# Targeting MRP3 in Pancreatic Cancer *In vitro*

Daniel Deveraux Estevan Dantzic

February 2020

A thesis submitted in complete fulfilment of the requirements for the degree of Doctor of Philosophy, Auckland University of Technology, 2020.

## Abstract

Pancreatic cancer is currently one of the most aggressive and resistant cancers. The incidences rates of pancreatic cancer are comparatively low. However, the death rates of pancreatic cancer are within the top 10 of all cancers worldwide. The five-year survival rate is currently 5%, meaning that 95% of patients diagnosed with pancreatic cancer will not live more than five years. Most pancreatic cancer patients will succumb to the disease within one year of diagnosis. The current treatments for pancreatic cancer have not been significantly improved over the past three decades. The mechanism of action for gemcitabine in cancer killing is that the nucleoside analogue prevents cell cycle progression and proliferation. However, the major limiting factor with the use of gemcitabine and many other drugs is multidrug resistance. Multidrug resistance is the resistance of cancer towards multiple drugs that are distinct both in structure and pharmacological target. ABC transporters have modulated multidrug resistance across a wide range of cancers. Each ABC transporter has displayed unique substrate specificity, tissue distribution and unique molecules that inhibited its activity. P-gp, BCRP2 and MRP1 were among the first ABC transporters discovered and are the best characterized of the ABC transporters. However, recent studies have shown that other ABC transporters such as MRP2, MRP3 and MRP5 are also overexpressed in a variety of cancer types, which have been suggested to confer multidrug resistance. MRP3 has for instance, shown overexpression in pancreatic cancer cells, has a unique affinity for glucuronide metabolites and has modulated anticancer drug resistance (MTX, teniposide and etoposide). This study initially investigated the expression of MRP3 across three bioinformatic platforms (ONCOMINE, Kmplot and STRING). The results confirmed the wide-reaching overexpression of ABCC3/MRP3 in kidney, lung and pancreatic cancer. The well-established genomic editing tool CRISPR-Cas9 was used to knockout the expression of MRP3 in PANC1 cells by liposome-delivered three guide RNAs and Cas9 protein. Silencing MRP3 in knockout cell lines increased cellular accumulation of a model MRP3 substrate, 5-chloromethylfluorescein (CMF) by 47%-fold, 76% and 38%. The same mixed knockout populations also showed decreased resistance towards methotrexate (MTX, a well-characterised MRP3 drug substrate) and gemcitabine (GEM). In addition to CRISPR-Cas9 modulation, the activity of MRP3 was also targeted using the potential inhibitors, suramin, curcumin and EF24. Suramin, curcumin and EF24 all successfully increased CMF accumulation by 2.11-fold, 2.43-fold and 2.4-fold. Whether this would translate into reduced resistance was investigated. Within PANC1 cells, the combination of MTX and EF24 proved to be the most promising, with synergistic values ranging from 0.137 to 0.412. While, MIAPACA2 cells showed highly synergistic results across all combinations tested, especially the combination of MTX and suramin. This

study was able to identify suramin, curcumin and EF24, three novel MRP3 inhibitors. Furthermore, for the first-time gemcitabine resistance was modulated by MRP3 expression in PANC1 cells. Taken together, our results suggest that MRP3 confers resistance to gemcitabine. Modulation of ABCC3 increased the sensitivity of PANC-1 and MiaPaCa-2 cells to gemcitabine and modulation of ABCC3 activity may represent a novel strategy to reverse gemcitabine resistance in pancreatic cancer cells. Screening tumour MRP3 expression levels to select patients for treatment with gemcitabine-based regimen alone or in combination with MRP3 modulation, could improve outcomes of pancreatic cancer treatment.

## Publications from this thesis

Dantzic, D., Noel, P., Merien, F., Liu, D. X., Lu, J., Han, H., … Li, Y. (2018). The Effects of Synthetically Modified Natural Compounds on ABC Transporters. *Pharmaceutics*, *10*(3), 127. doi:10.3390/pharmaceutics10030127
(Impact Factor: 4.773, 2018)


## Acknowledgements

I would like to firstly acknowledge Dr Yan Li. Without your support I would have never been able to achieve what I have achieved. The gentile, nurturing and helpful spirit that you carry with you will be something that I will try to replicate if I ever get the privilege to mentor someone. Not only did you support my studies, but you also showed interest in me as a person. I have been lucky with the supervisors that I have had over my scientific career thus far. The trust that you place in your students to find their own solutions to issues has also helped me to develop my confidence and problem-solving skills.

I would also like to acknowledge my secondary supervisor Prof. Fabrice Merien. I will always remember your willingness and eagerness to help whenever I needed it. So, I thank you for your support. I would also like to thank Piyush Budge and Riya Biswas my lab colleagues for all the help, support and friendship given during my time at AUT.

I would also like to thank my beautiful wife Edwina Dantzic, she got to see me go through the whole process. All the disappointments and joys of this perilous but rewarding PhD journey. I will be forever grateful for you. I would also like to thank my family, the support from my parents Joseph and Monica Dantzic and pride that they imbued on me really motivated me to keep striving towards this goal. I would not be the person I am today without both of you. I would also like to thank my siblings Chantelle Cooper and Charles Dantzic. I know that you were fully supportive of all my achievements and I am glad that I was able to achieve this feat for our family. I would like to thank my extended family for all the support that they showed during these last four years. Mālō e lelei!

Lastly, I would like to acknowledge the financial support that I was privileged to receive during the first three years of my PhD. Without this support, this journey would have been so much more difficult. Thank you to:

- Dr Yan Li and the AUT scholarships office for the PhD stipend
- The school of science for the Doctoral Fee scholarship

# Contents

# Figures and Tables List

## Figures

## Tables

## Attestation of Authorship

I hereby declare that this submission is my own work and that, to the best of my knowledge and belief, it contains no material previously published or written by another person (except where explicitly defined in the acknowledgements), nor material which to a substantial extent has been submitted for the award of any other degree or diploma of a university or other institution of higher learning.

Signed:

Date: 21 February 2020

# Chapter 1 Introduction

## Cancer review

### Hallmarks of Cancer

In 2000, Hanahan et al., sought to characterise the biological changes in normal cells that allow for the formation of cancer [1]. These multistep processes allow cancers to acquire six functions that enable cancers to grow and develop [1]. The ability for cancer to overexpress growth signals, supress anti-growth signals, evade apoptosis, sustain proliferation, sustain angiogenesis and cause tissue invasion and metastasis mechanisms all enable cancer growth [1]. The overexpression of growth factor (GF) receptors such as epidermal growth factor receptor (EGFR), allows cancers cells to respond to GFs more sensitively than normal cells [1]. Therefore, lower concentrations of GF can activate proliferation in cancerous cells [1]. Cancers also induce the production of growth factors and signalling to promote further growth signals, creating a feedback loop that promotes the continual growth of cancer cells [1]. Mutations in the Ras protein can lead to the upregulation of the PI3K signalling pathway which also modulates cell growth, motility, metabolism and survival in cancer [2].

Cancers supress anti-growth signals which, in normal cells allows the body and tissues to maintain cellular homeostasis [1]. Quiescence or cell cycle arrest prevent cells from further proliferation which may become permanent, depending on the cellular environment and the signals present [1]. The majority of antiproliferative signals pass through the retinoblastoma protein (pRb), p107 and P130 [1]. The E2F transcription factors are key factors in cell cycle progression between the G1 and S phase of the cell cycle [1]. The E2F transcription factors have been modified to block proliferation in cancer cells [1]. The expression of the growth factor TGFβ is able to dysregulate the phosphorylation of pRb [1]. A variety of cancers can utilise the activity of TGFβ to restore G1/S phase transition and subsequent proliferation [1].

Apoptosis once signalled caused cells to undergo a well characterised pathway of cell death [1]. In order for effective signalling the presence of sensors and effectors are necessary to both monitor and respond to cell death or cell survival signal levels, respectively [1]. The mitochondria is an organelle that the cell uses to accumulate apoptotic signals and respond by releasing more signals such as cytochrome C to further stimulate apoptosis [1]. This antiproliferative activity by cytochrome C can be governed by the B-cell lymphoma 2 (BCL2) family of mitochondrial proteins which either promote (BAX, BAK, BID, BIM) or supress apoptosis (BCL-2, BCL-XL, BCL-W) [1]. The upregulation of the tumour protein 53 (p53) protein results in the upregulation of BCL2-associated X protein (BAX) in response to DNA damage, thereby promoting apoptosis

[1]. However, mutation of the p53 gene has been seen across a variety of cancers and limits the ability of cancer cells to respond to DNA damage via BAX/cytochrome C dependent apoptosis [1]. Furthermore, some cancers have utilised the PI3K/AKT/PKB pathway to supress the transmission of signals that promote apoptosis [1].

The limitation of apoptosis, stimulation of growth factors and receptors and the suppression of cell death signals all contribute to the uncontrolled growth that we see in cancer [1]. Telomere length can be used to measure the amount of generations of cell division that a cell has undergone [1]. In normal cells the telomere degrades after each division by approximately 50-100 base pairs at the ends of chromosomes [1]. The continual degradation of the chromosome telomere ultimately leads to chromosomal degradation which results in death signalling and cell death of the affected cell [1]. However, cancer cells avoid this process by overexpression of the telomerase enzyme, which maintains the length of the telomere by adding hexanucleotides to the ends of telomeres [1].

In normal tissues, angiogenesis is transiently activated to repair tissue, during the menstrual cycle and embryogenesis [3]. The angiogenic process begins with the breakdown of the basement membrane followed by cell proliferation, migration of vasculature and subsequent maturation of endothelial cells [4]. In cancerous tissues, cancer exhibit heightened metabolic activity and require increased vascularity to supply the necessary nutrient requirements to grow [3]. Cancer utilises growth factors such as PDGF to stimulate proliferation, survival, migration and angiogenesis [5-10]. During tumorigenesis, angiogenesis is highly active, causing a constant sprouting of new vessels to supply the growing tumour [3]. Pathological angiogenesis is an incomplete process resulting in vascularity that is often morphologically abnormal and highly permeable [11].

The last characteristic for cancer establishment and progression is invasion and metastasis of cancer cells to adjacent and secondary tumour sites [1]. Metastasis begins with the entry of cancer cells into the blood, followed by the survival of cancer cells in the vascular system, invasion of distant tissue and establishment of tumour growth in the new location [12]. Many complex molecular changes facilitate cancerous metastasis and invasion [1]. The activity of E-Cadherin a cell-cell interaction molecule is lost in cancers, but by forced expression, E-Cadherin expression can limit cancers ability to invade and metastasise [1]. Once cells are able to invade a new region the remaining hallmarks of cancers are required to develop and establish secondary tumours, resulting in further stress, rerouting of bodily resources and degradation of the body [1].

**Cancer Treatments**

The most recent epidemiological estimates for cancer incidence and death rates where characterised by the GLOBOCAN project in 2018 [13]. The most common cancer types worldwide are lung, breast, prostate, colon and nonmelanoma skin cancers which were responsible for 11.6%, 11.6%, 7.1%, 6.1% and 5.8% of all (~18,100,000) cancer cases, respectively [13]. However, the death rates weren't directly proportional, lung, stomach, liver, breast and colon cancers showed 18.4%, 8.2%, 8.2%, 6.6% and 5.8%, of the deaths (~9,500,000) in 2018, respectively [13]. The inclusion of cancer prevention into the strategy of cancer treatment is needed to improve the cancer rates of the past [14]. The improvements of our understanding of cancer has significantly improved treatment and detection of cancers however, the incidence rates continue to rise despite these advances [14]. This has been attributed to a number of factors including increased rates of obesity and increases in the median population age [14]. Progress in various cancer analyses has revealed the heterogeneity of cancers, suggesting that prevention may also require a multifaceted approach [14]. The prevention of cancer is not a simple task to undertake [14]. Improved health education, reduction in lifestyle risk factors such as tobacco use, poor diet and physical inactivity may lead to improved incidence rates [14]. While preventative measures can be taken, it is not always possible to identify the reason that patients get cancer [14]. Therefore, we must also find ways to treat cancer when it does arise.

According to the national cancer institute the current cancer therapies include chemotherapy, hormone therapy, targeted therapy, stem cell transplants, immunotherapy, resection and radiotherapy (www.cancer.gov). For a long time the clinical efficacy of immunotherapy was limited by cancers ability to avoid detection and destruction by the immune system [15]. More recently, immune system targeting has vastly improved, with a number of successful clinical trials [16]. Immunotherapy was designated the 'breakthrough of the year' by Science magazine in 2013 [16]. Immunotherapy has shown some encouraging *in clinic* results, especially when using the chimeric antigen receptor (CAR) therapy [16]. CAR therapy is a personalised therapy that extracts a patient's T-cells, modifies them to recognise cancer cells and reintroduces them into the patient [16]. However, this is very expensive treatment that makes this treatment at this stage inaccessible for the general population [17]. Combinations of chemotherapy and immunotherapy have also exhibited improvements in patient survival [16].

In some cancers such as renal cell carcinoma (RCC), hormone receptors were dysregulated [18]. Dysregulated paracrine and autocrine hormone signalling modulates several cancerous hallmarks including proliferation, migration, angiogenesis and drug resistance [18]. Inhibiting cancer promoting hormones and their receptor signalling has

shown therapeutic benefit in RCC [18]. Breast cancers have also shown overexpressed hormone receptors including oestrogen receptors (ER) or progesterone receptors (PR) [19]. Tamoxifen, a hormonal therapy, prevents oestrogen and the ER from binding by competitive inhibition [19]. Reduction of ER activation reduces breast cancer growth in metastatic breast cancer [19]. Although there is still no cure for metastatic breast cancer, hormonal therapy demonstrated less toxicity and more prolonged palliative effects [19]. EGFR is a well-known oncogene that has been associated with poorer outcomes and prognoses in cancer patients [20]. Since the discovery of EGFR, targeting EGFR has undergone extensive research [20, 21]. In head and neck cancers, EGFR is overexpressed in 90% of tumours [20]. Cetuximab a monoclonal antibody remains the only FDA approved EGFR-targeted treatment [20].

However, much like other treatment modalities, the long term survival rates for head and neck cancers has remained unchanged, even in combination with radiotherapy and chemotherapy [20]. Radiotherapy is the treatment most commonly used in combination with other treatment types [22]. More than 50% of cancer patients undergo a radiotherapy regime [22]. Radiotherapy acts by delivering high physical energy to cancer cells, damaging DNA leading to death of the cancer cell [22]. The rapidly dividing cancer cells are more sensitive towards radiotherapy than normal cells, therefore radiotherapy should selectively target cancer [22]. Radiotherapy includes the use of gamma rays, x-rays and protons [22]. Recent evidence has suggested that radiotherapy can break down local tumours, but these destroyed tumours may also damage both local and distant tissues by releasing cytokines and activating oncogenic signals [22]. The degraded tumour debris circulating within the blood can increase the chance of relapse or metastasis [22].

Stem cells are cells that can indefinitely self-renew, form single cell-derived homogenous cell populations and differentiate into a variety of cell types [23]. There are several different stem cell types that can be classified based on their tissue origins [23]. Normal stem cells are involved in tissue regeneration and homeostasis [23]. In cancer therapy, stem cells can be modified to express GFs and cytokines producing stem cells which can act as a delivery mechanism to target tumours [23]. These modifications include the addition of chemokine and growth receptors which improve the stem cell tumour-homing ability [23]. Stem cell transplantation can be limited by dosing difficulties with insufficient or abundant stem cell transplants resulting in different challenges [23]. Low stem cell levels resulted in low responses and increased relapse levels, while too many transplanted stem cells increased the risk of tumorigenesis [23].

Pancreatic cancer in most cases is discovered in a state that is unresectable (non R0) limiting the patient's median survival to between 4 and 6 months [24-26]. In pancreatic ductal adenocarcinoma (PDAC), only 10-20% of patients diagnosed, present

with a tumour that can undergo surgery [27]. This limitation is in part due to the lack of distinguishing symptoms but also due to the lack of detection methods for early stage pancreatic cancer [24]. Resection is currently the only curative method for pancreatic cancer [27]. Patients that undergo surgery showed an improved median survival rate between 20.1 and 28 months [27]. Advances in imaging, patient care, accurate staging and clearly defined resection parameters have also improved pancreatic cancer treatment [27]. However, the prognosis remains poor, even when surgery is possible the five-year survival rate of pancreatic cancer remains only 25% [27].

Pancreatic cancer is treated where possible with surgery followed by treatment with either FOLFIRINOX or gemcitabine + nab-paclitaxel combination [28]. Gemcitabine has been used to treat pancreatic cancer for a number of years, however, the improvements in overall survival were significantly improved by the introduction of another anticancer drug nab-paclitaxel [28, 29]. The nab-paclitaxel and gemcitabine combination exhibited an improved median overall 1-year and 2-year survival in comparison to gemcitabine alone [28]. While there has been some advancements in the use of chemotherapy, the major limitations to successful cancer treatment are still efficacy, toxicity and drug resistance [28, 30].

**Pancreatic cancer**

The most aggressive cancers were those that show high levels of death rates in comparison to their respective incidence rates [13]. Pancreatic, liver, oesophagus, lung and mesothelioma cancers showed the closest mortality and incidence rates [13]. Due to the relative decline in breast cancer rates worldwide, it is predicted that pancreatic cancer may soon surpass breast cancer related deaths [13]. Over the next eight years the New Zealand's ministry of health forecasted an increase in the mortality, morbidity and overall burden of pancreatic cancer [31]. The 5-year survival rate for pancreatic cancer patients is approximately 5%, with most deaths occurring within the first year [24, 32, 33]. Approximately 53% of pancreatic cancer patients at the point of diagnosis had already developed distant metastasis [24]. 90% of pancreatic cancer patients were diagnosed with pancreatic ductal adenocarcinoma (PDAC) [34]. The five year survival rate for PDAC was <10%, ranking PDAC within the top five most common causes of cancer-related death [34]. The cloaked nature of pancreatic cancer symptoms have prevented the development of screening strategies to detect early stages of pancreatic cancer [25]. Early symptoms of pancreatic cancer can range from anorexia to skin changes which are precursors for a variety of diseases [25]. The first line treatment for pancreatic cancer for the past three decades has been gemcitabine an antimetabolite drug that has only yielded a marginal increase in patient survival [35, 36]. Pancreatic cancer is notoriously resistant to chemotherapeutics which has halted the improvements

in treatment for the last thirty years [37]. Pancreatic cancer shows a series of resistance mechanisms that prevent its destruction [37]. These include overexpression of efflux transporters (MRP1, MRP3, MRP4 and MRP5), mutations in key genes (BRCA, PARP, p53), and dysregulation of signalling pathways (NF-κB, P13K/AKT) [37]. Targeting the high levels of drug resistance is essential in successfully treating cancer and pancreatic cancer in particular [37].

**Drug Resistance**

Drug resistance is the primary limiting factor in the treatment of cancer [30]. The wide spread resistance seen towards cancer treatment requires further understanding and improved treatment options [30]. The mechanisms that drive drug resistance include drug inactivation, drug target alterations, DNA damage repair and drug accumulation modulation [1, 30]. Drug inactivation is a complex mechanism that encompasses the pharmacological interactions of drugs with various proteins and metabolites which modify, breakdown or indirectly inactivate drugs [30]. Drug target alterations are usually a result of mutations within cancers that cause the drug targets to no longer respond to drugs as effectively [30]. In cancer, some drugs were designed to disrupt DNA either directly or indirectly [30]. Damaged DNA repair mechanism may cause resistance simply carrying out what they were designed to do, repair DNA [30]. Lastly, efflux modulation which has prevented the accumulation of a number of different anticancer drugs [30, 38].

The process by which cells become resistant to multiple unrelated drugs is called multidrug resistance (MDR) is [39, 40]. Efflux modulation in cancer by up-regulation of various ABC transporters such as P-glycoprotein (P-gp), Breast Cancer Resistant Protein (BCRP) and Multidrug Resistant Proteins 1-5 (MRP1-5) efficiently remove drugs from the cell, thus preventing the drug from achieving its desired level and effect [30, 41, 42]. The activity of ABC transporters has become an essential consideration when designing drugs, as they can greatly affect pharmacokinetics, toxicity and efficacy of drugs [43]. Absorption, distribution, metabolism, excretion and toxicity are the properties that most dictate the success of a new drug, all of which can be affected by the expression of ABC transporters [44]. ABC transporters are present in key organs and blood/organ barriers such as the intestines, liver, kidneys, blood-brain barrier and blood placental barrier [45].

**ABC Transporters**

There are 48 human ABC transporters, all with the ability to utilise ATP as an energy source to transport substrates across cell membranes [41, 46]. ABC transporters are made up of two components, the transmembrane domain (TMD) which creates the passageway in the membrane for substrates to pass through and the nucleotide-binding

domain (NBD), where ATP is hydrolysed [47]. ATP hydrolysis provides the energy required for the conformational change of the TMD from the closed to the open conformation which is essential for the effective transport [47]. Cellular accumulation of anticancer drugs is attenuated by select ABC transporters because of their ability to efflux anticancer substrates out of cancer cells independent of concentration gradients (Figure 1—1) [48]. The ability to re-sensitise cancer cells to chemotherapeutics has been extensively studied as it is believed that when the limitation of resistance is removed, the efficacy of cancer treatment will be restored (Figure 1—1) [49, 50].

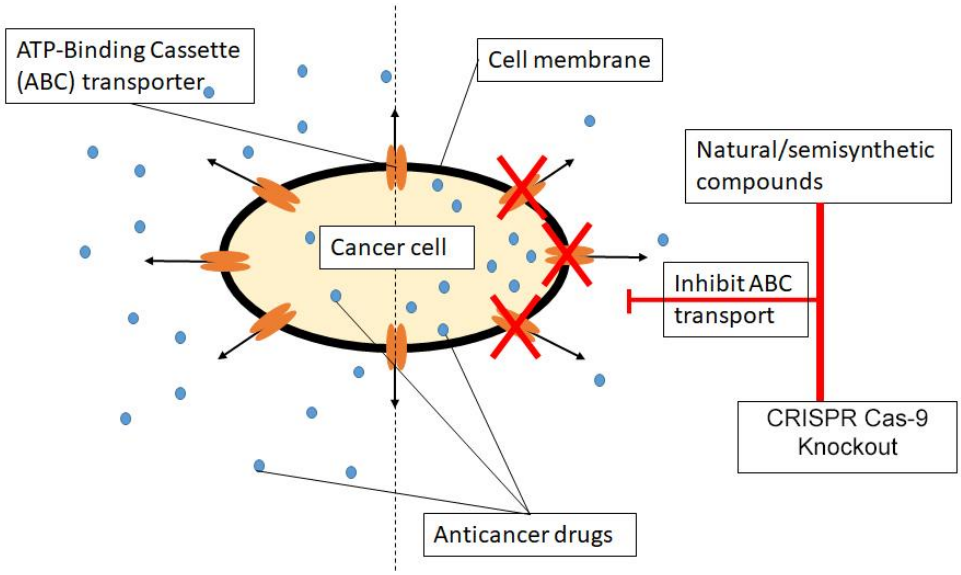


Figure 1—1. Multidrug resistance mechanism caused by ABC transporters and the targeting strategies. Modified from dantzic et al., [51].

In 1973, it was observed that daunorubicin, vincristine, and vinblastine all appeared to be actively transported from resistant Ehrlich ascite tumour cells [52]. In 1976, P-gp a surface glycoprotein was isolated from a colchine-resistant cell line [53]. It was found that the amount P-gp present correlated with the resistance observed against colchine [53]. The MDR1/ABCB1 gene, discovered in 1986, encodes the P-gp protein [54]. P-gp is a 170 kDa protein with 1280 residues in a single polypeptide chain [53, 55]. P-gp is expressed at various crucial barriers within the body, including the intestinal wall, the blood–brain barrier (BBB), the placental barrier and in key waste organs, including the liver and kidneys (Figure 1—2) [41, 56, 57]. The expression of P-gp at the apical side of the intestinal wall and the BBB predicates its role in limiting the entry of drugs into the bloodstream and the central nervous system, by pumping drugs either back into the gut lumen or back into the bloodstream, which under normal circumstances would act as a protective measure against toxins (Figure 1—2) [41, 58]. However, in the context of drug development and cancer treatment ABC transporters can play a large role in drug pharmacokinetics and therapeutic efficacy [58, 59]. It was for this reason that the

American Food and Drug Administration (FDA, Silver Spring, MD, USA) created strict guidelines on how drug and ABC transporter interactions should be evaluated during drug development [59]. Each ABC transporter has exhibited unique tissue distribution, substrate specificity and expression levels across both normal and cancerous tissues [55, 60]. P-gp transports a variety of anticancer agents against concentration gradients, including vinblastine, paclitaxel, doxorubicin, erlotinib, colchicine, and teniposide [55, 61]. Given the widespread use of these chemotherapeutics, inhibition of P-gp may transform relatively poorly performing cytotoxic drugs into exceptional ones.

Breast cancer resistance protein (BCRP) is another well studied member of the ABC transporter family [62]. The BCRP transporter has a unique structure and is considered a half transporter, as it is formed from only six TMDs and one NBD [63]. However, in order to function two BCRP molecules must dimerise to create a functional BCRP unit [63]. BCRP is distributed within the placenta, bile duct, colon, small bowel, brain and endothelium [62]. The localisation of BCRP permits it to act as a barrier, limiting the accumulation of toxins to the foetus, brain and prevent absorption of toxins into the blood stream (Figure 1—2) [42]. However, in cancerous cells, BCRP modulates the resistance of a variety of anticancer drugs including but not limited to gemcitabine mitoxantrone, topotecan, irinotecan, doxorubicin, SN-38, flavopiridol, and methotrexate (MTX) [62, 64-66]. Much like P-gp, the inhibition of BCRP reverses MDR, which could lead to improved therapeutic outcomes [62, 64]. BCRP has displayed the broadest substrate specificity and the most known phytochemical inhibitors of all ABC transporters [42]. To increase potency, specificity and inhibition of ABC transporters some natural compounds have been synthetically modified into new derivatives, which have been reviewed in detail below [51].

MRP1 is an ABC transporter that has been found in all areas of the body [63]. MRP1 transports a wide variety of xenobiotics and metabolites essential for cancer treatment and much like P-gp has been associated with poor prognosis [67, 68]. However, unlike P-gp, MRP1 is localised to the basolateral membrane of mucosal cells [69]. Therefore, under normal conditions MRP1 transports substrates into the bloodstream [69]. Much like BCRP, MRP1 is also localized to the BBB and transports substrates from the brain back into the blood stream (Figure 1—2) [38]. The complexity and cross-reactivity of these transport mechanisms were well exhibited by MRP1, with high substrate overlap between MRP1 and P-gp [60]. Unlike P-gp, MRP1 transports glutathione (GSH), glucuronate and sulphate conjugates which extends the scope of MRP1 specificity [60]. MRP1, MRP2, MRP5 and MRP6 all share the preferential transport GSH conjugates, while MRP3 preferentially transports glucuronide conjugates [42]. The glutathione conjugates created by xenobiotics such as methotrexate can also

be transported out of cells thereby limiting overall drug activity [60, 70]. MRP1 also transports doxorubicin, vincristine, etoposide, camptothecin, CPT-II and SN-38.

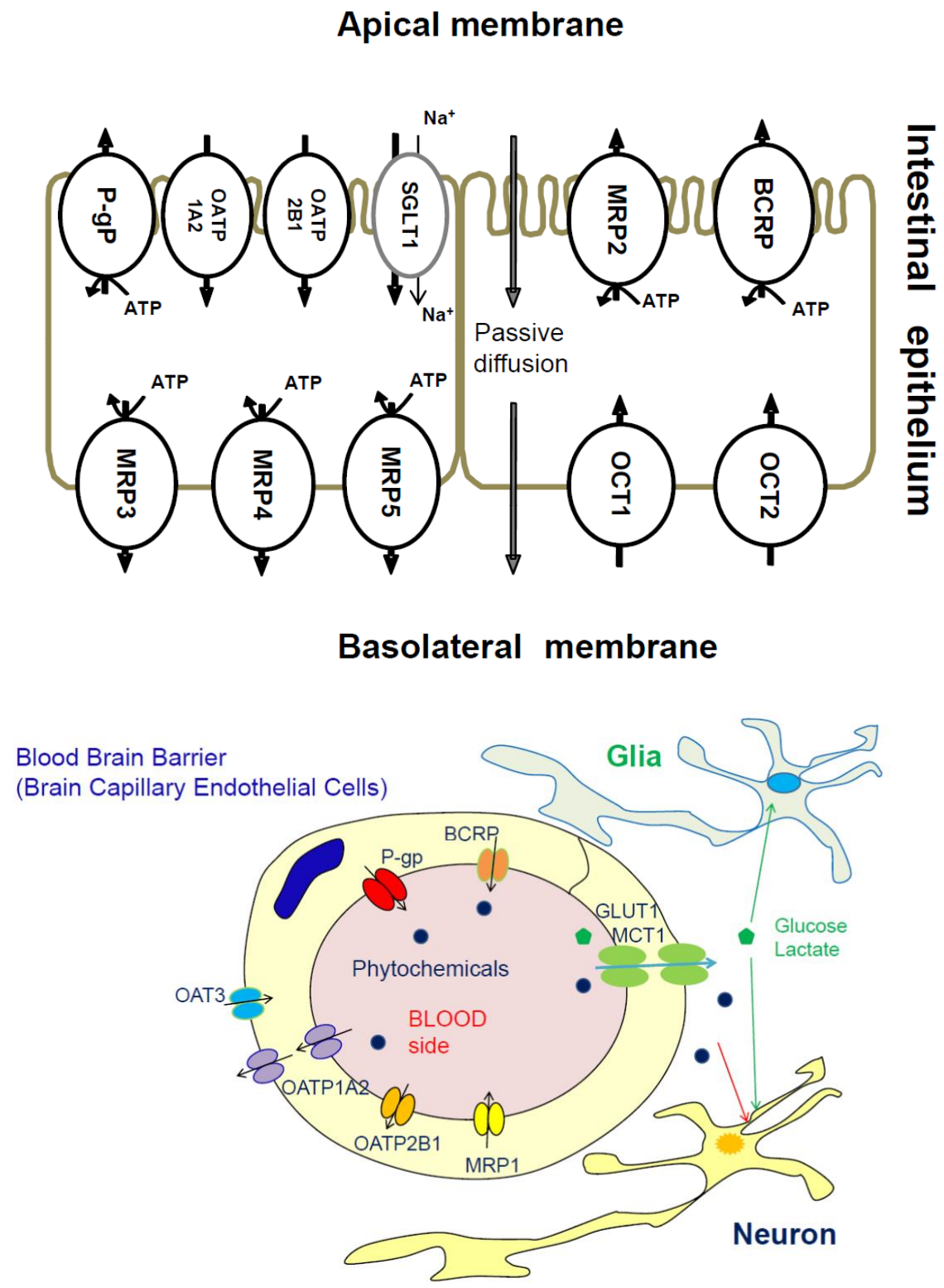


Figure 1—2. Localization of ABC and SLC transporters in the human small intestine and blood brain barrier [38].

However, in the transport of daunorubicin and vincristine, MRP1 transport showed dependence on GSH levels [71]. Therefore, MRP1 transport of GSH-conjugates may only occur when sufficient levels of GSH are available [71]. P-gp did not show the same dependence on GSH levels and resistance remained unaffected by changes in GSH levels [71].Highlighting the subtle but important differences in ABC transporter activity and substrate specificities.

MRP3 is located within the liver, adrenal glands, colon, pancreas, kidney and the gut [60, 72]. MRP3 (ABCC3), under healthy conditions is an important transporter in liver function due to its localisation in the hepatic basolateral membrane [73]. MRP3 expression within the basolateral membrane can increase the transport of MRP3 specific substrates including excess bile acids [73]. MRP3 alongside MRP4 and MRP5 are also localized to the basolateral membrane of the intestine facilitation the transport of substrates from the intestine into the blood stream (Figure 1—2) [38]. MRP2 and MRP3 were the only transporters able to transport conjugated bilirubin [72]. Unconjugated bilirubin is a potential neurotoxic compound that has been associated with a number of pathologies [72]. While MRP3 may not be the most expressed transporter in the liver, it can act as a compensatory transporter of MRP2 in the export of bile acids [73]. In the absence of MRP2, MRP3 moves the conjugated bilirubin from hepatocytes back into the blood stream which is subsequently removed from the body by the excretory system [72]. Conjugated bilirubin cannot be reabsorbed by the intestine, therefore MRP3 transport results in excretion of the conjugates [72]. This demonstrates in normal cells that MRP3 protects cells from the accumulation of glucuronide conjugates and in particular, bilirubin conjugates [72].

The preference for transport of glucuronide conjugates over glutathione conjugates differentiates MRP3 from MRP1 and MRP2 [60]. The transport of a number of glucuronide conjugates by MRP3 may affect the accumulation, function and destruction of other compounds and their respective conjugates [72]. These include normal metabolites (folic acid, bilirubin glucuronide), therapeutic drugs (methotrexate, etoposide, teniposide) and their respective metabolites (curcumin-O-glucuronide) and environmental contaminants (Bisphenol A glucuronide, Resveratrol glucuronide and Genistein) [72]. In the case of COG, an *in vivo* study demonstrated that the knockout of MRP3 in mice significantly decreased the concentration of COG in plasma samples [74]. MRP3 inside-out membrane vesicles showed the accumulation of COG in an ATP-dependent manner further validating that COG is an MRP3 substrate [74]. While, *in vivo,* MRP3$^{-/-}$ mice showed a significant decrease in the rate of absorption of folic acid into the blood stream [75]. Folic acids are key dietary vitamins essential in a number of metabolic processes, especially in purine and pyrimidine biosynthesis and amino acid metabolism [76]. Folate deficiencies can be related to several diseases including Alzheimer's, heart

disease, hearing loss and osteoporosis [76]. MRP3 has exhibited detrimental clinical activities by preventing the accumulation of pain medications such as diclofenac and morphine glucuronide (M6G) in their target sites [77, 78].

In some liver diseases MRP3 expression is upregulated in order to defend against cytotoxins [73, 79]. In cancer, ABCC3/MRP3 has shown overexpression in pancreatic cancer, renal cell carcinoma (RCC), transitional cell carcinoma (TCC), squamous cell carcinoma (SCC), resistant hepatocellular carcinoma cells, breast cancer, non-small cell lung cancer, bone cancer and cholangiocarcinoma [79-82]. Pancreatic cancer tissue samples underwent gene expression profiling and tissue microarray experiments [83]. The expression levels of 2177 cell-surface genes across four normal and 28 pancreatic cancer samples were evaluated and further investigated using immunohistochemistry [83]. TLR2 and ABCC3 were selected for further analysis from the 170 targets found to be overexpressed in two or more cancerous samples and not it normal samples [83]. ABCC3 and TRL2 showed 75% and 64% DNA array coverage, respectively across the pancreatic cancer samples [83]. Further *in vitro* validation by immunohistochemistry (IHC) confirmed that both ABCC3 and TLR2 exhibited differential protein expressions across normal and tumour tissue [83].

MRP3, much like other members of the ABC transporter family, can confer multidrug resistance in cancer cell lines towards specific substrates [79, 82]. In 1999, MRP3 was investigated for its localisation, expression and ability to induce multidrug resistance [79]. Cytotoxicity was analysed in MRP3 overexpressing cell lines against a variety of drugs, using cell viability assays [79]. MRP3 inhibited the cytotoxicity of etoposide, teniposide and MTX in a concentration dependant manner [79]. In another model, MRP3 mRNA levels were analysed in primary untreated transitional cell carcinoma (TCC), squamous cell carcinoma (SCC) and normal tissue [82]. Expression of MRP3 was significantly increased in cancerous samples in comparison to normal tissues with approximately 13-fold increase in mRNA expression [82]. The expression levels of MRP3 was also significantly higher in TCC cells when compared to SCC cells [82]. In hepatocellular carcinoma, sorafenib resistant PLC/PR5 cell lines were created by incubating cells with increasing concentrations of sorafenib over 24 months [84]. The $IC_{50}$ values of the two cell lines increased over this time by 1.8-fold and 4.6-fold that of the untreated PLC/PR5 cell line [84]. MRP3 expression was significantly upregulated in the resistant cell lines, while knockdown of MRP3 restored sensitivity to sorafenib [84]. Inhibition of MRP3 is essential to the reversal of resistance and treatment of a variety of cancers that overexpress MRP3 [79, 85].

ABCC3 mRNA and protein expression were overexpressed in Capan-2 and HPAFII PDAC cell lines as well as in tissue tumour specimens [36]. The stable (shRNA) and transient (siRNA) knockdown of ABCC3 both *in vitro* and *in vivo* reduced growth

rates, suggesting a role for MRP3 expression in PDAC proliferation [36]. Lysophosphatidylinositol (LPI) previously stimulated the proliferation of PDAC in cells with p53 mutations [36]. It was suggested that the efflux of LPI by MRP3 was the basis for the increase of PDAC proliferation [36]. These examples demonstrated the role of MRP3 in cancer biology and progression [36, 86]. ABCC3 mRNA was also overexpressed in breast cancer samples and breast cancer cell lines (BT-474, MCF-7, MDA-MB-231 and HCC-1805) [87]. In HER2 breast cancer cells, ABCC3 modulation of paclitaxel and monomethyl-auristatin-E (MMAE) was investigated [88]. Knockdown of ABCC3 increased sensitivity towards paclitaxel and MMAE, while overexpression of ABCC3 increased resistance in HER2 breast cancer cells [88]. Further analysis revealed that the overexpression of ABCC3 was found in HER2 upregulated tumours [89]. MRP3 expression was also upregulated in non-small cell lung cancer (NSCLC) [81]. When comparing resistant and sensitive NSCLC, 44 genes were found to be upregulated in resistant cell lines, ABCC3 was among the most overexpressed genes found [81]. The expression of ABCC3 has influenced key pathophysiological stages including lymph node involvement, malignant histological indicators, decreased OS and resistance to chemotherapeutics [81]. The expression of MRP3 shows key roles both in normal and cancerous samples, however, there is still much to be learned about MRP3.

**The Effects of Synthetically Modified Natural Compounds on ABC Transporters**

Recent efforts to reverse ABC transporter dependent MDR by natural compounds was reviewed in detail [51]. The natural compound camptothecin (CPT) and its derivatives displayed a variety of antitumor activities [90]. However, high BCRP expression caused a 400–1000-fold increase in resistance towards camptothecin derivatives [91]. CPT, a substrate of P-gp and MRP2 has unpredictable oral bioavailability which has been attributed to the intestinal and biliary excretion mediated by P-gp and MRP2 [92]. Resveratrol another natural compound effects different diseases such as cardiovascular disease, cancer and neurodegenerative diseases [93]. The efficient elimination by intestinal BCRP and phase II metabolism limit the bioavailability of resveratrol [93]. The natural compound apigenin has been highlighted for its chemo preventative affects [94]. There has been a large amount of *in vivo* data showing the anticancer effects of apigenin against multidrug resistant tumours, leukaemia models and osteosarcoma xenografts [95-97]. Saeed et al., investigated the relationship between apigenin and ABC transporter expression [98]. Apigenin accumulation did not show P-gp dependence, while, apigenin treatments showed inhibition of both P-gp and BCRP expression [98]. Genistein much like resveratrol exhibits low bioavailability *in clinic* which could be related to its broad interactions with BCRP, P-gp and MRP2 [99-101]. Natural, highly bioactive,

poorly bioavailable compounds may respond to chemical modification to produce ABC transporter inhibitors with improved activity *in clinic*.

The first generation of P-gp modulators verapamil and cyclosporine A were approved for treatment of other diseases, suggesting these could be used safely as MDR reversal agents, which was tested *in clinic* [59, 102]. However, these synthetic compounds exhibited little MDR reversal, low potency and poor pharmacokinetics [102]. Verapamil and cyclosporine A also exhibited high toxicity and serious off target effects such as increased cardiovascular toxicity [102]. The second generation of P-gp modulators included valspodar and dexverapamil, derivatives of first generation P-gp inhibitors [59]. *In vitro,* results showed higher potency and specificity however, *in clinic* the second generation modulators showed little MDR reversal effects and side effects such as neutropenia and high toxicity [102]. CYP450-mediated anti-cancer drug metabolism was also inhibited, leading to increased systemic exposure of cytotoxins and enhanced toxicity [102]. Third generation inhibitors, tariquidar and zosuquidar were developed with improved potency and minimise CYP450 inhibitory activity [102]. They were more potent with less pharmacokinetic interactions [59]. However, increased toxicity of chemotherapy regimens was still seen with limited clinical benefit [59]. These purely synthetic compounds were limited by toxicity, but dietary phytochemicals are hypothesised to be better tolerated.

**Ningalin B**

The P-gp inhibitory activity of natural marine compounds including Ningalin B and terpenoids were comprehensively summarised in the review article by Long et al. [103]. Ningalin B is a natural marine product isolated from the ascidian (sea squirt) family of the genus *Didemnum* [104-106]. In the earliest ningalin study a number of synthetic intermediates (e.g., *O*-methyl ningalin B, compounds 10, 11, 13 and 14) were synthesised from the ningalin isolate [104]. Ningalin B displayed moderate cytotoxicity in L1210 and HCT116 cell lines with $IC_{50}$ values of 10 and 12 µM, respectively [104]. The synthetic analogue *O*-methyl ningalin B was 5-fold and 2.5-fold less cytotoxic than ningalin B, in L1210 and HCT116 cell lines, respectively [104]. P-gp overexpressing HCT116/VM46 cells demonstrated increased resistance to doxorubicin and vinblastine [104]. Ningalin compounds 10, 11, 13 and 14 at 1 µM potently sensitised HCT116/VM46 cells towards doxorubicin and vinblastine [104]. Compound 14 (1 µM) increased the cytotoxicity of vinblastine to the point where the HCT116/VM46 resistant cells became more sensitive to vinblastine than the HCT116 wild type cells [104]. Meanwhile, ningalin B was unable to reverse MDR in HCT116/VM46 cells [107]. This suggests that synthetic modification of natural products can generate more potent, moderately toxic, P-gp specific, MDR reversal agents. Subsequent studies of other ningalin B analogues

demonstrated low toxicity and potent MDR reversibility towards doxorubicin and vinblastine in HCT116/VM46 resistant cells [107, 108]. Ningalin B analogues 3 and 4 (1 μM) caused a complete reversal of vinblastine resistance and halved the resistance towards doxorubicin in a P-gp dependent manner [107]. Further modification of compound 3 led to the generation of ningalin B derivatives 19, 20 and 21, which exhibited complete MDR reversal towards doxorubicin and vinblastine without the toxicity associated with compound 3 [107, 108].

Six additional ningalin analogues (N1-N6) reported by Chou and colleagues showed a wide range of cytotoxic responses, with $IC_{50}$ values ranging from 13 μM (N3) to 150 μM (N4) in vinblastine-sensitive cells (CCRF-CEM), and 18 μM (N5) to 250 μM (N2) in vinblastine-resistant cells (CCRF-CEM/VBL100) [109]. All the ningalin analogues except N5 displayed lower toxicity in vinblastine-resistant cells (CCRF-CEM/VBL100) compared with vinblastine-sensitive cells (CCRF-CEM), suggesting that N1-N4 and N6 were P-gp substrates [109]. This is hypothesised because the lowered toxicity in resistance cells suggests that the ningalin compound could be exported from the cells by P-gp. Ningalin analogues (10 μM) resulted in an increase in sensitivity ranging from 210-fold (N1) to $6.2 \times 10_6$-fold (N3) was observed in CCRF-CEM/$VBL_{100}$ cells [109]. N3, (Figure 1—3) showed strong resistance reversal in vinblastine-resistant cells (CCRF-CEM/$VBL_{100}$) towards vinblastine and paclitaxel to a level beyond that measured in vinblastine-sensitive cells (CCRF-CEM) [109]. This combination study revealed that combining ningalins and doxorubicin resulted in a reduction in the $IC_{50}$ of both compounds. The strong synergism between ningalins and doxorubicin in doxorubicin resistance cells was confirmed using the chou-talalay method [109]. *In vivo*, whilst paclitaxel treatment slowed tumour progression, the addition of N3 resulted in tumour shrinkage, and, in one case, complete elimination of the tumour [109]. Several *in vitro* P-gp functional assays demonstrated that ningalins compete for [$_3$H]azidopine binding to P-gp, increased the cellular accumulation of VBL or paclitaxel, and inhibited drug efflux from the tumour cells [109]. These results indicated that the synergistic antitumor activity between ningalins and chemotherapeutic drugs was dependent on the inhibition of P-gp by ningalins.

The P-gp overexpressing breast cancer cell line MDA435/LCC6MDR was used to investigate the most recently designed ningalin analogues [105, 110-112]. Doxorubicin accumulation assays revealed that compounds 6, 25, 12, 23, 35 and 37 caused a 3.0, 2.1, 2.6, 2.4, 2.2 and 2.3-fold increase in doxorubicin accumulation in resistant cell lines, respectively [105, 110, 111]. The potency of compounds based on the doxorubicin accumulation from the most to the least potent were as follows: 37 > 35 > 23 > 12 > 6 > 25 [105, 110, 111]. The combination of compounds 6 and 23 exhibited a greater response towards doxorubicin accumulation than when used individually [111].

Compounds 35 and 37 selectivity inhibited P-gp while they only moderately reduced BCRP transport and did not inhibit MRP1 transport [110].

Table 1—1.Comparison of the potent synthetic modulators in vitro.

| Reference | Compound | Target | Cytotoxicity (μM) | | | |
|---|---|---|---|---|---|---|
| Ting-Chao Chou [109] | N3 | P-gp | CCRF-CEM: 13 | CCRF-CEM/VBL1000: 100 | | |
| Bin [110] | Compound 35 | P-gp | L292: >100 | MDA435/LCC6: >100 | MDA435/LCC6MDR: >100 | |
| Yang [105] | Compound 23 | P-gp | L292: >100 | MDA435/LCC6: >100 | MDA435/LCC6MDR: >100 | |
| Wang [112] | Compound 12 | P-gp | L292: >100 | MDA435/LCC6: >100 | MDA435/LCC6MDR: >100 | |
| Chen [113] | 5 Bromo-tetrandrine | P-gp | KB: 5.14 | KBv200: 6.17 | | |
| Sun [114] | W6 | P-gp | KB: ~2 | KBv200: ~4 | MCF-7: ~4.5 | MCF-7/DOX: ~5 |
| Zhu [115] | Compound 26 | P-gp | HepG2/ADR: >150 | MCF-7/ADR: >150 | | |
| Kraege [116] | GO-Y078 | BCRP | K562/BCRP: 0.31 | | | |
| Wong [117] | Compound 51 | MRP1, P-gp and BCRP | L292: >100 | LCC6: >100 | LCC6MDR: >100 | |
| Wong [117] | 4e | MRP1 | L292: >100 | LCC6: >100 | LCC6MDR: >100 | |

Doxorubicin and rhodamine 123 are relatively specific substrates of P-gp [118]. Quantifying the accumulation levels of specific P-gp substrates within the cell correlates with the activity of the P-gp transporter [105, 110, 111]. Compounds 12 (Figure 1—3) (2 μM) and 23 (2 μM) increased rhodamine 123 accumulation by 3.9 and 4.8-fold, respectively [105, 112]. Compound 23 showed an $EC_{50}$ of 78 nM which was 4.7-fold less than the typical P-gp inhibitor verapamil [105]. The synthetic ningalin compounds 6, 25, 35, 37, 12 and 23 proved nontoxic and a more potent P-gp transport inhibitors than verapamil [104, 105, 110-112]. Furthermore, compounds 12, 23, 35 and 37 were more effective in reversing MDR towards vinblastine than verapamil and re-sensitizing resistant cells towards other drugs beyond that of non-resistant cells [104, 105, 110-112].

Structure-activity analysis (SAR) studies were carried out to investigate whether increasing the number of methoxy groups on ring B of ningalin B, changing the polarity, extending the linking chain, and substituting ring C with other functional groups would improve the potency and cytotoxicity of permethyl ningalin B analogues [110]. A significant improvement in potency and cytotoxicity was observed when the benzyloxy group was attached at the C ring in compounds 35 and 37 [110]. It was found that the number of methoxy substituents played a role in determining P-gp modulation, although

to what extent was not precisely established [110]. There was also evidence that more polar N substituents at the ring C decreased the P-gp activity [110]. SAR analysis of other ningalin compounds synthesised by Yang et al. including compound 23, showed that the addition of a para-trimethoxybenzyloxy, an ortho-bromo and a meta-methoxy group at ring C was an important pharmacophore for P-gp modulation in ningalin compounds [105].

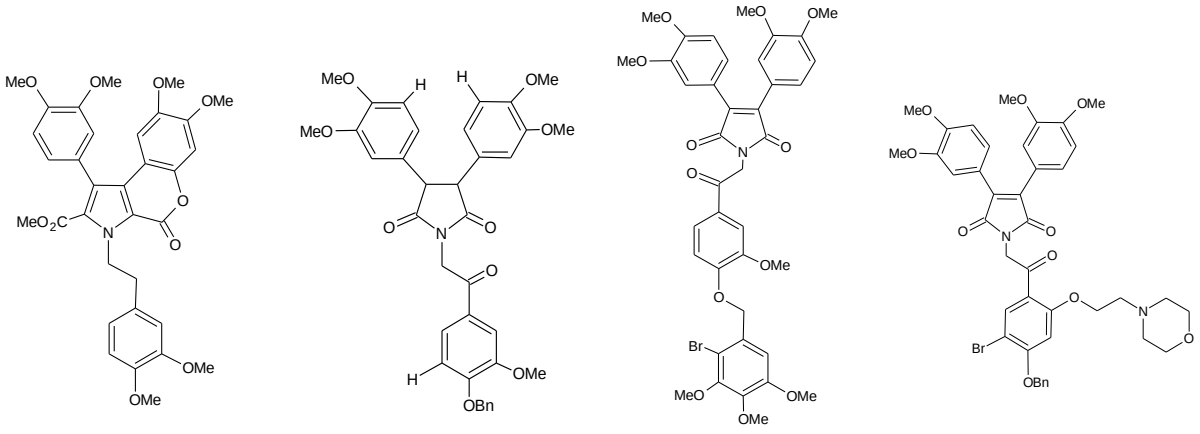

A B C D

Figure 1—3. Ningalin B compounds which act as potent P-gp inhibitors, from references 45, 49, 50 and 51. (A) N3 [49]. (B) Compound 35. 1-(2-(4-(benzyloxy)-3-methoxyphenyl)-2-oxoethyl)-3,4- bis(3,4-dimethoxyphenyl)-1H-pyrrole-2,5-dione1-(2-(2-bromo-5-methoxy-4-((3,4,5-trimethoxybenzyl)oxy)phenyl)-2-oxoethyl)-3,4-bis(3,4-dimethoxyphenyl)-1H-pyrrole-2,5-dione [50]. (C) Compound 23. 1-(2-(2-bromo-5-methoxy-4-((3,4,5-trimethoxybenzyl)oxy) phenyl)-2-oxoethyl)-3,4-bis(3,4-dimethoxyphenyl)-1H-pyrrole-2,5-dione [105]. (D) Compound 12. 1-(2-(4-(Benzyloxy)-5-bromo-2-(2-morpholinoethoxy)-phenyl)-2-oxoethyl)-3,4-bis(3,4-dimethoxy-phenyl)-1H-pyrrole2,5-dione [112].

**Tetrandrine**

The phytochemical tetrandrine (TET) is a bisbenzylisoquinoline, isolated from *Stephania tetrandra* roots which has been used in Chinese medicine since the 1960s for treatment of silicosis lesions [119, 120]. TET was shown by Fu et al. to increase the cellular accumulation of the P-gp substrate Fura-2 in a concentration-dependent manner [119]. In the presence of TET (0.625, 1.25 and 2.5 μM), doxorubicin-resistant cells (MCF-7/ADR) were re-sensitised to doxorubicin by 5.4, 11.8 and 20.4-fold, respectively [119]. Mice bearing subcutaneous MCF-7/ADR tumour xenografts were also re-sensitised to doxorubicin by combined treatment with TET without a significant increase in toxicity [119].

A brominated analogue of TET, bromotetrandrine (bromoTET, Figure 1—4), was reported to have a significant sensitizing effect on vincristine, doxorubicin, paclitaxel, docetaxel and epirubicin in P-gp overexpressing KBv200 (multidrug resistant) cells but not in the parental KB cells [113]. BromoTET was able to produce a significant increase

in doxorubicin accumulation in a concentration dependent manner in KBv200 cells [113]. *In vivo*, BromoTET alone resulted in a reduction of tumour growth at 7.5 mg/kg and 10 mg/kg by 14.8 and 23.5%, respectively, in KBv200 xenograft nude mice [113]. Co-administration of Bromo-TET (10 mg/kg) and epirubicin (2 mg/kg) significantly enhanced the antitumor activity of epirubicin without increasing toxicity [113]. BromoTET also increased the accumulation of doxorubicin within the KBv200 xenograft tissue while leaving the P-gp mRNA and protein expression unaffected [113]. Indicating that TET derivatives specifically inhibited P-gp transport function and not expression [113]. However, bromoTET showed some limitations, because of high toxicity in cancerous KB and KBv200 cell lines ($IC_{50}$ values of 5.14 and 6.17 µM, respectively) [113].

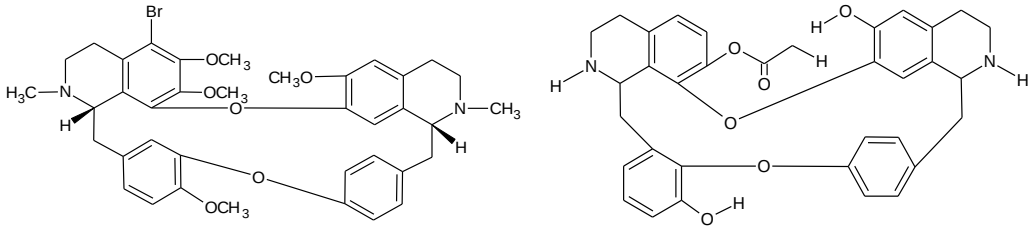


(**a**) (**b**)

Figure 1—4. Structures of 5-bromotetrandrine and W6. (a) Bromotetrandrine (11S,31S)-35-bromo-16,36,37,54-tetramethoxy-12,32-dimethyl-11,12,13,14,31,32,33,34-octahydro-2,6-dioxa-1(7,1),3(8,1)-diisoquinolina-5(1,3),7(1,4)-dibenzenacyclooctaphane [113]; (b) W6 [114]

H1, another synthetic derivative of TET, also displayed P-gp inhibition evidenced by increased doxorubicin and rhodamine 123 accumulation (3.7 and 29.7-fold increase) in KBv200 cells when treated with H1 (0.5 µM) [120]. H1 caused a complete reversal of resistance to doxorubicin and a partial reversal of resistance to vincristine and paclitaxel in KBv200 cells [120]. KB-sensitive cells remained unaffected by H1 in cellular accumulation experiments [120]. Cisplatin toxicity remained unaffected by incubation with H1, exhibiting the selectivity of H1, since cisplatin is not transported by P-gp [120]. P-gp interaction was studied using an ATPase assay which indicated NBD binding and transport activation [120]. Compounds interacting with an ABC transporter can stimulate or inhibit its ATPase activity, which is measured by the amount of inorganic phosphate generated by ATP hydrolysis [120]. H1 inhibited ATPase activity of P-gp but also showed that it was not a P-gp substrate due to the lack of ATPase stimulation effects [120]. P-gp protein expression decreased in the presence of H1 in a concentration dependent manner, while the P-gp mRNA levels remained unaffected [120]. Further analysis revealed P-gp expression was reduced by ubiquitination via by the MEK-ERK signalling pathway [120]. Similar to bromoTET, H1 was inherently cytotoxic, with $IC_{50}$ values ranging from 2-10 µM in the cell lines investigated [120].

W6 (Figure 1—4), was another highly potent MDR reversal agent [114]. In the drug resistant KBv200 and MCF-7/DOX cells, W6 (1 µM) increased the accumulation of doxorubicin by 4 and 5.3-fold, respectively [114]. W6 (0.25 µM, 0.5 µM and 1 µM) demonstrated MDR reversal, by lowering the $IC_{50}$ values of vincristine by 27.8, 29.2 and 1050-fold, respectively, in resistant KBv200 cells, and 64.5, 30.3 and 99.3, respectively [114]. W6 (0.25 µM, 0.5 µM and 1 µM) also lowered the $IC_{50}$ values of doxorubicin by 14.5, 14.6 and 27.8-fold and paclitaxel by 134.3, 274.5 and 1050-fold ,respectively, in resistant KBv200 cells [114]. Much like H1, W6 inhibited ATPase in a dose-dependent manner and decreased the protein expression of P-gp while the mRNA levels were unaltered [114]. These results suggested that W6 inhibited P-gp in a non-competitive manner, which was confirmed by photo labelling experiments [114]. Knockdown of ERK1/2 inhibited the expression of P-gp, while W6 significantly decreased the expression of ERK1/2 in a time dependent manner [114]. H1 and W6 appeared to show some commonality in the mode of action and the extent of cytotoxicity [114].

**Terpenes**

*Celastraceae* sesquiterpenes were isolated from the *Celastraceae* plant family which for centuries has been used to treat a variety of diseases [121]. Sesquiterpenes exhibit a wide range of biological activities, suggesting that they can interact with multiple proteins, including P-gp [121, 122]. The terpenoid compounds which are structurally diverse secondary metabolites modulate a variety of biological activities [122]. *Celastraceae* is also made up of non-terpenoid secondary metabolites such as quercetin, another natural product that has exhibited MDR reversal activities [122]. Twenty eight dihydro-β-agarofuran sesquiterpenes isolated from various *celastraceae* plants reduced cytotoxicity in the drug-sensitive NIH-3T3 cell line, while showing increased cytotoxicity in the P-gp expressing cells, suggesting some collateral sensitivity [109, 121]. Collateral sensitivity is a phenomenon by which cells resistant to one drug become hyposensitised to another [123]. Machu4 and Mama12 sesquiterpenes displayed the most potent inhibition of P-gp-mediated daunorubicin efflux, with $IC_{50}$ values of 0.24 and 0.33 µM, respectively [121].

Machu4, Mama5, and Mama12 reversed vinblastine resistance at 1 µM and were 5 to 9-fold more potent than verapamil [121]. Compounds that can dislodge [$^{3}$H] Azidopine from the binding pocket are likely to interact directly with the P-gp binding site [121]. The most potent daunorubicin efflux inhibitor, Machu4, did not decrease [$^{3}$H] Azidopine photolabeling, while, Mama12 dislodged [$^{3}$H] Azidopine [121]. These compounds presented no MRP1, MRP2 and BCRP modulation demonstrating their specificity as P-gp inhibitors [121]. Callies and co-workers prepared 58 dihydro-B-agarofuran sesquiterpene derivatives that showed a greater inhibitory activity against P-

gp mediated efflux of daunorubicin then with verapamil [124]. Six of the analogues (6, 24, 50, 57, 58 and 59) showed higher inhibitory potency than the lead dihydro-B-agarofuran compound [124]. Eighteen of the compounds displayed vinblastine re-sensitization, while five compounds exhibited greater MDR reversal activity than verapamil, with compound 48 completely reversed MDR at 3 µM [124]. Dihydro-B-agarofuran sesquiterpenes showed weak binding affinities and similar cytotoxic levels across control and MDR cell lines, suggesting that sesquiterpenes inhibited P-gp in a non-competitive manner [124].

Jatrophane diterpenoids were isolated from the *Euphorbia* family of plants and have shown potent and specific inhibition of P-gp [115, 125]. Compound 6 was twice as potent as cyclosporine A [125]. Further *in vitro* and *in vivo* evaluation of the jatrophane diterpenoid synthetic derivatives revealed that several compounds (12, 26, 29 and 35) inhibited rhodamine 123 efflux more efficiently than verapamil at 1 µM [115]. These unique compounds were non-cytotoxic in resistant (up to 150 µM) and sensitive cell lines (up to 100 µM), while displaying strong MDR reversal towards doxorubicin [115]. Compound 26 (Figure 1—5) was the most potent jatrophane MDR reversal agent, reducing doxorubicin $IC_{50}$ values by 61 and 36-fold in HepG2/ADR and MCF-7/ADR resistant cells, respectively [115]. *In vivo*, a combination of compound 26 and doxorubicin demonstrated a significant reduction in the final tumour volume and an increase in overall survival in a HepG2/ADR xenograft model [115].

**Other Notable Synthetic P-gp Inhibitors**

The broad activity and substrate specificity of P-gp can be further exhibited by the broad structural diversity of potential P-gp inhibitors. Methylated epigallocatechin, gallocatechin, and dihydromyricetin derivatives (compounds 23, 35, and 36) were not cytotoxic (>100 µM) in LCC6, LCC6MDR (a P-gp overexpressing breast cancer cell line) and L929 fibroblast cell lines [117]. The nontoxic compounds 23 and 35 significantly inhibited doxorubicin efflux at concentrations as low as 0.1 µM, while at 3 µM compounds 23 and 36 completely reversed MDR [117]. Methylated epigallocatechin and gallocatechin derivatives reversed MDR towards paclitaxel, vinblastine, vincristine, and doxorubicin in the nanomolar range ($EC_{50}$ between 102 to 280 nM) [117]. Intracellular accumulation of compounds 23 and 51 (Figure 1—5) in both MDR and parental cells were comparable, suggesting that they were not P-gp substrates [117].

Structure-activity analysis revealed some important P-gp inhibition pharmacophores including methoxy, allyloxy, or acetylamino substitutions at ring D and rigid linkers of oxycarbonylvinyl and oxycarbonylphenylcarbamoyl with optimal link lengths ranging from 7.75 to 13.37 Å between the D and C3 rings [126].

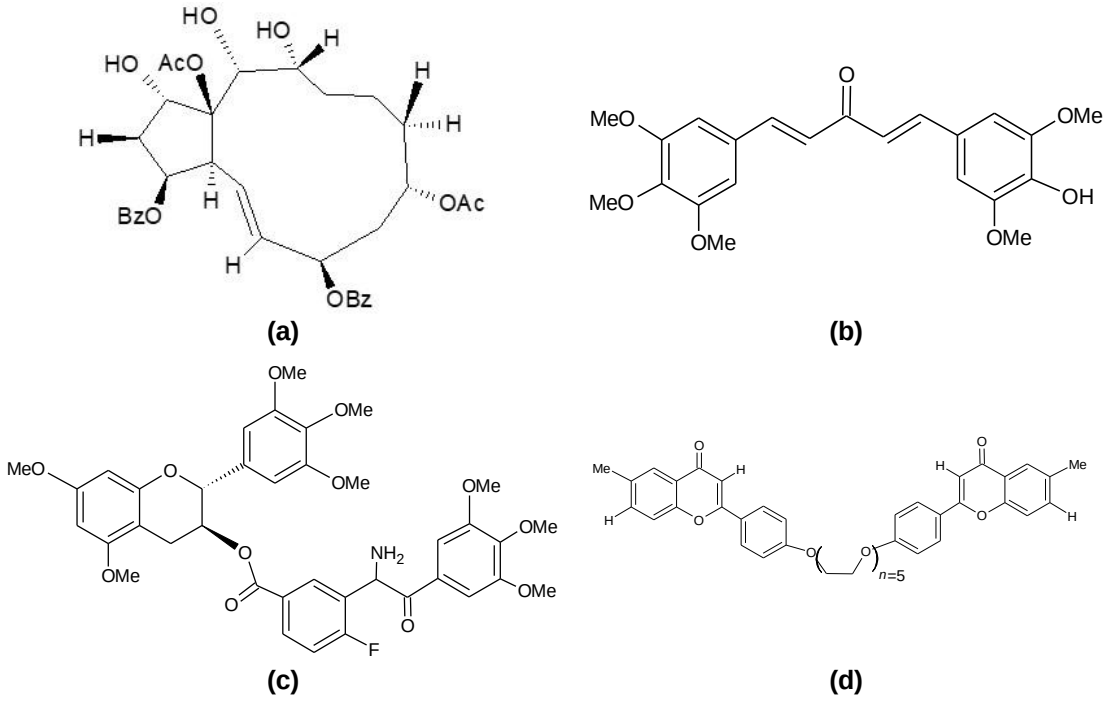


Figure 1—5. Other Potent MDR reversal agents. (a) Compound 26. (1S,2S,3S,4S,7R,9R,13R,14R,15S)-9,15-Fiacetoxy-3,7-dibenzoyloxy-1,13,14-trihydroxyjatropha-5E-ene [62]. (b) GO-Y078. (1E,4E)-1-(4-hydroxy-3,5-dimethoxyphenyl)-5-(3,4,5-trimethoxyphenyl)penta-1,4-dien-3-one [29]. (c) Compound 51. (2R,3S)-5,7-Dimethoxy-2-(3,4,5-trimethoxyphenyl)chroman-3-yl. 3-(3,4,5-trimethoxybenzamido)-4-fluorobenzoate [65]. (d) Compound 4e. 1,16-Bis[40-((6-methyl)-4H-chromen-4-on-2-yl)phenyl]-1,4,7,10,13,16-hexaoxahexadecane [65].

Several coumarin derivatives were reported to be more potent in blocking P-gp mediated rhodamine 123 efflux than verapamil [127]. Exhibiting high cytotoxicity across the sensitive and resistant cell lines studied [127]. However, compounds 1a, 1e, 1f, 1g, and 1h all exhibited collateral sensitivity with more than a two-fold increase in cytotoxicity against the doxorubicin-resistant Lovo/Dox cells in comparison to sensitive cells [127]. Cell cycle analysis revealed that the coumarin derivatives induced significant cell cycle changes [127]. Compound 1b induced significant G0/G1 arrest, 1c caused S-phase arrest, while 1e at lower concentrations caused the G0/G1 arrest and at high concentrations caused G2/M block [127].

Tiamulin, a nontoxic semi-synthetic antibiotic, was capable of reversing MDR against colchine, doxorubicin, and vinblastine [128]. Daunorubicin accumulation was increased after treatment with 2 μM tiamulin by 5.3-, 2.3- and 4.0-fold in P-gp expressing AS30-D/COL5, CEM/VLB3.6, and P388/ADR25 cells, respectively [128]. *In vivo*, overall animal survival was increased by 29% with tiamulin treatment [128]. Reserpine and yohimbine analogues also showed high vinblastine MDR reversal, unfortunately, these analogues also displayed high cytotoxicity [61].

Table 1—2. Effects of the potent synthetic modulators on cellular accumulation and cytotoxicity of substrates of ABC transporters

| Compound | Target | Cellular Accumulation in MDR Cells (Relative fold) | | MDR Reversal in MDR Cells (Relative fold) | | | | |
|---|---|---|---|---|---|---|---|---|
| N3 [109] | P-gp | | | Vinblastine: 440 | | | | |
| Compound 35 [110] | P-gp | Doxorubicin 1 μM: 2.2 | | Paclitaxel: 42.7 | | | | |
| Compound 23 [105] | P-gp | Doxorubicin 1 μM: 2.4 | | Paclitaxel: 48.0 | | | | |
| Compound 12 [112] | P-gp | Doxorubicin 1 μM: 2.6 | | Paclitaxel: 39.8 | | | | |
| 5 Bromo-tetrandrine [113] | P-gp | Doxorubicin 1.5 μM: ~1.2 | | Doxorubicin: 15.6 | Vincristine: 109.4 | Paclitaxel: 78.4 | Docetaxel: 57.8 | Epirubicin: 25.1 |
| W6 [114] | P-gp | Doxorubicin KBv200 1 μM: 4 | Doxorubicin MCF-7/DOX 1 μM: 5.3 | KBv200 Doxorubicin: 27.8 MCF-7/DOX Doxorubicin: 30.3 | KBv200 Vincristine: 29.2 MCF-7/DOX Vincristine: 64.5 | KBv200 Paclitaxel:1049.6 MCF-7/DOX Paclitaxel: 99.3 | | |
| Compound 26 [115] | P-gp | Rhodamine 123 HepG2/ADR 2 μM: 2.74 | | HepG2/ADR 100 nM Doxorubicin: 71 | MCF-7/ADR 200 nM Doxorubicin: 36 | | | |
| GO-Y078 [116] | BCRP | Pheophorbide A 1 μM: >3 | | SN-38: 1.18 | | | | |
| Compound 51 [117] | MRP1, P-gp and BCRP | Doxorubicin 2008/MRP1 1 μM: 2.6 | Doxorubicin HEK293/R2 (BCRP expressing) 1 μM: 10.4 | Paclitaxel: 31.4 | | | | |
| 4e [117] | MRP1 | Doxorubicin 2008/MRP1 1 μM: 8.9 | | | | | | |
| 4e [129] | MRP1 | Doxorubicin 3 μM: 2.1 | | 0.5 μM Doxorubicin: 13.7 | 0.5 μM Etoposide: 10.2 | | | |

Certain flavone derivatives, especially the aurone derivatives, significantly increased paclitaxel accumulation in MDR cells and bound strongly to P-gp [130]. All methoxyflavones tested in the study showed significant inhibition of [$_3$H] vincristine at 0.2 µM [130]. While, quercetagetin, a methoxyflavone, was the most potent [$_3$H] vincristine efflux inhibitor [35]. Hydrocinchonine, cinchonine, and quinidine reversed MDR against paclitaxel and docetaxel in MDR cells by activation of PARP [35]. P-gp specific modulation by hydrocinchonine, cinchonine, and quinidine was also confirmed by increased rhodamine 123 accumulation [131].

Quercetin modulated multiple ABC transporters including P-gp, BCRP and MRP1 [55, 132]. Active quercetin derivatives displayed low toxicity ($IC_{50}$ > 100 µM) while displaying high P-gp modulating activity [132]. Compound 17 (1 µM) increased paclitaxel sensitivity by 11.3-fold [132]. Bivalent quinine inhibitors Q(6′,6′) and Q(6′,4′) inhibited calcein AM efflux [133]. Honokiol, Magnolol and 4-*O*-Methylhonokiol compounds were nontoxic and improved daunorubicin resistance, however, honokiol was the only compound capable of weakly inhibiting calcein-AM efflux [134]. Alpha-tocopherol metabolites and gamma-tocotrienol weakly inhibited rhodamine 123 efflux, while gammaT3 was the only compound to significantly inhibit rhodamine 123 transport [135]. Typically, inhibitors reduce P-gp expression but gammaT3 increased P-gp protein expression while downregulating its transport [135].

ABCG2/BCRP

Ko143, a third generation synthetic inhibitor of BCRP performed poorly *in vivo* [59]. Ko143 displayed highly potent inhibition of BCRP *in vitro* however *in vivo* Ko143 exhibited a short plasma half-life of approximately 1 h and was highly cytotoxic [136]. Natural compounds including flavonoid scaffolds, aurones, marine products, quinazoline and chalcone moieties and protoflavones were all modified to investigate BCRP reversibility [65, 66, 137-140].

Aurones are a family of flavonoids previously shown to reverse MDR towards mitoxantrone in ABCG2-overexpressing cells [138]. Mitoxantrone, pheophorbide A and Hoechst 33342 are fluorescent BCRP substrates which can be detected by flow cytometry, permitting the quantification of BCRP transport activity [66, 138, 139]. Aurone analogues A-2, A-3, I-2, I-3, F-2 and F-3 exhibited considerable cellular accumulation of mitoxantrone, up to levels comparable to fumitremorgin C (FTC), a well-defined BCRP inhibitor [138]. Four methoxylated aurone compounds at 50 nM significantly reduced the $IC_{50}$ of mitoxantrone [138]. Mitoxantrone was combined with 0.5 µM of a series of chalcone (A-2, A-3, I-2, C-2) compounds and the F-2 aurone compound which resulted in complete MDR reversal in resistant cells [138]. Moreover, I-2 sensitised resistant cells towards mitoxantrone to a higher extent than those observed in control

cells [138]. ATPase assays revealed that the potent analogues A-2, A-3, I-2, F-2 were strong ATPase stimulators [138]. However, they do not inhibit cell viability differentially in ABCG2-overexpressing (MDA-MB-231/R) and parental (MDA-MB-231/V) breast cancer cells [138]. Compounds A-2, I-2 and F-2 weakly associated with the [I]IAAP/BCRP binding site, whereas A-3 completely inhibited [I]IAAP photolabeling [138]. These compounds all uniquely bound to and inhibited BCRP. *In vivo* the combination of A-2 and mitoxantrone significantly improved overall survival when compared with mitoxantrone treatment alone [138].

Quinazoline and chalcone compounds both inhibited BCRP at high nanomolar to low micromolar concentrations [139]. By combining the two moieties to generate new synthetic derivatives, Kraege et al. endeavoured to obtain more potent BCRP inhibitors [139]. Compound 35 inhibited pheophorbide A efflux in a BCRP overexpressing cell line with an $IC_{50}$ of 0.19 µM, which was well below cytotoxic levels [139]. Compound 35 also inhibited BCRP, with a 10-fold larger therapeutic ratio than that of Ko143 [139, 141]. Compound 35 revealed no selective difference in toxicity for MDR and sensitive cells, suggesting that compound 35 was not a substrate of BCRP [139]. However, compound 35 still potently reversed SN-38 resistance at 0.01 µM and 0.1 µM [139]. Compound 35 displayed high specificity towards BCRP in comparison to P-gp [139]. Compound 35 potently inhibited BCRP, slightly modulated P-gp, but did not affect MRP1 transport [139]. Most of the quinazoline compounds were highly toxic, with $IC_{50}$ values of less than 10 µM across the sensitive and resistant cell lines [66]. The therapeutic ratio of drugs was dependent upon the toxicity shown in comparison to the intended inhibitory activity [66]. Quinazoline derivatives 21, 54 and 60 exhibited improved therapeutic ratios in comparison to Ko143 even when considering these compounds' high cytotoxicity [66]. The large therapeutic window can mainly be attributed to the potent inhibition of Hoechst 33342 efflux by compounds 21, 54 and 60, with $IC_{50}$ values of 55.6, 44.2 and 47.5 nM, respectively [66]. Compounds 54 and 60 also potently sensitised MDR cells towards SN-38 ($EC_{50}$ values of 12.7 nM and 15.6 nM respectively) and mitoxantrone ($EC_{50}$ values 7.4 nM and 9.7 nM respectively) [66]. ATPase analysis revealed that these potent inhibitors followed a bell-shaped curve [66].

**ABCC1/MRP1**

The nontoxic bivalent apigenin homodimer compound 4e (Figure 1—5, $IC_{50}$>100 µM) potently inhibited MRP1-dependent doxorubicin efflux and completely reversed MDR against both doxorubicin and etoposide at 0.5 µM (Table 1—1) [117, 129]. SAR revealed that removal of OH groups at the C-5 and C-7 positions of the A-ring from apigenin dimers and methyl substitutions at the C-6 or C-7 or fluorine substitution at the C-7 position of the Å ring of the dimer showed the highest increase in MRP1-modulating

activity [129]. The high binding affinity of 4e within the MRP1 substrate/doxorubicin binding site showed that 4e inhibited transport by competitive inhibition [129].

The investigation of BCPCF (2′,7′-bis-(3-carboxy-propyl)-5-(and-6)-carboxyfluorescein) accumulation, an MRP1 specific substrate, resulted in relatively low potencies with $IC_{50}$ values of 13, 16, 16, 7, 5 and 7 μM for Licoisofalvone B, IFG10, IFG12, morin, silybin and indomethacin, respectively [142]. Several nontoxic lignan derivatives displayed even less potency upon BCPCF accumulation, with $IC_{50}$ values ranging from 50 to 125 μM [142]. The naturally occurring compound oleanolic acid which exhibits anticancer properties was synthetically modified creating DIOXOL and HIMOXOL derivatives [143]. DIOXOL and HIMOXOL showed an 8-fold increase in calcein-AM fluorescence in comparison to MK-571, a potent MRP1 inhibitor [143]. DIOXOL and HIMOXOL both inhibited MRP1-mediated transport in MDR cells and demonstrated strong anti-proliferative activities such as DNA fragmentation, increased BAX expression and decreased BCL-2 expression [143].

**Multi-Specific ABC Transporter Inhibitors**

In some cases, researchers have examined how their inhibitors react with multiple ABC transporters, which lets researchers further evaluate the specificity of these compounds across different ABC transporters. This was especially important when considering the broad overlap in inhibition and substrate specificity of ABC transporters [144]. *In vivo*, it was shown that knocking out both BCRP and P-gp increased drug accumulation 43-fold compared with the knockout of BCRP or P-gp alone [145]. As previously mentioned P-gp, BRCP and MRP1 all had some overlap in the substrates and co-localise at the same tissue [146, 147]. A potent multi-specific ABC transporter inhibitor could simultaneously block multiple efflux pathways and potentially increase the efficacy of anti-cancer drugs.

Cyclosporine A is an example of a multi-specific ABC transporter inhibitor in that it can inhibit MRP1, BCRP and P-gp [148]. Cyclosporine A showed an increase in disease-free survival, *in clinic* [148]. PSC-833, a derivative of cyclosporine A only inhibited P-gp, but did not show improved survival [148]. Quercetin derivatives such as compound 17 was not only the most potent P-gp inhibitor but also inhibited BCRP [132]. Quinazoline and chalcone derivative 24 were designed to inhibit BCRP, yet they showed equipotent inhibition against P-gp, with $IC_{50}$ values of 0.6 and 0.48 μM, respectively [139]. Compounds 19 and 27 both inhibited P-gp more potently then BCRP and MRP1 transport inhibition [139]. Methylated epigallocatechin, gallocatechin and dihydromyricetin derivatives inhibited multiple ABC transporters [117]. While compounds 23 and 35 completely reversed P-gp dependent doxorubicin resistance, they also displayed strong MDR reversal towards BCRP [117]. Moreover, derivatives 50 and 51 showed activity against all three ABC transporters MRP1, BCRP and P-gp [117]. High specificity to a

single target is usually a highly regarded characteristic for drug design, however further investigation into multi-specific ABC transport inhibitors could prove essential when multiple ABC transporters are overexpressed [59, 149]. These multi-specific inhibitors may be required to substantially reduce MDR *in clinic* [59, 149].

Furthermore*, in clinic,* high expression of P-gp was only found in a few tumour types such as renal cancer and pheochromocytoma [150, 151]. Many tumour samples exhibited much less expression when compared with resistant cell lines [150, 151]. While some inhibitors (nilotinib) have not shown success when inhibiting P-gp at high concentrations, as in overexpression models, in lower P-gp expressing cells the inhibition of nilotinib becomes useful [152]. The MDR reversal capabilities of nilotinib and imatinib both successfully reversed MDR when the expression of P-gp was at low to moderate levels, however, at higher P-gp expression levels nilotinib MDR reversal required higher concentrations which initiated off target affects [152]. The antiproliferative, anticancer agent ABT-263 and ABT-199 is another compound that is able to reverse MDR but only when BCRP expression is low [153]. This research suggests a potential clinical relevance for using inhibitors with different efficacies depending on the ABC transporter expressed within the tumours. Demonstrating that even non-potent compounds can be highly beneficial.

**Curcumin**

Curcumin is a phytochemical derived from the readily available spice turmeric which has been extensively investigated for its biological activity [154-156]. Observed activities include MDR reversal, antioxidant, anti-inflammatory, and anti-cancer activities [156-158]. However, the oral bioavailability of curcumin is very limited due to poor intestinal absorption, rapid metabolism into curcumin conjugates and a short half-life [159-161]. It was recently shown that the efflux of the predominant curcumin conjugate COG back into the blood was dependent upon the expression of MRP3 [74]. In addition, curcumin has showed broad spectrum inhibition of ABC transporters including P-gp, MRP1, MRP5 and BCRP transport across the relevant overexpressing cell lines [162]. It is still unknown whether curcumin and its metabolites are able to inhibit MRP3 activity [74]. Synthetically modifying well-tolerated natural compounds has the potential to create derivatives with increased specificity, potency, and improved bioavailability [116, 162] Curcumin analogues A12, B11 and C10 had increased potency and in some instances, specificity in comparison to curcumin but only inhibited a single ABC transporter [162]. A12 ($IC_{50}$: 1.2 µM) and B11 ($IC_{50}$: 5.2 µM) were more potent than curcumin ($IC_{50}$: 32 µM) in BCRP modulation [162]. C10 ($IC_{50}$: 2.8 µM) only inhibited P-gp, exhibiting enhanced specificity and potency when compared with curcumin (50.5 µM) [162]. However, A13 showed

multi-specific inhibition of BCRP, MRP1 and MRP5, with a higher potency in comparison to curcumin [162].

Murakami et al. screened 24 nontoxic synthetic curcumin analogues with increased bioavailability to evaluate their efficacy in BCRP modulation [116]. The curcumin analogues GO-Y078 (Figure 1—5), GO-Y0168, GO-Y0172 and GO-Y030 potently inhibited mitoxantrone transport, with $IC_{50}$ values of 0.51, 0.31, 0.25 and 0.37 µM, respectively, while curcumin exhibited an $IC_{50}$ of 0.62 µM [116]. GO-Y030 (1 µM) exhibited complete MDR reversal and GO-Y078 (1 µM) greatly enhanced SN-38 sensitivity in MDR cells [116]. GO-Y078, GO-Y0168, GO-Y0172 and GO-Y030 modulated ATPase activity and [I]IAAP binding at nanomolar concentrations, exhibiting high binding affinity the BCRP binding site [116]. This suggests that GO-Y030 and GO-Y078 competitively inhibited BCRP by competing for the BCRP substrate binding pocket [116]. However, GO-Y0168 and GO-Y0172 also bound strongly and inhibited mitoxantrone transport, yet only GO-Y078 and GO-Y0168 were able to reverse SN-38 resistance [116]. This suggested that curcumoid-mediated SN-38 MDR reversal was not entirely dependent on BCRP binding [116]. *In vivo*, GO-Y078 exhibited a 1.4-fold increase in survival that could be attributed to its increased solubility and bioavailability when compared with curcumin [163]. However, this *in vivo* activity could be attributed to the multi-specificity of these potent P-gp inhibitors which also showed some weak BCRP transporter inhibition [116]. Curcumin is another good example of when synthetic modification successfully improved the bioavailability, potency, and specificity in comparison to the lead bioactive compound [163].

Curcumin derivatives inhibited the widest range of ABC transporters in comparison to other natural derivatives, including P-gp, BCRP, MRP1 and MRP5 [51, 162]. Twenty-three heterocyclic cyclohexanone curcumoids were tested for P-gp, BCRP, MRP1 and MRP5 inhibition [162]. In cellular accumulation assays of transporter specific substrates, compound C10 demonstrated strong and specific P-gp inhibition ($IC_{50}$: 2.8 µM) in resistant cell lines [162]. While A13 inhibited BCRP, MRP1 and MRP5, with $IC_{50}$ values of 4.3, 11.9 and 11.7 µM, respectively [162]. Substrate inhibition translated into an increase in drug sensitivity, with compound C10 causing MDR reversal of paclitaxel resistance [162]. A12 and A13 resulted in MDR reversal of mitoxantrone resistance [162]. 6,7-Dimethoxy-2-phenethyl-1,2,3,4-tetrahydroisoquinoline derivatives 8, 9 and 12 were capable of modulating both calcein-AM and Hoechst 33342 efflux in their respective P-gp and BCRP expressing cell lines [126, 162].

**EF24**

5,5-bis[(2-fluorophenyl)methylene]-4-piperidinone (EF24), is another curcumoid derivative that has displayed promise [164]. EF24 was first synthesised by Adams et al.,

where EF24 demonstrated both the ability to arrest the cell cycle and induce apoptosis [165]. Since then, EF24 has inhibited NF-κβ and BCL2, indirectly enhancing BAX expression and cytochrome C mitochondrial release, stimulating apoptosis in a variety of cancer cells [164, 166, 167]. The additive effects of EF24 were shown in combination with the anticancer drug mitotane in adrenocortical tumour cell lines [168]. EF24 treatment also modulated Wnt/β-Catenin, NF-κβ, MAPK and P13K/AKT protein expression [168]. Furthermore, EF24 has showed inhibition of glucose uptake in ovarian cancer cells limiting the production of both lactate and glycolysis [169]. EF24 glucose modulation may be in response to EF24 inhibition of the glut1 transporter expression in a dose dependent manner [169]. EF24, glut1 inhibition and knockdown (siRNA) both impaired the tumorigenicity of ovarian cancer cells [169]. Curcumin has inhibited several ABC transporters including P-gp, MRP1, MRP5 and BCRP [170]. The ability for MRP3 to transport COG suggests a relationship between curcumin and MRP3, whether curcumin can inhibit MRP3 is unknown. It was of interest to determine whether curcumin and its derivate EF24 could also modulate MRP3 expression.

**Suramin**

Suramin (SUR) was initially synthesised in 1916 to treat trypanosomiasis, a parasitic infection [171]. In 1979, suramin displayed the ability to inhibit reverse transcriptase, a crucial enzyme in AIDs [172]. During experiments involving the treatment of AIDs, suramin demonstrated antitumor activity in AIDs specific cancers [173]. This discovery led to further investigation of suramin in the context of cancer therapy. Further investigation of the biological activity of the role of suramin showed suramin modulated infection, inflammation, proliferation, invasion, drug resistance, metastasis and angiogenesis [4, 174, 175]. Suramin also modulated Wnt signalling, telomere shortening, extracellular matrix breakdown, CD40-CD154 immunosuppression and MRP3 inhibition [73, 171, 174, 176, 177].

Drug induced liver injury (DILI) is a major safety concern that must be assessed during drug development [73]. DILI can be caused by insufficient secretion of bile acids and is one of the major reasons for rejection of transplanted livers [73]. In this model inhibition of MRP3 were screened to test compounds with the potential to cause DILI [73]. The Bayesian model's sensitivity of 64% and specificity of 70% was confirmed by *in vitro* testing [73]. $E_2$17G, a MRP3 dependant substrate was tested in a membrane vesicle model prepared from HEK293, MRP3 overexpressing cells [73]. Fidaxomicin, suramin and dronedarone were identified as the three strongest MRP3-dependent transport inhibitors [73]. Fidaxomicin, suramin and dronedarone were able to inhibit MRP3-dependant transport potently ($IC_{50}$ = 1.83±0.46 µM, 3.33±0.41 µM and 47.44±4.41

μM, respectively) [73]. Whether suramin can inhibit MRP3/ABCC3 in a cell or animal model remained untested.

**In Clinic**

A phase I trial of noncytotoxic concentrations of suramin coupled with either docetaxel or gemcitabine was implemented [178]. The purpose of this phase I trial was to assess the tolerability of the combination therapies and whether the plasma concentrations of suramin could be achieved [178]. Non-small cell lung cancer (NSCLC) was the most common form of lung cancer diagnosed [178]. Suramin was selected in this trial as NSCLC cancers highly express FGF, one of suramin's inhibitory targets [178, 179]. NSCLC patients were injected intravenously with suramin, plus either gemcitabine or docetaxel on days 1, 8 and 21 of each treatment phases [178]. After three phases, patients with partial responses or better continued the trial [178]. Patients with stable disease or worse were changed over to the other combination therapy [178]. The results showed some dose-limiting toxicity in the combination of suramin (10-50 μM) and docetaxel (75 mg/$m_2$), three of the six patients that received this combination exhibited febrile neutropenia [178]. However, no dose-limiting toxicities were seen with the combination of suramin (10-50 μM) and gemcitabine (1250 mg/ $m_2$) or at a lower concentration of docetaxel (56 mg/$m_2$) [178]. This phase I trial successfully proved that plasma concentrations of suramin could be achieved in the desired ranges and that combinations were well tolerated [178]. Furthermore, nine patients exhibited stable disease while two patients presented with a partial response to the treatment [178]. These results suggested that suramin combinations could be capable of antitumor activity and that further investigation was warranted [178].

**Methotrexate**

MTX is a substrate of MRP1, MRP5, BCRP2 and MRP3 [60, 62, 79, 180]. MTX is an antifolate and antimetabolite drug that has been used in the treatment of acute lymphocytic leukaemia, breast cancer, osteosarcoma, primary central nervous system lymphoma, and head and neck cancer [181]. Upon inhibition of carrier-mediated transport of MTX, P-gp also improved MTX accumulation resistance [182]. While, MTX enters cells predominantly via active or carrier mediated transport, it is also possible for MTX to passively diffuse into cells when MTX-carriers are inhibited [182]. MTX anticancer activity is dependent on the MTX metabolites ability to compete with enzymes involved in folate metabolism [181]. Primarily dihydrofolate reductase (DHFR) and to a lesser extent ribonucleotide transformylase (GARFT), 5′-amino-4′-imidazolecarboxamide ribonucleotide transformylase (AICARFT) and thymidylate

synthetase (TYMS) [181]. The competitive inhibition of GARFT and AICARFT by MTX impairs DNA/RNA synthesis by inhibiting purine synthesis and folate bioactivities [181].

**Gemcitabine**

Gemcitabine is a nucleoside analogue and an antimetabolite [178]. Gemcitabine di/triphosphate conformations are key antimetabolites that interfere with DNA synthesis and function [178]. In comparison to 5-FU, gemcitabine demonstrated improved clinical benefit response (5-fold) in pancreatic cancer patients [183]. However, Ciliberto D et al. (2013) stated that the therapeutic effects of gemcitabine were majorly putative and by no means curative [184]. Research responded to this crisis in pancreatic cancer treatment by studying combination treatments of gemcitabine with radiotherapy, resection, fluoropyrimidine-based therapies, platinum-based therapies, Kras-targeted therapies, nab-paclitaxel, EGFR-targeted therapies (erlotinib) and various phytochemical-based modulators [184-187]. Recent evidence showed a link between ABC transporters and gemcitabine [29, 188]. High gemcitabine (20 μM) concentrations over one hour increased the expression of MRP1, MRP3 and MRP5 [29]. MRP5 displayed the highest increase in expression in cells with gemcitabine resistance and subsequently studies have showed gemcitabine resistance was dependent on MRP5 expression [29, 188]. Whether MRP3 expression is able to modulate gemcitabine resistance was unknown.

**Bioinformatic Tools**

Since the inception of the microarray assay, the amount of genetic information available has grown [189]. The tissue microarray is a powerful tool that enables the user to simultaneously study the expression of thousands of genes or RNA products within a given cell or sample [189]. The use of DNA microarray data has been used to investigate the expression differences between cancerous and normal tissue types as well as across cancer types [190]. The advances in the quantification of genetic expression as well as advances in computing technologies has led to the creation of several bioinformatic databases including the Oncomine, KMplot and STRING databases. The oncomine database was created with the aim to collect, normalise, analyse and detect potential cancerous targets using published microarray data [190]. The KMplot platform also utilises microarray data but to plot Kaplan-Meier survival graphs that can be used to evaluate the impacts of low and high expression of a target gene on patient survival rates [191].

The levels of protein and mRNA do not always correlate, in fact it is difficult to predict protein levels based on RNA expression [192]. The STRING database is a platform dedicated to assessing a target's protein-protein interaction networks [193]. Proteins are among the most diverse, information-rich and specific molecules within the

body [193]. The STRING platform utilises protein expression from experimental data, text mining and coexpression analysis to evaluate the relationships between proteins [193]. These databases will be used to assess the RNA and protein expression of ABCC3/MRP3.

**Aims and Hypotheses**

The wealth of research into ABC transporters is vast, however research regarding MRP1, BCRP and P-gp has dominated multidrug resistance research [51]. The expression of MRP3 is emerging as a unique and important transporter in pancreatic cancer [36, 79, 83]. Pancreatic cancer is both highly resistant and aggressive and in need of new treatment avenues [13]. Simply put, if resistance can be reduced or eliminated, previously unsuccessful treatments can be improved. It is hypothesised that improving the understanding and targeting of MRP3 in pancreatic cancer will both improve and strengthen our knowledge of drug resistance mechanisms and restore cytotoxicity of previously ineffective drugs.

The aims for this research were as follows:

- To evaluate whether MRP3 expression was significant in pancreatic cancer and other cancers using ONCOMINE, KMplot and STRING databases.
- To investigate whether gemcitabine or methotrexate resistance in PANC1 cells was dependent on MRP3 expression and function by knocking our ABCC3 using the CRISPR-Cas9 system.
- To investigate whether MRP3 function could be inhibited by the natural compound curcumin and its derivate EF-24. Also, whether that inhibition could restore sensitivity of PANC1 cells to methotrexate or gemcitabine.
- To investigate whether MRP3 function could be inhibited by the synthetic compound suramin. Also, whether that inhibition could restore sensitivity of PANC1 cells to methotrexate or gemcitabine.

# Chapter 2 Methodology

## Bioinformatic Tools

### The ONCOMINE platform

To establish clinical associations between the ABCC3 gene sequence and mRNA expression level variations in cancer patients, retrospective analyses was undertaken using the Oncomine platform. Oncomine analysis is as defined by individual archived datasets which include analyses of differential expression, Cancer Outlier Profile Analysis (COPA), tumour response, recurrence-free survival, progression-free survival and overall survival.

### Differential Expression

Differential expression is the initial analysis type found within the ONCOMINE platform [194]. ONCOMINE is able to compare and differentiate expression between different cancers, cancer subtypes and normal samples [194]. This is an important tool when investigating genetic or pathological targets, especially when using the search function to investigate a target of interest across the vast oncomine database [194]. The threshold for used to search for ABCC3 was as follows: P-value = 0.0001, Fold Change=2 and Gene Rank = Top 10%. Some data outside of these ranges were also included in the analysis.

### Cancer versus Normal

The cancer versus normal analysis allowed the user to investigate whether a target was upregulated or downregulated in cancer in comparison to normal tissue samples [194]. A student's *t-test* was used for testing the significance when comparing two variables such as cancerous and normal expression [194]. The oncomine platform compared expression using a Pearson's correlation test to evaluate the significance of differences between three or more variables such as grade I, grade II and grade III breast cancer [194]. Using the ONCOMINE platform, the evaluation of ABCC3 gene would result in a disease summary graph. The disease summary graph automatically returns results for the differential expression analysis with significant results for both upregulation and downregulation of ABCC3 in comparison to normal tissue.

### Cancer versus Cancer

ONCOMINE uses the student's *t-test* in the cancer versus cancer analysis to assess the significance between cancer types and cancer subtypes [194]. Cancer versus cancer analyses include multi-cancer and histological analysis [194]. Multi-cancer datasets profile a number of cancer types and group their data accordingly [194]. The multi-cancer

datasets contain the expression levels of a variety of genes across several cancer types using the same reporter to permit more direct comparisons (oncomine.org). Multi-cancer datasets allow the cancer versus cancer analysis to compare expression levels across cancers [194]. The histological analysis compares the histologic subtype, grade and stage of the samples across the cancer sub-types [194]. “Misc” or miscellaneous searches allow for the comparison of samples based on other parameters such as treatment response, viral infection status, gene expression and biomarker results (e.g. the p-53 signalling pathway or the WNT signalling pathway) [194]. Both the cancer versus normal and cancer versus cancer analyses will be used to assess ABCC3 expression.

**Coexpression**

The ONCOMINE coexpression analysis aims to identify targets that follow the same expression patterns and that modulate similar biological pathways [194]. When the coexpression analysis is used in combination with the differential expression analysis, the identification of targets that are upregulated in cancer and coexpressed with the target gene can be achieved [194]. The ONCOMINE platform utilises a linked hierarchical clustering system to evaluate how synchronous other genes are with ABCC3 expression [194]. The top three ABCC3 overexpressing datasets had the top three performing coexpression genes extracted from ONCOMINE for further literature review. In accordance with a previous paper the threshold for coexpression correlation was set at 0.7, anything above this would be recognised as a gene that highly correlates with ABCC3 [195]. Genes that displayed coexpression were then be assessed by literature review to improve and strengthen the evidence of functional overlap. The WNT signalling pathway, sphingosine-1-phosphate pathway and p53-signalling pathway have shown association with ABCC3 expression [36, 196, 197]. Coexpression of targets with ABCC3 was firstly assessed with previously associated targets found in literature, followed by comparisons in cancer versus normal analysis.

The amount of data generated by these co-expression searches was vast and highly variable. To specifically analyse ABCC3 coexpression, a ranking system was used to find the top three overexpressing ABCC3 cancer types based on ONCOMINE’s differential expression and outlier analyses. The top three performing cancer types were taken from each of the differential analysis types cancer versus normal, cancer versus cancer (histology) and cancer versus cancer (multi-cancer). These were ranked from first to fourth and assigned a relative score based on their position from 4 for first position to 1 for fourth position. The positional scores were totalled, and the top three cancer types were revealed. These top three cancers were selected for coexpression analysis and further literature review.

### Outlier Analysis

COPA analysis allows for the user to distinguish overexpressing subsets within tumour types [194]. The heterogeneity seen in cancer is one of the major reasons that treatment fails [194, 198]. The COPA score calculates a median absolute deviation (MAD) which once calculated is normalised to a scale from 0-1 by dividing each sample expression by its MAD [194]. The use of median and MAD prevent the influence of outliers as well as limiting the influence of distribution estimates on calculations [194].The higher the COPA score the greater the evidence for consistent outlying expression seen in a cancer subset and the greater the difference in expression between the subsets of that gene. The $75_{th}$, $90_{th}$ and $95_{th}$ percentiles of the transformed data for each gene was calculated against the cancer datasets and then ranked by COPA scores [194]. The COPA scores were used to evaluate whether any ABCC3 expression heterogeneity occurred across the cancer samples. The ONCOMINE platform, includes the term 'gene rank' which represents how the gene of interest (ABCC3) ranks in comparison to other genes within that analysis type either in significance, COPA or overexpression scores.

### The Kaplan-Meier (Km) Plotter

The Kmplot database plots Kaplan-Meier plots based on the gene of interest and compares the overall survival of patients based on low and high mRNA expression of that target. The cancer types that were included were samples from bladder carcinoma (n = 405), breast cancer (n = 1090), cervical squamous cell carcinoma (SCC) (n = 304), oesophageal adenocarcinoma (n = 80), oesophageal SCC (n = 81), head-neck SCC (n = 500), kidney renal clear cell carcinoma (n = 530), kidney renal papillary cell carcinoma (n = 288), liver hepatocellular carcinoma (n = 371), lung adenocarcinoma (n = 513), lung SCC (n = 501), ovarian cancer (n = 374), pancreatic ductal adenocarcinoma (n = 177), pheochromocytoma and paraganglioma (n = 178), rectum adenocarcinoma (n = 165), sarcoma (n = 259), stomach adenocarcinoma (n = 375), testicular Germ Cell (n = 134), thymoma (n = 119), thyroid carcinoma (n = 502) and uterine corpus endometrial carcinoma (n = 543). In accordance with a previous paper and both the P-value and hazard ratio (HR) with 95% confidence intervals will be calculated by the KM plotter for ABCC3 [199]. Due to the sizes of datasets and possible compounding type I errors the false discovery rate (FDR) was also calculated to estimate the potential for false positives [200]. An FDR of 5% (0.05) indicates that 5% of the positive and significant results are actually negative results, which conversely means 95% of the positive results reflect actual positive results [200].

**STRING Platform (Protein-protein interactions)**

The aim of the STRING database is to collect, analyse and predict protein-protein interactions across a wide range of targets and organisms [193]. This platform aims to assemble all known protein-protein interactions based on word association algorithms, direct physical bonding and indirect functional relationships [193]. The STRING platform analyses data across a wide range of organisms using coexpression analysis, selective shared expression, text-mining software and computational prediction software [193]. The evidence used to assess interactions are divided into seven channels [193]. These include the experimental, database, text mining, and coexpression channels [193]. As well as the neighbourhood, fusion and co-occurrence channels which are also included in the STRING platform analysis but are considered more relevant to Bacteria/Archaea based studies and therefore will not be used for this research [193]. The experimental channel utilises previous findings from laboratory experiments that showed evidence of interactions [193]. While the database channel compares information from pathway databases to gather evidence for any possible interactions [193]. The text mining channel utilises software which scans a wide range of publications including but not limited to all PubMed abstracts for targets that consistently appear in text together [193]. Using the STRING database, current MRP3 protein-protein interactions will be analysed. It will be of interest whether these results overlap with mRNA/microarray database searches. ABCC3 will be used as the input protein, confidence threshold will be set at high (0.7) with no more than 50 interactions shown. Network edges are based on the strength and type of evidence available for each interaction. Across all experiments P-values: $<0.05$ will be considered significant and P-values: $<0.01$ will be considered very significant (Table 2—4).

**Cell Culture**

PANC1 cell line (ATCC), three PANC1 CRISPR ABCC3 knockout cells, MIAPACA2, HepG2 and A549 cells were used in this research project. All cells were grown and passaged in complete RMPI media (Thermofisher, NZ), unless otherwise stated during specific procedures. RMPI media was completed by supplementing RPMI with 10% FBS (Medica Pacifica, NZ), 100 units/ml penicillin (Life technologies, NZ), 100 µg/mL streptomycin Life technologies, NZ) and 2 mM of L-glutamine (Life technologies, NZ) [201]. Cells were grown and maintained in an incubator at 37°C, 95% humidity and 5% $CO_2$. The cell line integrity was confirmed by regular DNA profiling (DNA Diagnostics, Auckland NZ) [201]. Where needed, cells were harvested using TrypLE (Thermofisher, NZ) and incubated at 37°C in 5% $CO_2$ for 5 minutes, to achieve efficient cellular detachment from the surface of the flask. Cells were then stained by mixing trypan blue (Life Technologies, NZ) (80 µl) and cell suspension (20 µl) for 1 min at room temperature.

10 µl of the stained cells were placed in a haemocytometer and counted. The appropriate number of cells were counted and used for various experiments, plating, passaging and freezing.

**Flow Cytometry**

In 1954, Wallace Coulter designed the first basic flow analyser it was able to count and measure the size of a single cell flowing within a liquid, this liquid stream was focused to pass a specific measuring point [202]. In 1965, Kamentsky et al., described a flow cytometer that was able to measure absorption and back-scattered light of non-stained cells [203]. The absorption and back-scattered light measurements were used to infer the size and the amount of cellular nucleic acids [203]. The same year the first cell sorting device and use of electrostation ink-jet recording allowed the sorting of cells (1000cells/s) [204, 205]. Following these developments, in 1967, the electrostatic charging of droplets, further improved cell sorters and the development of cell extraction techniques led to the purification of human granulocytes and lymphocytes [202]. Cell sorting, preparation and separation allowed for more in-depth cellular investigation. The first clinical cytometer was implemented in 1983, further advances in technology and processing power led to the routine use to FLOW cytometry [202]. The creation of benchtop devices, the ability to measure five different parameters on 25,000 cells/s (1995), followed by the implementation of lasers and the use of fluorescent markers (1999) meant that the analytical power of flow cytometers exploded [206]. In 2003, the advances in digital technology allowed for the use of digitally based high-speed cell sorting [202]. The more that advances in computers, lasers, fluorophores, antibodies and optics improved the more prestigious flow cytometry became [207]. The most recent development in the field was the combination of flow cytometry and mass spectrometry [207]. The mass cytometer utilises stable element isotopes conjugated antibodies which enables the user to make at least 40 simultaneous measurements at one time [207]. Mass cytometry is limited by reduced sensitivity and throughput but displayed higher resolution and more comparisons when compared to flow cytometry [207]. The first commercially available mass cytometer was the Cytometry by Time-Of-Flight (CyTOF) which utilises probes that are able to bind to unique heavy-metal isotopes that allow specificity and limits signal overlap, a common limitation seen with antibodies [208]. Mass cytometry while not widely used may be the future of this field [207].

Flow cytometry can measure a variety of cellular features including cell size, cellular complexity/granularity, fluorescent features, intracellular/membrane proteins and nucleic acid levels [207, 209]. Thousands of cells per second can be analysed using the flow cytometry technique [207]. The flow cytometer design can be organised into fluidics, optics, detectors and analysers [207, 209]. The fluidics are responsible for directing

particles and or cells within a liquid to a precise location that can intersect a laser or light source [207, 209]. The sheath fluid and pressurised lines are the two main components of the fluidic system [209]. The sheath fluid is the liquid (most commonly PBS) that is forced through the flow chamber in between the pressurised lines [209]. The pressurised lines force the sample liquid stream through the flow chamber, while coaxial flow ensures that the sample stream becomes a central part of the sheath stream [209, 210]. The sample pressure is more than the sheath fluid, which focuses the sample stream into a stream of single cells [209, 210]. This is an essential requirement for accurate intersection of the fluid stream with the laser beam [209, 210]. The injection rate is the speed at which the sample passes through the flow cytometer and through the laser beam [209, 210]. The higher the injection rate the more events per second (EPS) can be analysed but the lower the resolution for each cell [209, 210]. Slower injection rates are needed for more resolution and detail and is sometimes needed in more complex models [209, 210]. To ensure accuracy the stream must not be compromised anything other than detection of the sample stream, including unwanted particles or bubbles could produce false readings [209].

The optics system can be divided into the excitation optics and collection optics which uses lasers and lenses to excite, collect and transmit various wavelengths by different reflection angles to detectors [207, 209]. The light produced by the lasers reflects off cells in ways that can be recorded by the FLOW cytometer, these include light scattered in the forward scatter (FSC) direction and side scatter (SSC) direction [207, 209]. Lasers can be used to excite fluorescent dyes and antibody conjugates (e.g. FITC) at specific wavelengths which can be used to further investigate specific cellular processes [207, 209]. Fluorescence based flow cytometry is limited by whether antibodies for your desired outcome actually exist and their specificity [207]. The FSC is light that is scattered along the same axis as the laser beam which means the FSC is used to detect differences in the sizes of the cells or particles used in the sample [209]. The SSC light is light that has been deflected to such a degree that it can be collected at approximately 90 degrees from the axis of the laser beam [207, 209]. The SSC results reflect the granularity and complexity of the cells or particles within the sample, the SSC includes the light detected from fluorescent signals [207, 209]. These light signals created by both the FSC and the SSC are collected using a series of lenses which gather, separate and focus specific wavelengths of light to the specific light detectors [207, 209]. Filters such as the long pass, short pass and band pass filters can be placed in the path of the light collected [209]. Long pass filters allow longer wavelengths of light to pass through the filter while short pass filters only allow shorter wavelengths of light to pass [209]. Band pass filters are a combination of short and long and can select which specific wavelengths should be captured [209]. These filters are used to sort the wavelengths

collected and ultimately detected which can increase the specificity of results [209]. Following the detection of the light signal the signals are digitised using amplifiers, processed and analysed using specifically designed computer programs [207, 209].

Through electrostatic cell sorting it is possible to collect and segregate cells based on set parameters [209]. It is now possible to sort cells based one or many parameters, resulting into specific populations of sorted cells that can used for further experimentation [209]. During electrostatic sorting, samples (cells/particles) are passed through lasers and depending on the predefined parameters become positively/negatively charged using a charging electrode [209]. The charged particles or cells can then be deflected into their respective containers using the charged plates [209].

**Current Uses for Flow Cytometry**

The current uses for flow cytometry are broad, including the identification of lymphoma and leukaemia in blood samples, detection of aneuploidy, patient prognoses and prediction of clinical outcomes [207]. Within the laboratory we used flow cytometry to quantify cell death signalling, cellular accumulation of drugs, cytokine detection, cell surface staining and intracellular protein expressionfc. DNA analysis of haematological malignancies such as leukaemia and lymphoma including minimal residual disease (MRD) and applications for *in vivo* analysis of cells within blood or lymph could be investigated using flow cytometry [207]. Fluorescent dyes stain specific areas or chemical structures, in this case DAPI can be used to stain and quantify DNA [207]. Aneuploidy describes cells that contain an abnormal number of chromosomes, flow cytometry can detect the differences in DNA amounts [207]. Aneuploidy is associated with a poor patient prognosis in many cancers, but could also indicate a favourable prognosis in rhabdomyosarcoma, neuroblastoma and acute lymphoblastic leukaemia (ALL) in children [207].

Flow cytometry can be used to detect and diagnose leukaemia and lymphoma carcinoma based on a set of morphological characteristics and cancerous markers [207]. The cancers that circulate within the blood and bone marrow are prime candidates for flow cytometry analysis [211]. For instance, the differences in the fluorescent detection of CD45 and SSC gating can be used to effectively detect blast cells and distinguish between mature lymphocytes, monocytes, maturing granulocytes, myeloid blasts, and lymphoid blasts [211]. A number of other markers can be used to detect these cancers, which in some cases can be detected simultaneously [207]. The clinical outcome can also be predicted based on the detection and classification of the cell type, facilitating the design of patient tailored treatment [207].

Flow cytometry has improved chemotherapeutic treatment in leukaemia and lymphoma cancers [207]. Non-Hodgkin lymphoma and plasma cells abundantly express CD20 which can be specifically targeted by rituximab [207]. Response to rituximab was directly dependent upon the cell surface expression of CD20 which is quantified using flow cytometry [207]. The past ten years have seen an expansion in the targeted therapies available for leukaemia patients [212]. In acute myeloid leukaemia (AML), 30% of patients exhibited *FLT3*-mutated AML [212]. The detection of the *FLT3* receptor CD135 in flow cytometry was successfully demonstrated [213]. The combination of midostaurin a tyrosine kinase inhibitor and chemotherapeutics improved the overall survival in *FLT3-mutated* AML patients [212].The experimentation and discovery of drugs that can target these specific populations is ongoing [212]. Midostaurin, could be replaced by the more specific and potent inhibitors of *FLT3* such as Quizartinib and Crenolanib [212]. However, the earlier detection of CD135 much like CD20 by flow cytometry may also improve the overall survival in *FLT3-mutated* AML patients. Flow cytometry has been commonly used to detect the presence of MRD in treated leukaemia and lymphoma carcinoma patients [207, 214]. MRD is a more accurate estimate of patient response to treatment than just morphological remission (>5%) [207, 214]. Highlighting the use of flow cytometry in predicting and assessing the success of a treatment via MRD assays [214]. Woo et al., highlighted that flow cytometry is becoming a more developed concept in, *in vivo* studies [207]. *In vivo,* flow cytometry permits the imaging of individual cells within blood or lymph of patients [207]. The idea was to detect cancerous cells within the vasculature of the animal/patient while limiting both alterations in normal cell biology and sensitivity seen in *ex vivo* techniques [207]. While the standardisation of techniques *in clinic* are still ongoing, the use of *in vivo* flow cytometry could impact many other diseases and scientific fields [207].

Epigallocatechin-3-gallate (EGCG) a component of green tea was investigated for its anticancer activity in oesophageal squamous cell carcinoma [215]. Flow cytometry was used to investigate the effects of EGCG alone and in combination with doxorubicin on cellular apoptosis, BCL-2, BAX, mitochondrial membrane potential and caspase protein levels in Eca109 and Ec9706 cancer cells [215]. The results showed that EGCG was able to cause apoptosis (100 µg – 300 µg), raise caspase-3 and BAX expression and limit the expression of BCL-2 [215]. Furthermore, the combination of EGCG (5 µg / 25 µg) and ADM (0.2 µg/ml) significantly improved the induction of apoptosis (P value: < 0.01) [215].

Flow cytometry is also commonly used for the quantification of several biological activities. These include quantifying cell death signalling, drug accumulation studies, cytokine detection, cell surface staining and intracellular protein expression [209, 216]. For instance, flow cytometry was used to quantify the intracellular and surface

expression of OATP1B1 and P-gp transporters in Caco-2, HEK293/OATP1B1 overexpressing and hepatocyte cells [216]. Hogg et al., compared the expression levels of these two transporters across mass spectrometry and flow cytometry [216]. Flow cytometry revealed that P-gp expression found on the surface of Caco-2 cells was only a fraction of the total expression of P-gp [216]. Suggesting a higher proportion of intracellular P-gp than previously thought [216]. While mass spectrometry did reveal higher expression levels and specificity, which was especially profound in OATP1B1 (~10-fold) expression [216]. The usability, speed and ease of the flow cytometry process as well as the ability to observe the major differences in transporter patterns made flow cytometry a favourable process to use for investigations of protein expression and distribution [216].

The uptake and cellular accumulation of transporter substrates is essential to better understand drug disposition, function and efficacy [217]. Flow cytometry was used to investigate the intracellular accumulation of drugs within HL60 leukemic cells [217]. The results showed that the prolonged incubation with drugs induced and sustained ABC expression, preventing the accumulation of doxorubicin [217]. Phorbol-12-myristate-13-acetate (PMA) is known to promote endocytosis, PMA reversed the P-gp dependent inhibition of doxorubicin cellular accumulation, while verapamil a known P-gp inhibitor did not [217]. Therefore, not only could P-gp be causing resistance by increasing efflux of anticancer drugs but that the endocytosis of drugs could also be a limiting factor in this model [217]. 5-chloromethylfluorescein diacetate (CMFDA) is a nonfluorescent lipophilic compound able to passively enter a cell, upon intracellular localisation cytosolic esterases cleave CMFDA acetate residues forming the 5-chloromethylfluorescein (CMF) products [218, 219]. The CMF product is fluorescent and membrane-impermeable, further modifications with glutathione continues to form fluorescent conjugates [218, 219]. The activity of MRP1, MRP2 and MRP3 when present are able to actively transport the CMF-glutathione conjugates out of the cell [218]. Therefore, CMF accumulation has be used to quantify the functional transport activity of these ABC transporters [218, 219]. Weiss et al., used this method to show the inhibitory potential of nucleoside, nucleotide, and non-nucleoside reverse transcriptase inhibitors on MRP1, MRP2 and MRP3 [218]. This method will also be used to investigate MRP3 modulation.

**Limitations**

Flow cytometry does have some limitations that must be considered. Firstly, the variety of uses for flow cytometry detection is limited by the number of antibodies available [216]. Not only must antibodies for the protein of interest be available, they need to target both internal and external epitopes depending on the target or distribution of interest [216]. Antibodies can also be limited by autofluorescence and background signals which make

observation of small changes in expression levels difficult [216]. When comparing flow cytometry to mass spectrometry the whole epitope is required for correct binding of antibodies which is not always possible within the cellular environment [216]. However, mass spectrometry can detect the presence of even fragments or partially degraded sections of the protein of interest [216]. The ability for flow cytometry to image tissue is not currently possible, flow cytometry can only analyse one cell at a time [207]. While the use of disassociating enzymes does allow for single-celled populations, the more laboratory manipulations done to a sample the more disruption of the normal cellular environment [207]. The vast applications require a sound foundation, grounded in a good knowledge of the background of the flow cytometry technology. These limitations can be reduced by careful experimental design, antibody selection and target selection. The usability, speed and range of applications make flow cytometry an essential tool for investigating the protein expression [216].

**Surface Staining**

The plasma membrane localisation of MRP3 has been documented in past publications [220, 221]. The detection of MRP3 protein expression was done by surface staining. Surface staining uses FLOW cytometry to detect the specifically selected antibodies' fluorescent signals from fluorescently conjugated antibodies. Cells were trypsinized and counted using a haemocytometer (as stated above) and $1.0x10_6$ cells were aliquoted into 1.5ml tubes and centrifuged at 350 x *g* for five minutes at 4°C. The supernatant was discarded, and cells were washed once in 1ml PBS-T (PBS + 0.2% Tween 20 (Thermofisher NZ)) in the centrifuge at 300 x *g* for 5 minutes at 4°C. Cells ($1.0x10_6$ cells) were fixed in tubes containing 100 µl of 1% paraformaldehyde for 15 minutes on ice, followed by two washes (PBS-T). Each wash was done in 150 µl of PBS-T (PBS + 20% tween 20) followed by centrifugation at 300 x *g* for 5 minutes at either 4°C or room temperature. Cell permeabilization was achieved by incubation of the cells in 100 µl of 0.2% saponin (in PBS) for 30 minutes at room temperature, followed by another two washes (room temperature). Blocking of non-specific antigen sites was achieved by incubating cells with 5% bovine albumin serum in PBS for 15 minutes. Cells were incubated in the dark, in 100 µl of either of anti-MRP3 (abcam, M3II-21, 2.5 µg/ml in 2% BSA in PBS) or IgG isotype control (Thermofisher, IgG2a, 2.5 µg/ml in 2% in BSA/PBS) for 60 minutes at room temperature. Following two washes (room temperature), cells were incubated in 100 µl of the Alexa Fluor® 488-labeled secondary antibody (1:1000 in 2% BSA/PBS) in the dark at room temperature for 60 minutes. Cells were then washed once at room temperature followed by a final centrifugation step at 350 x *g* for five minutes at room temperature and resuspension of cells in 200 µl of PBS at 4°C. Samples

were stored on ice and MRP3 surface staining was detected by flow cytometry immediately.

- Materials Used
    - PBS (Life Technologies, NZ)
    - Antibodies (primary: MRP3 antibody (abcam, M3II-21) secondary: Anti-Mouse IgG H&L (FITC) (abcam, ab6785), control: Mouse IgG2b kappa Isotype Control, Alexa Fluor 488 (Life Technologies, NZ, 53-4732-80)
    - Saponin – Sigma (Cat. No – BCBV8000)
    - MoFlow™ XDP flow cytometer (Beckman Coulter)
    - RPMI (phenol red free)
    - TrypLE Express (Life technologies, NZ)
    - Sheath fluid
    - Flow-Check™ Beads (Beckman Coulter) TrypLE Express (Life Technologies, NZ)
    - PBS (Life Technologies, NZ)
    - CMFDA (Life Technologies, C2925)
    - Software used: GraphPad prism 8, Summit 5.4 and Kaluza (Beckman Coulter)

**Drug Study**

In short, cells were grown in 75$cm_2$ flasks to an 80-90% confluence, trypsinized and counted (as above). Cells (0.5-1×$10_6$cells/ml) were then, centrifuged at 250 x *g* for 5 minutes and resuspended in phenol red free RPMI media supplemented with 10% FBS . The cell suspension was first incubated at 37°C for 10 minutes followed by the addition of CMFDA and the potential inhibitors EF24 (2.5,1.25 and 0.625 µM), suramin (20, 10 and 5 µM), benzbromarone (20 µM) or curcumin (20 µM). The accumulation study was initiated by spiking CMFDA (final concentration of 0.1% DMSO in RPMI phenol red free media) or BCECF (0.25 µM). After incubation for five minutes, cells were then washed in PBS (3ml, 4°C), centrifuged at 250 x *g* for 5 minutes, resuspended in PBS (4°C) and stored on ice. Measurement of CMF/BCECF fluorescence signal by flow cytometry immediately followed.

**MTT Assay**

Prior to 1983, the standard methods for analysing changes in cell death/proliferation involved laboriously counting cells with or without a specific dye or measuring the amount of 5aCr-labeled protein after lysis of cells or by measuring the accumulation of

radioactive nucleotide levels during cell proliferation [222]. The ability to quickly and efficiently measure cell viability across large samples was needed [222]. In 1983, Mossman et al., discovered a new assay now known as the MTT assay [222]. The ideal design for a viability assay would be void of washes, utilise the ELISA platform and contain a compound that was colourless but that would be modified within a living cell to become a new and distinguishable colour [222]. The tetrazolium salt 3-(4,5-dimethylthiazol-2-yl)-2,5-diphenyl tetrazolium bromide (MTT) is modified by reactions within the mitochondria to form a rapid colour change [222]. MTT is now regularly used to measure the amount of live cells contained within the sample, allowing the measurement of proliferation or cytotoxicity depending on the experimental model [222]. The initial yellow MTT substrate produces a dark blue formazan product in the presence of live cells [222].

As previously mentioned ECGC was investigated for its ability to modulate the anticancer drug ADM in oesophageal carcinoma [215]. The MTT assay displayed that ECGC was able to reduce cell viability in a time-dependant and concentration-dependant manner [215]. The MTT assay was used to assess $IC_{50}$ calculations of sorafenib in resistant PLC/PRF5 (R1 and R2) and wild type PLC/PRF5 cells [84]. The resistant cell lines showed significantly (P-value <0.01) higher $IC_{50}$ values than the wildtype cell line [84]. MTT results demonstrated that ABCC3 silencing by siRNA caused decreased cell viability and increased sorafenib cytotoxicity [84].

When considering the use of MTT as a cell viability/cytotoxicity assay it is important to consider the limitations. The MTT assay is limited by its insolubility in water and requires the organic solvent such as dimethyl sulfoxide (DMSO) or isopropanol in order to dissolve the MTT crystals [223]. The quality of DMSO used can affect the quality of MTT results [224]. In some instances, MTT assay has produced erroneous cell viability estimations [225, 226]. Many variations in methods during the MTT experiment can influence results including DMSO quality, presence of culture medium, and the exposure time of formazan to the air [224]. Morphological changes such as changes in size or cell contact may influence ability of cells to produce formazan products [224]. Notwithstanding, the variations between experiments are acceptable and with appropriate controls, MTT can produce reliable cell viability ($IC_{50}$) estimates [224].

**MTT methodology**

MTT was carried out in accordance with Myint et al [201]. Firstly, an MTT stock (5 mg/ml PBS or 12mM in PBS) was prepared and stored at 4°C protected from light. Cells (PANC1/A549) were then passaged and seeded into a 96 well plate with 8,000 cells per well. Immediately following 24 hours of cell incubation, media was removed, and cells were incubated with the chosen treatment arranged in a specific layout (Figure 2—1).

The MTT assay was used to investigate the cytotoxicity of suramin (abcam, ab120422), curcumin (sigma, C7727-500MG), EF24, benzbromarone, methotrexate and gemcitabine (abcam, ab145657). The cytotoxicity of each compound ($IC_{50}$) was investigated by observing the impact of a variety of concentrations (100 µM, 50 µM, 25 µM, 12.25 µM, 6.75 µM, 3.13 µM, 1.56 µM, 0.78 µM) on cell viability.

Figure 2—1. MTT Assay layout

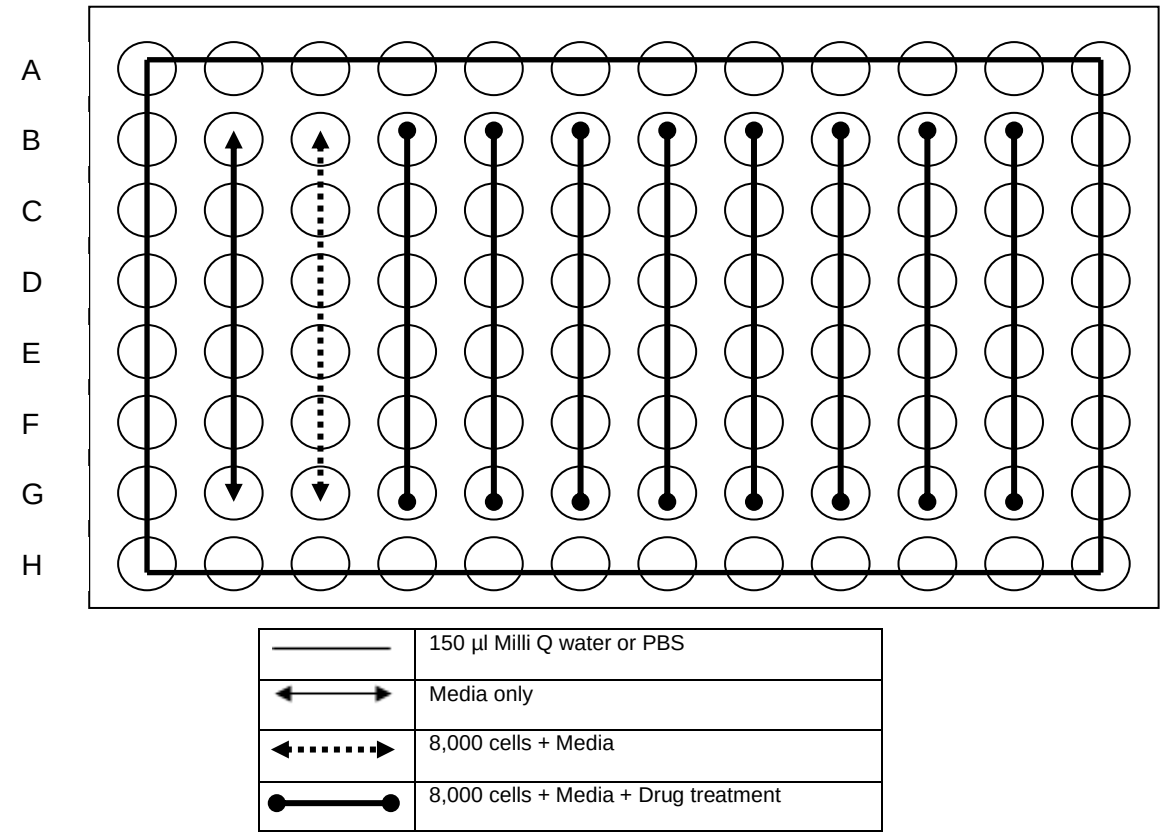


Once the treatments were completed and media/drugs were removed, MTT substrate was added (10 µl MTT in 100 µl RPMI non-supplemented) to each well. Followed by 3-4-hour incubation under normal cell culture parameters (37°C, 95% humidity and 5% $CO_2$). Most of the media was then removed leaving 25 µl in each well, which was combined with100 µl of DMSO, followed by mixing on an orbital shaker (10 minutes at RT). A further 10-minute incubation (at 37°C, 95% humidity and 5% $CO_2$) was followed by orbital shaker mixing (1 minute) and the absorbance of the formazan product was read at both 540 nm and 680 nm.

Table 2—1. Single agent MTT assays.

| Drug | Concentrations Tested |
|---|---|
| Suramin, Curcumin, Benzbromarone, Methotrexate, Gemcitabine | 100 µM, 50 µM, 25 µM, 12.25 µM, 6.75 µM, 3.125 µM, 1.5625 µM, 0.78125 µM |
| EF24 | 20 µM, 10 µM, 5 µM, 2.5 µM, 1.25 µM, 0.625 µM, 0.3125 µM, 0.15625 µM |

- Materials Used
    - 96-well plate
    - RPMI (Life Technologies, NZ) complete media
    - RPMI non-supplemented media (Life Technologies, NZ)
    - TrypLE Express (Life Technologies, NZ)
    - PBS (Life Technologies, NZ)
    - Suramin (Abcam, ab120422)
    - Benzbromarone (Abcam, 3562-84-3)
    - EF24 (Sigma, E8409)
    - Curcumin (Sigma, C7727-500MG)
    - Gemcitabine (Abcam, ab145657)
    - MTT reagent (Sigma, M5655)
    - Plate reader: Thermo Scientific™ Plate reader (Multiskan™ FC Microplate Photometer)
    - Dimethyl sulfoxide (DMSO) (Thermofisher, NZ)

**Combinatorial Treatment**

Following $IC_{50}$ calculations, the ability of the compounds to modulate the cytotoxicity of gemcitabine and methotrexate was then assessed across wild-type and ABCC3 knockout PANC1 cells. The simultaneous assay, incubated PANC1 and MIAPACA2 cells with suramin (100 µM, 50 µM, 25 µM, 12.5 µM, 6.25 µM and 3.125 µM) or EF24 (20 µM, 10 µM, 5 µM, 2.5 µM, 1.25 µM and 0.625 µM), in the presence of gemcitabine (100 µM, 50 µM, 25 µM, 12.5 µM, 6.25 µM and 3.125 µM) or methotrexate (100 µM, 50 µM, 25 µM, 12.5 µM, 6.25 µM and 3.125 µM) for 72 hours (Table 2—2). Followed by MTT detection (as above). The impact of the different concentrations on the number of live cells that remain would relate to which compounds and concentrations if any were able to significantly modulate gemcitabine or methotrexate cytotoxicity.

Table 2—2. MTT Simultaneous/Sequential Coincubation Treatment Layout (96-well plate)

| | | SUR or EF24 | SUR or CUC or EF24 | SUR or EF24 | SUR or EF24 | SUR or EF24 | SUR or EF24 |
|---|---|---|---|---|---|---|---|
| | Conc (µM) | 100 µM (SUR) or 20 µM (EF24) | 50 µM (SUR) or 10 µM (EF24) | 25 µM (SUR) or 5 µM (EF24) | 12.5 µM (SUR) or 2.5 µM (EF24) | 6.25 µM (SUR) or 1.25 µM (EF24) | 3.125 µM (SUR) or 0.625 µM (EF24) |
| **GEM or MTX** | **100 µM** | **100 µM** + 100 µM (SUR) or 20 µM (EF24) | **100 µM** + 50 µM (SUR) or | **100 µM** + 25 µM (SUR) or 5 µM (EF24) | **100 µM** + 12.5 µM (SUR) or 2.5 µM (EF24) | **100 µM** + 6.25 µM (SUR) or 1.25 µM (EF24) | **100 µM** + 3.125 µM (SUR) or 0.625 µM (EF24) |

| | | | | | | | |
|---|---|---|---|---|---|---|---|
| | | | 10 µM (EF24) | | | | |
| **GEM or MTX** | **50 µM** | **50 µM** + 100 µM (SUR) or 20 µM (EF24) | **50 µM** + 50 µM (SUR) or 10 µM (EF24) | **50 µM** + 25 µM (SUR) or 5 µM (EF24) | **50 µM** + 12.5 µM (SUR) or 2.5 µM (EF24) | **50 µM** + 6.25 µM (SUR) or 1.25 µM (EF24) | **50 µM** + 3.125 µM (SUR) or 0.625 µM (EF24) |
| **GEM or MTX** | **25 µM** | **25 µM** + 100 µM (SUR) or 20 µM (EF24) | **25 µM** + 50 µM (SUR) or 10 µM (EF24) | **25 µM** + 25 µM (SUR) or 5 µM (EF24) | **25 µM** + 12.5 µM (SUR) or 2.5 µM (EF24) | **25 µM** + 6.25 µM (SUR) or 1.25 µM (EF24) | **25 µM** + 3.125 µM (SUR) or 0.625 µM (EF24) |
| **GEM or MTX** | **12.5 µM** | **12.5 µM** + 100 µM (SUR) or 20 µM (EF24) | 12.5 µM + 50 µM (SUR) or 10 µM (EF24) | 12.5 µM + 25 µM (SUR) or 5 µM (EF24) | **12.5 µM** + 12.5 µM (SUR) or 2.5 µM (EF24) | **12.5 µM** + 6.25 µM (SUR) or 1.25 µM (EF24) | **12.5 µM** + 3.125 µM (SUR) or 0.625 µM (EF24) |
| **GEM or MTX** | **6.25 µM** | **6.25 µM** + 100 µM (SUR) or 20 µM (EF24) | 6.25 µM + 50 µM (SUR) or 10 µM (EF24) | 6.25 µM + 25 µM (SUR) or 5 µM (EF24) | **6.25 µM** + 12.5 µM (SUR) or 2.5 µM (EF24) | **6.25 µM** + 6.25 µM (SUR) or 1.25 µM (EF24) | **6.25 µM** + 3.125 µM (SUR) or 0.625 µM (EF24) |
| **GEM or MTX** | **3.125 µM** | 3.125 µM + 100 µM (SUR) or 20 µM (EF24) | 3.125 µM + 50 µM (SUR) or 10 µM (EF24) | 3.125 µM + 25 µM (SUR) or 5 µM (EF24) | **3.125 µM** + 12.5 µM (SUR) or 2.5 µM (EF24) | **3.125 µM** + 6.25 µM (SUR) or 1.25 µM (EF24) | **3.125 µM** + 3.125 µM (SUR) or 0.625 µM (EF24) |

### The Combination Index

The CompuSyn software was used to calculate the combination index of gemcitabine/methotrexate in combination with EF24 or suramin. This software was designed by Ting-Chao Chou and Nick Martin and correctly calculates drug combinations based on the Chou-Talalay equation [227]. This software calculates the potency (Dm), shape (m) and conformity (r) of the data to the parameters of the median-effect principles [227]. The combination index values can be interpreted as synergistic (CI<1), additive (CI=1) and antagonistic (CI>1) (Figure 2—2) [228]. The Dose-reduction index (DRI) values can be interpreted as favourable (DRI>1), unfavourable (DRI<1) or showing no difference (DRI=1) (Figure 2—2) [229].

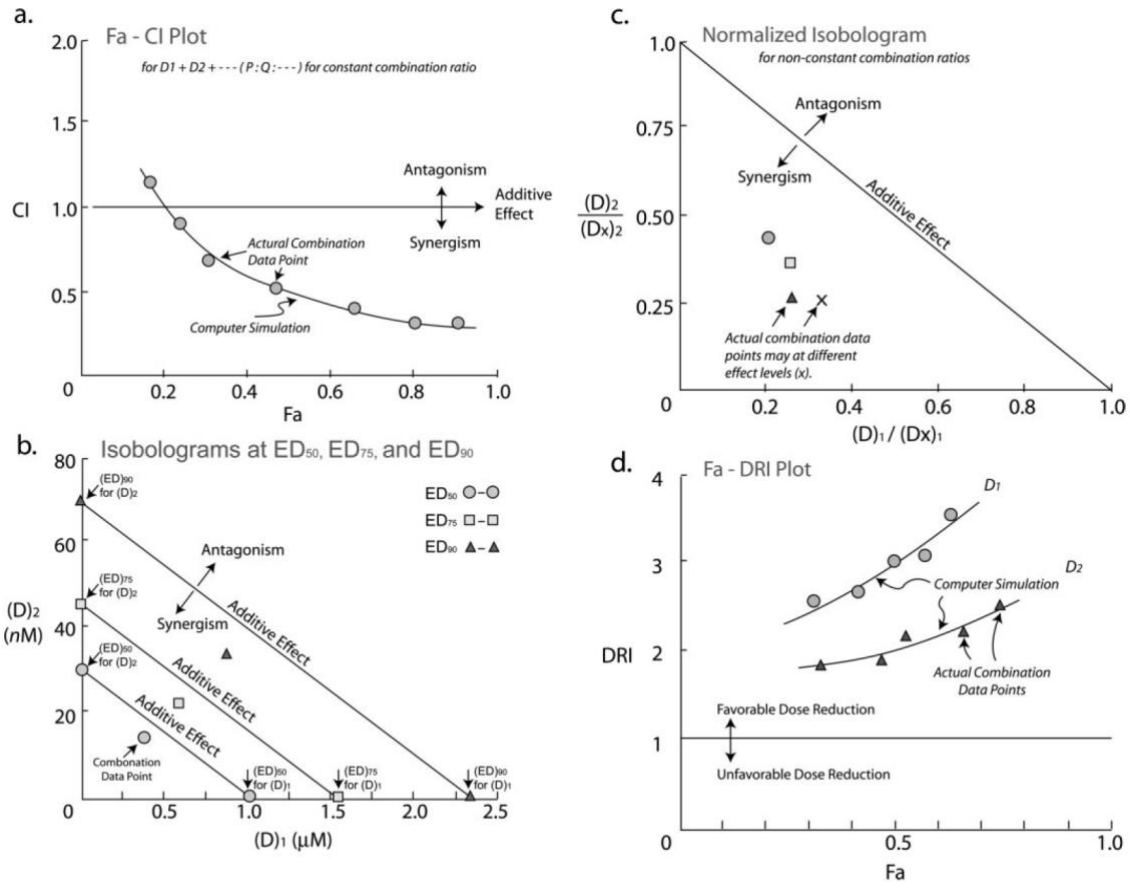


FIG. 8. Typical examples of drug combination plots and their interpretations based on the Chou and Talalay combination index theorem. a, $F_a$-CI plot. b, classic isobologram at $ED_{50}$, $ED_{75}$, and $ED_{90}$. c, normalized isobologram for combination at different combination ratios, and d, the $F_a$-DRI plot. All of these plots can be generated automatically by using CompuSyn (Chou and Martin, 2005).

Figure 2—2. Combination plots explained by chou et al., [229].

## ABCC3 Knockout (CRISPR)

The first method for the specific modification of genomic information was discovered in 1971 [230]. Kathleen Danna and Daniel Nathans used restriction enzymes from *Hemophilus influenzae* to cause double strand breaks in the small oncogenic SV60 virus double stranded DNA, producing specific DNA breaks [230]. Gel electrophoresis was used to separate the DNA fragments, resulting in 11 DNA fragments that were used to better characterise the SV60 virus [230]. Bacteria create endonucleases or restriction enzymes in an effort to protect themselves from viral attack or invading DNA [231]. The ability to create breaks in specific segments of DNA led to the creation of deletion mutants of SV60 [232]. SV60 mutants showed deletion in areas causing specific genetic disruption within the cleavage site of restriction enzymes as well as deletions beyond those cleavage sites [232]. The specific deletion of genetic material and the ability to compare mutant types allowed for the restriction mapping of the SV60 genome [233]. Furthermore, the ability to segment DNA in specific loci also produced fragments that were used to perfect DNA sequencing [233].

Modern genetic engineering utilises an approach called reverse engineering which uses various strategies to interrupt the target gene expression, followed by analysis of the corresponding phenotypic changes [234]. In 1971, Scherer and Davis developed the first method that allowed for the stable introduction of genetic material created *in vitro* into the genome of yeast (*Saccharomyces cerevisiae*) [235]. The system required an effective and selective marker and the insertion of DNA via homologous recombination [235]. Homologous recombination is the process that recombines an homologous DNA sequence bound to an exogenous DNA sequence at a desired locus [236]. The use of ampicillin resistance, selection genes and tetracycline sensitivity were used to ensure that the correct DNA sequences were inserted into the yeast plasmid [235]. In the early to mid-1980s, the ability to introduce foreign DNA into mammalian DNA was investigated in detail [236]. Combining specific restriction enzymes and homologous recombination smithies et al., was able to successfully and specifically insert exogenous genetic material into the β-globin locus [236]. This form of genetic editing relied heavily upon the availability of specific restriction enzymes that were able to cause DSBs in specific locations of the genome [237]. Although there have been several new restriction enzymes discovered, finding restriction enzymes, each with different recognition sequences for a specific genetic locus proved difficult [231, 237]. Further limitations of low rates (1 in $10_3$–$10_9$ cells) of successful spontaneous recombination and introduction of mistakes in the repair of DSBs by the non-homologous DNA repair (NHEJ) , meant that a faster more specific and efficient DNA editing tools were needed [237].

The specificity and targeted editing of genetic material progressed with the discovery of zinc finger proteins in 1991 [237]. Zinc finger proteins bind to DNA in a sequence specific manner with each zinc finger protein recognizing a 3 base pair DNA sequence [237]. The combination of zinc finger proteins could be combined into a sequence that could specifically bind to region of targeted DNA [237]. Fok1 DNA nuclease was modified to contain only its cleavage portion combined with zinc fingers allowed for targeted cleavage of select DNA sequence becoming the first “artificial” zinc finger nuclease (ZFN) [237, 238]. In 2006, transcription activator-like effector (TALE) proteins were discovered in the secretion of the *Xanthomonas* bacterial family [237]. Much like zinc finger proteins, TALE proteins could be combined with restriction enzyme to form a TALE nuclease (TALEN) [237]. TALE proteins however were able to recognise and bind to single nucleotides [237]. The ability to specify targeting of sequences was less restricted in TALEN gene editing in comparison to ZFN due to the ability to recognise single nucleotide molecule [239].

However, TALEN design and replication was more complicated and required several time-consuming critical production steps to ensure that the correct sequence of

polypeptides were created [240]. The specificity within the TALE was governed by a small region of the TALE amino acid sequence called the repeat variable diresidue (RVD) [240]. Joining a long sequence of these TALE proteins bound to endonucleases in a specific order with a number of repetitive regions make the synthesis of TALENs difficult [240]. However, these limitations have been greatly reduced by a number of methods which rapidly assemble custom TALE arrays [239]. The difficulty of creating and validating a specific amino acid chain and the inherent protein engineering has greatly limited the use of both ZFN and TALEN in the wider scientific community [237].

In 1987, the clustered regularly interspaced short palindromic repeats (CRISPR) sequence was discovered as a 29 nucleotide long series of fragments within the E.coli genome [241]. The investigation of the non-repeating sequences called spacers accelerated during the human genome project (HGP) where sequencing of different bacteriophages with key features of repeat and spacer regions of CRISPR were noticed [237]. This led to the discovery of the abundance of CRISPR sequences in bacteria (40%) and archaea (90%) and their proximity to CRISPR-associated (Cas) highly conserved genes [237]. The abundance of CRISPR-Cas sequences is matched by its diversity, within the CRISPR-Cas family there are six types and currently 29 known subtypes [242]. Class I, CRISPR-Cas systems contain multiprotein effector complexes while class II CRISPR-Cas systems only contain single protein effector complexes [242]. The class II, CRISPR-Cas9 system has become the most commonly used editing tool of the CRISPR-Cas family [242].

Theories that CRISPR-Cas was used as an immune response by bacteria began with the discovery that spacer regions encoded DNA that belonged to bacteriophages [237]. Proceeding viral infection, bacteria synthesised new spacer sequences derived from the attacking bacteriophage genome [243]. The newly integrated spacers were able to improve viral resistance [243]. However, this was dependent on the level of similarity between the spacer sequence and that of the targeted bacteriophage sequence [243]. This discovery was quickly followed by the realization that short CRISPR RNA (crRNA) transcribed from spacer regions guided the Cas enzymes to their targets [243]. The discovery of protospacer-adjacent motifs (PAMs) which were regions that were highly conserved in particular areas within the spacer sequences was the next critical finding in the creation of the CRISPR technology [237]. The first uses of CRISPR-Cas as an editing tool was shown in bacteria [244]. Earlier tools utilised mature crRNA and trans-activating crRNA (tracrRNA) separately which required independent binding to Cas proteins [244]. This was later simplified into a single short RNA that was a union of the tracrRNA and crRNA strand into a single guide RNA (sgRNA) [244]. Following experimentation in bacteria, the power of CRISPR as a gene editing tool was further established in eukaryote cells *in vivo* [237, 245].

The most used CRISPR-Cas system, utilises the Cas9 protein and more specifically the SpCas9 derived from *Streptococcus pyogenes* [242]. SpCas9 is especially used due to the simple PAM sequence (5'-NGG), the 20nt long spacer and the ability to form a complex with sgRNAs [242]. Modifications of the Cas9 protein has led to a wider variety of PAM sequences and a wider range of sequences that can be targeted [242]. More recent modifications have conjugated sgRNA and donor DNA together, increasing the transfection efficiency and increasing the use of the homologous directed repair (HDR) system [246]. It is suggested that cell or tissue type targeting could be the eventual outcome of these modified sgRNA and donor DNA sequences [246].

The future of CRISPR-Cas technology is yet unknown but at the present it is a widely accepted method used to reverse genetic expression of a wide variety of targets [247-250]. *Bacillus thurigiensis* (Bt) is a pervasive gram-positive soil bacterium that can release insecticidal toxins which kills insects [247]. In the fields of agriculture, forestry and public health, Bt has been extensively used, so much so that the resistance towards Bt toxins has increased within the insect population [247]. Modulation of both ABCC2 and ABCC3 genes have previously shown modulation of resistance towards *P.xylostella* (Px) [247]. Using the CRISPR-Cas9 system, both PxABCC2 and PxABCC3 knockouts decreased in resistance towards Bt toxins [247]. Concluding that, PxABCC2 and PxABCC3 expression were responsible for the resistance towards Bt toxins [247]. Cystic fibrosis (CF) is a fatal genetic disorder that is characterised by abnormal secretions in the lungs and the pancreas [251]. CF causes blockages that lead to inflammation, tissue damage and the destruction of organs [251]. CF is characterised by a mutation in the CF gene and a defect in the expression of CFTR, an ABCC family member [251]. Using CRISP-Cas9 the correct genetic code for CF was re-inserted into organoids that had the mutated CFTR function to restore the expression and activity [248].

As previously stated, P-gp has been one of the most studied ABC transporters [252]. The expression of canine P-gp was assessed in Madin-Darby canine kidney II cell line using CRISPR-Cas9 [249]. The interference of canine P-gp expression affected the feasibility of using MDCKII to study pharmacological responses to test compounds [249]. Therefore, CRISPR-Cas9 was used to remove canine P-gp genetic expression from MDCKII cells [249]. While, CRISPR-Cas9 successfully knocked out P-gp the expression levels, it also caused a slight decrease in ABCC2 expression, while the levels of canine ABCC3 remained constant [249]. Suggesting some off target effects as well as a possible compensatory relationship between certain transporters. The knockout of P-gp CRISPR-Cas9 also significantly enhanced sensitivity towards vincristine, doxorubicin and cisplatin in HCT-8/V and $KB_{v200}$ cells [118]. The knockout of P-gp was confirmed by western blot, PCR and rhodamine/doxorubicin cellular accumulation studies [118]. This study

displayed the impact of P-gp expression on multidrug resistance in two MDR cell lines as well as further validation of the MDR phenotype of ABC transporters [118].

There are some important limitations to consider when designing CRISPR-Cas experiments and translating CRISPR-Cas systems into the clinic. The design of the sgRNA is the most important step to ensure targeted gene editing [237]. The induction of NHEJ repair system to repair the DSBs introduces errors into DSB repairs by randomly inserting or deleting DNA pieces into the repair site [242]. This inherently introduces variability into the system which may contribute to a random editing efficiency within the target location. The homology-directed repair system is a more specific repair mechanism that can be used to insert a modified sequence which contain homology arms and DNA inserts into the DSB loci [242]. Researchers are searching for ways to select HDR for when genetic insertion using CRISPR-Cas9 is desired [242]. NHEJ is the most commonly used repair mechanism in eukaryotes and while random insertion or deletion may occur, this may be used to effectively cause knockout of genes [242]. There is also some variability within the CRISPR-Cas system that cannot be explained, some sgRNA's may simply not work [253]. While the CRISPR-Cas system is able to target specific regions of DNA, there are still some off-target effects [237]. These off-target effects may arise from mismatches within the PAM sequence [237]. However, the specificity of the CRISPR-Cas9 system has been proven in ABC transporters with previous P-gp knockout models [249]. Further modifications to the spCas9 protein has improved the specificity of the CRISPR-Cas9 system which indirectly reduces off-target effects [237].

While, successful genomic editing should result in successful protein editing. Smits et al., demonstrated that in one third of CRISPR gene knockout models, residual protein expression ranging from low to normal expression occurs [254]. The two suggested mechanisms for the rescue of protein expression were translation of the cleaved portions of DNA leading to truncated target proteins or by skipping the edited regions of DNA leading to protein isoforms with internal sequence deletions [254]. Allowing the synthesis of truncated proteins that can act to partially perform the duties of normal, unedited protein expression [254] .

Table 2—3. ABCC3 CRISPR-Cas9 target sequences and primers

| Primers | Primer Sequence | crRNA (Thermofisher) | crRNA target sequence | PCR product size | Pam Sequence |
|---|---|---|---|---|---|
| CRISPR1 FWD | CTCTGGGGAT GCGGATTCCA | CRISPR957583 _CR | GATACAGTAT GAGCGGCTGC (FWD strand) | 604bp | AGG |
| CRISPR1 RVS | GGGACCCAGC AGTGACTTTGA | | | | |

| | | | | | |
|---|---|---|---|---|---|
| CRISPR2 FWD | GGTGCAGTTTTTGTTGCCCTTA | CRISPR957588_CR | GGATGATGTAGCCACGACAA (FWD strand) | 608bp | TGG |
| CRISPR2 RVS | AGAAGGCAGAGGTTGCAGTGAG | | | | |
| CRISPR3 FWD | TGCTTGGGGTCATGGGAATC | CRISPR957600_CR | GGAGTAAAAAAGGTCCGCCC (reverse strand) | 422bp | AGG |
| CRISPR3 RVS | AGACCTCCCCCATCCACTTT | | GGGCGGACCTTTTTTACTCC (complementary 5' to 3' sequence) | | |

**CRIPSR Methodology**

The CRISPR-Cas9 system was used to knockout the ABCC3 gene in PANC1 (ATCC) cells in accordance with the manufacturer's protocol (Thermofisher). The crRNAs were predesigned and designated CRISPR1 (CRISPR957583_CR), CRISPR 2(CRISPR957588_CR) and CRISPR3 (CRISPR957600_CR) (Thermofisher). Firstly, the three TrueGuide™ synthetic sgRNA's (Thermofisher) were created by annealing the tracrRNA (Thermofisher) and the crRNA (Thermofisher) together in accordance with the manufacturer's protocol (Thermofisher). PANC1 cells were seeded at 50,000 cells per well in a 24 well plate. The following day the TrueGuide™ synthetic sgRNA and the Cas9 protein v2 (Thermofisher) were transfected into PANC1 cells using Lipofectamine™ RNAiMAX™ transfection reagent within OPTIMEM serum free media.

The cells were passaged twice after CRISPR-Cas9 transfection in accordance with the manufacturers protocol. Cleavage efficiency was then detected using the GeneArt® Genomic Cleavage Detection Kit and PCR, as below (life technologies). Cells ($0.25x10_6$) were harvested (200 x *g*, 5 mins, at 4˚C), supernatant was removed, and pellet was frozen (-80 ˚C). Cells were then lysed, and cell contents were exposed. Cell lysate was mixed with FWD/RVS primers or control primers, AmpliTaq Gold® 360 master mix and water to create a PCR mix. PCR was done in accordance with manufacturers PCR reaction. PCR product was verified by 2% agarose gel and SYBR™ Gold. The resultant PCR product was re-annealed and combined with the detection enzyme which cleaves any DNA mismatches created by the CRISPR knockout. After enzyme digestion was complete, samples were analysed in a 2% agarose gel supplemented with SYBR™ Gold. Gels were captured using SmartView Pro 2100 Imager System. The intensity of each band was calculated using ImageJ and cleavage efficiency was calculated as below.

Equation 2-1.Cleavage efficiency equation.

| |
|---|
| Cleavage efficiency = 1- [(1-fraction cleaved)$_{1/2}$] |
| Fraction cleaved = sum of cleaved band intensities/ (sum of the total bands intensities) |

- Materials Used
    - Opti-MEM™ Reduced Serum medium (Life Technologies, NZ, 31985070)
    - CRISPRMAX™ (Thermofisher, NZ)
    - crRNA (Life Technologies, NZ, A35509)
    - TrueCut Cas9 Protein v2 (Life Technologies, NZ, A36498)
    - GeneArt Genomic Cleavage Selection Kit (Life Technologies, A24372)
    - Primers (Table 2—3) (Life Technologies, NZ)
    - PCR facilities (see PCR methodology).

**PCR**

The polymerase chain reaction (PCR) was introduced into the scientific community by Dr Kary Mullis [255]. The polymerase chain reaction allows researchers to detect and amplify a region of DNA [255]. Mullis et al., stated that PCR "lets you pick the piece of DNA you're interested in and have as much of it as you want" [255]. This process enables trace amounts of DNA to be isolated and amplified until there is enough material to analyse [255]. Qualitative PCR identifies whether a specific gene is present or absent within a sample [255]. Quantitative PCR (qPCR) or real-time PCR (rtPCR) can be used to detect the amount of a gene target within a DNA sample [255]. Real-time PCR can utilise reverse transcription to convert RNA molecules into cDNA molecules which can subsequently be quantified by PCR [255]. Therefore, RNA molecules can also quantified by the PCR system [255].

A DNA template, primers, nucleotides and DNA polymerases are required to make the PCR [255]. The four nucleotides which make up the DNA strand are adenine (A), thymine (T), cytosine (C) and guanine (G) [255].The enzyme DNA polymerase is responsible for adding new nucleotides to form template strands of replicating DNA [255]. Primers were used to select the specific region of DNA to be amplified [255]. Primers highlight the region of DNA for DNA polymerases to build on [255]. The thermocycler uses heat cycles in a specific manner to induce DNA denaturation, annealing of primers and extension of DNA polymerases [255]. Each cycle of this process causes the amount of target DNA to double [255]. Cleavage detection primers were designed using the Primer-blast platform in accordance with the manufacturers protocol.

Detection of PCR products occurs either by direct staining of DNA using ethidium bromide or by labelling PCR primers or DNA fluorescent dyes (SYBR™ Gold) [255]. Agarose gel electrophoresis is the most common detection method for PCR [255].

Electrophoresis was used to separate and differentiate between different sizes and charges of DNA samples [255]. A DNA ladder containing DNA products with known sizes can be used to predict sample DNA size [255]. SYBR™ Gold (Thermofisher, NZ) is the most sensitive fluorescent nucleic acid stain that Thermofisher has available. In the detection of double/single stranded DNA and RNA SYBR™ Gold (at 300 nm excitation) was more sensitive than ethidium bromide, SYBR Green I stains and SYBR Green II stains [256]. The increase in sensitivity is due to the increased fluorescence signal upon binding (~1000-fold) [256]. PCR can be limited by the improved sensitivity of the PCR system which means that any contaminant can be amplified, greatly altering the result [255]. This can be the greatest strength and weakness of the PCR system, therefore extreme care is needed during sample preparation [255]. Primer design requires previous knowledge of the genetic sequence being investigated. Therefore, the PCR system cannot necessarily be used as an exploratory tool for unknown gene expression [255]. Lastly the non-specific binding and binding of primer dimers can also limit the efficacy of the PCR reaction [255, 257]. PCR will be used to assess the cleavage efficacy of CRISPR-Cas9 in knockout cells by amplifying the CRISPR-Cas9 target region combined with the endonuclease activity which cuts at hetero-duplex mismatches (Thermofisher, NZ) [258].

- Materials Used
    - SYBR Gold (Thermofisher, NZ)
    - PCR System: Roche Light Cycler® 2.0 (Roche Diagnostics, NZ)
    - Eppendorf Mastercycler® pro
    - Temperature profile: 95 °C for 10 min, and then 40 cycles of 95 °C for 15 s and 60 °C for 1 min. The threshold cycle (Ct) values were obtained for each sample.
    - Primers (Table 2—3).

**Statistics**

Statistical analysis was completed using the GraphPad Prism 8 software (San Diego, CA, USA). Each experiment when testing significance was done across three independent experiments. Significance was established across two sample averages using a student's t-test and one-way analysis of variance (ANOVA) across multiple data sets. The post-hoc Dunnett and Tukey test was applied when appropriate. P-values were considered as significant in accordance with Table 2—4**Error! Reference source not found.**

Table 2—4. GraphPad Prism wording for signficance tests and p-values

| P value | Wording | Summary |
|---|---|---|
| 0.0001 to 0.001 | Extremely significant | *** |
| 0.001 to 0.01 | Very significant | ** |
| 0.01 to 0.05 | Significant | * |
| ≥ 0.05 | Not significant | ns |

# Chapter 3 ABCC3 Bioinformatic Study

## Introduction

Cancer has become one of the most feared diseases in the world and according to the world health organization is ranked among the top ten causes of death worldwide [259]. Cancer is also second leading cause of death in the US with the number of new cases continually on the rise [260]. In 2018, there was an estimated 18.1 million newly diagnosed cancer cases and 9.6 million cancer related deaths worldwide [13]. Lung, breast and prostate cancers presented the highest number of new cases in 2018, with an estimated 2.093 million, 2.088 million and 1.276 million new cases, respectively [13]. Some cancers like pancreas, liver and lung cancer show a higher percentage of total deaths than new cases by 1.8-fold, 1.74-fold and 1.58-fold [13]. Pancreatic cancer is especially known for a poor outcome, while ranked as the fourteenth most common cancer, it also ranked as the seventh leading cause of death [13]. The five year survival rate for pancreatic cancer in the United States was at approximately 9% [261]. However, a recent study showed that these survival rates could vary depending on the country [262]. New Zealand showed less improvement in survival rates than other developed countries such as Australia, Canada, Norway, Denmark and Ireland [262]. There is clearly a need for improved, effective and targeted cancer therapies that will improve these poor survival rates especially within New Zealand.

Effective treatment of cancer patients can be limited by failed chemotherapy treatments, brought about by the increased efflux of anticancer drugs [86]. The reduction in cellular accumulation of anticancer drugs has resulted in reduced cancer killing and an increased multi drug resistance [86]. Multidrug resistance is the development or an inherent resistance of cancer to a multitude of drugs that are unrelated in structure or target [88]. The ATP binding cassette (ABC) family are made up of transport proteins that require the energy released from ATP hydrolysis to achieve protein reconfiguration, enabling active transport of substrates across the membrane [263]. This type of transport allows the transport of substrates against concentration gradients [263]. ABCC3/MRP3 has emerged as another important drug transporter in cancer [36, 79, 81]. It was our aim to investigate and analyse ABCC3 expression across normal and cancerous tissues using the ONCOMINE, Kaplan-Meier plotter (KMplot) and Search Tool for Retrieval of Interacting Genes/Proteins (STRING) platforms.

The ONCOMINE platform has collected and organised several cancerous microarray datasets from a number of sources into one platform [190, 194]. In 2007, ONCOMINE contained 264 independent cancerous datasets containing approximately 18,000 microarray samples of cancerous gene expression, with 2,000 normal samples for comparison [194]. To date, the number of samples within the ONCOMINE database

has expanded to 71,765 cancerous samples and 12,764 normal samples (oncomine.org). ONCOMINE was designed not only to contain a large amount of microarray data but was also designed to ensure usability and ease of comparison, in order to quickly find potential cancer targets [190]. Each new dataset was processed and normalised to allow for further comparisons between datasets [190]. The ONCOMINE database has integrated the data from the GenBank, Entrez Gene, Swissprot/Trembl, Unigene, InterPro, Biocarta, KEGG, HPRD, Cancer Gene Database, Gene Ontology, Inparanoid, Pin database, Therapeutic target database and TRANSFAC/Match databases [194]. The ONCOMINE platform was used to assess the ABCC3 expression across the datasets and analyses provided.

The Kaplan-Meier survival curve represents the probability of surviving a certain amount of time, in this case probability of surviving a specific expression profile [264]. The Kaplan-Meier method uses nonparametric methods to estimate this survival probability which remains constant between events [264]. The vertical drop in the KM plot indicates that the predefined event has occurred, in this case patient mortality [264]. The median survival time can be calculated as the point at which 50% of the patients have died [264]. The KM plotter (www.kmplot.com) is an online database which compares the survival time stored within the KM plot clinical database with the high and low mRNA expression of a specific gene [199]. To date, the online database contained 7,462 clinical samples across several cancer types (www.kmplot.com). The log-rank P produced by the KMplot informs the user as to whether a significant difference between the curves exists, it cannot however, attest to the magnitude of those differences [264]. For this reason the KM plot platform also produces a hazard ratio (HR) which is an indirect estimation of the length of a patient survival [264]. The higher the HR the shorter the estimated patient survival and the lower the HR the more prolonged the patient was estimated to survive [264]. It was our aim to use the Kmplot platform to assess the impact of high/low ABCC3 expression on the overall survival of cancer patients.

Although the expression of RNA/microarray data is highly informative, the mRNA expression does not always translate into protein expression [265]. In some cases, mRNA expression only weakly correlates with protein expression across a number of different organisms [265]. The recent advances in technology has further highlighted mechanisms that are able to regulate protein expression post mRNA manufacture [265]. The STRING platform is an online database which like ONCOMINE contains a vast amount of data, prioritises usability and is constantly maintained [190, 193]. However, unlike ONCOMINE, the STRING platform assesses and analyses protein-protein interactions [193]. The goal of the STRING platform is to predict functional interactions between not only proteins that structurally bind with each other but also proteins that indirectly regulate each other by transcriptional modulation, formation of reacting

compounds, signal transduction and functional homology [193]. Among all the interacting molecules, proteins could be deemed the most important, ranging in biochemical activity, information and specificity [193]. Therefore, it was our aim to use the STRING platform to investigate possible protein-protein interactions of MRP3. It was also our aim to assess whether these platforms would have any overlapping patterns for MRP3 expression.

## Results

### ABCC3 Disease Summary

The ONCOMINE database at the time of this search (August 2019) contained 71,765 cancerous datasets and 12,764 normal samples (oncomine.org). The initial ABCC3 gene search within the ONCOMINE database returned a disease summary which showed the amount of significant analyses returned by the ONCOMINE platform (Table 3—1). The search of ABCC3 expression returned 2,291 unique analyses with 350 significant analyses returned (Table 3—1). The ABCC3 disease summary presented a higher number of significantly overexpressing analyses, than of significantly downregulated analyses (Table 3—1). The cancer versus normal analyses exposed several cancer types that significantly dysregulated the expression of ABCC3 (Table 3—1). The lung, kidney, oesophageal and brain carcinoma showed the highest amount of significant ABCC3 overexpressing analyses. In the cancer versus cancer (histological) analyses lung, bladder and brain carcinoma displayed the most analyses that returned significant results (Table 3—1). The multi-cancer datasets showed that colorectal, pancreatic and kidney carcinoma had highest number of significant ABCC3 overexpression analyses while melanoma, leukaemia and lymphoma showed the highest number of significant analyses that under expressed ABCC3 (Table 3—1). The amount of significant results returned within the outlier analysis for breast, brain, leukaemia and lung cancer suggested that subsets of these cancers differentially expressed ABCC3. Although the disease summary was a useful tool, it took further interrogation of the data to accurately interpret the ABCC3 expression results.

Table 3—1. Disease Summary for ABCC3 (ONCOMINE). Threshold was set at a P-value = 0.0001, Fold Change=2 and Gene Rank = Top 10%. Cell colour was an indicator of the best gene rank percentile for each analysis.

| Analysis Type by Cancer | Cancer Vs Normal | | Cancer vs cancer | | | | Outliers | |
|---|---|---|---|---|---|---|---|---|
| | | | Histology | | Multi-cancer | | | |
| Bladder Cancer | 1 | | 4 | 4 | | | 2 | 3 |
| Brain/CNS Cancer | 6 | | 3 | 3 | | | 12 | 4 |
| Breast Cancer | 1 | | | | | 2 | 32 | 8 |
| Cervical Cancer | | | 1 | 1 | | | 4 | 3 |

| | | | | | | | | |
|---|---|---|---|---|---|---|---|---|
| Colorectal Cancer | | 2 | | | 4 | | 3 | 8 |
| Esophageal Cancer | 5 | | 1 | 1 | 1 | | 2 | 3 |
| Gastric Cancer | | | | | | | 2 | 3 |
| Head and Neck Cancer | 1 | | | | | | 7 | 6 |
| Kidney Cancer | 5 | | 1 | 2 | 3 | | 3 | 8 |
| Leukemia | 1 | | | | | 4 | 17 | 13 |
| Liver Cancer | | | | | | | | 4 |
| Lung Cancer | 6 | 1 | 7 | 7 | | | 11 | 10 |
| Lymphoma | 1 | | 1 | 1 | | 4 | 4 | 9 |
| Melanoma | | 1 | | | | 5 | 8 | 3 |
| Myeloma | | | | | | 1 | 8 | 1 |
| Other Cancer | | | 1 | | | 1 | 12 | 13 |
| Ovarian Cancer | | | | | | 1 | 9 | 1 |
| Pancreatic Cancer | 1 | | | | 2 | | 4 | 3 |
| Prostate Cancer | | 1 | | | | 2 | 7 | 8 |
| Sarcoma | | 1 | 2 | 1 | 1 | 1 | 8 | 7 |
| | | | | | | | | |
| Significant Unique Analyses | 28 | 6 | 20 | 19 | 10 | 18 | 143 | 106 |
| Total unique analyses | 426 | | 700 | | 255 | | 910 | |

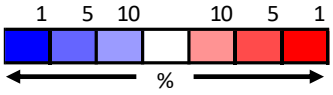


**Differential ABCC3 Expression in Cancer versus Normal**

In order to better understand the differential expression shown in the ABCC3 disease summary, the data from the cancer versus normal analysis was extracted (Figure 3—1). All data was presented with significant differences in ABCC3 expression when comparing normal and cancerous samples with P-values ranging from 0.025 to 7.20E-20 (Figure 3—1). The Gumz renal, kidney carcinoma dataset upon comparison of ABCC3 expression in clear cell renal cell carcinoma and normal kidney expression showed the greatest difference in ABCC3 expression levels of all datasets analysed, with a fold change of 15.06 (P-value = 2.38E-9, gene rank: top 1%) (Figure 3—1). ABCC3 expression was not only the largest in the Gumz renal dataset, but also showed the highest, significantly different genes expressed across the cancer versus normal comparison. The other highly overexpressing kidney carcinoma datasets Higgins Renal and Jones Renal also showed a significantly increased ABCC3 expression in cancer samples with a fold change of 5.153 and 4.577 respectively (Figure 3—1). The Gumz renal and Higgins Renal showed a gene rank of 1%, the Jones Renal dataset resulted in a gene rank of 3% (Table 3—2). Demonstrating the greater importance of ABCC3 expression in the Gumz renal and Higgins renal datasets.

The lymphoma carcinoma type showed the second highest fold change (12.487) of all cancerous versus normal analyses (Figure 3—1). The ABCC3 expression within the Basso Lymphoma dataset was significantly (P-value = 7.19E-19) higher in centroblastic lymphoma in comparison to normal lymphocyte expression (Table 3—2). However, the next strongest overexpressing lymphoma carcinoma dataset (lymphoma Ma Breast) although significant, exhibited a much lower differential ABCC3 expression (Table 3—2). The remaining datasets Brune Lymphoma and Compagno Lymphoma showed an ABCC3 overexpression of 1.349 and 1.393-fold, respectively (Figure 3—1). The gene rank of ABCC3 in the top 3 and 5% of both Compagno Lymphoma and Brune Lymphoma showed that other genes were more significantly differentially expressed within these datasets (Figure 3—1). The third highest overexpressing ABCC3 cancer type was found in the Sanchez-Carbayo Bladder 2 dataset which compared superficial bladder cancer mRNA expression with normal bladder samples (Fold Change: 12.216, P-value = 7.46E-16) (Figure 3—1). However, this was the only bladder carcinoma dataset to show any significant over or under expression of ABCC3 (Table 3—2).

The Su Lung carcinoma dataset showed the next highest fold change (10.261) in lung adenocarcinoma versus normal mRNA samples (P-values:1.04E-9) (Table 3—2). The Stearman Lung and Landi Lung datasets also showed ABCC3 overexpression in lung cancer samples with a fold change of 3.267 and 2.688, respectively (Table 3—2). The lung cancer type showed the widest range of ABCC3 expression of all cancer types and was the only cancer type to show both significant under and overexpression of ABCC3 (Figure 3—1). The lung cancer datasets ranged from the significant overexpression of the Su Lung dataset (Fold change: 10.261, P-value =1.04E-9) to the largest under expression of any cancer type found within the Bhattacharjee Lung dataset (Fold change: -26.3, P-value = 4.37E-5) (Table 3—2).

The pancreatic cancer datasets Pei Pancreas and Badea Pancreas both showed a significant overexpression of ABCC3 in pancreatic cancer samples in comparison to normal samples (Figure 3—1). While Pei Pancreas showed a fold change of 2.131, the Badea Pancreas dataset fell just outside of the disease summary threshold (Table 3—2).

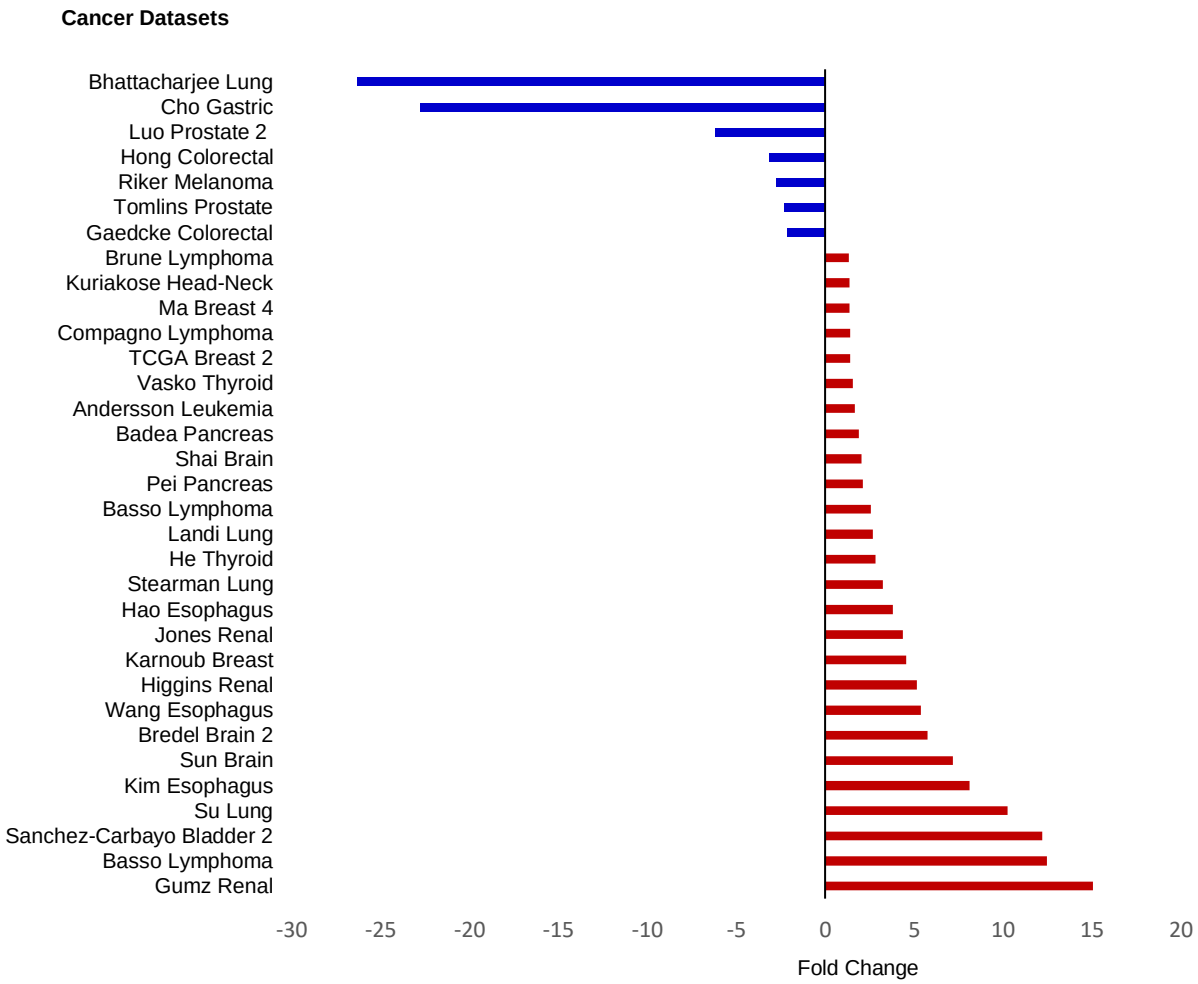


Figure 3—1. Cancer vs Normal. A list of the top over and under expressing ABCC3 cancer datasets across all cancer types. The top three databases of each cancer type that showed either a significant increase or decrease in ABCC3 expression were extracted (oncomine.org).

The Badea Pancreas dataset compared the mRNA expression of ABCC3 in pancreatic ductal adenocarcinoma with pancreas samples, which showed ABCC3 expression was significantly increased in pancreatic ductal adenocarcinoma (P-value = 8.75E-8), with a fold change of 1.887 (Table 3—2). Although, differences in expression levels were not large as other datasets, Pei Pancreas and Badea Pancreas still showed extremely significant and distinct ABCC3 overexpression in pancreatic cancer versus normal samples (Table 3—2,). The remaining cancer types that showed significant ABCC3 overexpression were the oesophageal cancer, brain and central nervous system cancer, breast cancer, head and neck cancer and leukaemia cancer (Table 3—2). The cancer versus normal analysis resulted in a differential expression of the oesophageal cancer ranging from 8.138 fold to 3.825 fold, brain and central nervous system cancer ranging from 7.2 fold to 2.067, breast cancer ranging from 4.577 fold and 1.365 fold, head and neck cancer ranging from 2.824 fold to 1.365 fold and leukaemia cancer ranging from 2.586 fold to 1.674 fold (Table 3—2). Prostate, melanoma and colorectal carcinoma

datasets all exclusively showed significantly lower ABCC3 expression in the cancerous samples in comparison to normal samples (Table 3—2). Prostate cancer datasets Cho Gastric and Luo Prostate 2, after Bhattacharjee Lung show the greatest ABCC3 under expression with fold changes of -22.777 and -6.151, respectively (Table 3—2). The range and prevalence of ABCC3 expression in cancerous samples in comparison to normal shows the importance of ABCC3 as a cancerous target.

Table 3—2. Differential analysis of ABCC3 expression (Cancer versus Normal)

| Cancer Type | Dataset | P-value | t-test | Expression (Under/Over) | Fold Change | Gene rank (%) | (n) | Reporter |
|---|---|---|---|---|---|---|---|---|
| Kidney Cancer | Gumz Renal | 2.38E-09 | 10.509 | Over | 15.08 | 1% | 20 | 209641_s_at |
| Lymphoma Cancer | Basso Lymphoma | 7.19E-19 | 14.163 | Over | 12.487 | 1% | 53 | 38261_at |
| Bladder Cancer | Sanchez-Carbayo Bladder 2 | 7.42E-16 | 10.592 | Over | 12.216 | 4% | 76 | 209641_s_at |
| Lung Cancer | Su Lung | 1.04E-09 | 8.443 | Over | 10.261 | 1% | 57 | 209641_s_at |
| Esophageal Cancer | Kim Esophagus | 3.53E-16 | 18.355 | Over | 8.138 | 1% | 43 | ILMN_1677814 |
| Brain/CNS Cancer | Sun Brain | 1.04E-18 | 10.729 | Over | 7.2 | 2% | 104 | 209641_s_at |
| Brain/CNS Cancer | Bredel Brain 2 | 4.23E-10 | 9.228 | Over | 5.779 | 2% | 31 | IMAGE:781139 |
| Esophageal Cancer | Wang Esophagus | 1.41E-08 | 7.169 | Over | 5.374 | 1% | 43 | AF083552 |
| Kidney Cancer | Higgins Renal | 8.94E-11 | 10.913 | Over | 5.153 | 1% | 27 | IMAGE:781139 |
| Breast Cancer | Karnoub Breast | 1.37E-05 | 5.427 | Over | 4.577 | 1% | 22 | 209641_s_at |
| Kidney Cancer | Jones Renal | 4.52E-10 | 19.224 | Over | 4.39 | 3% | 31 | 214979_at |
| Esophageal Cancer | Hao Esophagus | 1.62E-06 | 5.438 | Over | 3.825 | 2% | 27 | IMAGE:781139 |
| Lung Cancer | Stearman Lung | 1.61E-08 | 7.401 | Over | 3.267 | 1% | 39 | 38261_at |
| Head and Neck Cancer | He Thyroid | 1.98E-07 | 8.638 | Over | 2.824 | 1% | 18 | 209641_s_at |

| | | | | | | | | |
|---|---|---|---|---|---|---|---|---|
| Lung Cancer | Landi Lung | 7.20E-20 | 12.197 | Over | 2.688 | 1% | 107 | 209641_s_at |
| Leukemia Cancer | Basso Lymphoma | 3.82E-07 | 5.953 | Over | 2.586 | 6% | 41 | 1930_at |
| Pancreatic Cancer | Pei Pancreas | 0.0000817 | 4.274 | Over | 2.131 | 8% | 52 | 209641_s_at |
| Brain/CNS Cancer | Shai Brain | 1.25E-05 | 4.954 | Over | 2.067 | 6% | 34 | 38261_at |
| Pancreatic Cancer | Badea Pancreas | 8.75E-08 | 5.791 | Over | 1.887 | 11% | 78 | 209641_s_at |
| Leukemia Cancer | Andersson Leukemia | 8.15E-08 | 7.047 | Over | 1.671 | 5% | 29 | IMAGE:781139 |
| Head and Neck Cancer | Vasko Thyroid | 6.32E-04 | 4.075 | Over | 1.549 | 3% | 18 | 230682_x_at |
| Breast Cancer | TCGA Breast 2 | 6.17E-04 | 4.873 | Over | 1.429 | 3% | 822 | 17-046095638 |
| Lymphoma Cancer | Compagno Lymphoma | 3.98E-11 | 9.537 | Over | 1.393 | 3% | 37 | 239217_x_at |
| Breast Cancer | Ma Breast 4 | 7.13E-04 | 3.733 | Over | 1.365 | 3% | 23 | g9955971_3p_s_at |
| Head and Neck Cancer | Kuriakose Head-Neck | 2.50E-02 | 3.505 | Over | 1.365 | 5% | 25 | 1930_at |
| Lymphoma Cancer | Brune Lymphoma | 2.00E-03 | 4.857 | Over | 1.349 | 5% | 29 | 2062_x_at |
| Colorectal Cancer | Gaedcke Colorectal | 1.82E-18 | -10.792 | Under | -2.139 | 7% | 130 | A_23_P207507 |
| Prostate Cancer | Tomlins Prostate | 3.40E-06 | -5.06 | Under | -2.282 | 1% | 53 | IMAGE:781139 |
| Melanoma Cancer | Riker Melanoma | 3.74E-05 | -5.384 | Under | -2.758 | 2% | 18 | 239217_x_at |
| Colorectal Cancer | Hong Colorectal | 1.12E-08 | -7.803 | Under | -3.152 | 6% | 82 | 209641_s_at |
| Prostate Cancer | Luo Prostate 2 | 0.011 | -2.455 | Under | -6.151 | 4% | 30 | 38261_at |
| Prostate Cancer | Cho Gastric | 3.07E-07 | -17.153 | Under | -22.777 | 4% | 25 | ILMN_1677814 |
| Lung Cancer | Bhattacharjee Lung | 4.37E-05 | -5.065 | Under | -26.3 | 6% | 23 | 38261_at |

## Differential ABCC3 Expression across Cancer

### Cancer versus Cancer (Histological samples)

The differential analysis not only compares ABCC3 expression across cancerous and normal samples, but they also compare across cancer types. The cancer versus cancer analysis compares the ABCC3 expression in histological samples as well as in multi-cancer datasets (Table 3—3 & Table 3—4). The histological analysis compared samples within the same datasets, showing which of the cancer subtypes under/over express the ABCC3 target the most significantly and predominantly (Table 3—3). The top overexpressing ABCC3 dataset within the histological analysis was the Bhattacharjee Lung dataset (Table 3—3). Non-small cell carcinoma in comparison to small cell lung carcinoma and SCC showed a significant 16.482-fold increase in ABCC3 expression (P-value = 2.39E-6) (Table 3—3). The remaining lung cancer datasets TCGA Lung, Lee Lung, Bittner Lung and Bild Lung also show an overexpression of ABCC3 in non-small cell carcinoma samples in comparison to SCC (Table 3—3). The ABCC3 overexpression in non-small cell carcinoma samples in comparison to the squamous cell lung carcinoma in the TCGA Lung dataset resulted in a 5.207-fold increase in ABCC3 expression (P-value = 5.43E-12) (Figure 3—2). The Lee Lung, Bittner Lung and Bild Lung datasets showed increased ABCC3 expression in non-small cell lung carcinoma with ABCC3 expression by 5.0-fold (P-value = 2.59E-18), 3.96 fold (P-value = 1.61E-06) and 3.28 fold (P-value = 2.41E-13), respectively (Table 3—3). This expression pattern seen across four lung cancer datasets suggests that ABCC3 could be an effective target for non-small cell carcinoma treatment.

Following the Bhattacharjee lung dataset, the Segal Sarcoma 2 dataset showed the next highest ABCC3 overexpression with a 9.53-fold change when comparing cancerous histological samples (Table 3—3). The analysis showed that the ABCC3 expression in malignant fibrous histiocytoma was significantly (P-value = 1.92E-5) higher (9.53-fold) than fibrosarcoma, gastrointestinal stromal tumour, leiomyosarcoma, liposarcoma and soft tissue sarcoma (oncomine.org). Although, malignant fibrous histiocytoma showed ABCC3 overexpression in comparison to the other sarcoma types, the malignant fibrous histiocytoma still under expressed ABCC3 just to a lesser extent than other sarcomas (oncomine.org). Highlighting how important it was to further interrogate the results for correct interpretation. ABCC3 under expressing Segal Sarcoma 2 also showed significantly lower ABCC3 expression in gastrointestinal stromal tumour samples in comparison to fibrosarcoma, leiomyosarcoma, liposarcoma, malignant fibrous histiocytoma and soft tissue sarcoma (Figure 3—2). Therefore, Segal Sarcoma 2 samples ranged in ABCC3 under expression from weakly under expressing malignant fibrous histiocytoma samples to strongly under expressing gastrointestinal

stromal tumour samples (oncomine.org). The Nakayama Sarcoma dataset showed a different ABCC3 expression pattern, the malignant peripheral nerve sheath tumour showed a 5.92-fold increase in ABCC3 expression in comparison to fibrosarcoma, leiomyosarcoma, liposarcoma, malignant fibrous histiocytoma and soft tissue sarcoma (oncomine.org). When comparing cancer to cancer patterns the malignant peripheral nerve sheath tumour showed weak overexpression of ABCC3, with some samples showing ABCC3 $\log_2$ values close to zero (oncomine.org).

The bladder carcinoma dataset Sanchez-Carbayo Bladder 2 showed the next highest fold change across histological samples (Figure 3—2). The superficial bladder cancer significantly overexpressed ABCC3 (P-value = 7.90E-14, Fold Change: 8.32) in comparison to the urothelial carcinoma (Table 3—3). Unlike sarcoma samples the bladder carcinoma samples not only showed a significant difference in comparison across samples, the majority of the superficial bladder cancer samples also showed strong ABCC3 overexpression (Figure 3—2, oncomine.org). This suggested that ABCC3 would be a good target for the superficial bladder cancer subset of bladder carcinoma.

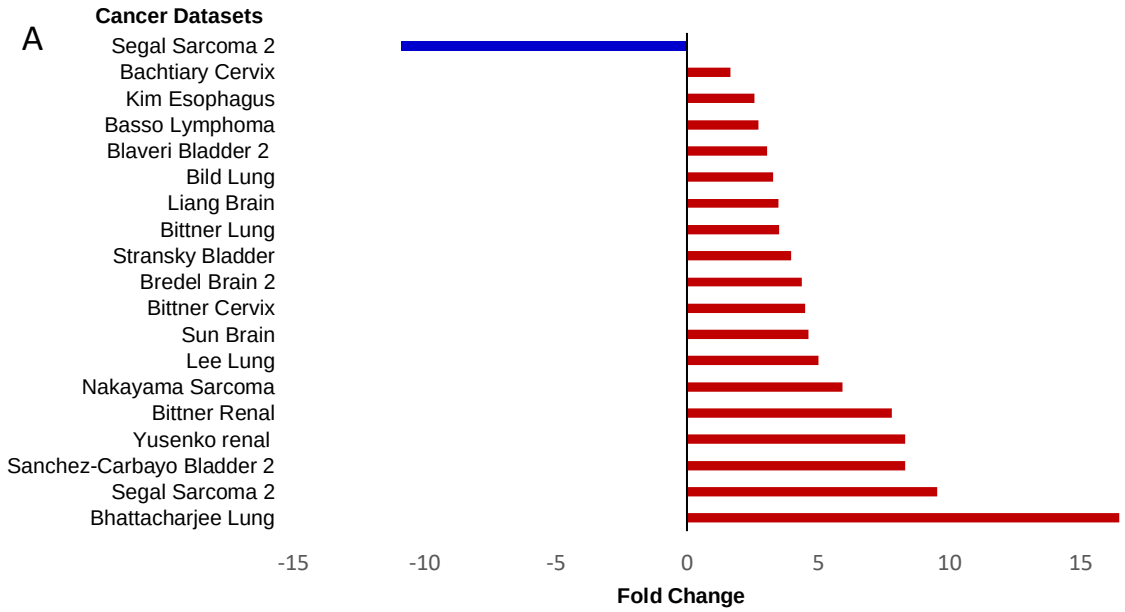

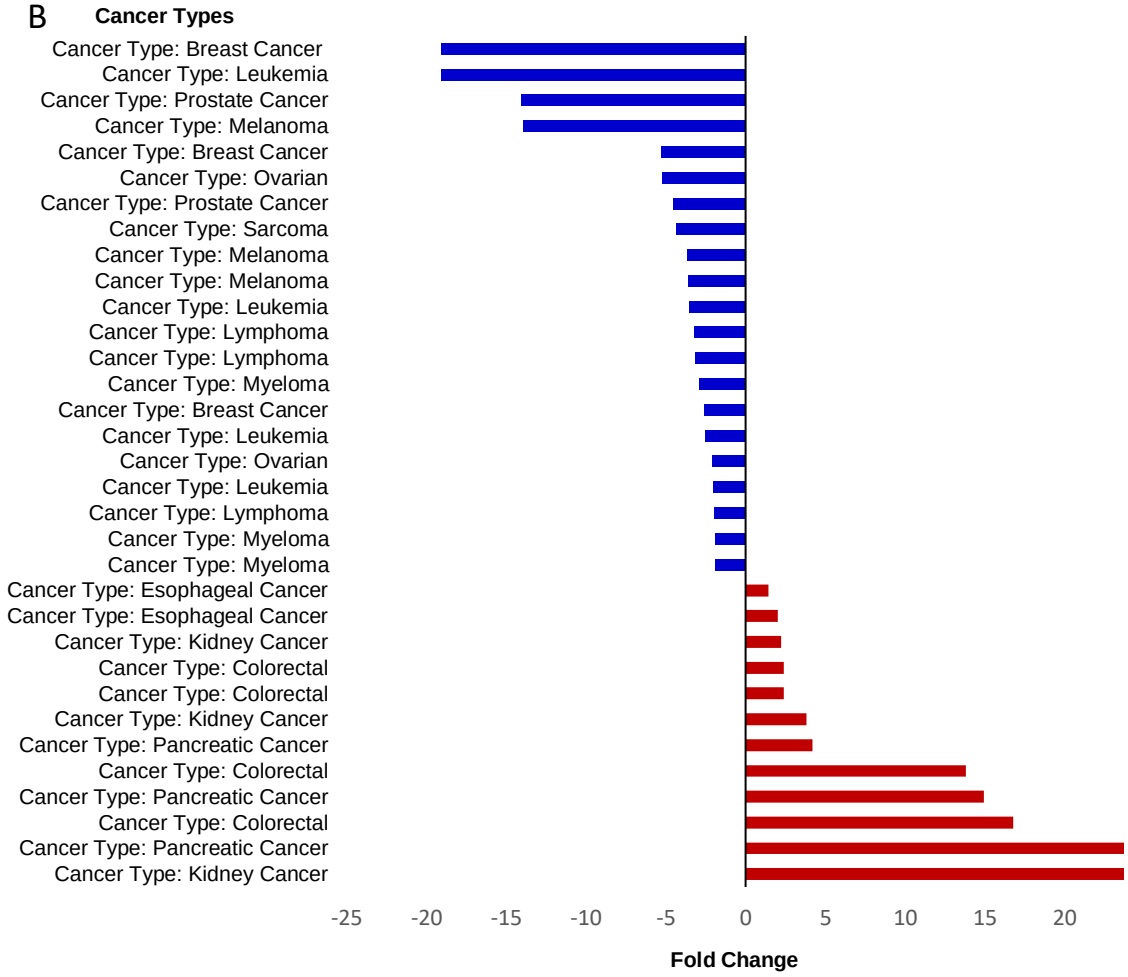


Figure 3—2. Cancer versus Cancer Analyses. The differential expression of ABCC3 across different cancer types was analysed. (A) Fold changes between the highest ABCC3 expressing histological sample type in comparison the other sample types across the cancer datasets. (B) Comparison of ABCC3 expression across different cancer types in multi-cancer databases. The top three databases **which** showed either a significant increase or decrease in ABCC3 expression were examined and the fold change expression was extracted**.**

In cancer versus normal analyses kidney carcinomas showed the highest fold change (Figure 3—1). The Yusenko renal dataset showed renal carcinoma expressed ABCC3 significantly higher (P-value = 3.66E-5, fold change: 8.32) than renal lipoma, renal oncocytoma, renal sarcoma, renal wilms tumour and rhabdoid tumour of the kidney (Table 3—3). The Bittner Renal dataset also showed a similar expression pattern to the Yusenko dataset (Table 3—3). Renal carcinoma samples were also significantly higher (P-value = 2.08E-4, fold change: 7.8) in comparison to renal angiomyolipoma and renal oncocytoma (Table 3—3).

The Brain/CNS carcinoma datasets showed significant ABCC3 overexpression in glioblastoma in comparison to other Brain/CNS cancer samples (Figure 3—2, Table 3—3). The Sun Brain, Bredal Brain 2 and Liang Brain datasets showed ABCC3 expression in glioblastoma to be 4.63-fold (P-value = 1.08E-12), 4.38-fold (P-value = 1.28E-5) and 3.48-fold (P-value = 2.84E-7) that of other Brain/CNS cancers (Table 3—3). The overexpression of ABCC3 was greater in glioblastoma than in astrocytoma,

oligodendroglial tumours and mixed glioma across the Sun Brian, Bredal Brain 2 and Liang Brain datasets (Figure 3—2, Table 3—3, oncomine.org). The lymphoma, oesophageal and cervical cancer types also showed significant overexpression of ABCC3 within the respective datasets. The Basso Lymphoma dataset revealed that diffuse large b-cell lymphoma significantly overexpressed ABCC3 (P-value = 4.32E-5, fold change: 2.72) in comparison to burkitt's lymphoma, mantle cell lymphoma, primary effusion lymphoma and follicular lymphoma (Table 3—3, oncomine.org). The Kim Esophagus dataset showed a significant (P-value = 1.13E-7) 2.564-fold increase in ABCC3 expression in oesophageal cancer precursor samples in comparison to oesophageal carcinoma (Table 3—3, oncomine.org). While the Bittner Cervix dataset showed ABCC3 expression in cervical adenocarcinoma was significantly (P-value = 2.95E-5) higher (4.5-fold) than in cervical adenosquamous carcinoma, cervical small cell carcinoma and cervical SCC samples (Table 3—3, oncomine.org). Although not as distinct, the Bachtiary Cervix dataset followed the same expression pattern as the Bittner Cervix dataset, with cervical adenocarcinoma significantly expressing ABCC3 higher (P-value = 0.002, fold change:1.65) than that of cervical SCC (Table 3—3, oncomine.org). The more these expression patterns were repeated across datasets the greater the evidence that these patterns were a true representation of clinical expression patterns.

Table 3—3. Differential analysis of ABCC3 expression (Cancer vs Cancer (Histology))

| Cancer Type | Dataset | Cancer type comparisons | P-value | t-test | ABCC3 Expression (Under/Over) | Fold Change | Gene rank (%) | (n) | Reporter |
|---|---|---|---|---|---|---|---|---|---|
| Lung Cancer | Bhattacharjee Lung | Lung Cancer Type: Non-Small Cell Lung Carcinoma | 2.39E-06 | 5.49 | Over | 16.482 | 1% | 159 | 38261_at |
| Sarcoma | Segal Sarcoma 2 | Sarcoma Type: Malignant Peripheral Nerve Sheath Tumor | 1.92E-05 | 4.62 | Under | 9.533 | 1% | 47 | 1930_at |
| Bladder Cancer | Sanchez-Carbayo Bladder 2 | Bladder Urothelial Carcinoma Type: Superficial Bladder Cancer | 7.90E-14 | 9.65 | Over | 8.323 | 2% | 109 | 209641_s_at |
| Kidney Cancer | Yusenko renal | Kidney Cancer: Renal Carcinoma | 3.66E-05 | 5.66 | Over | 8.316 | 2% | 62 | 23062_x_at |
| Kidney Cancer | Bittner Renal | Kidney Cancer: Renal Carcinoma | 2.00E+04 | 5.98 | Over | 7.81 | 2% | 253 | 209641_s_at |

| | | | | | | | | | |
|---|---|---|---|---|---|---|---|---|---|
| Sarcoma | Nakayama Sarcoma | Sarcoma Type: Malignant Peripheral Nerve Sheath Tumor | 1.32E-14 | 14.33 | Over | 5.92 | 1% | 99 | 209641_s_at |
| Lung Cancer | TCGA Lung | Lung Cancer Type: Non-Small Cell Carcinoma | 5.43E-12 | 8.673 | Over | 5.207 | 1% | 187 | A_23_P207507 |
| Lung Cancer | Lee Lung | Lung Cancer Type: Non-Small Cell Lung Carcinoma | 2.59E-18 | 10.94 | Over | 5.003 | 1% | 138 | 209641_s_at |
| Brain/CNS Cancer | Sun Brain | Brain and CNS Cancer Type: Glioblastoma | 1.08E-12 | 7.68 | Over | 4.63 | 1% | 157 | 209641_s_at |
| Cervical Cancer | Bittner Cervix | Cervical Cancer Type: Cervical Adenocarcinoma | 2.95E-05 | 4.74 | Over | 4.503 | 1% | 35 | 209641_s_at |
| Brain/CNS Cancer | Bredel Brain 2 | Brain and CNS Cancer Type: Glioblastoma | 1.28E-05 | 4.95 | Over | 4.375 | 4% | 49 | IMAGE:781139 |
| Bladder Cancer | Stransky Bladder | Bladder Urothelial Carcinoma Type: Superficial Bladder Cancer | 4.33E-06 | 4.96 | Over | 3.959 | 2% | 57 | 38261_at |
| Lung Cancer | Bittner Lung | Lung Cancer Type: Non-Small Cell Lung Carcinoma | 1.61E-06 | 4.99 | Over | 3.52 | 1% | 101 | 209641_s_at |
| Brain/CNS Cancer | Liang Brain | Brain and CNS Cancer Type: Glioblastoma | 2.84E-07 | 6.50 | Over | 3.476 | 2% | 33 | AA429895 |
| Lung Cancer | Bild Lung | Lung Cancer Type: Non-Small Cell Lung Carcinoma | 2.41E-13 | 8.24 | Over | 3.275 | 1% | 111 | 230682_x_at |
| Bladder Cancer | Blaveri Bladder 2 | Bladder Urothelial Carcinoma Type: Superficial Bladder Cancer | 1.52E-09 | 7.13 | Over | 3.049 | 1% | 65 | AA429895 |
| Lymphoma | Basso Lymphoma | Mature B-cell Non-Hodgkin's Lymphoma Type: Diffuse Large B-Cell Lymphoma | 4.32E-05 | 4.10 | Over | 2.72 | 2% | 100 | 38261_at |
| Esophageal Cancer | Kim Esophagus | Esophageal Cancer Type: Esophageal Cancer Precursor | 1.13E-07 | 5.75 | Over | 2.564 | 1% | 100 | ILMN_177814 |

| | | | | | | | | | |
|---|---|---|---|---|---|---|---|---|---|
| Cervical Cancer | Bachtiary Cervix | Cervical Cancer Type: Cervical Adenocarcinoma | 0.002 | 5.190 | Over | 1.645 | 5% | 32 | 239217_x_at |
| Sarcoma | Segal Sarcoma 2 | Sarcoma Type: Gastrointestinal Stromal Tumor | 1.76E-06 | -5.35 | Under | -10.898 | 2% | 37 | 38261_at |

**Cancer versus Cancer (Multi-cancer datasets)**

Kidney carcinoma once again showed the highest overexpression of ABCC3 but this time in comparison to other cancers (Figure 3—2). The Su Multi-cancer dataset showed a significantly higher fold change (P-value = 1.80E-18, fold change: 24.93) in the kidney cancer in comparison to bladder, breast, colorectal, liver, lung, ovarian, pancreatic and prostate cancer samples (Table 3—4). The high ABCC3 expression in kidney datasets was also seen in the Bittner Multi-cancer and Garnett CellLine datasets which also showed fold changes of 3.83 (P-value = 4.45E-6) and 2.25 (P-value = 369E-22), respectively (Table 3—4). Strengthening the evidence of a strong relationship between ABCC3 overexpression and kidney carcinoma (Table 3—5). However, within this analysis the pancreatic carcinoma type showed the most consistently high ABCC3 overexpression (Figure 3—2 & Table 3—5). The Su Multi-cancer dataset showed ABCC3 expression in the kidney cancer type was followed closely by the significant ABCC3 expression of the pancreatic type resulting in a 24.53-fold increase in comparison to bladder, breast, colorectal, kidney, liver, lung, ovarian and prostate cancers (oncomine.org, Table 3—4). Furthermore, ABCC3 expression in the pancreatic cancer type in comparison across other cancer types within both the Ramaswamy Multi-cancer and Barretina CellLine datasets reveal fold changes of 14.93 (P-value = 2.89E-4) and 4.21 (P-value = 8.71E-12), respectively (Table 3—4). The Ramaswamy Multi-cancer datasets analysed the ABCC3 expression across bladder, brain/CNS, breast, colorectal, oesophageal, gastric, head and neck, kidney, leukaemia, liver, lung, lymphoma, melanoma, myeloma, ovarian, pancreatic, prostate and sarcoma cancer samples (oncomine.org). This broad range of cancer types analysed showed that pancreatic cancer on average exhibited higher ABCC3 expression in comparison to other cancer types including kidney carcinoma (Table 3—4). The average fold change across datasets were 10.34-fold and 14.56-fold in kidney and pancreatic cancer datasets, respectively.

Colorectal carcinoma was the next highest overexpressing ABCC3 cancer type (Table 3—4). Across the Su Multi-cancer, Gyorffy CellLine 2, Bitnner Multi-cancer and Garnett CellLine datasets colorectal cancer showed a significant overexpression of ABCC3 by 16.8-fold (P-value = 1.8E-13), 13.8-fold (P-value = 5.82E-5), 2.41-fold (P-value = 8.44E-62) and 2.25-fold (P-value = 1.19E-6), respectively (Table 3—4). Much like pancreatic carcinoma, colorectal cancer also demonstrated high and consistent

expression of ABCC3 in comparison to other cancers (Table 3—4). Lastly within the Barretina CellLine and Bittner Multi-cancer datasets, oesophageal cancer showed significant ABCC3 in overexpression by 2.03-fold (P-value = 1.54E-5) and 1.41-fold (P-value = 4.6E-4). The cancer types that showed significant ABCC3 under expression in comparison to other cancers were breast, leukaemia, prostate, melanoma, ovarian, prostate, sarcoma, lymphoma and myeloma cancer (Table 3—4). The Su Multi-cancer dataset showed that breast cancer was the lowest ABCC3 expressing cancer within the dataset with -19.11-fold under expression in comparison to other cancers (P-value = 9.43E-10) (Table 3—4 & Figure 3—2). The Ramaswamy Multi-cancer 2 and Yu Multi-cancer datasets also showed breast cancer ABCC3 under expression, with -5.3-fold and -2.59-fold, respectively (Table 3—4).

Table 3—4. Differential analysis of ABCC3 expression (Cancer vs Cancer (Multi-cancer))

| Cancer Type | Dataset | Cancer type comparisons | P-value | t-test | Expression (Under/Over) | Fold Change | Gene rank (%) | n | Reporter |
|---|---|---|---|---|---|---|---|---|---|
| Kidney Cancer | Su Multi-cancer | Cancer Type: Kidney Cancer | 1.80E-18 | 11.67 | Over | 24.928 | 1% | 162 | 38261_at |
| Pancreatic Cancer | Su Multi-cancer | Cancer Type: Pancreatic Cancer | 4.86E-09 | 9.96 | Over | 24.526 | 1% | 162 | 38261_at |
| Colorectal Cancer | Su Multi-cancer | Cancer Type: Colorectal | 1.80E-13 | 8.65 | Over | 16.796 | 1% | 162 | 38261_at |
| Pancreatic Cancer | Ramaswamy Multi-cancer | Cancer Type: Pancreatic Cancer | 2.89E-04 | 4.56 | Over | 14.93 | 4% | 169 | U66674_at |
| Colorectal Cancer | Gyorffy CellLine 2 | Cancer Type: Colorectal | 5.82E-05 | 5.89 | Over | 13.793 | 1% | 16 | AA429895 |
| Pancreatic Cancer | Barretina CellLine | Cancer Type: Pancreatic Cancer | 8.71E-12 | 8.66 | Over | 4.206 | 2% | 875 | 209641_s_at |
| Kidney Cancer | Garnett CellLine | Cancer Type: Kidney Cancer | 4.45E-06 | 5.73 | Over | 3.831 | 3% | 690 | 209641_s_at |
| Colorectal Cancer | Bittner Multi-cancer | Cancer Type: Colorectal | 8.44E-62 | 17.92 | Over | 2.405 | 3% | 1468 | 230682_x_at |
| Colorectal Cancer | Garnett CellLine | Cancer Type: Colorectal | 1.19E-06 | 5.42 | Over | 2.395 | 5% | 690 | 209641_s_at |

| | | | | | | | | | |
|---|---|---|---|---|---|---|---|---|---|
| Kidney Cancer | Bittner Multi-cancer | Cancer Type: Kidney Cancer | 3.69E-22 | 10.15 | Over | 2.249 | 6% | 1468 | 209641_s_at |
| Esophageal Cancer | Barretina CellLine | Cancer Type: Esophageal Cancer | 1.54E-05 | 5.00 | Over | 2.031 | 4% | 875 | 230682_x_at |
| Esophageal Cancer | Bittner Multi-cancer | Cancer Type: Esophageal Cancer | 4.60E-04 | 5.47 | Over | 1.414 | 1% | 1468 | 214979_at |
| Myeloma | Wooster | Cancer Type: Myeloma | 3.73E-04 | -6.19 | Under | -1.896 | 6% | 298 | 209641_s_at |
| Myeloma | Garnett CellLine | Cancer Type: Myeloma | 1.38E-13 | -11.75 | Under | -1.909 | 2% | 690 | 209641_s_at |
| Lymphoma | Garnett CellLine | Cancer Type: Lymphoma | 5.82E-41 | -14.65 | Under | -1.966 | 1% | 690 | 209641_s_at |
| Leukemia | Garnett CellLine | Cancer Type: Leukemia | 3.14E-39 | -14.31 | Under | -2.037 | 2% | 690 | 209641_s_at |
| Ovarian Cancer | Bittner Multi-cancer | Cancer Type: Ovarian | 7.53E-11 | -6.74 | Under | -2.115 | 6% | 1468 | 209641_s_at |
| Leukemia | Shankavaram CellLine 2 | Cancer Type: Leukemia | 1.90E-07 | -5.86 | Under | -2.526 | 1% | 51 | 1930_at |
| Breast Cancer | Yu Multi-cancer | Cancer Type: Breast Cancer | 2.81E-08 | -5.79 | Under | -2.585 | 7% | 270 | 209641_s_at |
| Myeloma | Barretina CellLine | Cancer Type: Myeloma | 1.65E-36 | -17.96 | Under | -2.909 | 2% | 875 | 209641_s_at |
| Lymphoma | Barretina CellLine | Cancer Type: Lymphoma | 9.64E-72 | -21.31 | Under | -3.186 | 1% | 875 | 209641_s_at |
| Lymphoma | Bittner Multi-cancer | Cancer Type: Lymphoma | 7.17E-06 | -5.81 | Under | -3.207 | 5% | 1468 | 230682_x_at |
| Leukemia | Barretina CellLine | Cancer Type: Leukemia | 1.50E-105 | -25.23 | Under | -3.517 | 1% | 875 | 209641_s_at |
| Melanoma | Shankavaram CellLine | Cancer Type: Melanoma | 1.65E-08 | -6.40 | Under | -3.614 | 1% | 59 | 209641_s_at |
| Melanoma | Compendia CellLine | Cancer Type: Melanoma | 1.45E-08 | -3.65 | Under | -3.646 | 1% | 59 | 209641_s_at |

| | | | | | | | | | |
|---|---|---|---|---|---|---|---|---|---|
| Sarcoma | Bittner Multi-cancer | Cancer Type: Sarcoma | 5.51E-13 | -9.26 | Under | -4.332 | 2% | 1468 | 209641_s_at |
| Prostate Cancer | Bittner Multi-cancer | Cancer Type: Prostate Cancer | 1.60E-20 | -12.89 | Under | -4.525 | 2% | 1468 | 209641_s_at |
| Ovarian Cancer | Su Multi-cancer | Cancer Type: Ovarian | 3.38E-04 | -3.63 | Under | -5.254 | 6% | 162 | 38261_at |
| Breast Cancer | Ramaswamy Multi-cancer 2 | Cancer Type: Breast Cancer | 3.60E-03 | -1.94 | Under | -5.3 | 5% | 54 | U66674_at |
| Melanoma | Shankavaram CellLine 2 | Cancer Type: Melanoma | 4.73E-13 | -9.23 | Under | -13.921 | 1% | 60 | 38261_at |
| Prostate Cancer | Su Multi-cancer | Cancer Type: Prostate Cancer | 1.36E-10 | -7.33 | Under | -14.076 | 4% | 162 | 38261_at |
| Leukemia | Ramaswamy Multi-cancer | Cancer Type: Leukemia | 2.65E-12 | -8.47 | Under | -19.08 | 9% | 169 | U66674_at |
| Breast Cancer | Su Multi-cancer | Cancer Type: Breast Cancer | 9.43E-10 | -7.24 | Under | -19.114 | 1% | 162 | 38261_at |

Following breast cancer, the Ramaswamy Multi-cancer dataset showed leukaemia cancer as the next lowest ABCC3 expressing cancer type with -19.08-fold (P-value = 2.65E-12) under expression (Table 3—4 & Figure 3—2). The Barrentina CellLine, Shankavaram CellLine 2 and the Garnett CellLine datasets also showed ABCC3 reduced expression in leukaemia cancer types by -3.52-fold (P-value = 1.50E-105), -2.53-fold (P-value = 1.90E-7) and -2.04-fold (P-value = 3.14E-39), respectively (Table 3—4). The other cancer types prostate, melanoma and ovarian cancers all showed significantly lower expression of ABCC3 with -14.08-fold (P-value = 1.36E-10), -13.92-fold (P-value = 4.73E-13) and -5.25-fold (P-value = 3.38E-4), respectively (Table 3—4). The sarcoma, lymphoma and myeloma cancer types ranged in under expression from -4.33-fold to -1.9-fold in comparison to other cancers (Table 3—4). Suggesting that these cancers would not perform well under ABCC3 targeted therapies.

Table 3—5. Top ABCC3 Overexpresing cancer types across ONCOMINE analyses. The top three ABCC3 overexpressing cancer types based on a ranking system (Supplementary Table 1).

| Cancer Types | Cancer vs Normal | Cancer vs Cancer (Histology) | Cancer vs Cancer (Multi-Cancer) | Outlier Analysis | Total Score |
|---|---|---|---|---|---|
| Kidney Cancer | 5 | | 4 | | 9 |
| Pancreatic | | | 4 | 4 | 8 |
| Lung Cancer | | 5 | | | 5 |

| | | | | | | |
|---|---|---|---|---|---|---|
| Bladder | 2 | 2 | | | | 4 |
| Lymphoma | 3 | | | | | 3 |
| Melanoma | | | | | 3 | 3 |
| Colorectal | | | 2 | | | 2 |
| Brain/CNS Cancer | | | | | 1 | 1 |

**Heterogeneous ABCC3 Expression within Cancer Types (Outlier Analysis)**

The expression of ABCC3 within a cancer type may not be homogenous and some cancers may have a subset of samples that overexpresses ABCC3. Outlier analysis within the ONCOMINE platform endeavours to assess the significance of this type of heterogenous expression with the use of COPA analysis [194]. The cancer dataset that showed the highest COPA score (35.396) was a pancreatic cancer dataset (oncomine.org, **Error! Reference source not found.**). The TCGA pancreas dataset showed high ABCC3 expression in the 95$^{th}$ percentile across a subset of both the pancreatic adenocarcinoma and pancreatic ductal adenocarcinoma samples (oncomine.org, **Error! Reference source not found.**). The remaining pancreatic datasets Ishikawa Pancreas and Collison Pancreas datasets resulted in COPA scores of 3.821 and 2.1151, respectively (Table 3—6). These results would suggest that there may be some subsets of pancreatic cancer that greatly overexpress ABCC3 above that of other pancreatic samples. COPA scores ranged from 28.757 to 11.104 in the Lin CellLine3 (95$^{th}$ percentile), Segal Sarcoma 2 (75$^{th}$ percentile), Wang Neuroblastoma (90$^{th}$ percentile), Imadome Cervix (95$^{th}$ percentile), Welsh Prostate (75$^{th}$ percentile), Jones Renal (95$^{th}$ percentile) and Lenburg Renal (95$^{th}$ percentile) datasets (Table 3—6). The remaining datasets resulted in positive COPA scores spanning several cancer types. These cancer types resulted in COPA scores ranging from 9.83 to 1.213 (Table 3—6). This showed that ABCC3 expression was highly heterogenous across many cancer types and may be an ideal candidate for targeted therapies.

Tomlins et al., developed the COPA analysis and did not record COPA scores below 2, as the closer to zero the closer to the median and therefore the less outlying the expression profile [266]. The Nakayama Sarcoma, Zhan Myeloma 2, Sanchez-Carbayo Bladder 2, Palanisamy Gastric, Compagno Lymphoma, Dyrskjot Bladder 4, Ballester Lymphoma, Takeno Gastric and Lin Colon 2 datasets all resulted in COPA scores below 2 (Table 3—6). Suggesting weak outlier expression profiles and although the Tian Myeloma, Su Esophagus 2, Stransky Bladder, Biewenga Cervix, Estilo Head-Neck, Giordano Thyroid, Gaedcke Colorectal, Jorissen Colorectal 3 and Nutt Brain datasets resulted in negative COPA scores these did not exceed -2 (Table 3—6). Therefore, these datasets also showed weak outlier expression profile.

The more the expression levels deviate from the median the COPA score the more evidence of heterogeneity in both positive and negative directions. The lymphoma carcinoma Fan CellLine dataset showed the greatest deviation in the negative direction with a COPA score of -11.11 (Table 3—6 & **Error! Reference source not found.**). The remaining datasets including the Khatua Brain and Hao Esophagus also showed strong outlier expression in the lower 25$_{th}$ percentile resulting in COPA scores ranging from -10.709 to -2.084, respectively (Table 3—6 & **Error! Reference source not found.**). The range of COPA scores and strong outlier deviations although distinct also require further interrogation. Irrespective of COPA scores, datasets showed ABCC3 overexpression, under expression or a mixed population of ABCC3 expressing samples (Table 3—6). Excluding the samples that fall between the 2 and -2 threshold for COPA scores, 76% (65/86) of the databases showed both ABCC3 over and under expressing populations (Table 3—6). High COPA scores would be expected from expression patterns that showed some samples under expressing and some overexpressing ABCC3 (oncomine.org, Table 3—6).

However, some datasets also showed exclusively ABCC3 overexpression and some showed exclusive ABCC3 under expression (Table 3—6). Some datasets overexpressed ABCC3 and resulted in a positive COPA score, under expressed ABCC3 and resulted in a negative COPA score, overexpressed ABCC3 but resulted in a negative COPA score or under expressed ABCC3 but resulted in a positive COPA score (Table 3—6). Firstly, the Imadome Cervix, Lenburg Renal, Smith Colorectal, Smith Colorectal 2, Tan Renal and Collison Pancreas datasets all overexpressed ABCC3 and showed positive COPA results (Table 3—6). These datasets showed ABCC3 overexpression with some samples significantly overexpressing ABCC3 above that of the datasets median ABCC3 expression. Conversely, the Smith Skin, Symmans Breast 2, Nakayama Sarcoma 2 and Fan CellLine datasets all show exclusive ABCC3 under expression and negative COPA scores (Table 3—6). These datasets much like the previous datasets showed subsets that appear to extend to the extremes of ABCC3 expression (Table 3—6). Within these datasets that already showed under expressed ABCC3 there was evidence of a subset of samples that under expressed ABCC3 significantly lower than the dataset median (Table 3—6). These results showed ABCC3 heterogeneity samples under/overexpress ABCC3 in the extreme ranges of ABCC3 expression in both negative and positive directions.

Wang Neuroblastoma, Lenburg Renal, During Leukaemia and Koboyashi Sarcoma datasets showed under expression of ABCC3 and yet still yielded a positive COPA score (Table 3—6). Although the datasets exclusively showed ABCC3 under expression and most of these samples exhibited ABCC3 under expression at relatively

strong levels, a small subset of samples significantly showed only weakly ABCC3 under expression (oncomine.org, Table 3—6).

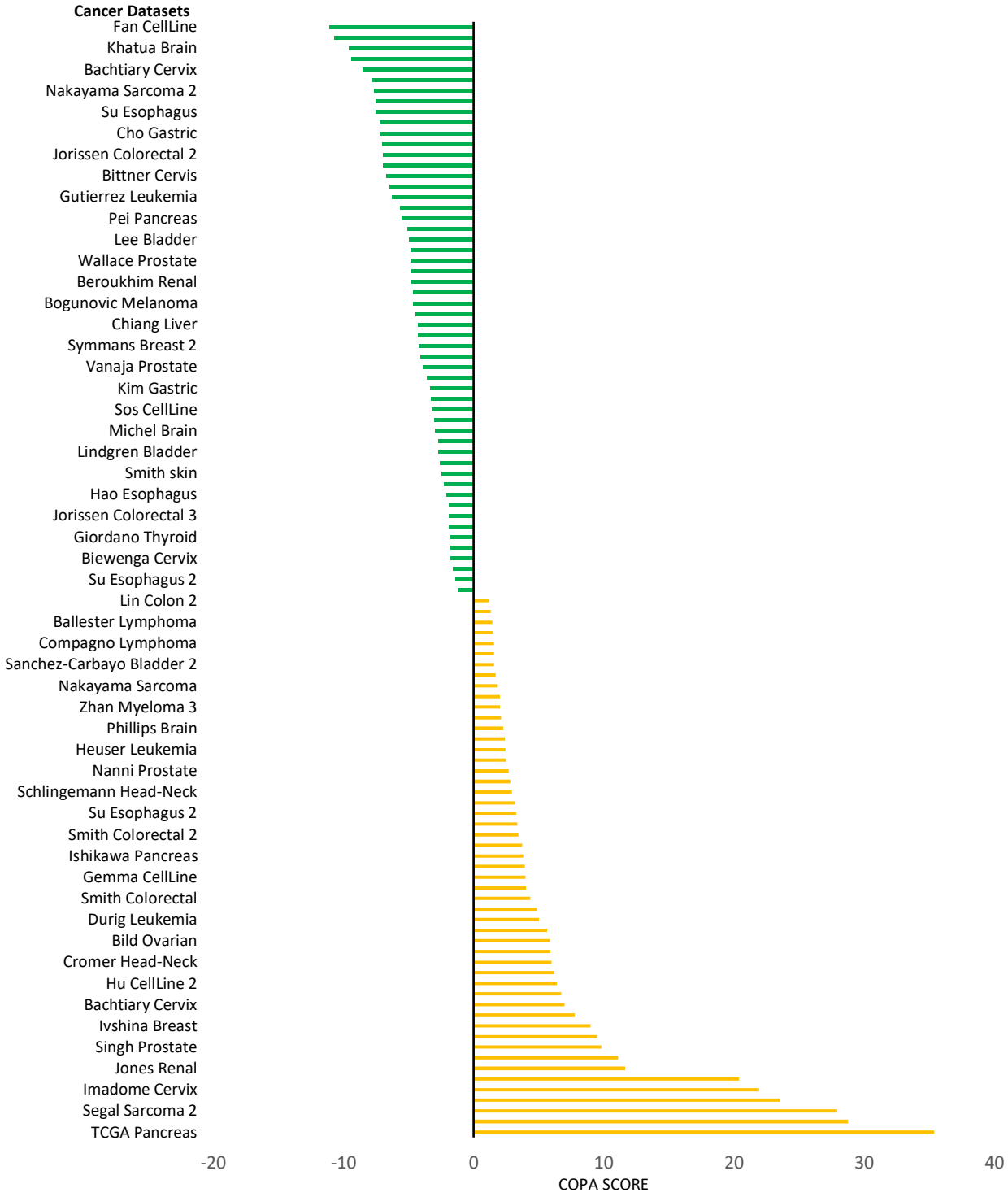


Figure 3—3. Outlier Analysis. The consistency of heterogenous ABCC3 expression across cancerous subsets was analysed. The top three databases that showed either a significant increase or decrease in the COPA score across cancer types was examined and the COPA score was extracted. The list of all the COPA scores across all databases were shown. Green represents the negative COPA scores and the orange represents the positive COPA scores.

These weakly under expressing ABCC3 samples lay within the upper 75th percentiles and were distinct enough from the median to give evidence of an outlying profile and the corresponding COPA score (Table 3—6). Conversely, the Roessler Liver 2, Vanaja Prostate, Ishikawa Pancreas, Chiang Liver, Lee Bladder, Pei Pancreas and Cho Gastric datasets showed negative COPA scores, while overexpressing ABCC3 (Table 3—6). These datasets had samples that showed high ABCC3 overexpression, yet within the dataset there were some samples that only weakly overexpressed ABCC3 below the 25th percentile (oncomine.org). These datasets highlighted data that consistently showed strong ABCC3 overexpression or under expression, with some samples showing less strong ABCC3 expression.

Table 3—6. Outlier analysis of ABCC3 expression across cancer datasets. The threshold for COPA scoring as extrapolated from the Tomlin et al., was shown between 2 and -2 by solid lines [266].

| Cancer Type | Dataset | Expression Over/Under | Gene Rank (%) | Percentile | COPA score | Reporter | (n) |
|---|---|---|---|---|---|---|---|
| Pancreatic Cancer | TCGA Pancreas | Both | 8% | 95th | 35.396 | 17-046095638 | 100 |
| Melanoma | Lin CellLine 3 | Both | 1% | 95th | 28.757 | 209641_s_at | 94 |
| Sarcoma | Segal Sarcoma 2 | Both | 3% | 75th | 27.933 | 38261_at | 51 |
| Brain/CNS Cancer | Wang Neuroblastoma | Under | 1% | 90th | 23.526 | 1930_at | 102 |
| Cervical Cancer | Imadome Cervix | Over | 3% | 95th | 21.926 | 354061 | 160 |
| Prostate Cancer | Welsh Prostate | Under | 3% | 75th | 20.387 | 38261_at | 34 |
| Kidney Cancer | Jones Renal | Both | 1% | 95th | 11.638 | 214979_at | 92 |
| Kidney Cancer | Lenburg Renal | Over | 7% | 95th | 11.104 | 230682_x_at | 18 |
| Prostate Cancer | Singh Prostate | Both | 4% | 90th | 9.828 | 38261_at | 102 |
| Ovarian Cancer | Jazaeri Ovarian | Both | 1% | 95th | 9.502 | IMAGE:781139 | 61 |
| Breast Cancer | Ivshina Breast | Both | 1% | 95th | 8.999 | 209641_s_at | 289 |
| Esophageal Cancer | Su Esophagus | Both | 6% | 95th | 7.783 | IMAGE:781139 | 19 |
| Cervical Cancer | Bachtiary Cervix | Both | 3% | 75th | 7 | 230682_x_at | 33 |
| Melanoma | Hoek Melanoma | Both | 1% | 90th | 6.74 | 209641_s_at | 45 |
| Melanoma | Hu CellLine 2 | Both | 1% | 95th | 6.409 | 17-046095638 | 45 |
| Breast Cancer | Schmidt Breast | Both | 1% | 90th | 6.181 | 209641_s_at | 200 |
| Head and Neck Cancer | Cromer Head-Neck | Both | 2% | 95th | 5.986 | 1930_at | 38 |
| Breast Cancer | Wang Breast | Both | 1% | 90th | 5.882 | 209641_s_at | 286 |
| Ovarian Cancer | Bild Ovarian | Both | 1% | 90th | 5.843 | 209641_s_at | 153 |

| | | | | | | | |
|---|---|---|---|---|---|---|---|
| Head and Neck Cancer | Ginos Head-Neck | Both | 1% | 90th | 5.643 | 209641_s_at | 54 |
| Leukemia | Durig Leukemia | Under | 1% | 75th | 5.033 | 209641_s_at | 14 |
| Cervical Cancer | Scotto Cervix 2 | Both | 1% | 90th | 4.88 | 209641_s_at | 66 |
| Colorectal Cancer | Smith Colorectal | Over | 9% | 95th | 4.357 | 209641_s_at | 177 |
| Lung Cancer | Su Lung | Both | 1% | 75th | 4.029 | 209641_s_at | 66 |
| Lung Cancer | Gemma CellLine | Both | 1% | 75th | 3.991 | 209641_s_at | 29 |
| Leukemia | TCGA Leukemia | Both | 1% | 90th | 3.935 | 209641_s_at | 197 |
| Pancreatic Cancer | Ishikawa Pancreas | Both | 3% | 90th | 3.821 | 239217_x_at | 49 |
| Ovarian Cancer | Schaner Ovarian | Both | 2% | 90th | 3.746 | IMAGE:781139 | 44 |
| Colorectal Cancer | Smith Colorectal 2 | Over | 10% | 90th | 3.437 | 230682_x_at | 55 |
| Lung Cancer | Raponi Lung | Both | 1% | 75th | 3.362 | 209641_s_at | 130 |
| Esophageal Cancer | Su Esophagus 2 | Both | 10% | 90th | 3.265 | 209641_s_at | 106 |
| Lymphoma | Dave Lymphoma | Both | 5% | 90th | 3.199 | 239217_x_at | 191 |
| Head and Neck Cancer | Schlingemann Head-Neck | Both | 3% | 75th | 2.95 | 209641_s_at | 12 |
| Kidney Cancer | Tan Renal | Over | 1% | 75th | 2.832 | 209641_s_at | 30 |
| Prostate Cancer | Nanni Prostate | Both | 1% | 75th | 2.684 | 209641_s_at | 30 |
| Sarcoma | Kobayashi Sarcoma | Under | 3% | 75th | 2.489 | 214979_at | 27 |
| Leukemia | Heuser Leukemia | Both | 1% | 75th | 2.449 | AA429895 | 35 |
| Brain/CNS Cancer | Sun Brain | Both | 1% | 75th | 2.411 | 209641_s_at | 180 |
| Brain/CNS Cancer | Phillips Brain | Both | 1% | 75th | 2.257 | 209641_s_at | 100 |
| Pancreatic Cancer | Collisson Pancreas | Over | 5% | 75th | 2.1151 | 239217_x_at | 27 |
| Myeloma | Zhan Myeloma 3 | Both | 2% | 75th | 2.02 | 209641_s_at | 78 |
| Myeloma | Zhou Myeloma | Both | 1% | 75th | 2.018 | 239217_x_at | 115 |
| Sarcoma | Nakayama Sarcoma | Both | 1% | 75th | 1.875 | 209641_s_at | 105 |
| Myeloma | Zhan Myeloma 2 | Both | 2% | 75th | 1.684 | 239217_x_at | 414 |
| Bladder Cancer | Sanchez-Carbayo Bladder 2 | Both | 3% | 75th | 1.588 | 209641_s_at | 157 |
| Gastric Cancer | Palanisamy Gastric | Both | 8% | 75th | 1.582 | 17046095638 | 93 |
| Lymphoma | Compagno Lymphoma | Under | 5% | 75th | 1.563 | 214979_at | 136 |
| Bladder Cancer | Dyrskjot Bladder 4 | Both | 9% | 75th | 1.492 | AW848421 | 29 |
| Lymphoma | Ballester Lymphoma | Both | 9% | 75th | 1.427 | IMAGE:208097 | 59 |

| | | | | | | | |
|---|---|---|---|---|---|---|---|
| Gastric Cancer | Takeno Gastric | Both | 4% | 75th | 1.323 | AGhsB030810 | 141 |
| Colorectal Cancer | Lin Colon 2 | Both | 9% | 75th | 1.213 | AF085692 | 149 |
| Myeloma | Tian Myeloma | Both | 18% | 25th | -1.241 | 1930_at | 173 |
| Esophageal Cancer | Su Esophagus 2 | Over | 2% | 25th | -1.4 | 239217_x_at | 106 |
| Bladder Cancer | Stransky Bladder | Both | 4% | 25th | -1.578 | 38261_at | 57 |
| Cervical Cancer | Biewenga Cervix | Both | 2% | 25th | -1.755 | A_23_P207507 | 45 |
| Head and Neck Cancer | Estilo Head-Neck | Both | 4% | 25th | -1.782 | 38261_at | 58 |
| Head and Neck Cancer | Giordano Thyroid | Both | 1% | 25th | -1.787 | 209641_s_at | 99 |
| Colorectal Cancer | Gaedcke Colorectal | Over | 1% | 25th | -1.883 | A_23_P207507 | 130 |
| Colorectal Cancer | Jorissen Colorectal 3 | Both | 2% | 25th | -1.907 | 209641_s_at | 154 |
| Brain/CNS Cancer | Nutt Brain | Both | 4% | 25th | -1.922 | 1930_at | 50 |
| Esophageal Cancer | Hao Esophagus | Both | 2% | 25th | -2.084 | IMAGE:781139 | 48 |
| Lung Cancer | Zhou CellLine | Both | 1% | 25th | -2.26 | 209641_s_at | 44 |
| Melanoma | Smith skin | Under | 4% | 25th | -2.491 | 214979_at | 18 |
| Prostate Cancer | Bittner Prostate | Both | 1% | 25th | -2.608 | 230682_x_at | 60 |
| Bladder Cancer | Lindgren Bladder | Both | 9% | 10th | -2.698 | AA429895 | 75 |
| Head and Neck Cancer | FriersonHF Salivary-gland | Both | 8% | 25th | -2.725 | 1930_at | 22 |
| Brain/CNS Cancer | Michel Brain | Both | 10% | 10th | -2.975 | 1930_at | 29 |
| Lymphoma | Shaknovich Lymphoma | Both | 1% | 25th | -3.031 | 230682_x_at | 69 |
| Lung Cancer | Sos CellLine | Both | 1% | 10th | -3.189 | 17-046095638 | 84 |
| Liver Cancer | Roessler Liver 2 | Over | 3% | 10th | -3.311 | 209641_s_at | 445 |
| Gastric Cancer | Kim Gastric | Both | 8% | 5th | -3.366 | 209641_s_at | 123 |
| Melanoma | Hoeflich CellLine 2 | Both | 10% | 10th | -3.569 | 239217_x_at | 51 |
| Prostate Cancer | Vanaja Prostate | Over | 2% | 10th | -3.892 | 239217_x_at | 40 |
| Breast Cancer | Weigelt Breast | Both | 7% | 10th | -4.109 | AA429895 | 16 |
| Breast Cancer | Symmans Breast 2 | Under | 6% | 10th | -4.196 | 214979_at | 103 |
| Pancreatic Cancer | Ishikawa Pancreas | Over | 6% | 10th | -4.291 | 230682_x_at | 49 |
| Liver Cancer | Chiang Liver | Over | 5% | 5th | -4.3 | 209641_s_at | -4.3 |
| Myeloma | Mulligan Myeloma | Both | 4% | 5th | -4.482 | 214979_at | 264 |

| | | | | | | | |
|---|---|---|---|---|---|---|---|
| Melanoma | Bogunovic Melanoma | Both | 10% | 10th | -4.627 | 239217_x_at | 44 |
| Leukemia | TCGA Leukemia | Both | 2% | 10th | -4.647 | 214979_at | 197 |
| Kidney Cancer | Beroukhim Renal | Both | 1% | 10th | -4.767 | 209641_s_at | 70 |
| Gastric Cancer | Ooi Gastric | Both | 2% | 10th | -4.772 | 209641_s_at | 31 |
| Prostate Cancer | Wallace Prostate | Both | 2% | 10th | -4.821 | 209641_s_at | 89 |
| Pancreatic Cancer | Iacobuzio-Donahue Pancreas 2 | Both | 10% | 5th | -4.823 | IMAGE:781139 | 36 |
| Bladder Cancer | Lee Bladder | Over | 3% | 5th | -4.942 | ILMN_1677814 | 256 |
| Ovarian Cancer | Bittner Ovarian | Both | 5% | 5th | -5.101 | 214979_at | 241 |
| Pancreatic Cancer | Pei Pancreas | Over | 4% | 5th | -5.534 | 230682_x_at | 52 |
| Breast Cancer | Bittner Breast | Both | 4% | 5th | -5.65 | 214979_at | 336 |
| Leukemia | Gutierrez Leukemia | Both | 4% | 5th | -6.28 | 214979_at | 43 |
| Sarcoma | Bittner Endometrium | Both | 2% | 5th | -6.481 | 214979_at | 177 |
| Cervical Cancer | Bittner Cervix | Both | 8% | 5th | -6.7 | 214979_at | 36 |
| Lung Cancer | Bittner Lung | Both | 1% | 5th | -6.967 | 214979_at | 109 |
| Colorectal Cancer | Jorissen Colorectal 2 | Both | 1% | 5th | -6.987 | 214979_at | 155 |
| Kidney Cancer | Bittner Renal | Both | 1% | 5th | -7.011 | 239217_x_at | 256 |
| Gastric Cancer | Cho Gastric | Over | 1% | 5th | -7.213 | ILMN_1677814 | 90 |
| Esophageal Cancer | Su Esophagus | Both | 4% | 5th | -7.502 | IMAGE:781139 | 19 |
| Kidney Cancer | TCGA Renal | Both | 1% | 5th | -7.521 | A_23_P207507 | 88 |
| Sarcoma | Nakayama Sarcoma 2 | Under | 1% | 10th | -7.649 | 214979_at | 34 |
| Lymphoma | Hartmann Lymphoma | Both | 1% | 5th | -7.795 | 214979_at | 64 |
| Cervical Cancer | Bachtiary Cervix | Both | 3% | 5th | -8.5 | 230682_x_at | 33 |
| Leukemia | Raponi Leukemia | Both | 1% | 5th | -9.38 | 214979_at | 34 |
| Brain/CNS Cancer | Khatua Brain | Both | 4% | 10th | -9.594 | 1930_at | 13 |
| Liver Cancer | Liao Liver | Both | 4% | 5th | -10.709 | 230682_x_at | 13 |
| Lymphoma | Fan CellLine | Under | 1% | 5th | -11.11 | 214979_at | 21 |

## Coexpression Analysis

The coexpression analysis was an important part of the ONCOMINE platform as it allows the user to assess genes that are expressed alongside ABCC3 [194]. Possible targets that modulate ABCC3 expression were investigated using the coexpression analysis [36, 197]. There was a number of targets that strongly correlated with ABCC3 expression (Table 3—7). Members of the WNT signalling pathway, sphingosine-1-phosphate pathway and p53-signalling pathway also showed significant correlation with ABCC3 overexpression (Table 3—7). The sphingosine-1-phoshate receptors S1PR1 and S1PR3 where all found to be upregulated within the ABCC3 overexpressing datasets (Table 3—7). The increase in S1PR1 overexpression ranged from 1.67-fold (Beroukhim Renal: Non-Hereditary Clear Cell Renal Cell Carcinoma vs. Normal) to 6.71-fold (Su Multi-cancer: kidney cancer type) (Supplementary Table 2). While S1PR3 showed a 1.53-fold increase in expression in the Bild Lung dataset (comparing Lung cancer type: Non-small Cell Lung Carcinoma) (Supplementary Table 2).

Table 3—7. The identified targets that were also upregulated in ABCC3 overexpressing datasets across previously associated pathways. The top seven datasets which showed the highest gene ranks for ABCC3 where compared with pathways that showed ABCC3 modulation in literature (Supplementary Table 2). The frequency at which each target appeared across the seven datasets was recorded.

| ABCC3 & WNT signaling pathway | | ABCC3 & p53 signaling pathway | | ABCC3 & S1P receptor signaling pathway | |
|---|---|---|---|---|---|
| Gene | Frequency | Gene | Frequency | Gene | Frequency |
| CSNK1A1 | 5 | ATM | 3 | S1PR1 | 6 |
| CCND1 | 4 | CCND1 | 3 | S1PR3 | 1 |
| PPARD | 4 | BAX | 3 | | |
| FZD1 | 4 | BCL2 | 2 | | |
| MYC | 3 | TP53 | 2 | | |
| HNF1A | 2 | RB1 | 1 | | |
| SMAD4 | 2 | CDKN1A | 1 | | |
| MAP3K7 | 2 | TIMP3 | 1 | | |
| CNSK2A1 | 1 | GADD45A | 1 | | |
| CTNNB1 | 1 | PCNA | 1 | | |
| TLE1 | 1 | CDK2 | 1 | | |
| PPP2CA | 1 | CDK4 | 1 | | |
| CSNK1D | 1 | MDM2 | 1 | | |

In all datasets except for Bild Lung dataset, S1PR1 was found to be upregulated (Supplementary Table 2). These results suggest that S1PR1 overexpression may be linked with ABCC3 overexpression (Table 3—7).

The more complex WNT signalling pathway and p53 signalling pathway resulted in a greater number of targets found to be upregulated in ABCC3 overexpressing datasets (Table 3—7 & Supplementary Table 2). The results showed that in the presence of ABCC3 overexpression casein kinase 1 alpha 1 (CSNK1A1), cyclin D1 (CCND1), peroxisome proliferator-activated receptor delta (PPARD), frizzled homolog 1 (FZD1),

myelocytomatosis viral oncogene (MYC), HNF1A, SMAD4, mitogen-activated protein kinase 7 (MAP3K7), casein kinase 2 Alpha 1 (CNSK2A1), catenin (cadherin-associated protein) beta 1 (CTNNB1), TLE1, PPP2CA and CSNK1D were all upregulated (oncomine, Table 3—7).

Due to the broad nature of both the WNT signalling pathway and the p53 signalling pathway some overlap would be expected. CCND1 was the only target found common to both pathways (Table 3—7). The comparison of the p53 signalling pathway and ABCC3 overexpression also revealed the upregulation of mutated ataxia-telangiectasia (ATM), BAX, BCL2, p53, retinoblastoma 1 (RB1), cyclin-dependent kinase inhibitor 1A (CDKN1A), TIMP metallopeptidase inhibitor 3 (TIMP3), growth arrest and DNA-damage-inducible alpha (GADD45A), proliferating cell nuclear antigen (PCNA), cyclin-dependent kinase 2 (CDK2), cyclin-dependent kinase 4 (CDK4) and MDM2 p53 binding protein (MDM2). The frequency at which a target regularly appeared during this analysis bolsters the evidence that there was a correlation between that target and ABCC3 (Table 3—7).

The ONCOMINE platform also identified a number of targets whose expression strongly correlated (>0.7 correlation score) with the expression of ABCC3 (Table 3—8). Interestingly, very few of the gene targets were repeated across the datasets (Table 3—8). The only target to repeat across the coexpression analyses was the keratin protein 7 (KRT7) which was shown in both the Frasor CellLine 2 and Stansky Bladder datasets (Table 3—8). Furthermore, the cytoband locations of the coexpressing genes varied greatly, suggesting that ABCC3 expression may impact a wider range of genes and their corresponding functions than previously thought (Table 3—8).

Table 3—8. ABCC3 Coexpression Analysis across Cancer types. The top three coexpressing genes from the top three cancer datasets (Table 3—5). A coexpression correlation threshold of 0.7 was used to eliminate genes that aren't highly correlated with ABCC3.

| Cancer Type | Dataset | Coexpression correlation | Gene | Cytoband | Reporter | n |
|---|---|---|---|---|---|---|
| Head and Neck | Pramoonjago CellLine | 0.998 | CLDN7 | 17p13 | 202790_at | 6 |
| Head and Neck | Dohda CellLine | 0.998 | LHX4 | 1q25.2 | 1553157_at | 6 |
| Head and Neck | Pramoonjago CellLine | 0.997 | LRRN2 | 1q32.1 | 216167_at | 6 |
| Head and Neck | Pramoonjago CellLine | 0.996 | PRSS22 | 16p13.3 | 205847_at | 6 |
| Head and Neck | Dohda CellLine | 0.99 | CSHL | 17q42.2 | 208293_x_at | 6 |
| Head and Neck | Dohda CellLine | 0.985 | SARS2 | 19q13.2 | 218702_at | 6 |
| Colorectal | Connolly CellLine | 0.949 | CALCOCO2 | 17q21.32 | 210817_s_at | 18 |

| | | | | | | |
|---|---|---|---|---|---|---|
| Colorectal | Connolly CellLine | 0.942 | CRBN | 3q26.2 | 222533_at | 18 |
| Colorectal | Connolly CellLine | 0.937 | ZNF655 | 7q22.1 | 225945_at | 18 |
| Esophageal | Wang Esophagus | 0.906 | TSPAN1 | 1q34.1 | AF054838 | 52 |
| Esophageal | Wang Esophagus | 0.906 | LGALS4 | 19q13.2 | U82953 | 52 |
| Esophageal | Wang Esophagus | 0.888 | RHOC | 1q13.1 | A1685018 | 52 |
| Esophageal | Hao Esophagus | 0.885 | TSPAN8 | 12q14.1-q21.1 | IMAGE:509731 | 48 |
| Head and Neck | An CellLine | 0.882 | HSF2BP | 21q22.3 | 34044_at | 23 |
| Head and Neck | An CellLine | 0.882 | COL6A1 | 21q22.3 | 41350_at | 23 |
| Head and Neck | An CellLine | 0.882 | GAL3ST1 | 22q12.2 | 38565_at | 23 |
| Breast | Frasor CellLine 2 | 0.86 | KRT7 | 12q12-q13 | 41294_at | 30 |
| Breast | Pratilas CellLine | 0.857 | CYP2B6 | 19q13.2 | 206754_at | 32 |
| Lung Cancer | Gemma CellLine | 0.855 | KYNU | 2q22.2 | 204385_at | 29 |
| Esophageal | Hao Esophagus | 0.848 | SPINK1 | 5q32 | IMAGE:1412481 | 48 |
| Esophageal | Hao Esophagus | 0.848 | CDC42BPA | 1q42.11 | IMAGE:506523 | 48 |
| Pancreatic Cancer | Gyorffy CellLine 2 | 0.847 | TNFRSF21 | 6p21.1-p12.2 | AA490494 | 13 |
| Pancreatic Cancer | Gyorffy CellLine 2 | 0.847 | MAOA | Xp11.3 | AA011095 | 13 |
| Pancreatic Cancer | Collisson CellLine | 0.827 | TCF7L2 | 10q25.3 | 212762_s_at | 20 |
| Pancreatic Cancer | Gyorffy CellLine 2 | 0.818 | AKR1C2 | 10p15-p14 | AI924357 | 13 |
| Breast | Frasor CellLine 2 | 0.814 | GPC5 | 13q32 | 36788_at | 30 |
| Breast | Lin CellLine 3 | 0.81 | LTBP2 | 14q24 | 204682_at | 94 |
| Breast | Lin CellLine 3 | 0.81 | F3 | 1q22-p21 | 204363_at | 94 |
| Breast | Pratilas CellLine | 0.807 | GLS2 | 12q13 | 205531_at | 32 |
| Breast | Pratilas CellLine | 0.807 | CASP6 | 4q25 | 209790_s_at | 32 |
| Prostate | Welsh Prostate | 0.799 | EPN2 | 17q11.2 | 36121_at | 34 |
| Bladder | Stransky Bladder | 0.774 | KRT19 | 17q21.2 | 40899_at | 57 |
| Bladder | Stransky Bladder | 0.774 | KRT7 | 12q12-q13 | 41294_at | 57 |
| Breast | Lin CellLine 3 | 0.773 | PPP1R13L | 19q19.32 | 218849_at | 94 |

| | | | | | | |
|---|---|---|---|---|---|---|
| Bladder | Stransky Bladder | 0.764 | GATA3 | 10p15 | 40511_at | 57 |
| Breast | Frasor CellLine 2 | 0.764 | ENPP1 | 6q22-q23 | 342_at | 30 |
| Prostate | Welsh Prostate | 0.762 | CYPA411 | 1q33 | 35412_at | 34 |
| Colorectal | Tsuji Colorectal | 0.749 | PRPF18 | 10q13 | 232473_at | 83 |
| Colorectal | Tsuji Colorectal | 0.749 | RPA4 | Xq21.33 | 221143_at | 83 |
| Bladder | Sanchez-Carbayo Bladder 3 | 0.746 | PPFIBP2, or liprin-beta-2 | | | 157 |
| Bladder | Sanchez-Carbayo Bladder 2 | 0.746 | CTSH | 15q24-q25 | 202295_s_at | 157 |
| Colorectal | Watanabe Rectum | 0.743 | CAST | 5q15 | 41257_at | 46 |
| Lung Cancer | Gemma CellLine | 0.735 | S100A6 | 1q21 | 217728_at | 29 |
| Lung Cancer | Gemma CellLine | 0.735 | AHR | 7p15 | 202820_at | 29 |
| Prostate | LaTuplippe Prostate | 0.733 | LPCAT4 | 15q14 | 40472_at | 35 |
| Bladder | Sanchez-Carbayo Bladder 4 | 0.725 | UGT1A3 | | 208596_s_at | 157 |
| Melanoma | Hoek Melanoma | 0.722 | HAS1 | 19q13.4 | 207316_at | 45 |
| Melanoma | Hoek Melanoma | 0.722 | PTGS1 | 9q32-q33.3 | 205127_at | 45 |

### ABCC3 Modulation of Overall Survival

The overall survival in response to ABCC3 high/low expression was plotted by www.kmplot.com (Figure 3—4 & Figure 3—5). The graphs plotted displayed the survival over time (months) against the probability that the patients were still alive (Figure 3—4 & Figure 3—5). The cancer types that significantly predicted patients with high ABCC3 expression showed increased overall survival were breast carcinoma (HR 0.68 [0.48-0.94], P-value = 0.021), bladder cancer (HR 0.61 [0.45-0.83], P-value = 0.0014), uterine corpus endometrial carcinoma (HR 0.6 [0.39-0.941, P-value = 0.016), sarcoma (HR 0.6 [0.38-0.91], P-value = 0.026), rectum adenocarcinoma (HR 0.37 [0.16-0.89], P-value = 0.021) and oesophageal adenocarcinoma (HR 0.31 [0.12-0.81], P-value = 0.012) (Figure 3—4). These results suggested that some patients with certain cancer types may benefit from higher levels of ABCC3 expression. However, these patients also showed a much lower average HR estimate (0.528) across the six datasets, a 3.41-fold reduction when

compared to the average HR across the datasets in Figure 3—5. The lower HR suggests that these cancers showed an overall less aggressive cancer profile (Figure 3—5).

A

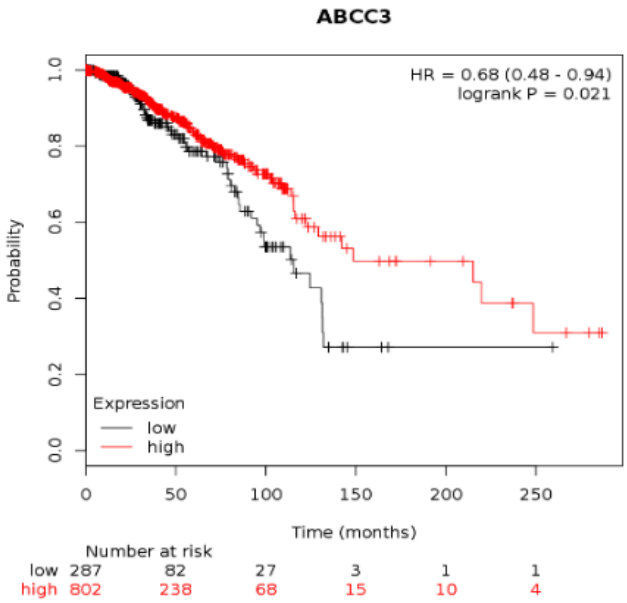
ABCC3
HR = 0.68 (0.48 - 0.94)
logrank P = 0.021
Probability
Expression
low
high
Time (months)
Number at risk
low 287 82 27 3 1 1
high 802 238 68 15 10 4

B

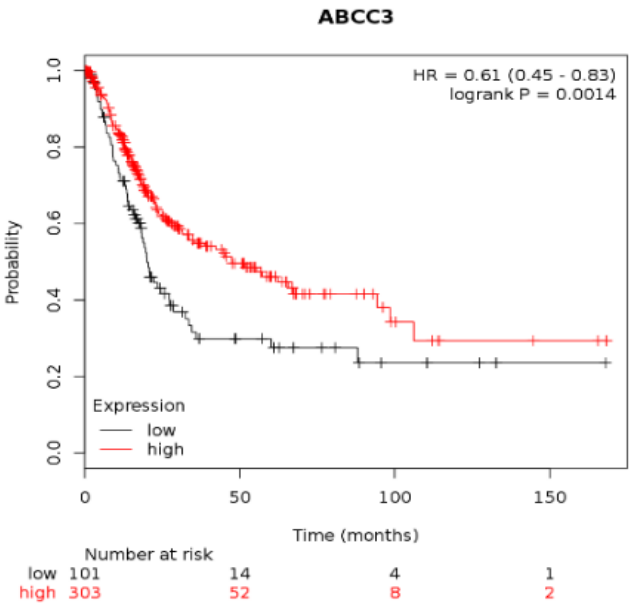
ABCC3
HR = 0.61 (0.45 - 0.83)
logrank P = 0.0014
Probability
Expression
low
high
Time (months)
Number at risk
low 101 14 4 1
high 303 52 8 2

C

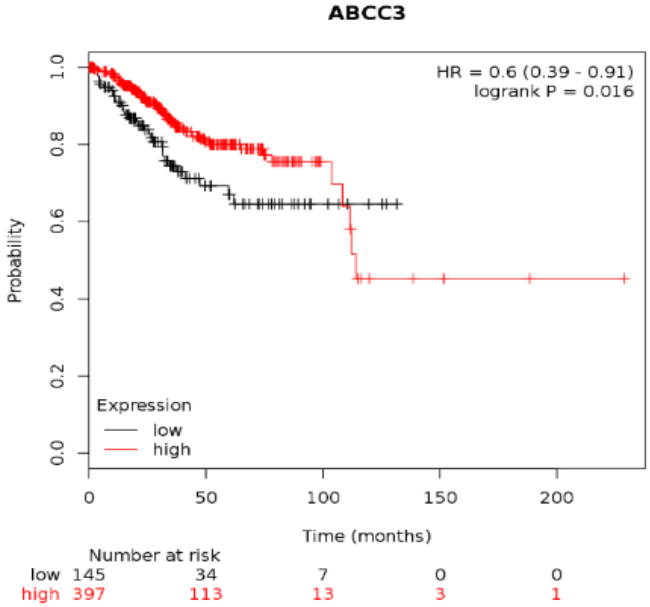
ABCC3
HR = 0.6 (0.39 - 0.91)
logrank P = 0.016
Probability
Expression
low
high
Time (months)
Number at risk
low 145 34 7 0 0
high 397 113 13 3 1

D

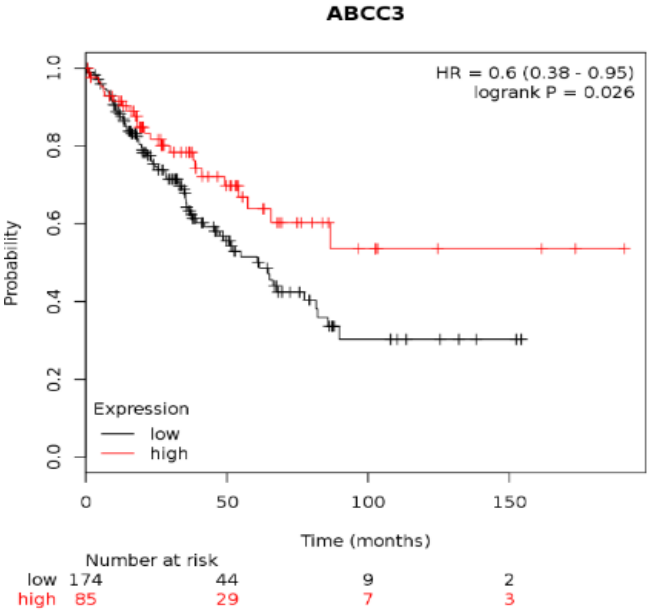
ABCC3
HR = 0.6 (0.38 - 0.95)
logrank P = 0.026
Probability
Expression
low
high
Time (months)
Number at risk
low 174 44 9 2
high 85 29 7 3

E

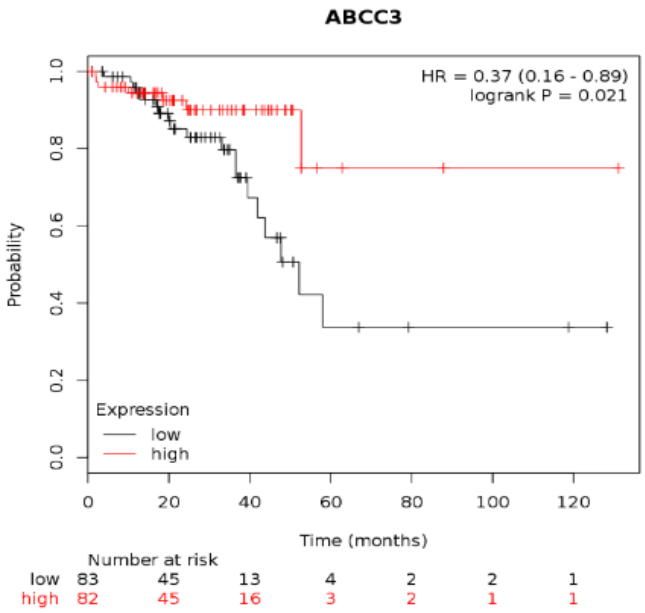


F

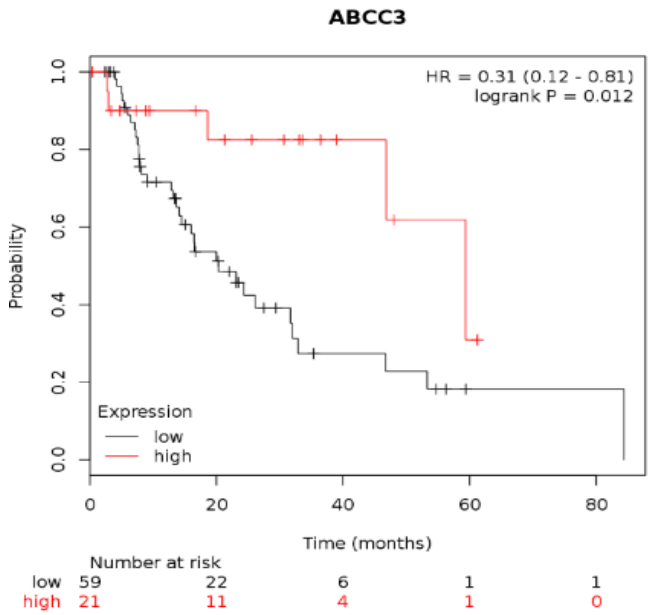


Figure 3—4. Kaplan Meier Survival Plots of ABCC3 expression. Cancer Types that showed improved survival with higher expression of ABCC3 Cancer types in which overall suvival was significantly improved by higher levels of ABCC3 expression includes (A) Breast Carcinoma, (B) Bladder Carcinoma, (C) Uterine Corpus Endometrial Carcinoma, (D) Sarcoma, (E) Rectum Adenocarcinoma and (F) Esophageal Adenocarcinoma.

However, in cancers where the high expression of ABCC3 limited overall survival, the HR and significance levels were much higher (Figure 3—5). The kidney renal papillary cell carcinoma (HR 2.6 [1.4-4.81], P-value = 0.0017), pancreatic ductal adenocarcinoma (HR 2.01 [1.32-3.06], P-value = 9.6E-4), kidney renal clear cell carcinoma (HR 1.68 [1.23-2.29], P-value = 0.001), lung SCC (HR 1.6 [1.02-2.52], P-value = 0.038), head and neck SCC (HR 1.46 [1.11-1.93], P-value = 0.0071) and liver hepatocellular carcinoma (HR 1.46 [1.07-1.99], P-value = 0.017) all showed that patients with high ABCC3 expression had reduced overall survival (Figure 3—5). The average HR across these datasets was 1.8, exhibiting that these cancers showed a more aggressive profile (Figure 3—5). Upon further interrogation the pancreatic adenocarcinoma was the only Kmplot to show an FDR of 5%, followed by bladder carcinoma (FDR: 20%), kidney renal clear cell carcinoma (FDR: 20%), kidney renal papillary cell carcinoma (FDR: 20%) and head and neck SCC (FDR:50%) (data not shown, kmplot.com). The remaining datasets all had FDRs over 50%, thereby limiting the robustness of those results. Suggesting that although, some cancers showed significant differences in low/high ABCC3 expression, that only a few results showed clear evidence of ABCC3 involvement in patient survival. Pancreatic adenocarcinoma, kidney renal clear cell carcinoma and kidney renal papillary cell carcinoma continue to show evidence that ABCC3 increased expression decreases overall survival in these cancer types (Figure 3—1)

A

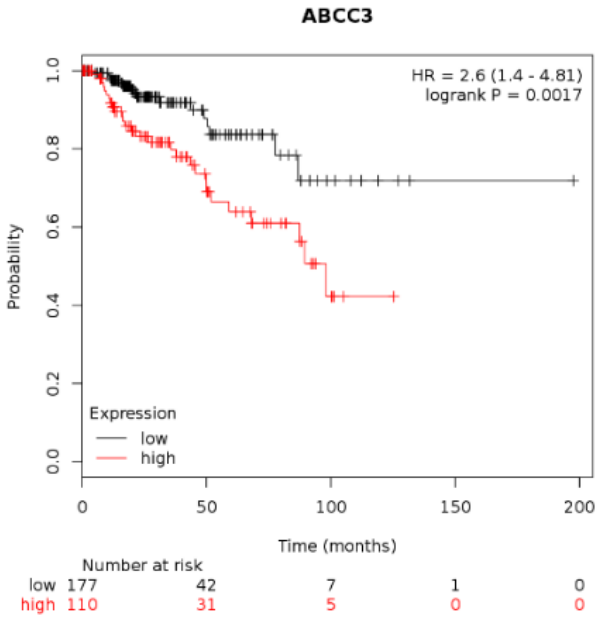
ABCC3
HR = 2.6 (1.4 - 4.81)
logrank P = 0.0017
Probability
Expression
low
high
Time (months)
Number at risk
low 177 42 7 1 0
high 110 31 5 0 0

B

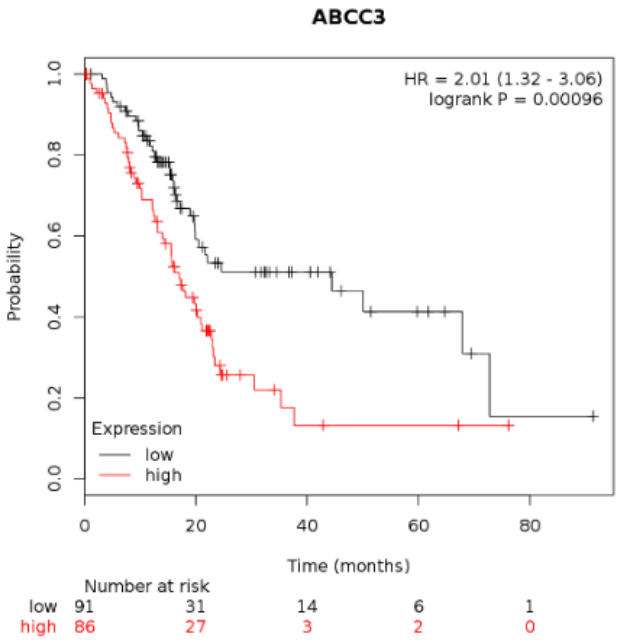
ABCC3
HR = 2.01 (1.32 - 3.06)
logrank P = 0.00096
Probability
Expression
low
high
Time (months)
Number at risk
low 91 31 14 6 1
high 86 27 3 2 0

C

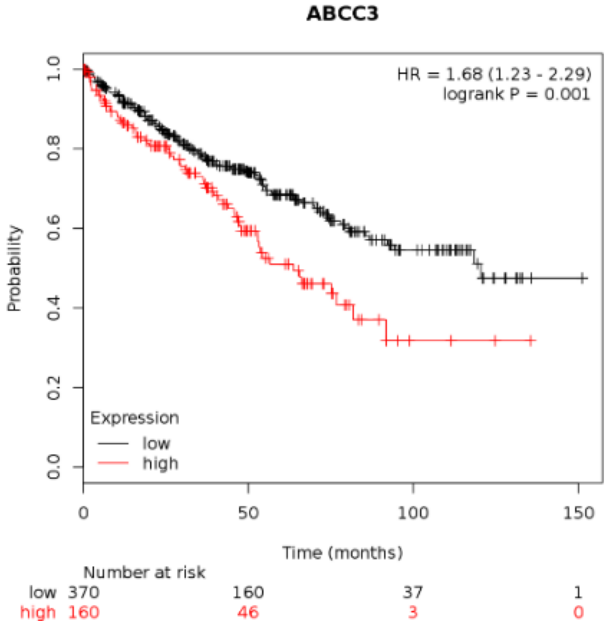
ABCC3
HR = 1.68 (1.23 - 2.29)
logrank P = 0.001
Probability
Expression
low
high
Time (months)
Number at risk
low 370 160 37 1
high 160 46 3 0

D

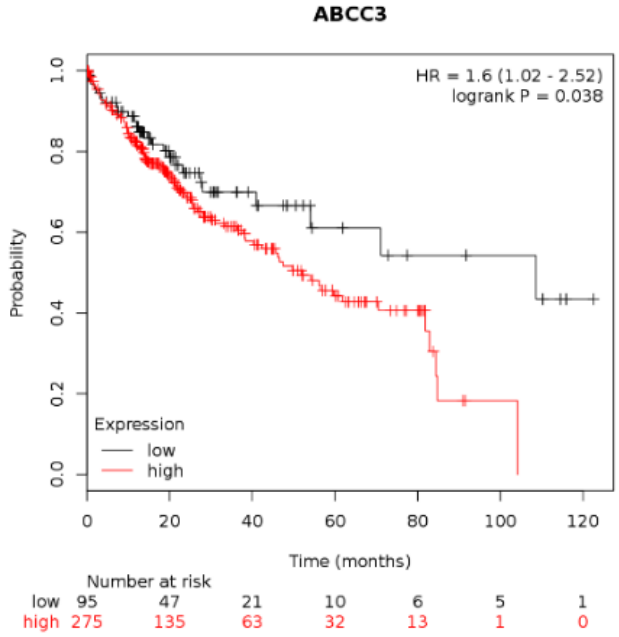
ABCC3
HR = 1.6 (1.02 - 2.52)
logrank P = 0.038
Probability
Expression
low
high
Time (months)
Number at risk
low 95 47 21 10 6 5 1
high 275 135 63 32 13 1 0

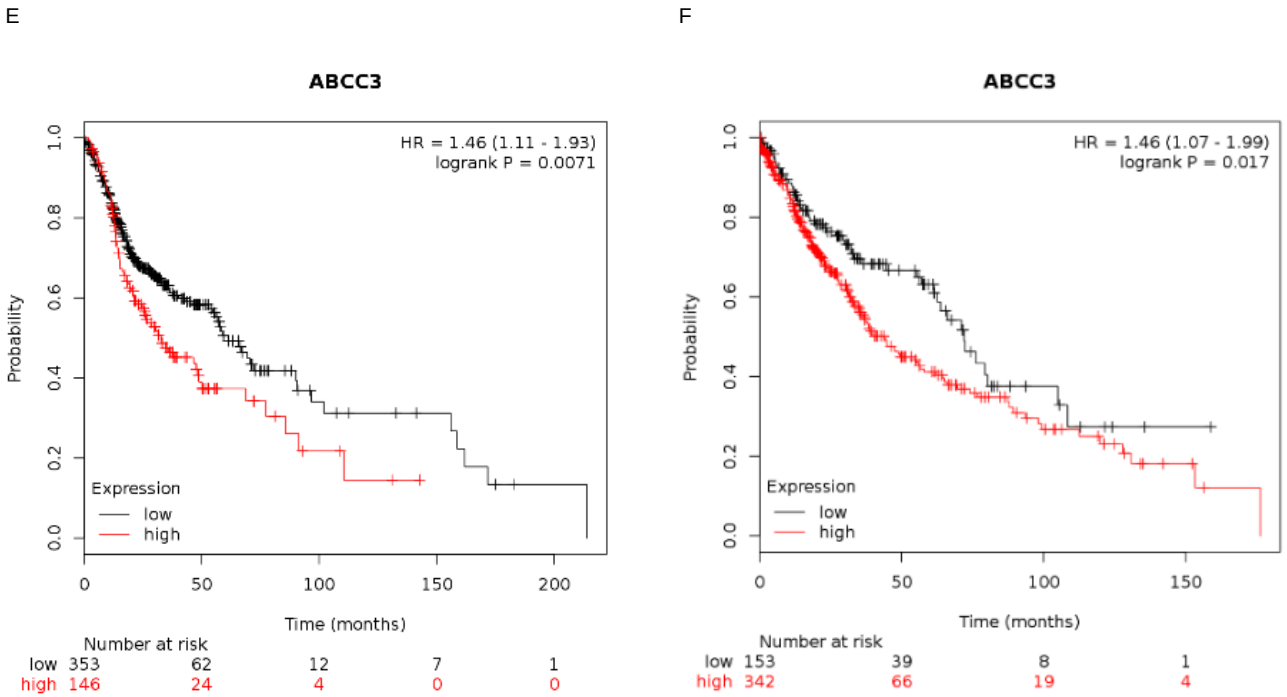


Figure 3—5. Kaplan Meier Survival Plots of ABCC3 expression. Cancer Types that show significantly improved survival with lower expression of ABCC3. Cancer types in which overall suvival was significantly improved by lower levels of ABCC3 expression included: (A) Kidney Renal Papillary Cell Carcinoma, (B) Pancreatic Ductal Adenocarcinoma, (C) Kidney Renal Clear Cell Carcinoma, (D) Lung SCC, (E) Head and Neck SCC and (F) Liver Hepatocellular Carcinoma.

### ABCC3 Predicted Functional Associations

The STRING database was used to predict potential protein-protein interactions of ABCC3. The STRING database revealed that the majority of proteins (>70%) with predicted ABCC3 association were also transport proteins (Table 3—9). The STRING database revealed that ABCG4 was associated with ABCC3 protein (Figure 3—6).

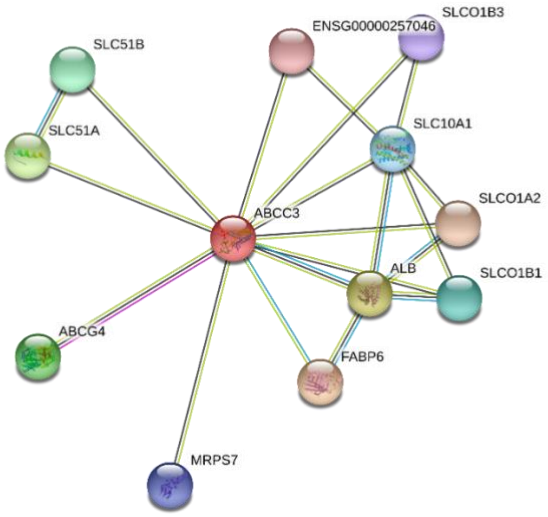


Figure 3—6. ABCC3 protein association network in the STRING database. This shows all the interactions that have been predicted to show functional association with ABCC3 with high confidence (>0.7) within the STRING database.

The solute carrier organic anion (SLC) transporters were the remaining transporters associated with MRP3 (Table 3—9 & Figure 3—6). SLC51A, SLC51B, SLCO1B1, SLC10A1, SLCO1B3, ENGS00000257046 and SLCO1A2 all showed association with ABCC3 (Table 3—9). The remaining proteins included gastrotropin/fatty acid binding protein 6 (FABP6), albumin (ALB) and mitochondrial ribosomal protein S7 (MRPS7) (Table 3—9). Although the functions of ABCC3 and the SLC transporters should show overlap of function they did not return the highest confidence score (Table 3—9). Both FABP6 and ALB showed strong confidence scores of 0.926 and 0.919 (Table 3—9).

| Predicted functional partners | Coexpression | Experiments | Databases | Text mining | Score |
|---|---|---|---|---|---|
| FABP6 | | | X | X | 0.926 |
| ALB | X | | X | X | 0.919 |
| SLC51A | X | | | X | 0.767 |
| ABCG4 | X | X | | X | 0.758 |
| SLC51B | X | | | X | 0.755 |
| SLCO1B1 | X | | | X | 0.751 |
| SLC10A1 | X | | | X | 0.745 |
| MRPS7 | X | | | X | 0.745 |
| SLCO1B3 | X | | | X | 0.738 |
| ENGS00000257046 | X | | | X | 0.732 |
| SLCO1A2 | X | | | X | 0.705 |

Table 3—9 ABCC3 STRING predicted functional partners. These results showed with strong predictive confidence (>0.7) that ABCC3 was associated with these targets across the four relevant analysis types held within the STRING database.

While, the coexpression, databases and text mining analyses were used as evidence for ALB, FABP6 confidence scores were calculated without showing coexpression (Table 3—9). ABCC3 association with MRPS7 and ABCG4 appear to show some exclusivity in that they do not overlap with any of the other strongly associated ABCC3 proteins (Figure 3—6). When comparing the associated proteins found from the STRING database and the targets found in the ONCOMINE database there was no overlap (Table 3—9, Table 3—8 & Table 3—7).

## Discussion

### Coexpression Analysis

The coexpression analyses revealed a number of targets that were either coexpressed or upregulated alongside ABCC3 expression (Table 3—7 & Table 3—8). Cytochrome P450 enzymes (P450s) are able to modulate the metabolism of several drugs especially within the nervous system [267]. In normal tissue, ABC transporters aid in the removal of xenobiotics and certain toxins alongside P450s activity [268]. The P450s CYP2B6 and the cytochrome enzyme CYPA411 were both found to co-express (0.857 and 0.762) with ABCC3 expression within breast and prostate cancer datasets, respectively (Table 3—7). The co-expression of CYP2B6 and other P450s were also shown with ABCG2 and ABCA1 in the amygdala and the prefrontal cortex of the brain [268]. Asfar et al., showed that within the Pakistani population overexpression of both P450s (including CYP2B6) and ABC transporters ABCB1 and ABCC2 were found [269]. Furthermore, the functional activity of CYP2B6 and CYP3A4 were shown in peripheral blood mononuclear cells (PBMC) treated with cytokines over 48 hours, [270]. It appears that the mechanism that modulate P450s may be linked to ABC transporter modulation [270]. Yang et al., investigated the effects of the cytokine, interleukin-6 (IL-6) over 48 hours on the expressions of P450s including CYP2B6 and transporters including ABCC3 [271]. The general pattern showed that P450s expression generally reduced in the presence of IL-6, while the expression of efflux transporters like ABCC3 generally remained constant or increased in expression [271].

Ectonucleotide pyrophosphatase/phosphodiesterase 1 (ENPP1) is a cell surface protein that catalyses the reaction of ATP to AMP [272]. The generalised arterial calcification of infancy (GACI) is a rare disease that causes calcification of the internal lamina in large and medium arteries leading to infant heart failure within the first months of life [272]. Inactivation via mutation of ENPP1 has been shown to cause 75% of the GACI diagnosed [272]. The literature associating ENPP1 with ABC transporters was demonstrated by the ABCC6 mutation which also accounted for a significant amount of GACI diagnosed [272]. Within cancer ENPP1 expression has been linked to malignancy and chemotherapeutic response in breast cancer tissues [273]. ENPP1 expression also promoted the localization of ABCG2 to the surface of breast cancer cells [273]. The coexpression of ENPP1 and ABCC3 (0.764) as shown in a breast cancer dataset may suggest that ENPP1 also promotes the cell surface localization of ABCC3 or be involved in ATP phosphorylation, an essential reaction in ABC transport (Table 3—8) [272].

The inhibition of WNT signalling via the inhibition of TCF7L2 and β-catenin stimulated the expression of ABCC3 [197]. The binding locus for both TCF7L2 and ABCC3 showed nine common binding regions suggesting a common binding region

between the two targets [197]. There was a number of p53 and WNT signalling pathway members that showed upregulation alongside ABCC3 overexpression (Table 3—7). The WNT signalling members CSNK1A1, CCND1, PPARD and FZD1 showed the most consistent upregulation alongside ABCC3 (Table 3—7). ABCC3 expression in the presence of wild-type p53 was lower than in the presence of p53 mutations [36]. The p53 signalling members ATM, CCND1 and BAX/BCL2 showed the most consistent upregulation alongside ABCC3 (Table 3—7). Increased CCND1 expression has been linked to a poor prognosis in glioblastoma [274]. CCND1 was responsible for cell signal integration and cell cycle regulation [274]. CCND1 overexpression has previously been associated with MDR1 and BCL2 upregulation, while CCND1 inhibition showed a decrease in MDR1 and BCL2 expression [274]. Knockdown of WNT receptor Frizzled-1 (FZD1) much like CCND1 also reduced MDR1 expression [275]. The leukemic cells responded to the knockdown of FZD1 and downregulation of MDR1 with increased sensitivity towards chemotherapy [275]. Within lung cancer, interleukin 6 (IL-6) showed the ability to stimulate the expression of Ataxia-telangiectasia mutated (ATM) which in turn increased the expression of BCL2, BAX and ABCG2 [276]. The ability for CCND1 and FZD1 activity to modulate MDR1 activity may also translate towards modulation of ABCC3 expression.

ABCC3 was predicted to associate with several transporters including SLC51A, SLC51B, SLCO1B1, SLC10A1, SLCO1B3, ENGS00000257046, SLCO1A2 and ABCG4 (Table 3—9). Yan et al., showed the role of ABC transporters and SLC transporters in the absorption and distribution of phytochemicals [38]. The reason ABC and SLC transporters have such a link to absorption was that both are localised within the GI tract (Figure 1—2) [38]. ABCC3/MRP3, SLCO1A2/OATP1A2 and SLCO1B1/OATP1B1 have all been identified within different areas of the GI tract [38]. SLCO1A2 and SLCO1B1 are both located on the apical membrane while MRP3 is located on the basolateral side of the membrane [38]. Unlike P-gp and BCRP2, it appears that the normal action of MRP3, SLCO1A2 and SLCO1B1 all appear to aid in the absorption of chemicals into the blood circulation (Figure 1—2) [38]. The absorption of the SLCO1A2 drug substrates imatinib, talinolol, levofloxacin and MTX can be reduced upon SLCO1A2 inhibition [38]. MTX is also a substrate of ABCC3, inhibition of MRP3 expression improved methotrexate cytotoxicity [79, 277]. The functional link between SLC and ABC transporters has been well established, reinforcing the validity of the STRING platform [38, 278].

Fatty acid binding protein 6 (FABP6/IBABP/ILBP) preferentially binds to bile acids and is almost completely localised in the ileum [279]. *In vivo,* ABCC3 double knockout in mice had altered transport of bile acids in hepatocytes revealing ABCC3's ability to modulate liver regeneration [280]. Although no direct link between FABP6 and ABCC3 has been shown, the proximity of these bile acid functions would warrant further

investigation. MRPS7 is a small mitochondrial, ribosomal protein and in accordance with other ribosomal proteins plays a role in translation, a key cellular process [281]. Little is known about MRPS7, however a recent study showed that two siblings both affected with congenital sensorineural deafness and hepatic and renal impairments also showed a mutation in the MRPS7 gene [281]. Moreover, mutations in the MRPS7 gene caused a reduction in mitochondrial protein synthesis, while exogeneous addition of wild-type MRPS7 restored mitochondrial protein synthesis [281]. The link between ABCC3 and MRPS7 could not be established in literature. However, this does not detract from this current research, it further demonstrates how much is still yet unknown about both cancer and MRP3. The fact that the STRING platform returned expected, weakly associated and unknown protein-protein interactions may also prove the usefulness of the platform.

**ABCC3 Expression analyses**

The top three ABCC3 overexpressing cancer types were found to be kidney cancer, pancreatic cancer, and lung cancer (Table 3—5). In 2012, Kidney cancer made up a total of 2.4% of new cancer cases worldwide, with approximately 338,000 new kidney cancer cases [282]. This rose to 403,262 new cases in 2018 and resulted in 175,098 deaths in 2018 alone [13]. The most common form of kidney cancer, renal cell carcinoma (RCC) is highly aggressive and resistant to therapy with 5-year recurrence rates ranging from 30 to 60% [283]. RCC presents symptoms late and is inherently resistant to chemotherapy [284]. As previously shown by a number of studies, ABC transporters and ABCC3 in particular was able to limit the effectiveness of several anticancer drugs including platinum based drugs, methotrexate, paclitaxel, doxorubicin and gemcitabine [81, 88, 277, 285]. Although, the link between RCC or kidney carcinoma and ABCC3 has not been well characterised it would be plausible to hypothesise that the high ABCC3 expression seen in this study could contribute to RCC resistance. Kool et al., used a Madin-Darby canine kidney II cell to better characterise the function of ABCC3 [79]. The expression levels of P-gp, MRP1 and LRP were quantified in 47 RCC samples with the aim of assessing any possible linkages between multidrug resistant protein expression and clinically relevant parameters [286]. Although RCC showed expression of all three MDR proteins no correlations between clinical parameters could be made [286]. However, in Figure 3—5, the patient's overall survival (OS) was significantly (P-value = 0.0017) increased when ABCC3 expression in low. The results also showed that kidney carcinoma and ABCC3 differential expression between cancerous and normal samples, was the highest of all cancer types (Figure 3—1 & Figure 3—2). An ideal target is one that is differentially expressed when comparing cancerous and normal samples [287].

Pancreatic cancer much like RCC is also recognized as an aggressive and resistant form of cancer [24, 37]. Pancreatic cancer death rates are currently listed in the top four of all cancer related deaths and expected to rise to second by 2030 [288]. New Zealand's ministry of health in 2010 forecasted an increase in the mortality, morbidity and overall burden of pancreatic cancer within New Zealand in the next 8 years [31]. The five year survival rate for pancreatic cancer in the United States is at approximately 9% [261]. However, a recent study also showed that these survival rates can vary depending on the country [262]. In 2012, there was estimated 338,000 newly diagnosed pancreatic cancer patients, with 331,000 deaths that same year [282]. In 2018, there was approximately 459,000 new cases of pancreatic cancer worldwide with approximately 432,000 deaths [13]. These findings not only highlight the need for new therapies but demonstrate the need for better preventative strategies where possible. This study found pancreatic cancer to be on average the highest ABCC3 overexpressing cancer type in comparison to other cancers (Figure 3—2). High ABCC3 expression was also shown to have a significantly negative impact on overall survival in pancreatic cancer (Figure 3—5). Pancreatic cancer versus normal analysis also showed that pancreatic cancer exhibited ABCC3 overexpression, although not as strongly as other cancers (Figure 3—1). The outlier analysis revealed that the TCGA pancreas dataset exhibited the highest COPA score, suggesting a portion of the pancreatic cancer samples strongly and heterogeneously overexpress ABCC3 (**Error! Reference source not found.**).

The average expression of ABCC3 may veil the complexity of the ABCC3 expression due to the high heterogeneity as seen in the ONCOMINE platform (**Error! Reference source not found.**). In literature, pancreatic cancer has already shown differential expression of both ABCC3 and ABCC5 across normal and cancerous mRNA samples [289]. Further examination of the expression profiles of 2177 cell-surface genes across samples of both cancerous and normal pancreas tissues revealed that, ABCC3 and TLR2 were robust targets [83]. A recent paper by Adamska et al., showed that not only was ABCC3 overexpressed in pancreatic cancer but also that the knockdown (siRNA) of ABCC3 was able to modulate pancreatic cancer proliferation [36]. The identification of the relationship between ABCC3 and pancreatic cancer through these results as well as validation in literature attests to the value of these bioinformatic studies.

Lung carcinoma exhibited ABCC3 overexpression and performed especially well when comparing histological samples within the cancer types (Table 3—5 & Figure 3—2). The overexpression of ABCC3 was specifically shown within non-small cell carcinoma samples in comparison to SCC, across multiple lung cancer datasets (Table 3—3). This pattern was seen across multiple lung carcinoma datasets. The non-small cell carcinoma subtype was the most common form of lung cancer diagnosed (80-85%) and has a resistant phenotype although not to the same extent as renal carcinoma or pancreatic

carcinoma, with a 5-year survival rate of 15% [13, 81]. The reason for the low 5-year survival rate is the high recurrence rate of 30-70% and the resistance to multiple drugs [81]. The upregulation of ABCC3 in non-small cell carcinoma was linked to the increased multidrug resistance and a failure of chemotherapy [81]. The cancer types and cancer subsets identified by this study which showed overexpression of ABCC3 have also been linked with aggressive and resistance cancers. This data suggests RCC, pancreatic and non-small cell cancers would be good targets for ABCC3 modulation.

The cancer versus cancer (histology) analysis also identified malignant fibrous histiocytoma which showed the highest expression of ABCC3 across the sarcoma cancer type (Table 3—3). However, this comparison was across a dataset that all showed low ABCC3 expression, therefore the malignant fibrous histiocytoma demonstrated weak ABCC3 under expression (Table 3—3, oncomine.org). Soft-tissue sarcoma diagnoses are rare with only 12,000 new cases estimated in the US, each year [290]. The five-year survival rate for soft-tissue sarcoma ranges from 90% to 56% depending on the stage of the cancer [291]. The Ewing sarcoma, a rare form of bone carcinoma has a five-year survival rate of less than 20% [292, 293]. Within this Ewing sarcoma subtype the mechanisms underlying Ewing sarcoma drug resistant was investigated [292]. The A673, Ewing sarcoma cell line was exposed to increasing concentrations of SP-2509, a small molecule reversible lysine specific demethylase (LSD1/KDM1A) inhibitor over a seventh month time period [292]. The expression of the intended target KDM1A remained unchanged in the newly created a multidrug resistant Ewing sarcoma cell line. While the expression of of ABCC3, ABCB1 and ABCC5 all increased [292]. This revealed the importance of ABC expression in drug resistance. The danger of ABCC3 overexpression was seen in this sarcoma model [292]. Sarcoma usually exhibits relatively high survival rates, this exhibits that the overexpression of ABC transporters could change this [292].

Lung cancer, gastric cancer and prostate cancer all exhibited datasets that showed significant under expression of ABCC3 in cancer versus normal analyses (Figure 3—1). Breast cancer, leukaemia and prostate all showed significant under expression in comparison to other cancer samples (Figure 3—2). Suggesting that these cancers would not be good targets for ABCC3 targeted treatments. However, Breast cancer which showed the strongest ABCC3 under expression across cancer types (Table 3—4), also showed an increase in ABCC3 expression in patient samples that underwent chemotherapy [87]. Both Ewing sarcoma and breast carcinoma showed that ABCC3 upregulation may also occur in these under expressing cancers resulting in increased drug resistance [292]. These under expressing cancers may like Ewing sarcoma and breast cancer develop resistance to drugs via overexpression of ABCC3 [292].

## Limitations

There a number of limitations that must be considered while interpreting the results of these bioinformatic tools [189, 294]. DNA microarrays allow for the simultaneous comparison of the expression of thousands of genes [189]. The ONCOMINE platform has gathered and normalised thousands of microarray samples [194]. However, microarray data was limited firstly by the quality of samples, this concerns both the sample and tissue quality and the quality of the RNA extracted [189]. The extraction of RNA and the processing time is so important that any degradation in mRNA can result in false microarray results [189]. The sample quality can be affected by sample selection, as many tissues especially in the context of cancer contain heterogenous populations of different cell types and healthy/diseased cells [294]. The ONCOMINE platform has no control over the quality of a dataset other than the fact that it has been published in a recognized journal [190]. The inherent assumption that these published datasets have been well constructed is a reasonable assumption. However, while the chance is low, this could provide opportunity for some ill-prepared data to slip through. Secondly, Microarray datasets are also limited by the genes/probes that have been used. Therefore, they may paint a limited picture of the total genetic expression in the samples. As ABCC3 is a relatively new ABC transporter member being studied there may be some expression patterns that have been missed because ABCC3 was not included as part of the study. Lastly, microarray data utilise various forms of nucleic acids (mRNA, cDNA, PCR products) to measure gene expression [294]. Quite simply the expression of nucleic acids does not always translate into functional protein expression [294].

Subsequently, the STRING database was used to address protein-protein functional relations. However, the string database much like any database platform including the ONCOMINE and the KMplot was limited by the data contained within the database, and the analyses available. The STRING database while it was designed for the evaluation of protein-protein interactions, was not equipped to compare cancerous versus normal samples [193]. Although there were several proteins that were identified as functionally associated with ABCC3 in the context of cancer these may not be pathologically relevant (Table 3—9). However, all of these limitations can be resolved by further validation of the expression patterns seen across these databases. This can be done by other quantification methods such as RT-PCR and Western blotting [294].

## Conclusion

In conclusion, the expression of ABCC3 was shown across a wide range of cancers, which may be targeted by ABCC3 inhibition. The top overexpressing ABCC3 cancers based on the oncomine platform were kidney, lymphoma, bladder, lung, sarcoma, colorectal, melanoma, brain/CNS and pancreatic cancer (Table 3—1). Pancreatic cancer

exemplified the importance of heterogeneous expression. While pancreatic cancer did not show strong ABCC3 overexpression in comparison to normal pancreatic cells, it showed the highest COPA score and strong expression in comparison to other cancer types (Figure 3—1, Figure 3—2 & **Error! Reference source not found.**). High ABCC3 expression was also shown by the KMplot platform to be a modulator of overall survival across kidney renal papillary cell carcinoma, PDAC, kidney renal clear cell carcinoma, Lung SCC, Head and Neck SCC and Liver Hepatocellular Carcinoma (Figure 3—5). This was especially true for pancreatic cancer which showed significant (P-value = 9.6E-4) and statistically robust (FDR: 5%) modulation of survival rates (Figure 3—5). The discovery that cancer types and subtypes which do overexpress ABCC3 were more resistant and aggressive, reinforced ABCC3's role in creating a resistant phenotype. The amount of information and analyses that were recorded from the ONCOMINE, STRING and KMplot platforms as well as the ability to correlate these findings with previous literature attests to the value of these kinds of studies. The three cancers that would be ideal candidates for a validation of ABCC3 expression and targeting would be pancreatic, kidney and lung carcinoma.

# Chapter 4 CRISPR-Cas9 Knockout of ABCC3

## Introduction

The ATP binding cassette (ABC) family are made up of transport proteins that require the energy released from ATP hydrolysis to achieve protein reconfiguration, which transport substrates across the membrane [263]. This type of transport allows the movement of substrates against their concentration gradients [263]. The ABC family is divided into a number of subfamilies, ABCC, also known as the multidrug resistance protein (MRP) family contains the most multidrug resistance transporters [86]. Multidrug resistance is the development or inherent resistance of cancer to a multitude of drugs that are unrelated in structure or function [88]. ABCC1 (or MRP1), P-glycoprotein (P-gp) and breast cancer resistance protein (BCRP/2) were the first ABC transporters to be associated with a multidrug resistance [86, 186, 295, 296]. ABC transporters also play an essential role in a number biological processes because of their ability to transport proteins and essential signalling molecules [86]. ABC transporters have been able to modulate the "hallmarks of cancer" as stated by Hanahan and Weinberg (2000) [1, 86]. Forced expression of BCRP in bone marrow both *in vitro* and *in vivo* showed a reduction in mature progenitor cells displaying BCRP modulation of differentiation in cancer cells [86]. Furthermore, the sole treatment of valspodar, a P-gp inhibitor also promoted apoptosis *in vitro* [86]. P-gp also conferred survival in the presence of apoptotic stimuli, supposedly without active transport [86]. The knockdown of MRP1 both *in vitro* and *in vivo* resulted in spontaneous cell death [86]. Other hallmarks associated with ABC transporter expression include cell migration, invasion and metastasis which are essential in of cancer progression [86].

More recent analysis revealed that MRP3 and MRP5 could also cause multidrug resistance [79, 186]. MRP3 was located in several locations including the liver, colon, small intestine, adrenal gland and at lower levels in the lung, pancreas, kidneys and prostate [79]. MRP3 has the closest sequence homology to MRP1, however it has not been as extensively characterised [79]. The canonical mechanism for which ABC transporters can confer resistance is by actively transporting drugs away from their target sites [79, 186, 295, 296]. The manipulation of ABC transporters to decrease multidrug resistance in cancer has been a well-recognised therapeutic strategy [86, 297, 298]. ABCC3 has also been associated with differentiation, a key biological necessity of cancer [86]. The TNM staging or tumour grading is associated with tumour differentiation with the majority of tumour cells being differentiated resulting in grade I [289]. While the more undifferentiated cells within a tumour the higher the grade, with grade III representing tumours that are predominantly undifferentiated [289]. ABCC3 mRNA expression was correlated with tumour grading and differentiation in pancreatic cancer [289]. Tumour

growth and differentiation are also related, less differentiated tumours have an increased potential for proliferation [86]. In order to sustain tumour growth, it is essential to keep a major proportion of the tumour undifferentiated [86].

MRP3 expression has affected numerous drugs and their metabolites in several cancer types [36, 80, 81, 87, 89, 186, 285, 299-301]. Cancerous pancreatic tissues significantly overexpressed MRP3 and MRP5 mRNA in comparison to normal tissue [186, 289]. The upregulation of ABCC3 mRNA expression in HER2 positive breast cancer samples and cell lines has also been shown [89]. As previously shown *in vitro* by O'Brien et al., ABCC3 can mediate paclitaxel and MMAE resistance in HER2 positive breast cancer cell lines [88]. Luminal cancers which are predominantly ER positive cancers, usually yield a relatively good prognoses and respond well to hormonal therapies [88]. ABCC3 was shown not only to confer resistance to paclitaxel and the antimitotic monomethyl-auristatin-E (MMAE), ABCC3 was also highly expressed in 25% of HER2-positive breast tumours and in 11% of luminal tumours [88]. In non-small cell lung cancer, ABCC3 was identified as one of the most of upregulated genes in the chemo resistant samples/cell lines [81]. In osteosarcoma, the expression of ABCC3 increased the likelihood of a poorer prognosis with a reduced disease-free survival (DFS) and overall survival (OS) [80]. Osteosarcoma is one of the leading causes of cancer related deaths in children and adolescents [80]. Patients expressing the ABCC3 (rs4148416 TT genotype) showed a significant reduction in the response to chemotherapy [80]. ABCC3 expression also limited platinum-based chemotherapies within NSCLC patients being treated [81].

90% of pancreatic cancer patients are diagnosed with pancreatic ductal adenocarcinoma (PDAC) [34]. The five year survival rate for PDAC is <10%, ranking PDAC in the five highest cancers causing death [34]. The first line treatment for pancreatic cancer in the past three decades has been gemcitabine, an antimetabolite drug that has only yielded a marginal increases in patient survival [35, 36]. More recently, Abraxane (albumin-bound paclitaxel) and FOLFIRINOX have been included in the standard treatment for pancreatic cancer, with improved survival estimates but is limited by increased side effects [36]. ABCC3 is highly expressed in PDAC tumours and the knockdown of ABCC3 caused reduced PDAC cell proliferation [36]. Analysis of public datasets revealed that the differential upregulation of ABCC3 in PDAC correlates with a poor prognosis and reduced survival rates [36]. *In vitro* and *in vivo* models revealed that knockdown of ABCC3 was able to reduce the proliferation rates of pancreatic cancer cells and greatly reduced the growth rate in tumours [36].

Modern genetic engineering utilises an approach called reverse engineering which uses various strategies to interrupt gene expression of a target [234]. The corresponding phenotypic changes can be attributed to the specific changes in the

genome [234]. The CRISPR-Cas9 system has been extensively utilised to investigate such changes. CRISPR-Cas9 was used to successfully investigate P-gp expression by creating P-gp knockout cell lines [249]. The CRISPR-Cas9 system successfully modulated genomic, protein and functional activities of P-gp, establishing a precedence for the success of CRISPR-Cas9 in drug transport mechanisms [249].

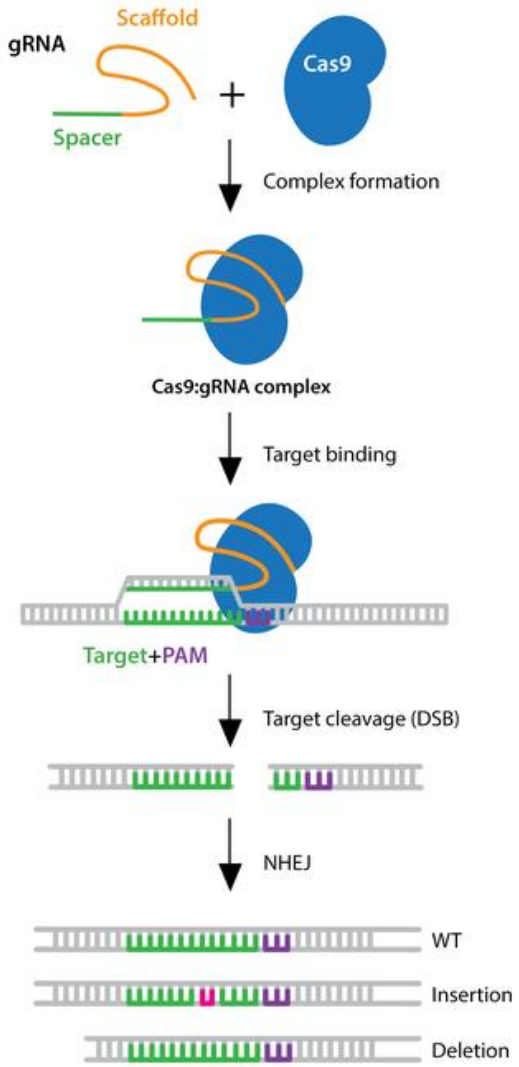


Figure 4—1.CRISPR-Cas9 mechanism. Modified from (https://www.addgene.org/guides/crispr/)

P-gp knockout by CRISPR-Cas9 was also able to significantly enhance sensitivity towards vincristine, doxorubicin and cisplatin in HCT-8/V and $KB_{v200}$ cells [118]. The knockout of P-gp was confirmed by western blot, PCR and rhodamine/doxorubicin cellular accumulation studies [118]. The CRISPR-Cas9 system has been reviewed in detail in the methodology chapter. In short, three gRNA sequences designed by Thermofisher scientific were used to target a specific ABCC3 loci, binding and guiding the cas9 protein cause a double strand break within the target site (Figure 4—1 & Table 4—1). The CRISPR-Cas9 was introduced to the cell by transfection in accordance with the manufacturer's instructions. Using the CRISPR-Cas9 system, ABCC3 expression was knocked out in pancreatic cancer (PANC1) cells and the phenotypic and genomic

effects were investigated (Figure 4—1). Whether the modulation of ABCC3 activity affects gemcitabine or methotrexate drug resistance was also investigated.

## Results

### ABCC3 Expression in PANC1 Cells

The MRP3 protein levels was confirmed in PANC1 cells by flow cytometry and surface staining of the ABC transporter membrane proteins in accordance with a previously established protocol [201]. The MRP3 expression was investigated in both PANC1 and HepG2 cells (Figure 4—2). In PANC1 cells, MRP3 protein expression was shown to be significantly (P-value = 0.0055) higher than its IgG control by 3.5-fold (Figure 4—2) across three independent experiments. During the initial optimization of the protocol, HepG2 cells were used to validate MRP3 expression (Figure 4—2). HepG2 surface staining showed a significant (P-value = 0.03) 3.07-fold difference between the average MRP3 (X-GMean = 1.135) expression and the IgG (X-GMean = 0.37) control. The strong differences in surface staining in comparison to IgG control in HepG2 cells suggested that the protocol being used was selective and sensitive to MRP3 expression.

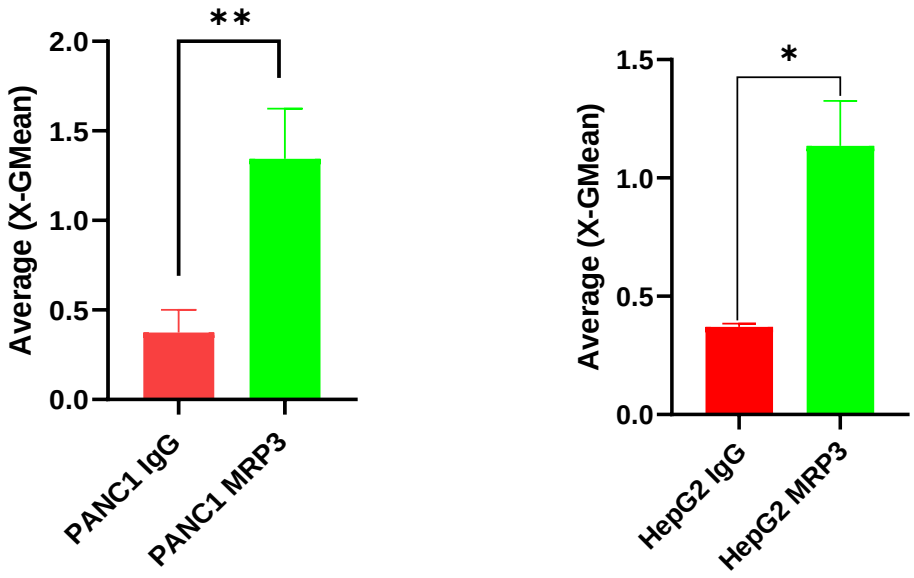


(A) (B)

Figure 4—2. MRP3 expression in PANC1 and HepG2 cells. The surface staining of PANC1 cells with an MRP3 antibody confirmed the presence of MRP3 membrane protein expression in PANC1 and HepG2 cells. (A) MRP3 expression was significantly higher than IgG controls (P-value = 0.0055). (B) HepG2 cells which also express MRP3 were used to optimise surface staining and act as a positive control for MRP3 expression, significance was not calculated as this was only repeated twice [302].

**Targeting ABCC3 using CRISPR-Cas9**

Three gRNA sequences that target the ABCC3 gene were acquired from Thermofisher (Table 4—2). As previously stated, gRNA's can for unknown reasons be unable to knockout the selected gene target [253]. Therefore, three different gRNA sequences that target different loci within the ABCC3 gene were selected (Table 4—2). When possible different PAM sequences were also selected to ensure a variation in targeting could be achieved [242]. Each gRNA sequence was designated a number to ease subsequent data analysis (Table 4—2). The initial round of CRISPR-Cas9 transfection was done in triplicate with the resultant cells named gRNA1 (a, b and c), gRNA2 (a, b and c) and gRNA (a, b and c). Initially the knockout of ABCC3 was assessed by quantifying the cellular accumulation of CMF within the cell to select the transfected replicate with the highest functional inhibition (see below). The selected replicates for gRNA1, 2 and 3 (mixed population) were tested for cleavage efficiency.

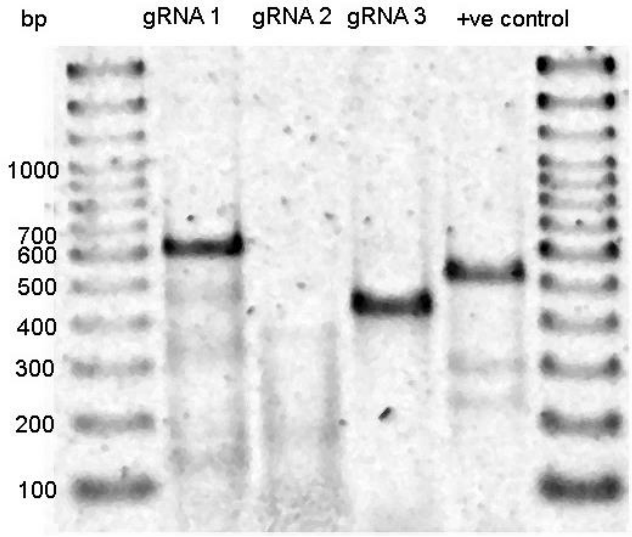


Figure 4—3. CRISPR-Cas9 cleavage detection

The enzyme (T7EI) contained in the kit targets the DNA mismatches caused by Cas9 activity and the corresponding double strand breaks, creating two smaller DNA fragments. The forward and reverse primers for gRNA3 were redesigned using the BLAST platform (Table 4—1). The cleavage detection kit exhibited three different results for the three gRNA sequences used (Figure 4—3). The cleavage results showed that gRNA1 was the only gRNA to demonstrate clear cleavage with a cleavage efficiency of 0.267 (Figure 4—3 & Equation 2-1). gRNA3 did not show any cleavage detection, while

gRNA2 exhibited some cleaved products but no uncleaved DNA (Figure 4—3). This data suggests that knockout of ABCC3 was most successfully achieved in the gRNA1 cell lines. The positive control was also clearly seen and resulted in a cleavage efficiency of 0.291 (Equation 2-1).

| Primers | Primer Sequence | PCR product size | crRNA (Thermofisher) | crRNA target sequence | Pam Sequence |
|---|---|---|---|---|---|
| CRISPR 1 FWD | CTCTGGGGATGCGGATTCCA | 604bp | CRISPR957583_CR | GATACAGTATGAGCGGCTGC | AGG |
| CRISPR 1 RVS | GGGACCCAGCAGTGACTTTGA | | | | |
| CRISPR 2 FWD | GGTGCAGTTTTTGTTGCCCTTA | 608bp | CRISPR957588_CR | GGATGATGTAGCCACGACAA | TGG |
| CRISPR 2 RVS | AGAAGGCAGAGGTTGCAGTGAG | | | | |
| CRISPR 3 FWD | TGCTTGGGGTCATGGGAATC | 422bp | CRISPR957600_CR (Reverse Strand) | GGAGTAAAAAAGGTCCGCCC | AGG |
| CRISPR 3 RVS | AGACCTCCCCCATCCACTTT | | | | |

Table 4—1. ABCC3 gRNA sequences and primers.

### Functional Modulation of MRP3 Activity

ABCC3 knockout should result in the modulation of MRP3 transport function. Flow cytometry outputs include the geometric mean which is predominantly used to calculate the mean of values on a logarithmic scale [303]. While, the arithmetic mean is simply the value that divides the total acquired across the entire dataset by the number of observations recorded [303, 304]. The median on the other hand is the value that lies between the highest observed results and the lowest results observed [304]. The median values can be used to remove outliers from the overall summary values that is sometimes seen in mean calculations. This is usually why the median is utilised in flow cytometry experiments [304].

Table 4—2. gRNA Targets

| gRNA | Thermofisher catalog number | Target DNA sequence | PAM sequence |
|---|---|---|---|
| 1 | CRISPR957583_CR | GATACAGTATGAGCGGCTGC (FWD strand) | AGG |
| 2 | CRISPR957588_CR | GGATGATGTAGCCACGACAA (FWD strand) | TGG |
| 3 | CRISPR957600_CR | GGAGTAAAAAAGGTCCGCCC (reverse strand) | AGG |

The initial round of CRISPR-Cas9 transfection showed increased CMF cellular accumulation above that of the WT PANC1 cancer cells (Figure 4—4). Both the median and the geometric mean (x-GMean) results were displayed (Figure 4—4). These results showed that in mixed knockout populations, gRNA2 exhibited the highest increase in CMF accumulation by 84% (x-GMean) (Figure 4—4). The highest increase of CMF accumulation across gRNA1 and gRNA3, were 47% and 33% respectively (Figure 4—4). However, the average across the triplicate experiments gRNA1 and gRNA3 cell lines showed a conservative increase in CMF accumulation of 0.8% and decrease of 0.63%, respectively (Figure 4—4).

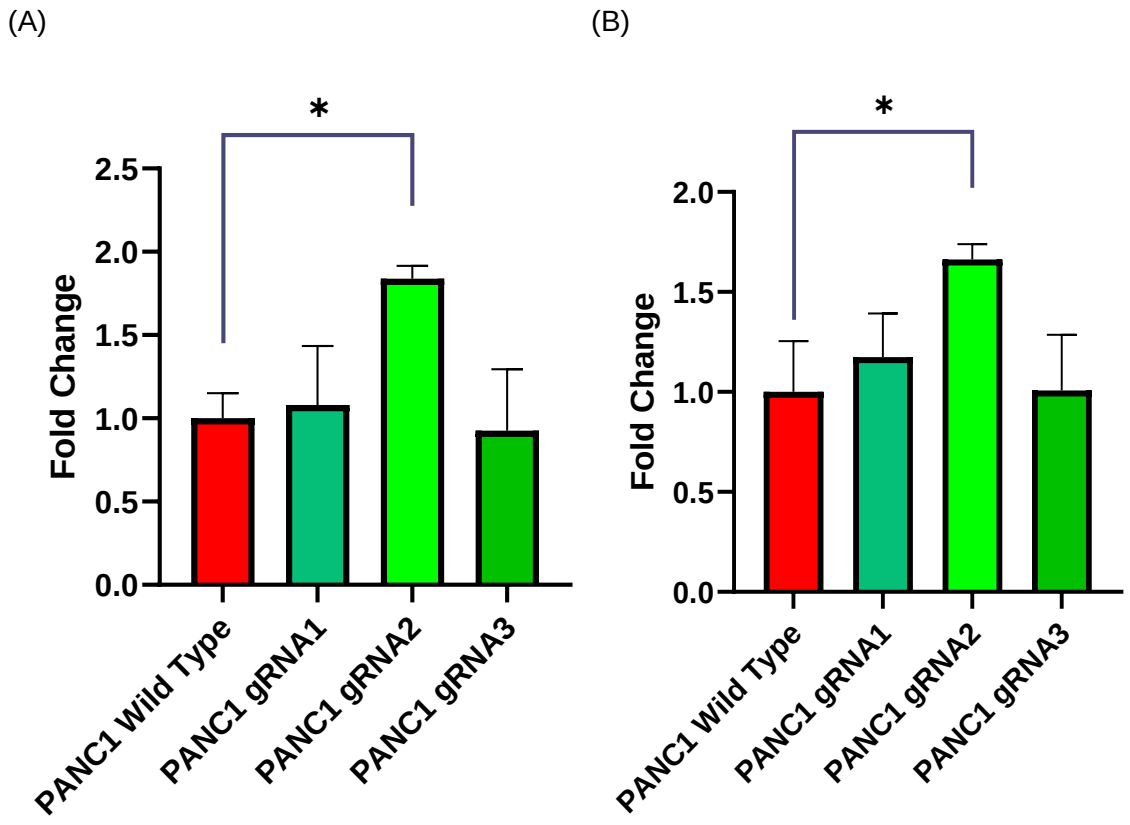


Figure 4—4. Accumulation of CMF across wild-type and K/O PANC1 cells. Initial screening of mixed K/O cell population showed substantial differences between WT and K/O CMF uptake levels. (A) Compares the differences in geometric mean of CMF fluorescence. gRNA2 showed a significant increase in CMF accumulation in comparison to WT cells (P-value = 0.0131). (B) Compares the differences in the median CMF fluorescence values. gRNA2 showed a significant increase in CMF accumulation in comparison to WT cells (P-value = 0.0159).

Median results showed a more conservative increase in CMF accumulation across the datasets, although the overall expression pattern remained unchanged (Figure 4—4). The average median significantly increased in CMF accumulation across gRNA2 knockout cells was 66.3%. The average median values for gRNA1 and gRNA3 showed CMF increases of 17% and 0.1%, respectively. These results suggested that the transfection efficiency for gRNA2 was consistent across the PANC1 cells, however

gRNA1 and gRNA3 both showed large variations in transfection efficiency across the CRISPR-Cas9 repeats. The CMF accumulation assay was used to screen the functional effects of ABCC3 knockout using the CRISPR-Cas9 system.

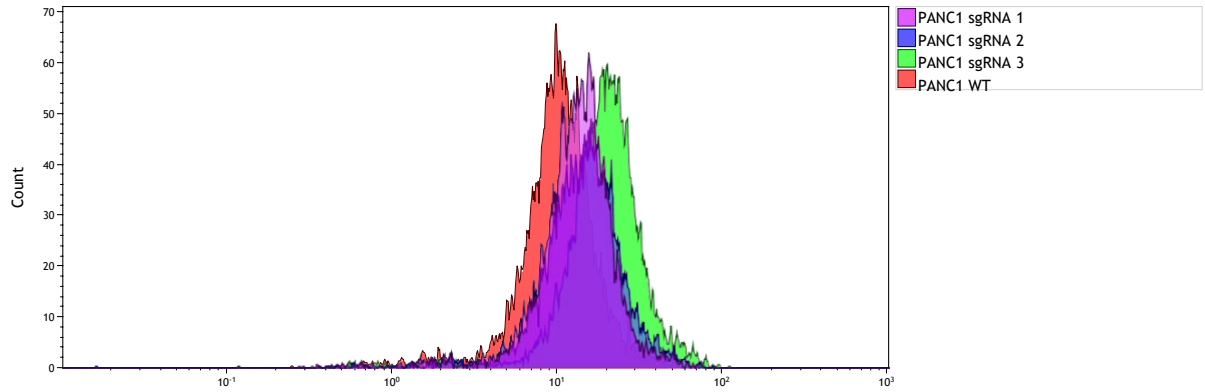


Figure 4—5. Accumulation of CMF across wild-type and the K/O PANC1 cells. The overlay revealed the average differences in CMDFA accumulation levels across WT and MRP3 K/O cells (n = 2). The replicate with the highest accumulation was chosen in this overlay.

The overlay of the fluorescence across the samples exhibiting the highest CMF accumulation showed a clear shift of the knockout cells in the log scale (Figure 4—5). While, gRNA2 showed the highest average increase in CMF accumulation across cell lines, gRNA3 clearly showed the highest fluorescence in comparison to all cell lines (Figure 4—5).

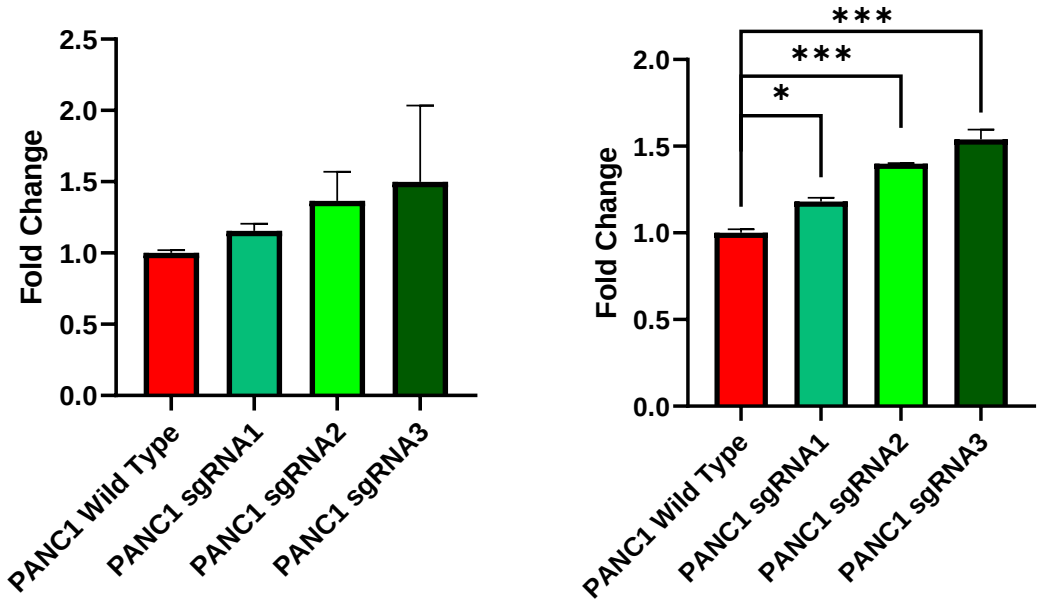


(A) (B)

Figure 4—6. Accumulation of CMF across wild-type and knockout PANC1 cells. The second repeat of CRISPR-Cas9 experiments also revealed differences in average CMDFA accumulation levels across WT and mixed MRP3 knockout populations (fold-change) (n = 2). (A) Average geometric mean fold change. (B) Average median fold change.

The second round of CRISPR-Cas9 transfection also showed increased CMF accumulation in PANC1 ABCC3 knockout cells in comparison to wild-type PANC1 cells (Figure 4—6). In this second round the transfected, mixed cell populations showed an increase in CMF accumulation (x-GMean) above that of wild-type PANC1 by 1.499-fold, 1.36-fold and 1.15-fold across gRNA3, gRNA2 and gRNA1 cells, respectively (Figure 4—6). While, the average x-GMean fluorescence seen across gRNA samples was the highest in gRNA3 , the highest levels of fluorescence (x-GMean and median) seen in any of the replicates was seen in a replicate of the gRNA2 mixed populations (Figure 4—7). The variation in CMF accumulation showed that while an upward trend was seen in x-GMean significance could not be established.

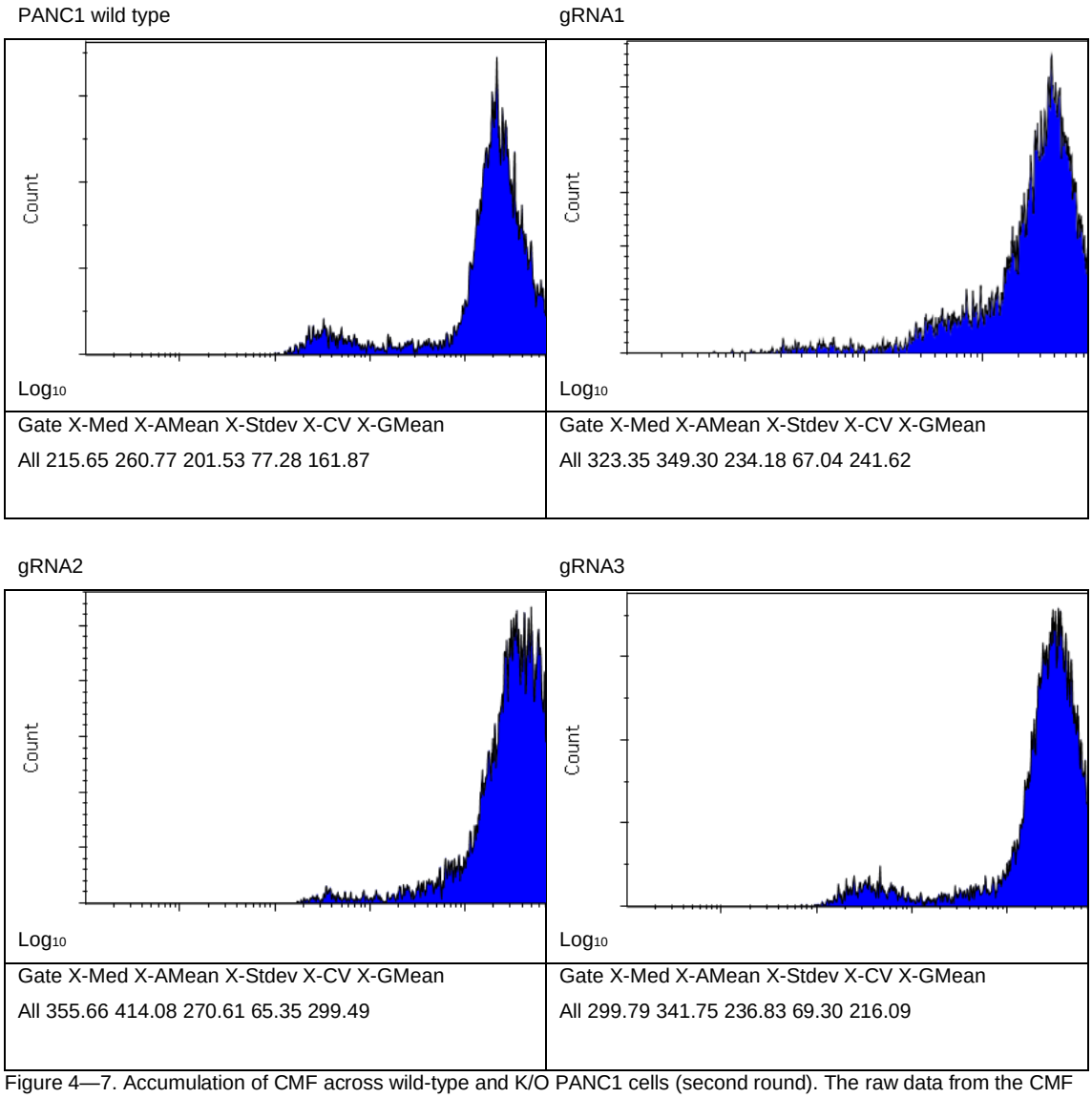


Figure 4—7. Accumulation of CMF across wild-type and K/O PANC1 cells (second round). The raw data from the CMF accumulation study of the second round of the CRISP-Cas9 experiments. The highest CMDFA accumulation levels across WT and mixed knockout populations were extracted from the Kaluza software.

However, median fluorescence results across the same cells and data sets showed that CMF accumulation was significantly (P-values = 0.0112, 0.0006 and 0.002, respectively)

increased in gRNA1, gRNA2 and gRNA3 cells by 18.1%, 39.8 and 53.9% (Figure 4—6). The median values showed much less variations across gRNA samples tested, lowering the standard deviation and highlighting the differences in CMF accumulation levels (Figure 4—6).Furthermore, according to the average median results, gRNA2 cells accumulated the highest amount of CMF (Figure 4—6). The average median fluorescence across duplicates was 1.47-fold, 1.76-fold and 1.38-fold in gRNA1, gRNA2 and gRNA3 mixed populations, respectively (Figure 4—6).

## Modulation of Drug Resistance in ABCC3 Knockout Cell Lines

(A)

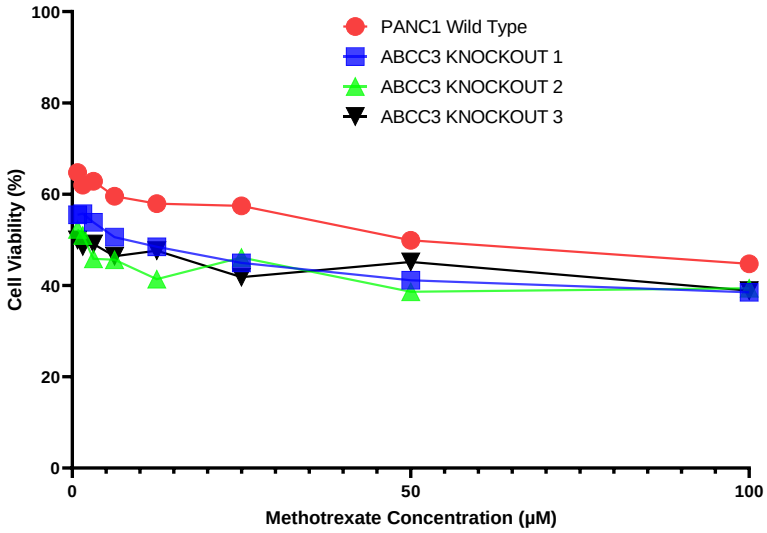


(B)

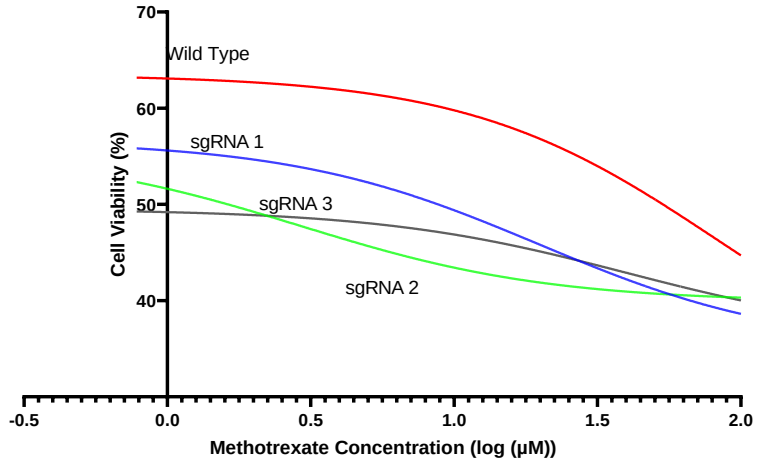


Figure 4—8. Cell viability across WT and K/O cell lines non-linear regression models. (A) Cell viability across K/O and WT cell lines in response to methotrexate concentrations (linear graph). (B) Cell viability across K/O and WT cell lines in response to methotrexate concentrations (log graph).

While these results did not line up exactly with the initial round of CRISPR-cas9 results, the general increase especially in gRNA2 samples were consistent across the two rounds of transfection (Figure 4—4 & Figure 4—6). The shift in fluorescence peaks was also seen across both initial and subsequent transfection experiments in comparison to wild-type PANC1 cells (Figure 4—7). The modulation of ABCC3/MRP3 transport function was established. Whether this modulation would affect drug resistance in PANC1 cells was investigated. The PANC1 cells and knockout cells were grown alongside each other since transfection. The PANC1 cells showed an unusually high resistance towards gemcitabine showing an $IC_{50}$ > 100 µM (Table 4—3). These same cells showed a slightly more sensitive response towards methotrexate ($IC_{50}$ = 81.5 µM) (Table 4—3). In the mixed cell populations, the knockout of ABCC3 showed decreased resistance towards both methotrexate and gemcitabine (Figure 4—8 & Figure 4—9).

Nonlinear regression analysis in GraphPad prism displayed this increase in sensitivity clearly (Figure 4—9 & Figure 4—8). The $IC_{50}$ of methotrexate in wild type cells of 81.5 µM was reduced in gRNA1, gRNA2 and gRNA3 knockout cells with each knockout cell line showing a more potent methotrexate $IC_{50}$ of 19.76 µM, 2.91 µM and 40.33 µM, respectively (Table 4—3). The $IC_{50}$ calculations of gemcitabine in wild type cells (>100 µM) was also reduced in gRNA2 knockout cells to 3.53 µM (Table 4—3). While the remaining knockout cells also showed large gemcitabine $IC_{50}$ values (>100 µM), both gRNA1 and gRNA3 cells both exhibited a downward shift in both the linear and nonlinear graphs, suggesting a decrease in resistance towards gemcitabine than wild type cells (Figure 4—8).

(A)

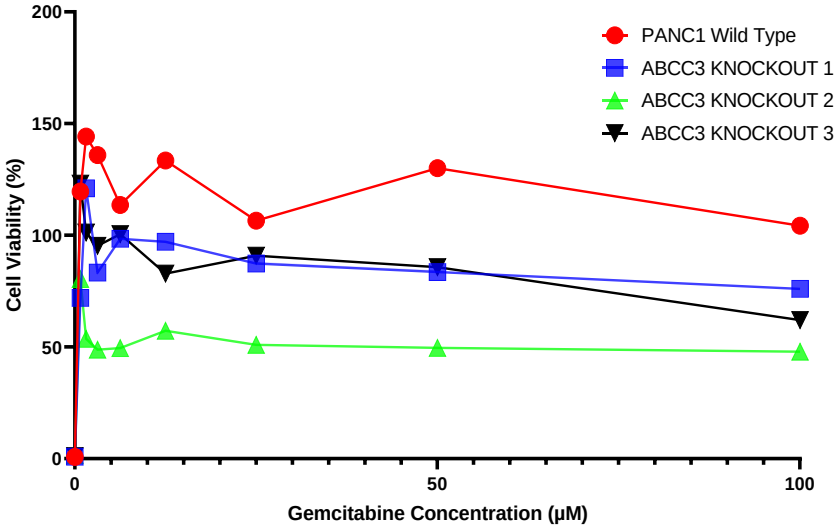

(B)

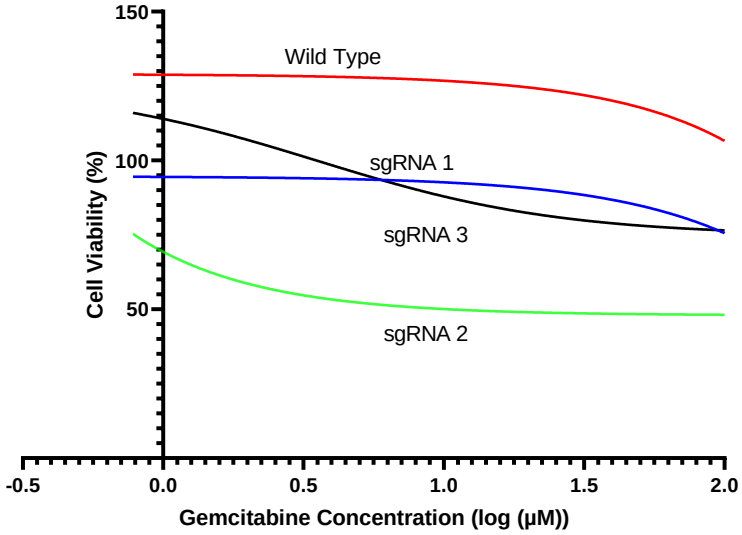


Figure 4—9. Cell viability across WT and K/O cell lines non-linear regression models. (A) Cell viability across K/O and WT cell lines in response to gemcitabine concentrations (linear graph). (B) Cell viability across K/O and WT cell lines in response to gemcitabine concentrations (log graph).

Methotrexate and gemcitabine both showed increased sensitivity in knockout cells in comparison to wild-type, especially ABCC3 knockout 2 cells (Table 4—3, Figure 4—8 & Figure 4—9). Further analysis revealed that the mean cell viability in wild-type PANC1 cells in the presence of methotrexate and gemcitabine were 57.39% and 109.8%, respectively (Table 4—3).

$IC_{50}$ (µM)

| | PANC1 Wild-Type | PANC1 ABCC3 K/O 1 | PANC1 ABCC3 K/O 2 | PANC1 ABCC3 K/O 3 |
|---|---|---|---|---|
| MTX $IC_{50}$ values | 81.5 µM | 19.76 µM | 2.913 µM | 40.33 µM |
| GEM values $IC_{50}$ | >100 µM | >100 µM | 3.530 µM | >100 µM |
| One-way ANOVA results | | | | |
| Mean cellular viability results MTX | 57.39 | 48.59 | 45.03 | 45.94 |
| Dunnett's Test (P-values) MTX | | 0.0122 | 0.0005 | 0.0011 |
| Mean cellular viability results GEM | 109.8 | 79.93 | 48.84 | 82.51 |
| Dunnett's Test (P-values) GEM | | 0.1684 | 0.0016 | 0.2256 |

Table 4—3. Gemcitabine and Methotrexate cytotoxicity across PANC1 wild-type and knockout cells. MTT assay was used to investigate the differences in cytotoxicity between wild-type and knockout cells.

Whereas, across the knockout cells the average cell viability in the presence of varied concentrations of methotrexate significantly dropped to 48.59 (P-value = 0.012), 45.03

(P-value = 0.0005), 45.94 (P-value = 0.0011) in gRNA1, gRNA2 and gRNA3 knockout cells respectively (Table 4—3). The average cell viability across different concentrations of gemcitabine also dropped significantly in gRNA2 cells to 48.84 (P-value = 0.0016) but not the remaining knockout cells (Table 4—3).

**Discussion**

The CRISPR-Cas9 knockout of MRP3 showed reduced functional activity of MRP3 with gRNA2 and gRNA3 knockout cells competing for the highest inhibition in CMF accumulation (Figure 4—4 & Figure 4—7). The subsequent loss in MRP3 function also resulted in the reduction of MRP3-dependent resistance of methotrexate and gemcitabine (Table 4—3). The use of both the geometric mean and the median in the interpretation of flow cytometry results was necessary [303, 304]. While the median value does reduce the effects of outliers, the cells that had high CMF fluorescence may be the very cells that the CRISPR-Cas9 system was meant to create. The results clearly showed that gRNA2 within the mixed population was the most successful increasing CMF accumulation which can be related to a decrease in MRP3 function and multidrug resistance (Figure 4—6, Figure 4—8 & Figure 4—9). MRP1, MRP5, BCRP2 and MRP3 transport has been previously established in literature to transport methotrexate [277, 305]. Therefore, the knockout of MRP3/ABCC3 would be expected to increase sensitivity towards methotrexate. However, gemcitabine has only been previously shown to increase the expression levels of MRP1, MRP5 and MRP3 [29, 302]. This was the first time that modulation of gemcitabine resistance has shown dependence on MRP3 expression, which was highlighted in ABCC3 gRNA2 knockout cells (Table 4—3). These results showed a clear logical flow from knockout to limited function including increased model substrate CMF accumulation and enhanced drug sensitivity. Further validating ABCC3/MRP3 as a viable anticancer target.

The cleavage detection results suggest that the cleavage efficiency in the mixed gRNA populations for both gRNA2 and gRNA3 was low or non-existent. However, these cells showed the highest modulation of CMF accumulation and the most significant changes to drug resistance. Mutations in PANC1 DNA or gRNA could affect both the target sequence and the binding site utilised by Cas9 for double stranded breaks [306]. While the mixed populations of the knockout cells all showed reductions in ABCC3/MRP3 expression, function and multidrug resistance, establishing single clone populations is necessary to fully investigate the extent at which transport and drug resistance of gemcitabine and methotrexate is dependent on ABCC3/MRP3 expression. Furthermore, gene sequencing could be used detect the genomic changes that have allowed the phenotypic changes seen in these cell lines. Further validation across other pancreatic cancer cell lines and comparison between knockout and ABCC3 overexpressing cell

lines would bolster the results found in this study. A recent paper also suggested that truncated versions of proteins may compensate in part for the loss of function caused by CRISPR-Cas9 [254]. Whether this is the reason for the lower CMF accumulation should be investigated.

The successful modulation of ABCC3/MRP3 expression has far reaching applications. The overexpression of ABCC3/MRP3 has been shown as previously stated across several different cancer types. These include pancreatic cancer, breast cancer, lung cancer, bone cancer, and urinary bladder cancer [80, 81, 283, 307]. The ability to successfully target ABCC3 using the CRISPR-Cas9 system will inform our understanding of the dependence of these cancers on the expression of ABCC3/MRP3. Furthermore, ABCC3/MRP3 has been shown to transport a number of anticancer drugs including methotrexate, paclitaxel and monomethyl-auristatin-E (MMAE), sorafenib, etoposide, teniposide and glucuronide conjugates and possibly gemcitabine [60, 79, 88]. These knockout cells can also be used to investigate other drug targets and substrates that could modulated by ABCC3/MRP3 activity.

# Chapter 5 The Role of MRP3 in Drug Resistance

## Introduction

MRP3 expression has transported anticancer drugs and modulated resistance in cancer [36, 277]. The modulation of cytotoxicity was analysed in MRP3 overexpressing cell lines against a variety of drugs [79]. MRP3 was able to inhibit etoposide, teniposide and methotrexate in a concentration and time dependant manner [79]. In normal cells, MRP3 expression is key in the transport of key bile acids [73]. MRP3 expression is also key in the pharmacological activities of drug development and distribution, especially in the context of drug induced liver injury (DILI) [43, 73]. MRP3 expression was able to modulate bile acid homeostasis, a key factor in DILI [73]. MRP3 also showed extensive overexpression in pancreatic, kidney and lung cancer as exhibited by the bioinformatics chapter. MRP3 inhibition by suramin, curcumin and EF24 were investigated in pancreatic cancer cell lines PANC1 and MIAPACA2.

Suramin, was first synthesised in 1916 to treat the parasitic infection, trypanosomiasis (Figure 5—1) [171]. Trypanosomiasis more commonly known as sleeping sickness is a disease that is caused by the *Trypanosoma brucei, T. b. rhodesiense* and *T. b. gambiense* parasites [308]. The disease is transmitted by the bite of the tsetse fly (*Glossina spp*) found in different regions of Africa [308]. The parasites infect and multiply within the blood causing a variety of initial symptoms including fever, headaches and joint pain [308]. These minor symptoms are followed by more serious neurological and endocrinal disorders, which if untreated would result in death within months of initial infection [308]. After extensive characterization of over 1000 naphthalene ureas, germanin (suramin) was discovered to cure trypanosomiasis [308]. Parasites require energy provided by glycolysis in order to multiply within the blood [309]. Suramin inhibits the glycosomal enzymes within the cytosol, directly limiting the energy required to sustain parasitic life [309]. Suramin also showed a wide variety of biological activities including modulation of angiogenesis, WNT signalling, telomere shortening, extracellular matrix (ECM) breakdown, CD40-CD154 immunosuppression and more recently MRP3 inhibition [73, 171, 174, 176, 177]. This has led to the investigation of suramin in several anticancer studies [73, 171, 174, 176, 177].

Suramin has also shown the ability to inhibit angiogenesis in several different models [310, 311]. In ovarian and cervical cancer the overexpression of Hpa was correlated with a poor prognosis [310]. The endo-β-glucuronidase, Hpa is a compound that aids in the breakdown of the ECM, basement membrane by cleaving heparan sulphate proteoglycans [310]. The breakdown of the ECM and the basement membrane are crucial steps in cancer invasion, migration and metastasis [310]. In primary breast tumours, overexpression of Hpa resulted in increased tumour growth, survival and

angiogenesis [312]. Suramin (300-600 µg/ml) was able to significantly inhibit Hpa protein and mRNA expression as well as cell growth in HO-8910PM and HeLa cells in a concentration and time dependent manner [310].

Suramin also inhibited Wnt signalling in triple-negative breast cancer (TNBC) cells [174]. The Wnt signalling proteins play an important role in normal and cancerous cellular processes [313]. The canonical Wnt signalling has been shown to modulate epithelial cell differentiation, endothelial-mesenchymal transition Notch-induced cell cycle arrest and stabilization of vasculature [313]. The non-canonical, Ca2+, Wnt signalling pathway was able to stimulate the nuclear factor of activated T-cells (NFAT) downstream [313]. The transcription factor NFAT is key in the upregulation of VEGF-induced angiogenesis [314]. Canonical Wnt signalling also modulates vascularization of the central nervous system and is responsible for blood-brain barrier (BBB) induction [315, 316]. The ability to inhibit Wnt signalling may explain the wide range of biological activities that suramin can inhibit. The mechanism of suramin inhibition appeared to be the targeting of plasma membrane components of the Wnt signalling pathway by inhibiting g-protein dependent endocytosis [174]. While, the biological activities of suramin has shown vast biological activities, more recently suramin also exhibited the ability to modulate MRP3 [73]. Using a computational, Bayesian model to predict novel MRP3 inhibitors, Ali et al., identified suramin as a potential inhibitor [73]. The accumulation of $E_2$17G, like CMF was dependent on the activity of MRP3 transport across the cell membrane [73, 218, 219]. Further *In vitro* validation revealed suramin to be one of the top three inhibitors of MRP3 dependent transport of $E_2$17G in a membrane vesicle study [7].

Curcumin, a phytochemical derived from the readily available spice turmeric has been extensively investigated in cancer (Figure 5—1) [154-158]. Earlier studies investigated curcumin's clinical activity, apoptotic activity and ABC transporter modulations [154-158]. In cancer, NF-κB modulated apoptosis, tumour proliferation, invasion, angiogenesis and metastasis [154]. Curcumin targeted NF-κB by reducing NF-κB activation, suppressing NF-κB downstream gene products thereby inhibiting proliferation [154]. In pancreatic cancer, a phase II trial testing the clinical effectiveness of curcumin was carried out [154]. Curcumin showed no cytotoxicity across the 25 patients, but bioavailability was limited [154]. However, even with limited bioavailability, two patients still demonstrated positive responses with one patient exhibiting >18 months stable disease [154]. The remaining patient showed a marked reversal in tumour size (73%), which was unfortunately followed by a rapid disease progression [154]. The tumours that regressed continued to do so under curcumin treatment while other tumours that were originally smaller continued to grow, suggesting a heterogeneous population of curcumin-sensitive and resistant cells within the tumour population [154].

Figure 5—1.Chemical structures of Suramin, benzbromarone, curcumin and EF24.

Suramin

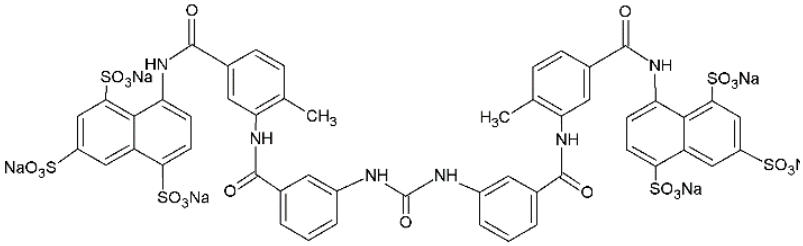

[317]

Benzbromarone

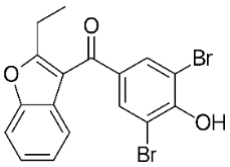

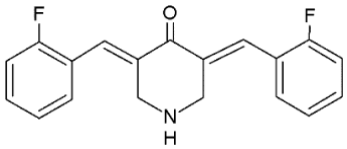

EF24 [318]

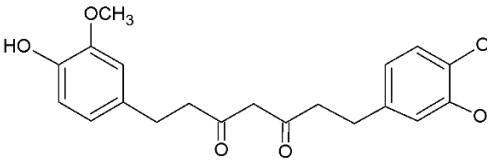

Curcumin [318]

As previously stated, ABC transporters and especially those of the MDR family have shown strong regulation of multidrug resistance in cancer cells and can affect drug disposition and absorption in both normal and cancerous cells [30, 44, 55]. The multidrug resistant cervical cancer cell line (KB-V1) was used to investigate the effects of curcumoids on P-gp expression and function [156]. Curcumin and two closely related compounds showed reduction in both the expression and function of the ABC transporter P-gp [156]. The treatment with curcumin increased the sensitivity of KB-V1 cells to vinblastine above that of the other curcumoids tested [156]. Curcumin also showed the strongest inhibition of verapamil stimulated ATPase activity when compared to the other curcumoids tested [156]. Curcumin also showed the ability to inhibit a broad spectrum of ABC transporters including P-gp, MRP1, MRP5 and BCRP transport across the respective overexpressing cell lines [55, 162]. As previously mentioned, *in vivo* MRP3 knockout mice showed significantly less COG plasma levels of MRP3 suggesting that the loss of MRP3 decreased the accumulation of COG within the plasma and increased in accumulation within the cells [74]. Therefore, COG could be a substrate of MRP3 and possibly a competitive inhibitor as well. Whether curcumin can also inhibit MRP3 was investigated.

The oral bioavailability of curcumin was limited due to poor intestinal absorption, rapid metabolism into curcumin conjugates and a short half-life [159-161]. The intestinal transport of curcumin and two novel derivatives was investigated using a Caco-2 cell monolayer [157]. A chamber designed with both an apical and basolateral compartment was used to detect changes in concentrations across the Caco-2-cell monolayer [157]. Transport rates were calculated and the results demonstrated that curcumin derivatives exhibited improved membrane permeability, suggesting improved bioavailability [157].

The chemical modulation of curcumin in order to improve the specificity, potency and bioavailability has been extensively studied [157, 162]. Monocarbonyl analogues of curcumin (MACs) were created without the unstable β-diketone moiety, improving upon curcumin's *in vivo* pharmacology [162]. 23 MACs were investigated for their ability to improve upon curcumin's inhibition of P-gp, BCRP, MRP1 and MRP5 [162]. These MACs showed improved potency in the inhibition of the ABC transporters tested in comparison to curcumin [162]. The greatest improvements were seen in BCRP transport inhibition [162].

A curcumin MAC EF24, also showed improved biological activity and anticancer affects (Figure 5—1) [162]. EF24 exhibited increased cytotoxicity in a variety of cancer cells in comparison to curcumin and cisplatin [166]. EF24, much like curcumin, interrupted cell cycle progression, induced apoptosis and inhibited cancer cell proliferation by modulating the NF-κB pathway [166]. Whether curcumin's ability to inhibit ABC transporters has translated to EF24 remains unknown. Curcumin, EF24 and suramin inhibition of MRP3 function and reversal of MRP3 dependent drug resistance was investigated.

## Results

### Cytotoxicity

The MTT assay was used to calculate the modulation of cell viability when treated with EF24, suramin, benzbromarone, curcumin, methotrexate and gemcitabine across PANC1 and A549 cells (Table 5—1). The protein atlas database showed that A549 cells showed the highest mRNA expression of ABCC3 across a wide variety of cell lines, not including PANC1 (www.proteinatlas.org). A549 was therefore included in this study as a control for highly expressing ABCC3 cells when needed. In PANC1 and A549 cells, EF24 showed the most potent inhibition of cellular viability across PANC1 ($IC_{50}$: 1.7 μM) and A549 ($IC_{50}$: 2.2 μM) cells (Table 5—1). Curcumin also showed inhibition of cellular viability across PANC1 ($IC_{50}$: 24.81 μM) and A540 ($IC_{50}$: 34.49 μM) cells (Table 5—1). PANC1 cells showed a much higher resistance toward gemcitabine ($IC_{50}$ >100 μM) than in A549 ($IC_{50}$: 17.92 μM) cells (Table 5—1). While A549 cells showed much higher resistance towards methotrexate than in PANC1 cells exhibiting $IC_{50}$ values of 47 μM and >100 μM, respectively (Table 5—1). The nonlinear regression graphs of the tested compounds showed a wide the variety of slopes and curves (Figure 5—2). Suramin, benzbromarone, and curcumin (≥20 μM) all increased cell viability or proliferation beyond that of untreated PANC1 cells (Figure 5—2). This initial stimulation by suramin and curcumin decreased as concentrations increased (Figure 5—2). However, benzbromarone continued to stimulate cell viability up to 100 μM (Figure 5—2).

Figure 5—2. MTT Cell viability results (Log10) of 72-hour incubations (PANC1). All experimental results were averages across three separate experiments. Data was transformed using the GraphPad prism software 8.3.2. The graph with the highest R-value was selected.

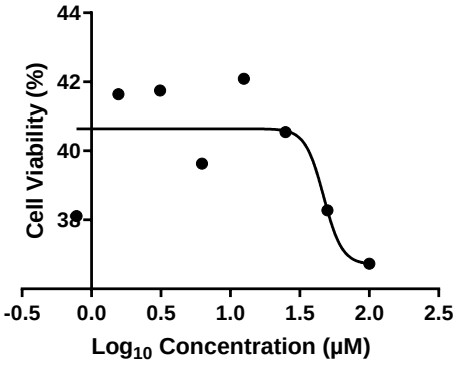


Methotrexate cell viability results.

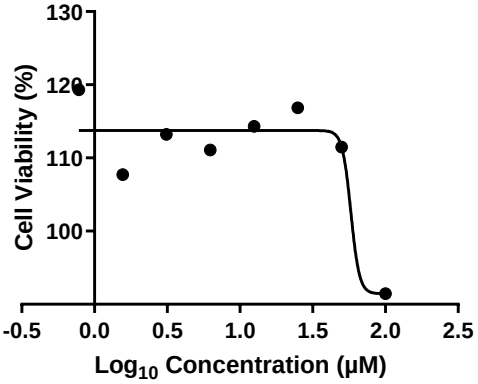


Suramin cell viability results.

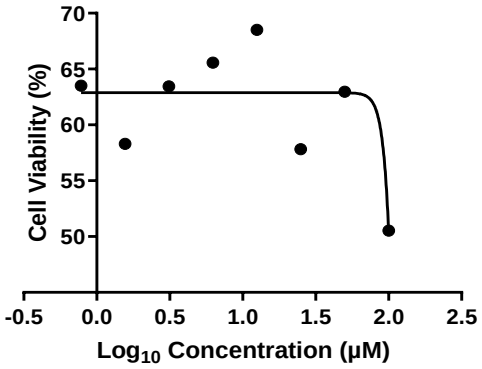


Gemcitabine cell viability results.

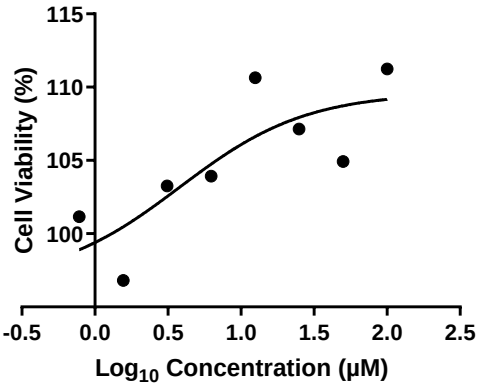


Benzbromarone cell viability results.

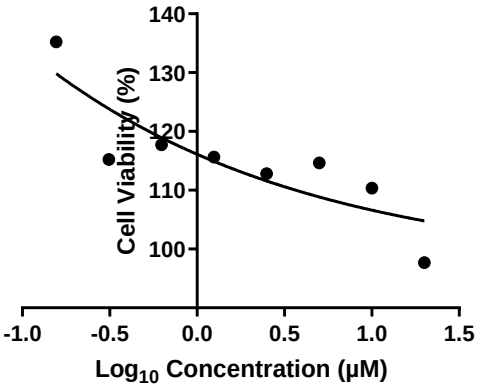


Cell viability of curcumin with the highest concentration ending at 20 μM.

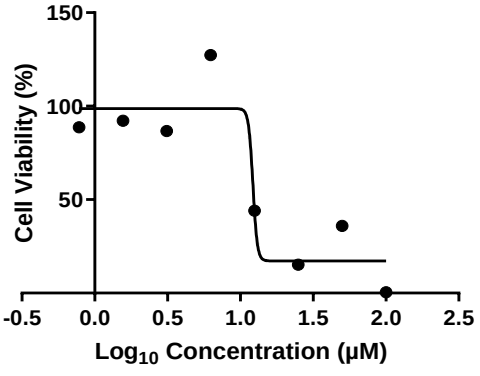


Cell viability of curcumin with the highest concentration ending at 100 μM.

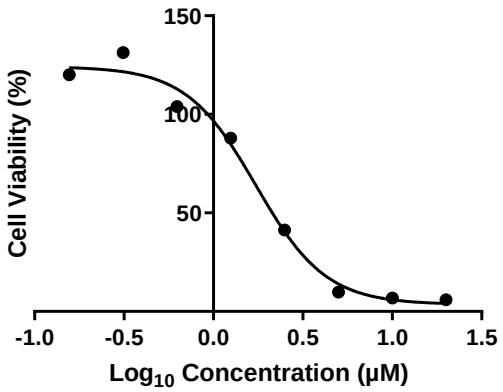


EF24 treated PANC1 cell viability results.

The anticancer drugs methotrexate and gemcitabine both decreased cell viability of PANC1 cells in a concentration dependent manner (Figure 5—2). Methotrexate even at low concentrations caused an initial 60-70% drop in cell viability, which continued to drop at higher concentrations (Figure 5—2). However, gemcitabine treatment up to 100 μM was unable to decrease cell viability by more than 50% (Figure 5—2). Curcumin at higher concentrations (with an final concentration of 100 μM) and EF24 were both able to cause close to 100% cell death, decreasing cell viability in a concentration dependent manner (Figure 5—2).

| | PANC1 | A549 | MIAPACA2 |
|---|---|---|---|
| Suramin | >100 μM | >100 μM | >100 μM |
| EF24 | 1.76 μM | 2.2 μM | 821 nM |
| Gemcitabine | >100 μM | 17.92 μM | 14.88 μM |
| Methotrexate | 47 μM | >100 μM | 3.07 μM |
| Benzbromarone | >100 μM | >100 μM | |
| Curcumin | 24.81 μM | 34.49 μM | |

Table 5—1. Cytotoxicity across PANC1, MIAPACA2 and A549 cells. MTT assay was used to investigate the cytotoxicity ($IC_{50}$) of treatment compounds: suramin, benzbromarone, curcumin, EF24, methotrexate and gemcitabine after 72 hours incubation.

### MRP3 Transport Inhibition

The effects of suramin and benzbromarone on the cellular accumulation of CMF was tested in pancreatic cancer cells (MIAPACA2 and PANC1). The fluorescent CMF signals were detected using flow cytometry which showed that the highest signals were detected after five minutes incubation (Figure 5—3). BCECF a specific substrate of MRP5 transport was also initially tested in MIAPACA2 cells in combination with DMSO (negative control), curcumin, EF24 and benzbromarone (Figure 5—3). The results showed that curcumin (20 μM) significantly increased the geometric mean of BCECF accumulation (P-value = 0.0371) by 2.17-fold (Figure 5—3).

(A)

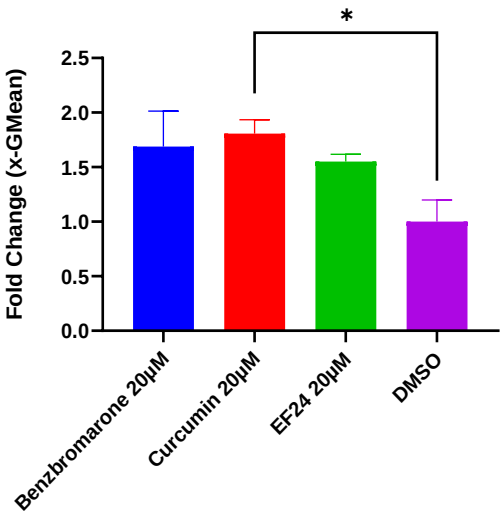
*
Fold Change (x-GMean)
2.5
2.0
1.5
1.0
0.5
0.0
Benzbromarone 20µM
Curcumin 20µM
EF24 20µM
DMSO

(B)

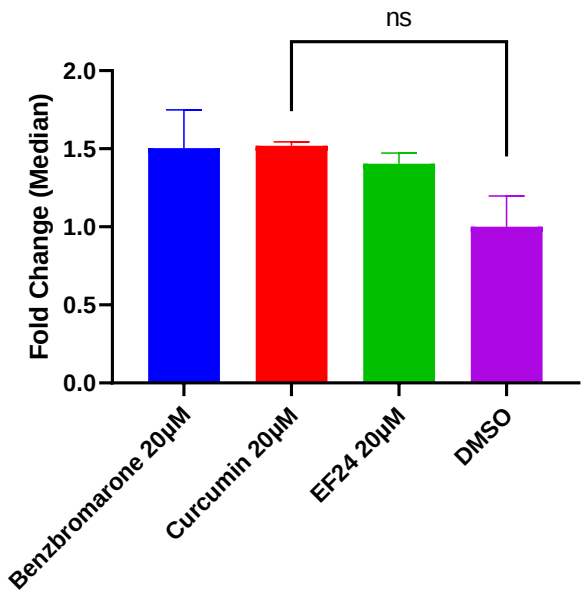
ns
Fold Change (Median)
2.0
1.5
1.0
0.5
0.0
Benzbromarone 20µM
Curcumin 20µM
EF24 20µM
DMSO

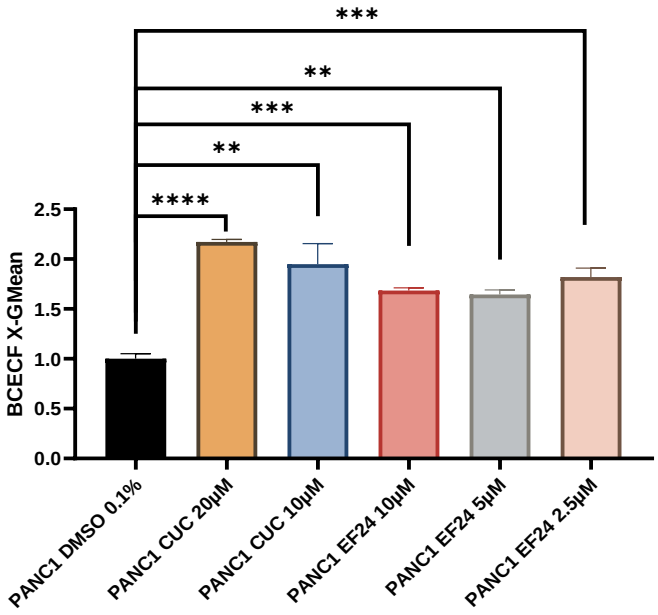
***
**
***
**
****
BCECF X-GMean
2.5
2.0
1.5
1.0
0.5
0.0
PANC1 DMSO 0.1%
PANC1 CUC 20µM
PANC1 CUC 10µM
PANC1 EF24 10µM
PANC1 EF24 5µM
PANC1 EF24 2.5µM

(C)

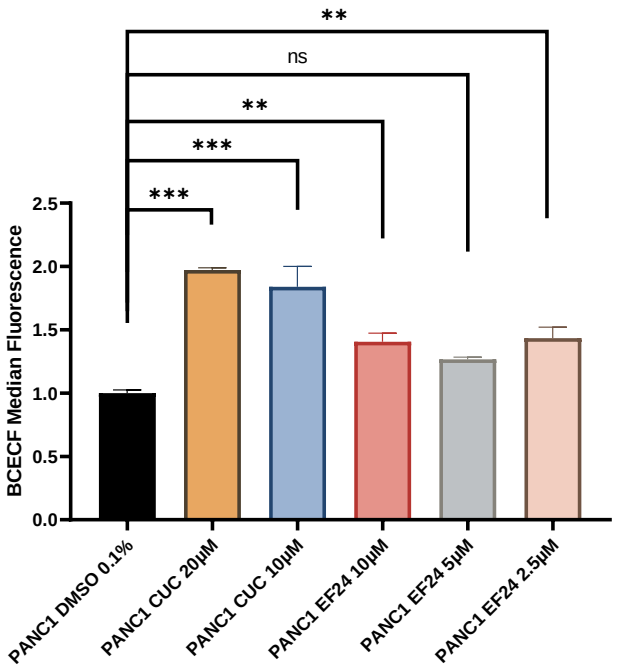


(D)

Figure 5—3. Initial assessment of BCECF (0.25 µM) accumulation (X-gMean or Median fluoresence). MIAPACA2 cells were incubated with DMSO (0.1% in RPMI phenol red free, serum free media), benzbromarone, curcumin and EF24 in combination with BCECF (A) x-GMean or (B) median fluoresence. PANC1 cells were also incubated with a combination of DMSO, CUC or EF24 and BCECF in PANC1 cells at different concentrations (C) x-GMean or (D) median flouresence.

The BCECF accumulation was increased by benzbromarone (20 µM) and EF24 (20 µM) by 1.68 and 1.56-fold (P-values = 0.0614 and 0.1163, respectively). These results also showed an increase in median fluorescence (X-med) by 1.5.17-fold, 1.519-fold and 1.4-fold for benzbromarone, curcumin and EF24, (P-values = 0.079, 0.073, 0.144) respectively (Figure 5—3). Upon further investigation, BCECF accumulation significantly increased in PANC1 cells when treated with curcumin also at 10 µM and at varied concentrations of EF24 (10 µM and 2.5 µM). Curcumin at 10 µM and 20 µM was able to significantly increase BCECF accumulation (x-GMean) by 1.94-fold and 2.17-fold (P-value = 0.0003 and <0.0001) concentrations, respectively (Figure 5—3).

While EF24 at 10 µM, 5 µM and 2.5 µM was able to significantly (P-values = 0.0015, 0.0021 and 0.0006, respectively) increase BCECF (x-GMean) accumulation by 1.68-fold, 1.65-fold and 1.82-fold, respectively (Figure 5—3). The median BCECF accumulation results showed similar but more conservative increases (Figure 5—3). Median BCECF accumulation increased under curcumin (20 µM and 10 µM) and EF24 (10 µM, 5 µM and 2.5) treatment by 1.97-fold, 1.84-fold, 1.41-fold, 1.27-fold and 1.43-fold, respectively (Figure 5—3). Suggesting some evidence of heterogeneity within the sample cells and that 2.5 µM would be a good concentration for MRP5/BCECF inhibition (Figure 5—3 & Table 5—1).

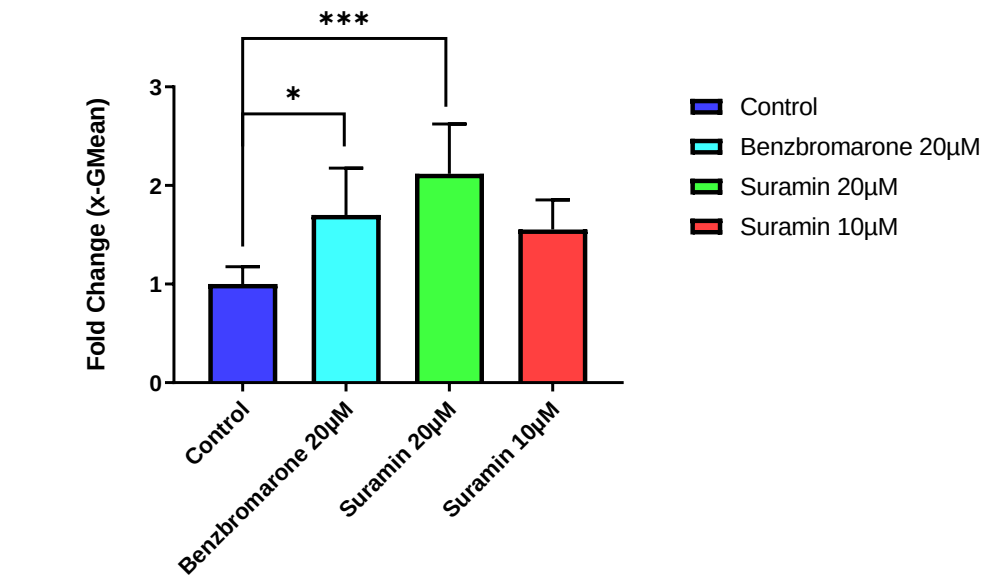


(A)

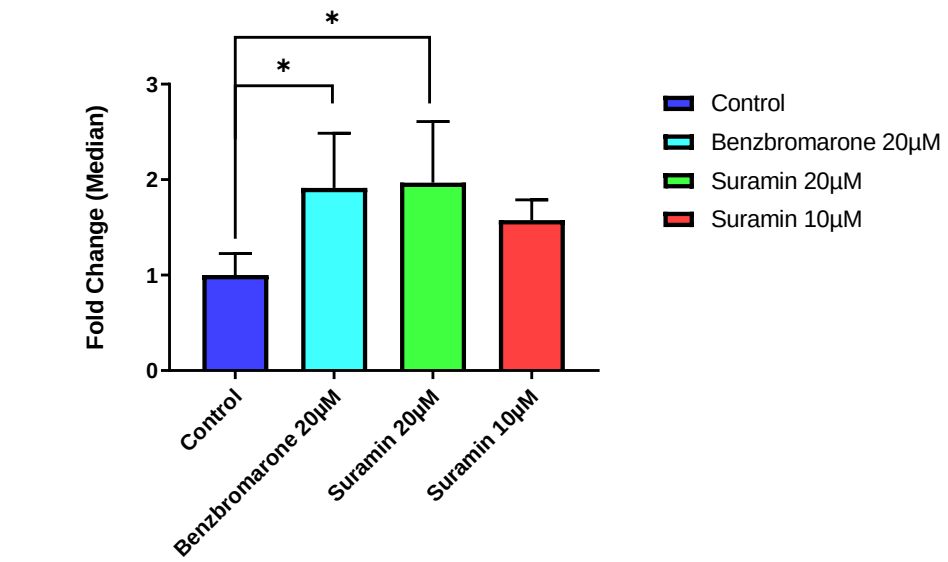


(B)

Figure 5—4. PANC1 accumulation of CMF in the presence of Suramin/Benzbromarone (five minutes). The comparison of fluorescent signals between control (0.1% DMSO in RPMI phenol red free, serum free media), benzbromarone (20 µM) and suramin (20 µM or 10 µM) in PANC1 cells. (A) x-GMean and (B) Median.

CMF accumulation was initially optimised, and the five-minute time point was selected as it showed the highest CMF accumulation (Supplementary Figure 3). PANC1 cells treated with suramin (20 µM) and benzbromarone (20 µM) significantly (P-value = 0.001 and 0.029, respectively) increased the cellular accumulation of CMF by 2.11-fold and 1.7-fold (Figure 5—4). While suramin (10 µM) showed an average increase in CMF accumulation by 1.55-fold. However, this increase was unable to produce significance (P-value = 0.15) (Figure 5—4). The CMF accumulation median showed suramin (20 µM)

and benzbromarone (20 µM) were also able to significantly (P-value = 0.011 and 0.016, respectively) increase CMF across median fluorescence levels by 1.97-fold and1.91-fold, respectively (Figure 5—4). Suramin at 20 µM, 10 µM and 5 µM was also able to increase CMF accumulation in HepG2 cells by 1.55-fold, 2.81-fold and 2.02-fold respectively (data not shown).

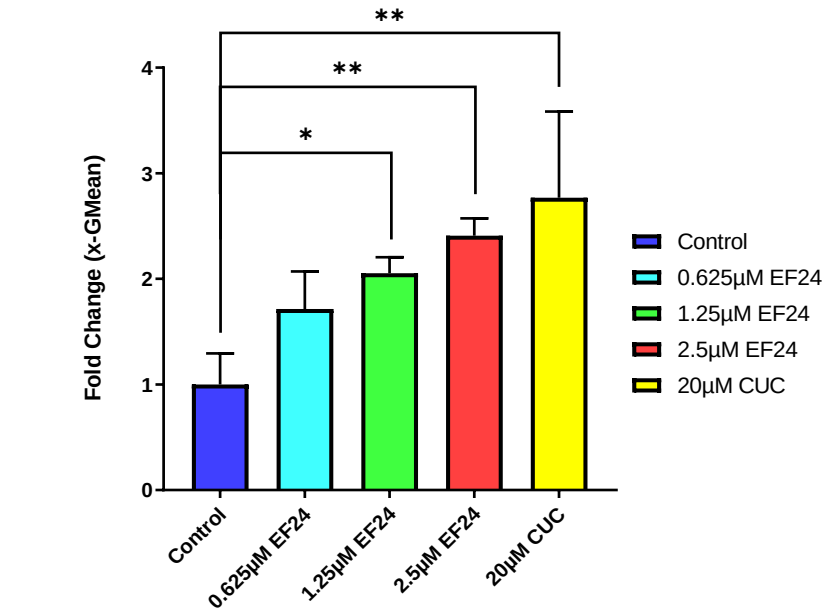


(A)

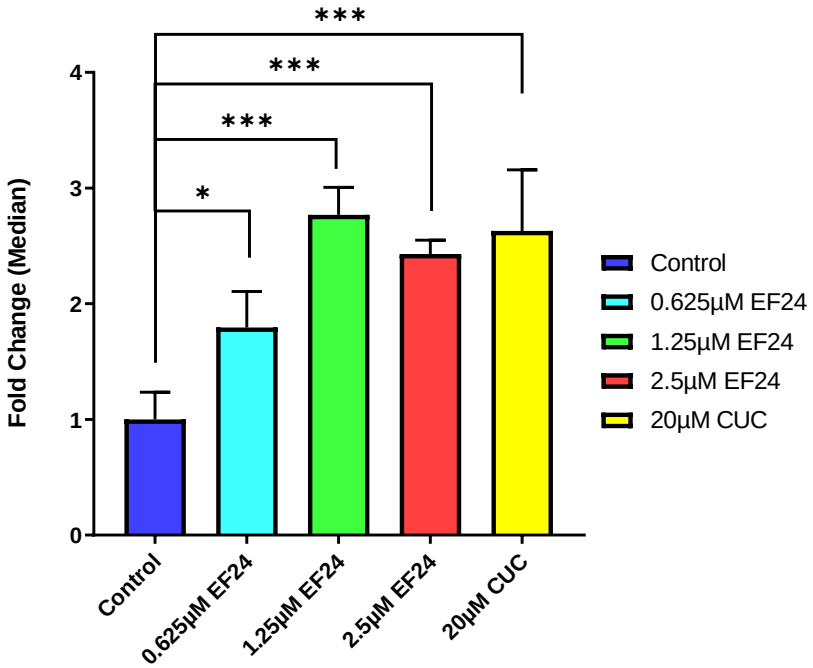


(B)

Figure 5—5. PANC1 accumulation of CMF in the presence of EF24/Curcumin/EF24 (five minutes). The comparison of fluorescent signals between control (DMSO: 0.1%), curcumin (20 µM) and EF24 (2.5 µM, 1.25 µM or 0.625 µM) in PANC1 cells. (A) x-GMean or (B) median fluorescence.

Curcumin and EF24 also showed inhibition of MRP3 in the CMF accumulation assay (Figure 5—5). The same protocol used for the assessment of suramin/benzbromarone modulation of CMF accumulation was used to evaluate curcumin and EF24. EF24 showed a much higher potency than the other compounds tested to illicit inhibition of MRP3-dependent, CMF accumulation (Figure 5—5). EF24 at 2.5 µM had already shown the ability to significantly increase the accumulation of BCECF in PANC1 cells (Figure 5—3). EF24 at 2.5 µM and 1.25 µM was also able to significantly (P-value = 0.0083 and 0.0425, respectively) increased CMF cellular accumulation (x-GMean) by 2.43-fold and 2.05-fold, respectively (Figure 5—5). Even at 0.625 µM, EF24 was also able to increase CMF accumulation by 1.96-fold (P-value = 0.1786) (Figure 5—5). Curcumin (20 µM) also significantly (P-value = 0.0018) increased CMF accumulation within PANC1 cells by 2.77-fold (P-value = 0.0421) (Figure 5—5). For the first time the median CMF fluorescence exhibited stronger evidence that CMF accumulation had increased (Figure 5—5). All compounds tested showed significant increase in the median CMF accumulation (Figure 5—5). Curcumin (20 µM) and EF24 (2.5 µM, 1.25 µM or 0.625 µM) significantly (P-values = 0.0003, 0.0009, 0.0002 and 0.0371, respectively) increased CMF accumulation (median) by 2.63-fold, 2.43-fold, 2.77-fold and 1.79-fold, respectively (Figure 5—5). Curcumin has already showed inhibition a number of other ABC transporters including P-gp, MRP1, MRP5 and BCRP transport across the respective overexpressing cell lines [55, 162]. These results showed that curcumin (20 µM) also increased CMF accumulation, displaying that MRP3 was also inhibited by curcumin (Figure 5—5). Furthermore, these results showed potent and significant inhibition of MRP3 function at 2.5 µM, 1.25 µM and 0.625 µM (Figure 5—5).

**Combination of EF24 and Suramin with Anticancer Drugs in PANC1 cells**

The inhibition of MRP3 function should translate into a reduction in anticancer drug resistance, this was investigated. The use of the diagonal combination design with a ratio of 1:1 drug combinations were recommended for the initial experiment [229]. The CompuSyn software was used to calculate the combination index (CI) and dose-reduction index (DRI) values of the various combinations of the anticancer drugs (MTX or GEM), with the MRP3 inhibitors (SUR or EF24) [229]. The CI can be used to effectively define whether a combination of drugs were synergistic, antagonistic or additive [229]. The DRI is a measure of how many fold the dose of one drug may be reduced in the presence of another drug in comparison to the sole treatment of either drug [229]. The data was interpreted as suggested in a previous paper by chou at al., (Figure 5—6) [229].

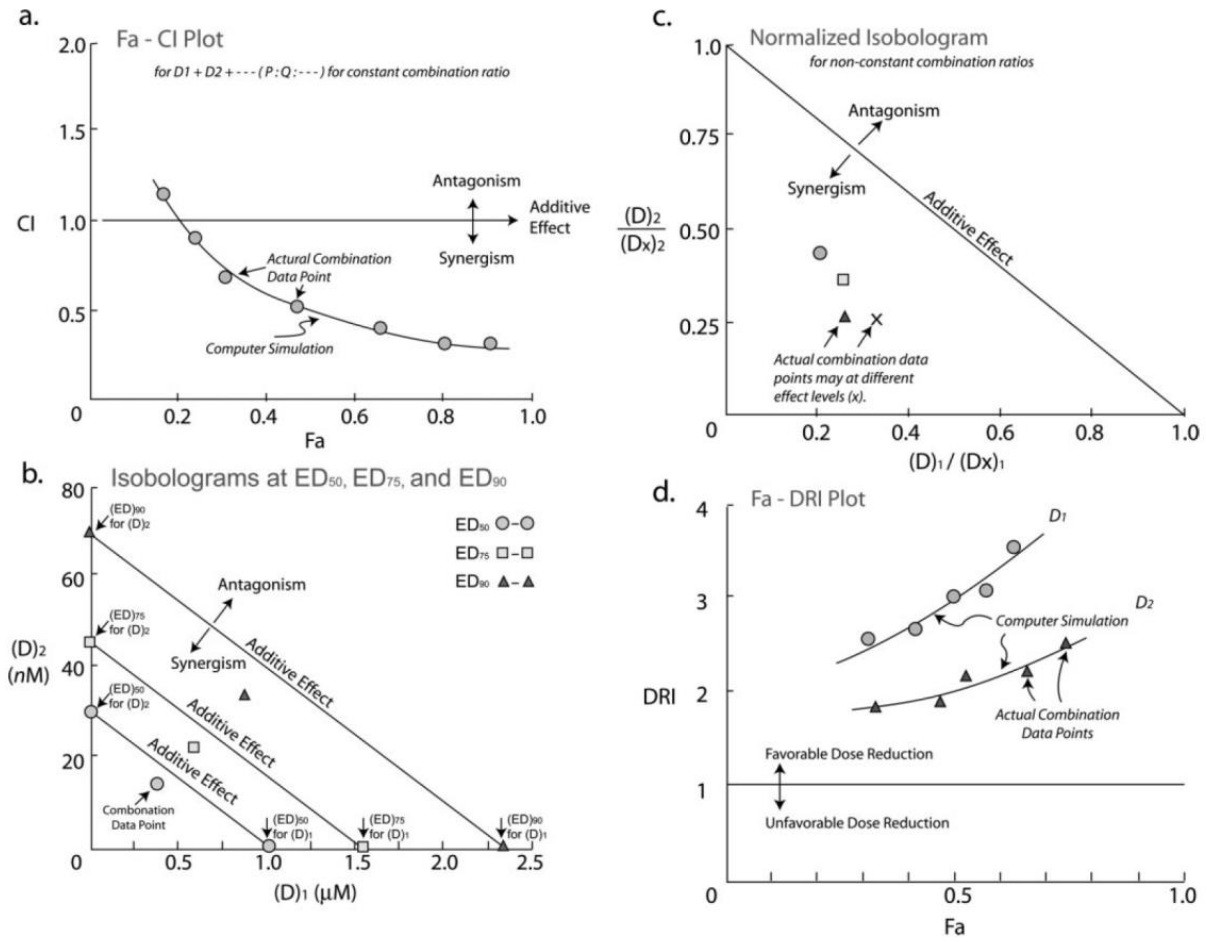


FIG. 8. Typical examples of drug combination plots and their interpretations based on the Chou and Talalay combination index theorem. a, $F_a$-CI plot. b, classic isobologram at $ED_{50}$, $ED_{75}$, and $ED_{90}$. c, normalized isobologram for combination at different combination ratios, and d, the $F_a$-DRI plot. All of these plots can be generated automatically by using CompuSyn (Chou and Martin, 2005).

Figure 5—6. Combination plots explained by chou et al., [229].

### Gemcitabine and EF24

The CompuSyn analysis showed high inhibition of PANC1 cell viability by EF24 and low inhibition of cell viability by GEM, which is consistent with previous results (Table 5—2 & Table 5—1). The analysis parameters of slope (m), potency (Dm) and goodness of fit (r) revealed that gemcitabine showed low conformity (r-value = -0.2068) to the median effect principle (MEP) and therefore, Dm and m values could not be trusted (Table 5—2). This result was most likely due to the fact that gemcitabine did not previously show more than a 50% reduction in cell viability up to 100 μM (data not shown). The slope (m) is an important parameter as it is used to calculate the CI [229]. Conversely, EF24 showed a strong r-value (0.944), with a sigmoidal curve (m>1) and a low Dm (0.647 μM) (Table 5—2). The combination of gemcitabine and EF24 the data showed a higher Dm than EF24 or gemcitabine alone (3.44834) which would suggest a less potent combination than EF24 alone (Table 5—2). The combination of EF24 and gemcitabine also showed less conformity to the MEP (r-value = 0.895) (Table 5—2).

| Compound | | Fractional Inhibition | Parameters | | | CI [DRI (GEM); DRI (EF24)] |
|---|---|---|---|---|---|---|
| GEM (µM) | EF24 (µM) | (Fa) | m | Dm | r | |
| 100 | | 0.323 | -0.0672 +/- 0.15907 | 4.33E-05 | -0.2068 | |
| 50 | | 0.221 | | | | |
| 25 | | 0.234 | | | | |
| 12.5 | | 0.334 | | | | |
| 6.25 | | 0.459 | | | | |
| 3.125 | | 0.237 | | | | |
| | 20 | 0.996 | 1.45122 +/- 0.25452 | 0.6426 | 0.94363 | |
| | 10 | 0.986 | | | | |
| | 5 | 0.880 | | | | |
| | 2.5 | 0.794 | | | | |
| | 1.25 | 0.752 | | | | |
| | 0.625 | 0.637 | | | | |
| 100 + 20 | | 0.999 | 1.60679 +/- 0.39931 | 3.44834 | 0.89549 | 1.59E49 [6.3E-50;3.10467] |
| 50 + 10 | | 0.984 | | | | 5.47E32 [1.8E-33;1.10679] |
| 25 + 5 | | 0.975 | | | | 2.43E29 [4.1E-30;1.59850] |
| 12.5 + 2.5 | | 0.627 | | | | 6.367E8 [1.57E-9;0.36724] |
| 6.25 + 1.25 | | 0.829 | | | | 2.24E15 [4.5E-16;1.52493] |
| 3.125 + 0.625 | | 0.730 | | | | 1.98E11 [5.1E-12;2.04348] |
| | | Simulation | | | | |
| | | 0.05 | | | | 1.08851 [9.76E14;0.91869] |
| | | 0.1 | | | | 1.03557 [9.162E9;0.96565] |
| | | 0.15 | | | | 1.00410 [7068269;0.996] |
| | | 0.2 | | | | 0.98107 [32047.0;1.01933] |
| | | 0.25 | | | | 0.96508 [371.677;1.039] |
| | | 0.3 | | | | 1.07844 [7.57246;1.05665] |
| | | 0.5 | | | | 66324.8 [1.51E-5;1.11810] |
| | | 0.65 | | | | 9.700E8 [1.03E-9;1.16525] |
| | | 0.75 | | | | 1.63E12 [6.1E-13;1.20313] |
| | | 0.95 | | | | 4.29E24 [2.3E-25;1.36080] |

Table 5—2. Dose and effect data were obtained from the MTT assay (average value of triplicate) and were subjected to CompuSyn analysis in accordance chou et al., [229]. The combination index values can be interpreted as synergistic (CI<1), additive (CI=1) and antagonistic (CI>1) [228]. The combination of gemcitabine and EF24 was compared.

Gemcitabine and EF24 at low concentrations demonstrated a slightly synergistic or additive effect with combination indexes ranging from 0.965 to 1.08851 between fa values of 0.005 and 0.3 (Table 5—2). While the fa values under 0.3 would usually be considered small inhibitory effects, it was at this inhibition level that gemcitabine was able to show any inhibition in the highly resistant PANC1 cells (Table 5—2). These data points also corresponded with highly favourable dose reduction indexes for gemcitabine (DRI>1) while, EF24 showed no dose reduction responses (Table 5—2). The remaining data including the combination index values for the actual/non-simulated data, showed that gemcitabine and EF24 at higher inhibition levels (Fa) returned highly antagonistic

results (CI>1) (Table 5—2). Gemcitabine also showed unfavourable does reductions (DRI), while EF24 showed moderately favourable (DRI) (Table 5—2). These results demonstrate that EF24 could add to the cytotoxic effects of gemcitabine across the ranges when gemcitabine was able to illicit cytotoxicity alone.

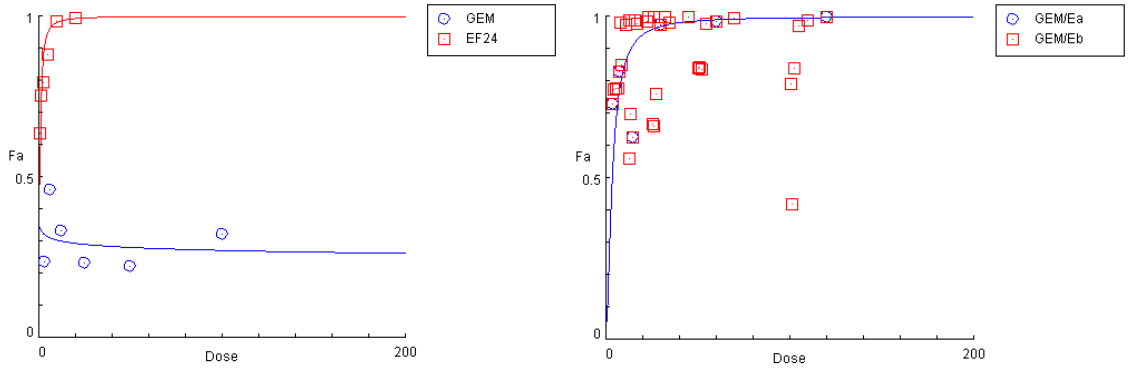


A B

Figure 5—7. The dose-response curves for inhibition of PANC1 cell viability. (A) Gemcitabine and EF24 dose-response curves were shown with a nonlinear curve fitted. (B) The simulated and actual data for the combination of gemcitabine and EF24.

These conclusions were consistent with the graphical outputs of the CompuSyn software (Figure 5—8). The combination plot for gemcitabine and EF24 clearly showed that at lower concentrations and inhibitory effects that the relationship between the two drugs appeared to centralise around additive (CI=1) CI values (Figure 5—8). While, at higher concentrations the relationship became clearly antagonistic (Figure 5—8). Both DRI curves exhibited what was previously shown, in that the initial concentrations of EF24 showed slight improvement in potency, but as the concentrations and effects of the combination increased the antagonistic characteristics increased (Figure 5—8). While, gemcitabine showed almost favourable DRI but only at levels lower than 0.4 (Fa) (Figure 5—8). At higher inhibitions DRI levels for gemcitabine became highly unfavourable (Table 5—2 & Figure 5—8).

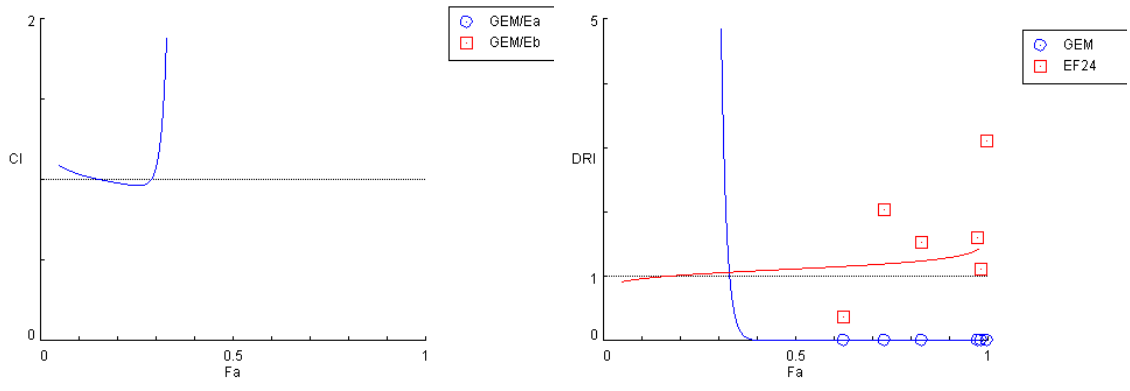


A B

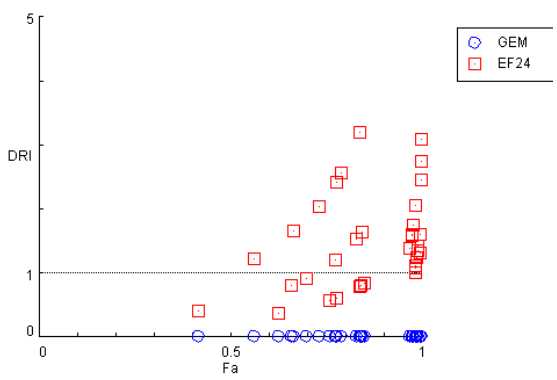
GEM
EF24
DRI
Fa

C

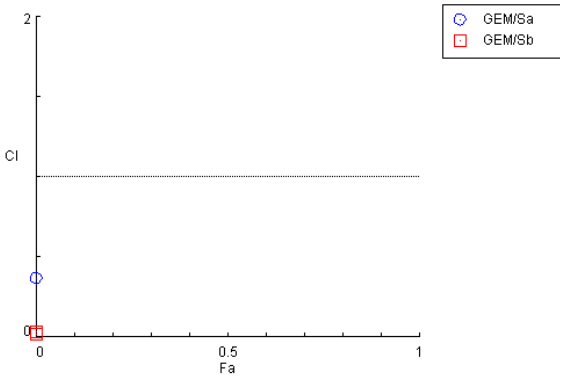
GEM/Sa
GEM/Sb
CI
Fa

D

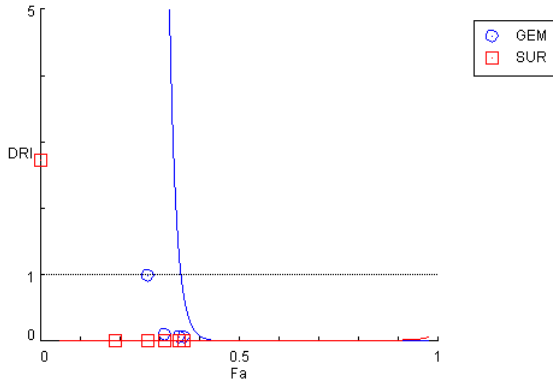
GEM
SUR
DRI
Fa

E

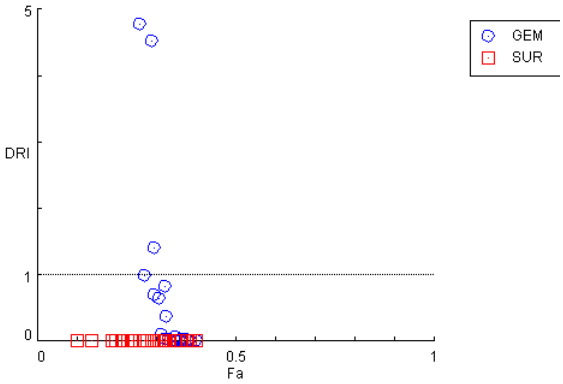
GEM
SUR
DRI
Fa

F

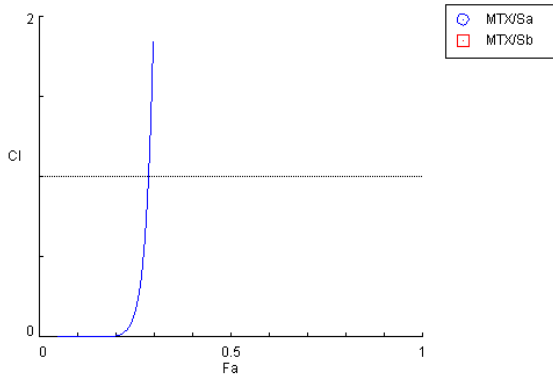
MTX/Sa
MTX/Sb
CI
Fa

G

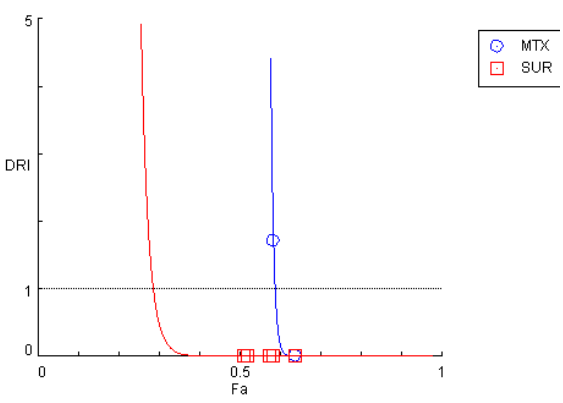
MTX
SUR
DRI
Fa

H

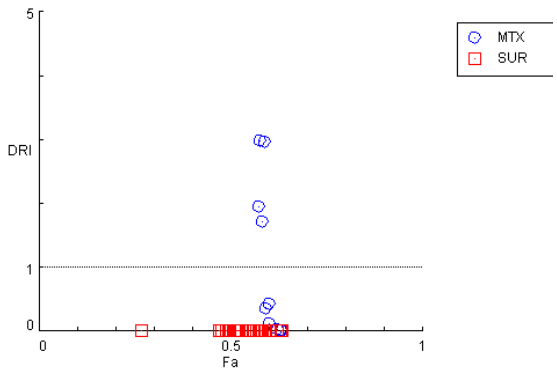
MTX
SUR
DRI
Fa

I

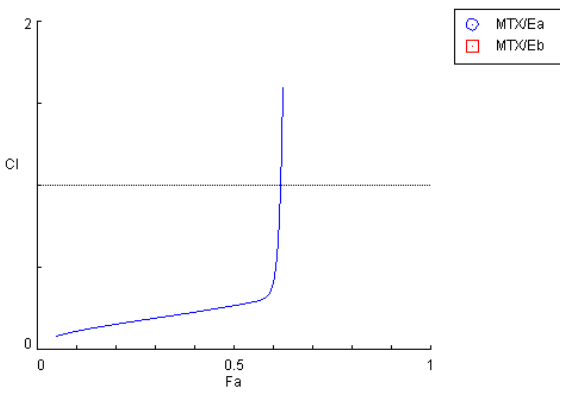
MTX/Ea
MTX/Eb
CI
Fa

J

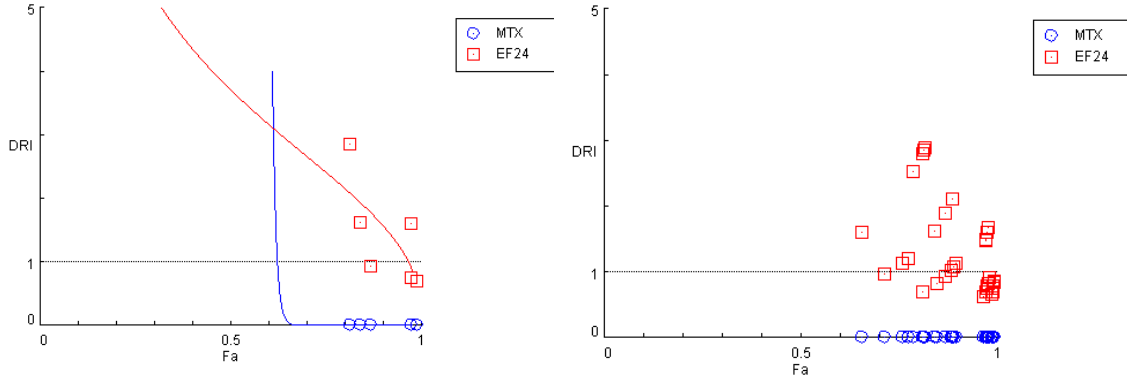


K L

Figure 5—8. Combination plot for the coincubation treatments of GEM and EF24 in panc1 cells. (A) Combination plot of gemcitabine and EF24. (B) The DRI plot in the combination of gemcitabine and EF24 (constant ratio). (C) The DRI plot in the combination of gemcitabine and EF24 (non-constant ratio). (D) Combination plot of gemcitabine and suramin. (E) The DRI plot in the combination of gemcitabine and suramin (constant ratio). (F) The DRI plot in the combination of gemcitabine and suramin (non-constant ratio). (G) Combination plot of methotrexate and suramin. (H) The DRI plot in the combination of methotrexate and suramin (constant ratio). (I) The DRI plot in the combination of methotrexate and suramin (non-constant ratio). (J) Combination plot of methotrexate and suramin. (K) The DRI plot in the combination of methotrexate and suramin (constant ratio). (L) The DRI plot in the combination of methotrexate and suramin (non-constant ratio).

## Gemcitabine and Suramin

The combination of suramin and gemcitabine was also investigated in PANC1 cells (Table 5—3). Much like gemcitabine, suramin did not fit the MEP model well (r-value = -0.3928) (Table 5—3). This could also be due to the lack of cytotoxicity of both compounds across these concentration ranges resulting in flat curves that do not fit the model well (Table 5—3). The combination of gemcitabine and suramin enhanced the divergence from the MEP model (r-value = -0.1617) (Table 5—3). Suggesting that the combination of gemcitabine and suramin did not fit the MEP model well.

| Compound | | Fractional Inhibition | Parameters | | | CI [DRI (GEM); DRI (Suramin)] |
|---|---|---|---|---|---|---|
| GEM (µM) | Suramin (µM) | (Fa) | m | Dm | r | |
| 100 | | 0.323 | -0.0672 +/- 0.15907 | 4.33E-05 | -0.2068 | |
| 50 | | 0.221 | | | | |
| 25 | | 0.234 | | | | |
| 12.5 | | 0.334 | | | | |
| 6.25 | | 0.459 | | | | |
| 3.125 | | 0.237 | | | | |
| | 100 | 0.0001 | -0.7141 +/- 0.83600 | 1.71E-4 | -0.3928 | |
| | 50 | 0.0001 | | | | |
| | 25 | 0.0001 | | | | |
| | 12.5 | 0.0001 | | | | |
| | 6.25 | 0.03122 | | | | |

| | | | | | | | |
|---|---|---|---|---|---|---|---|
| | 3.125 | 0.0001 | | | | | |
| 100 + 100 | | 0.272 | -0.4259 1.29938 | +/- | 0.17082 | -0.1617 | 147803 [0.98521;6.77E-6] |
| 50 + 50 | | 0.313 | | | | | 97819.9 [0.10042;1.02E-5] |
| 25 + 25 | | 0.0001 | | | | | 0.367 [5.24E53;2.7216] |
| 12.5 + 12.5 | | 0.188 | | | | | 9447.5 [9768.12;1.06E-4] |
| 6.25 + 6.25 | | 0.350 | | | | | 15452.5 [0.06750;6.48E-5] |
| 3.125 + 3.125 | | 0.362 | | | | | 8298.9 [0.06380;1.21E-4] |
| | | Simulation | | | | | |
| | | 0.15 | | | | | 2.20E-4 [1.10E30;4545.89] |
| | | 0.25 | | | | | 0.15873 [7.51E20;6.30010] |
| | | 0.5 | | | | | 13742.1 [111080.;7.28E-5] |
| | | 0.65 | | | | | 8328012 [1.34E-4;1.20E-7] |
| | | 0.75 | | | | | 6.21E10 [1.6E-11;8.4E-10] |
| | | 0.95 | | | | | 2.40E37 [4.2E-38;4.3E-18] |

Table 5—3. Dose and effect data were obtained from the MTT assay (average value of triplicate) and were subjected to CompuSyn analysis in accordance chou et al., [229]. The combination index values can be interpreted as synergistic (CI<1), additive (CI=1) and antagonistic (CI>1) [228]. The combination of gemcitabine and suramin was compared.

However, the results demonstrated that suramin (25 µM) and gemcitabine (25 µM) combined, exhibited moderate synergism with CI values of 0.367 (Table 5—3). The simulated data at lower inhibition levels (>0.25 fa) also showed moderate to strong synergism (Table 5—3). At inhibition levels of 0.15 (Fa) and 0.25 (Fa) the GEM:SUR combination resulted in CI values of 0.0002 and 0.159 (Table 5—3). The combination and sole treatments of gemcitabine and suramin both did not achieve higher inhibition (Fa) levels (Figure 5—9). Which explains the inability of the CompuSyn program to plot the Fa-CI plot (Figure 5—8). Therefore, while the r value is low the data would suggest that like EF24, suramin may be able to marginally enhance the cytotoxicity of gemcitabine at lower doses (Figure 5—9 & Table 5—3). Interestingly, the combination of GEM:SUR at these low doses also overcame the initial enhancement of proliferation exhibited by suramin (Figure 5—2).

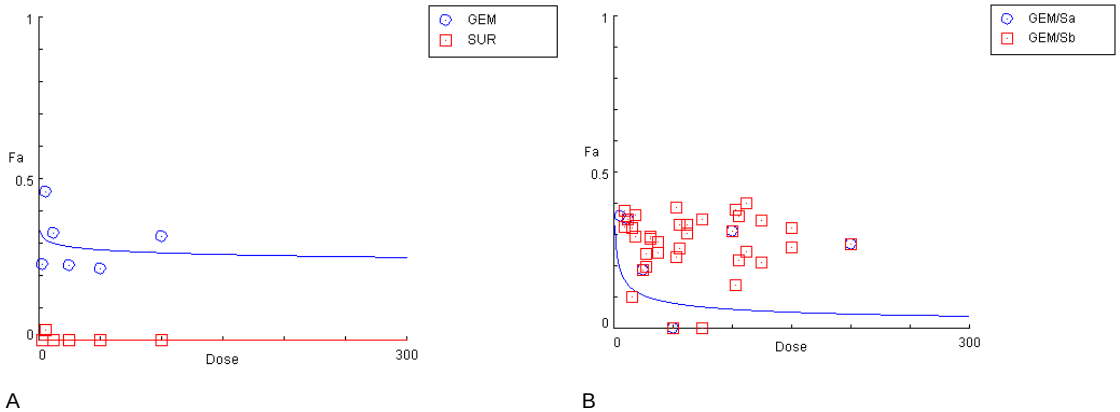


A B

Figure 5—9. The dose-response curves for inhibition of PANC1 cell viability. (A) Gemcitabine and suramin dose-response curves were shown with a nonlinear curve fitted. (B) The simulated and actual data for the combination of gemcitabine and suramin.

**Methotrexate and Suramin**

As previously shown, methotrexate was initially more cytotoxic than gemcitabine in PANC1 cells (Table 5—1). The conformity of both suramin and methotrexate was low in both single incubations (r values = -0.3928 and -0.3421, respectively). However, the combination of suramin and MTX showed good conformity (r-value = 0.94905) (Table 5—4). The combination of suramin and MTX showed improved potency (Dm = 1.04) above that of the ambiguous MTX Dm estimate (Dm = 260265). At the lower fa levels, the combination index showed strong synergism up to 0.25 (Fa) with CI values ≤ 0.159 (Table 5—4 & Figure 5—8). These synergistic combinations also exhibited corresponding highly favourable DRI values for MTX and SUR (DRI ≥ 7.51E20 and 4545.9, respectively) (Table 5—4 & Figure 5—8). The actual data showed approximately half of the combinations showed favourable DRI values for MTX (Figure 5—8). Suggesting that the addition of suramin increased the potency of MTX. However, the remaining combinations of suramin and MTX showed strong antagonism and unfavourable DRI values between the two drugs (Table 5—4). Suggesting that these combinations were unable to achieve strong cytotoxicity at the chosen concentrations.

| Compound | | Fractional Inhibition | Parameters | | | | CI [DRI (MTX); DRI (Suramin)] |
|---|---|---|---|---|---|---|---|
| MTX (µM) | Suramin (µM) | (Fa) | m | | Dm | r | |
| 100 | | 0.604 | -0.0413 | +/- 0.05667 | 260265 | -0.3421 | |
| 50 | | 0.568 | | | | | |
| 25 | | 0.586 | | | | | |
| 12.5 | | 0.563 | | | | | |
| 6.25 | | 0.665 | | | | | |
| 3.125 | | 0.597 | | | | | |
| | 100 | 0.0001 | -0.7141 | +/- 0.83600 | 1.71E-4 | -0.3928 | |
| | 50 | 0.0001 | | | | | |
| | 25 | 0.0001 | | | | | |
| | 12.5 | 0.0001 | | | | | |
| | 6.25 | 0.03122 | | | | | |
| | 3.125 | 0.0001 | | | | | |
| 100 + 20 | | 0.638 | 0.11176 | +/- 0.05870 | 1.04094 | 0.94905 | 1298106 [0.00280 7.71E-7] |
| 50 + 10 | | 0.582 | | | | | 466210 [1.70822;2.14E-6] |
| 25 + 5 | | 0.511 | | | | | 156098 [3524.55;6.41E-6] |
| 12.5 + 2.5 | | 0.519 | | | | | 81774.0 [3146.01;1.22E-5] |
| 6.25 + 1.25 | | 0.572 | | | | | 55249.8 [34.3878;1.81E-5] |
| 3.125 + 0.625 | | 0.510 | | | | | 19414.7 [30749.7;5.15E-5] |
| | | Simulation | | | | | |
| | | 0.15 | | | | | 2.20E-4 [1.10E30;4545.89] |
| | | 0.2 | | | | | 0.00809 [1.05E25;123.667] |

| | | | | | | |
|---|---|---|---|---|---|---|
| | | 0.25 | | | | 0.15873 [7.51E20;6.3001] |
| | | 0.5 | | | | 13742.1 [111080;7.28E-5] |
| | | 0.65 | | | | 8328012 [1.34E-4 1.20E-7] |
| | | 0.75 | | | | 6.21E10 [1.6E-11 8.4E-10] |
| | | 0.95 | | | | 2.40E37 [4.2E-38 4.3E-18] |

Table 5—4. Dose and effect data were obtained from the MTT assay (average value of triplicate) and were subjected to CompuSyn analysis in accordance chou et al., [229]. The combination index values can be interpreted as synergistic (CI<1), additive (CI=1) and antagonistic (CI>1) [228]. The combination of methotrexate and suramin was compared.

### Methotrexate and EF24

The combination of MTX and EF24 was the final combination tested in PANC1 cells yielding m, dm and r values of 1.60679 +/- 0.39931, 3.44834 and 0.89549 respectively (Table 5—5). At inhibition fractions (Fa) up until 0.6 the combination of MTX and EF24 showed moderate synergism with CI values ranging from 0.137 to 0.412 across fa values of 0.15 to 0.6, respectively (Table 5—5). The combination of MTX and EF24 also showed favourable dose reduction up to 0.6 Fa (Table 5—5). The remaining data showed that higher inhibition fractions, the combination of MTX and EF24, the relationship shifted from synergistic to antagonistic, most likely due to the maximum cytotoxicity of MTX being less than that of EF24 (Figure 5—8). This was supported by the fact that the DRI values of EF24 remained favourable over the entire simulated dataset (Figure 5—7 & Figure 5—8). The MTX:EF24 combination index showed the widest ranging synergistic effects in comparison to the other combinations, as shown by the combination plot (Figure 5—8). Suggesting that at the concentrations selected, this could be the most effective combination in PANC1 cells.

| Compound | | Fractional Inhibition | Parameters | | | CI [DRI (MTX); DRI (EF24)] |
|---|---|---|---|---|---|---|
| MTX (µM) | EF24 (µM) | (Fa) | m | Dm | r | |
| 100 | | 0.604 | -0.0413 +/- 0.05667 | 260265 | -0.3421 | |
| 50 | | 0.568 | | | | |
| 25 | | 0.586 | | | | |
| 12.5 | | 0.563 | | | | |
| 6.25 | | 0.665 | | | | |
| 3.125 | | 0.597 | | | | |
| | 20 | 0.996 | 1.45122 +/- 0.25452 | 0.6426 | 0.94363 | |
| | 10 | 0.986 | | | | |
| | 5 | 0.880 | | | | |
| | 2.5 | 0.794 | | | | |
| | 1.25 | 0.752 | | | | |
| | 0.625 | 0.637 | | | | |
| 100 + 20 | | 0.987 | 1.60679 +/- 0.39931 | 3.44834 | 0.89549 | 3.69E43 [2.7E-44 0.69667] |
| 50 + 10 | | 0.973 | | | | 8.21E33 [1.2E-34 0.75529] |

| | | |
|---|---|---|
| 25 + 5 | 0.975 | 2.74E34 [3.6E-35 1.59443] |
| 12.5 + 2.5 | 0.868 | 3.08E15 [3.3E-16 0.94031] |
| 6.25 + 1.25 | 0.840 | 7.13E12 [1.4E-13 1.61410] |
| 3.125 + 0.625 | 0.815 | 4.84E10 [2.1E-11 2.85669] |
| | Simulation | |
| | 0.15 | 0.13663 [3.51E24;7.31887] |
| | 0.2 | 0.15666 [5.20E20;6.38340] |
| | 0.25 | 0.17539 [3.58E17;5.70161] |
| | 0.3 | 0.19358 [6.18E14;5.16588] |
| | 0.35 | 0.21173 [1.91E12;4.72304] |
| | 0.5 | 0.26999 [300034; 3.70395] |
| | 0.6 | 0.41207 [10.4710;3.15883] |
| | 0.65 | 21.6150 [0.04701;2.90475] |
| | 0.75 | 3977566 [2.51E-7;2.40621] |
| | 0.95 | 7.77E26 [1.3E-27;1.16571] |

Table 5—5. Dose and effect data were obtained from the MTT assay (average value of triplicate) and were subjected to CompuSyn analysis in accordance chou et al., [229]. The combination index values can be interpreted as synergistic (CI<1), additive (CI=1) and antagonistic (CI>1) [228]. The combination of methotrexate and EF24 was compared.

## Combination of EF24 and Suramin with Anticancer Drugs in MIAPACA2 cells

### Gemcitabine and Suramin

The combination of suramin or EF24 with the anticancer drugs gemcitabine and methotrexate was also investigated in MIAPACA2 cells (Table 5—6). Much like in PANC1 cells, gemcitabine, did not fit the MEP model well (r-value = -0.166) (Table 5—6). However, the suramin model appeared to fit better in MIAPACA2 cells, which could also be due increased cytotoxicity exhibited by suramin in MIAPACA2 cells (r-value = 0.598) (Table 5—1 & Table 5—6). The conformity of the GEM:SUR model to the MEP slightly decreased when in combination (r-value = 0.574) (Table 5—6). While the r-value was lower in combination in MIAPACA2 cells, this combination still showed increased conformity in comparison to the gemcitabine and suramin combination in PANC1 cells.

| Compound | | Fractional Inhibition | Parameters | | | CI [DRI (GEM); DRI (Suramin)] |
|---|---|---|---|---|---|---|
| GEM (µM) | SUR (µM) | (Fa) | m | Dm | r | |
| 10 | | 0.613 | -0.0189+/-0.05602 | 2.56E14 | -0.1663 | |
| 5 | | 0.696 | | | | |
| 2.5 | | 0.609 | | | | |
| 1.25 | | 0.670 | | | | |
| 0.625 | | 0.657 | | | | |
| 0.3125 | | 0.647 | | | | |
| | 100 | 0.213 | -0.7701 +/-0.14402 | 67817.7 | 0.59827 | |
| | 50 | 0.283 | | | | |
| | 25 | 0.286 | | | | |

| | | | | | | | |
|---|---|---|---|---|---|---|---|
| | 12.5 | 0.151 | | | | | |
| | 6.25 | 0.203 | | | | | |
| | 3.125 | 0.161 | | | | | |
| 10 + 100 | | 0.610 | 2.42118 1.72598 | +/- | 0.37160 | 0.57423 | 7.97E-4 [1412.95;11162.2] |
| 5 + 50 | | 0.664 | | | | | 92.7686 [0.01078;98017.3] |
| 2.5 + 25 | | 0.535 | | | | | 1.52E-4 [5.83E10; 6578.86] |
| 1.25 + 12.5 | | 0.599 | | | | | 2.33E-5 [116742; 67702.1] |
| 0.625 + 6.25 | | 0.740 | | | | | 2.360E9 [4.2E-10;757895] |
| 0.3125 + 3.125 | | 0.676 | | | | | 105.061 [0.00952;221112] |
| | | Simulation | | | | | |
| | | 0.45 | | | | | 0.76708 [7.08E15;1.30365] |
| | | 0.5 | | | | | 0.03825 [9.87E11;26.1427] |
| | | 0.55 | | | | | 0.00191 [1.377E8;524.253] |
| | | 0.65 | | | | | 0.79296 [1.26111;271902] |
| | | 0.75 | | | | | 1.298E9 [7.7E-10;3.519E8] |
| | | 0.95 | | | | | 3.78E44 [2.6E-45;3.34E20] |

Table 5—6. Dose and effect data were obtained from the MTT assay (average value of triplicate) and were subjected to CompuSyn analysis in accordance chou et al., [229]. The combination index values can be interpreted as synergistic (CI<1), additive (CI=1) and antagonistic (CI>1) [228]. The combination of gemcitabine and suramin was compared.

The results demonstrated that suramin at 25 µM or 12.5 µM in combination with gemcitabine at 2.5 µM or 1.25 µM exhibited strong synergism with CI values of 1.52E-4 and 2.33E-5, respectively (Table 5—6). The simulated data across Fa levels (<0.45 fa) showed moderate synergism (Table 5—6). At inhibition levels from 0.45 (Fa) up to 0.65 (Fa) the GEM:SUR combination resulted in CI values ranging from 0.019 to 0.793 (Table 5—6). The DRI curve for both suramin and gemcitabine also suggested favourable dose reductions as each reaches medial Fa inhibition (Figure 5—11). Therefore, this data would suggest suramin and gemcitabine showed synergism especially at lower to middle concentrations (Figure 5—10 & Figure 5—11).

**Gemcitabine and EF24**

MIAPAC2 cell viability was more potently affected by EF24, SUR, MTX and GEM, demonstrating MIAPACA2 sensitivity, which was consistent with previous results (Table 5—1) [319]. While gemcitabine also showed a poor conformity to the MEP (r-value = -0.166) in MIAPACA2 cells it was able to cause a greater reduction in cell viability at a lower concentration (Figure 5—10). The inhibition of cell viability by EF24 in MIAPACA2 also did not fit well with MEP (r-value = 0.183). Most likely because of the high potency that EF24 exhibited against cell viability across all concentrations tested.

(A)

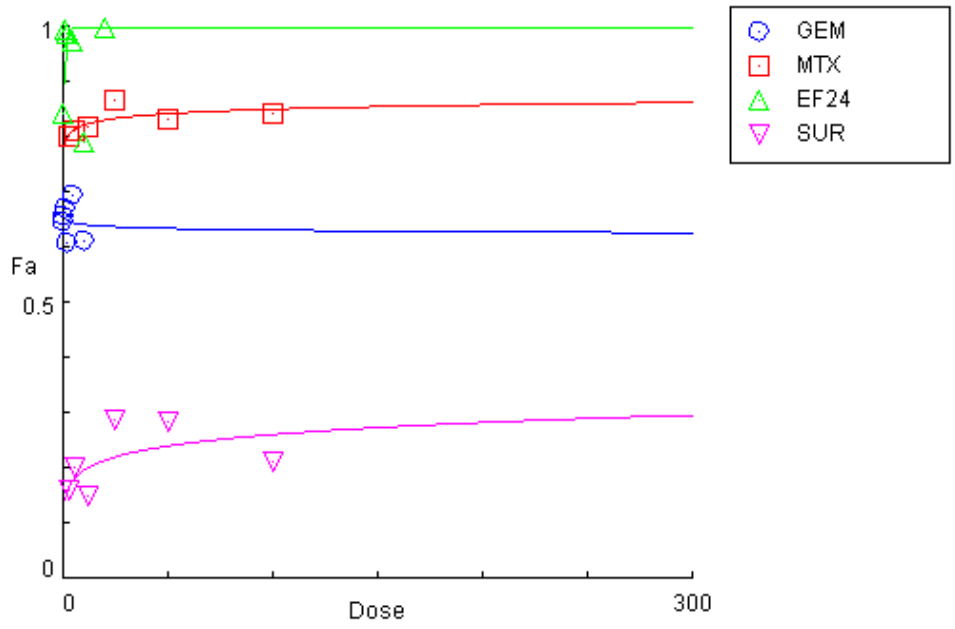


(B)

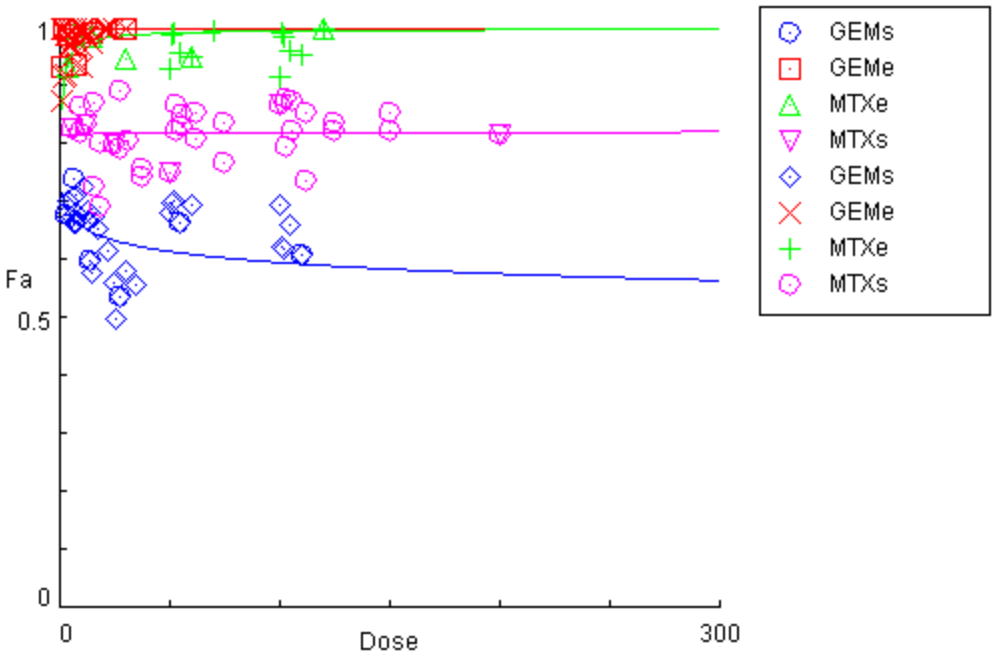


Figure 5—10. The dose-response curves for inhibition of MIAPA2 cell viability. (A) GEM, MTX, EF24 and SUR dose-response curves were shown with a nonlinear curve fitted. (B) The simulated and actual data for the combination of all the combinations including GEM:SUR (GEMs), GEM:EF24 (GEMe), MTX:EF24(MTXe) and MTX:SUR (MTXs).

The combination of gemcitabine and EF24 showed much more consistent synergistic effects (Table 5—7). The CI values from low fa values (0.05) to moderately high fa values (0.65) all showed synergistic effects (Table 5—7). The GEM:EF24 coincubation showed strong synergistic effects with CI values ranging from 7.69E-4 to 0.00276 (Table 5—7).

| Compound | | Fractional Inhibition | Parameters | | | CI [DRI (GEM); DRI (EF24)] |
|---|---|---|---|---|---|---|
| GEM (µM) | EF24 (µM) | (Fa) | m | Dm | r | |
| 10 | | 0.613 | -0.0189+/- 0.05602 | 2.56E14 | -0.1663 | |
| 5 | | 0.696 | | | | |
| 2.5 | | 0.609 | | | | |
| 1.25 | | 0.670 | | | | |
| 0.625 | | 0.657 | | | | |
| 0.3125 | | 0.647 | | | | |
| | 20 | 1 | 0.84369 +/- 2.26343 | 8.24E-4 | 0.18322 | |
| | 10 | 0.792 | | | | |
| | 5 | 0.975 | | | | |
| | 2.5 | 0.987 | | | | |
| | 1.25 | 0.996 | | | | |
| | 0.625 | 0.842 | | | | |
| 10 + 20 | | 1 | -0.1154 +/- 0.10632 | 2853.55 | -0.4769 | 1.1E304 [9.E-305; 5.58693] |
| 5 + 10 | | 0.992 | | | | 2.95E97 [3.4E-98; 0.27415] |
| 2.5 + 5 | | 0.936 | | | | 5.56E47 [1.8E-48; 0.22553] |
| 1.25 + 2.5 | | 0.987 | | | | 2.88E84 [3.5E-85; 0.87736] |
| 0.3125 + 0.625 | | 0.933 | | | | 3.66E45 2.7E-46; 1.76322] |
| | | Simulation | | | | |
| | | 0.05 | | | | 1.52E-4 [1.38E87; 6569.14] |
| | | 0.1 | | | | 2.71E-4 [3.87E69; 3688.97] |
| | | 0.15 | | | | 3.87E-4 [5.24E58; 2580.77] |
| | | 0.2 | | | | 5.07E-4 [3.44E50; 1972.12] |
| | | 0.25 | | | | 6.33E-4 [6.00E43; 1579.24] |
| | | 0.3 | | | | 7.69E-4 [7.49E37; 1300.66] |
| | | 0.4 | | | | 0.00108 [3.12E27; 924.65] |
| | | 0.5 | | | | 0.00148 [9.32E17; 676.07] |
| | | 0.65 | | | | 0.00276 [2670.80; 419.158] |
| | | 0.95 | | | | 1.59E51 [6.3E-52; 69.5789] |

Table 5—7. Dose and effect data were obtained from the MTT assay (average value of triplicate) and were subjected to CompuSyn analysis in accordance chou et al., [229]. The combination index values can be interpreted as synergistic (CI<1), additive (CI=1) and antagonistic (CI>1) [228]. The combination of gemcitabine and EF24 was compared.

These data points also corresponded with highly favourable dose reduction indexes for both gemcitabine (DRI>1) and EF24 (Table 5—7). The remaining data including the combination index values for the actual/non-simulated data, showed that gemcitabine and EF24 at high inhibition levels (0.65>Fa) returned highly antagonistic results (CI>1) (Table 5—7). Gemcitabine also showed unfavourable does reductions (DRI), while EF24 exclusively demonstrated favourable dose reductions (Figure 5—11).These results strongly demonstrated that EF24 could add to the cytotoxic effects of gemcitabine across the ranges that gemcitabine was able to illicit cytotoxicity alone. This is a feature that is consistent across both PANC1 and MIAPAC2 cells. The combination plot for gemcitabine and EF24 demonstrated synergistic (CI<1) CI values across the majority of this

combination (Figure 5—8). While, at higher concentrations the combination became antagonistic (Figure 5—8). The DRI plots showed that past fa 0.65 the DRI became favourable for gemcitabine, which could simply be because of the potency of EF24 (Figure 5—10).

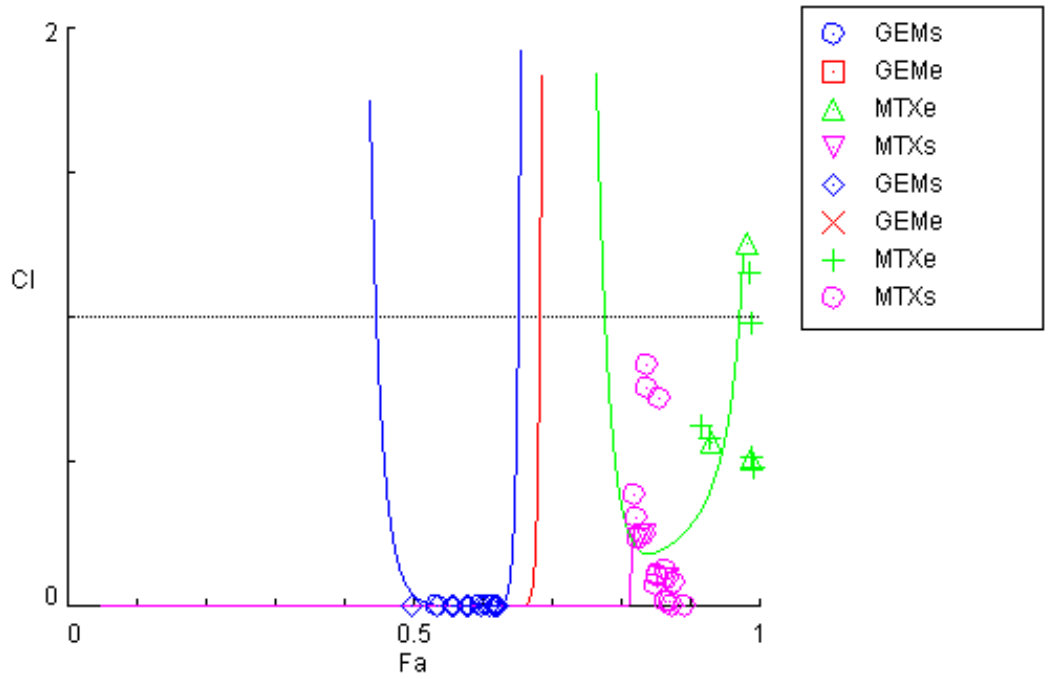


(A)

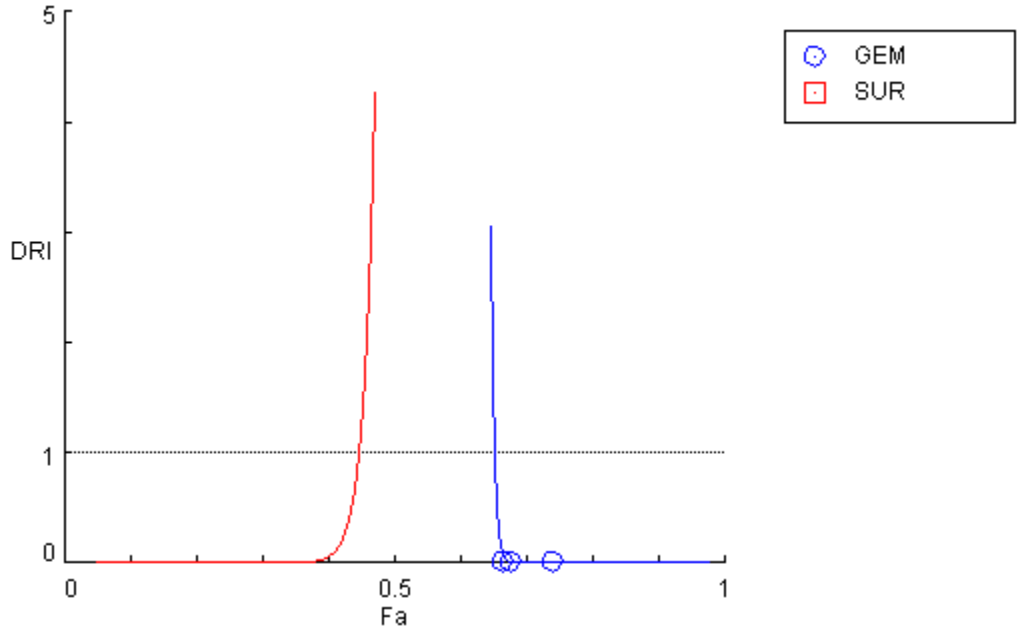


(B)

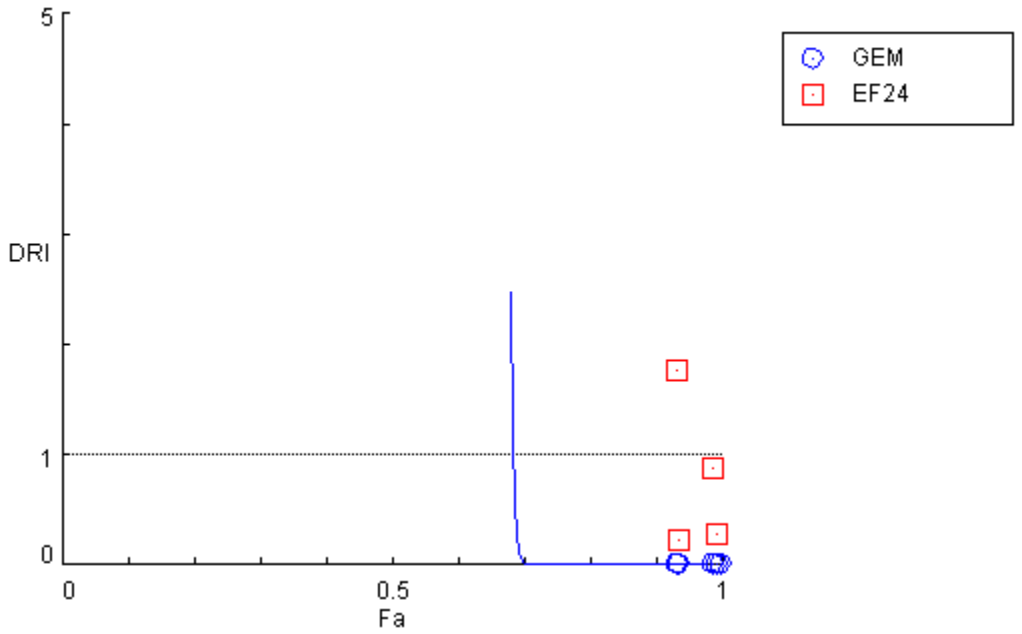


(C)

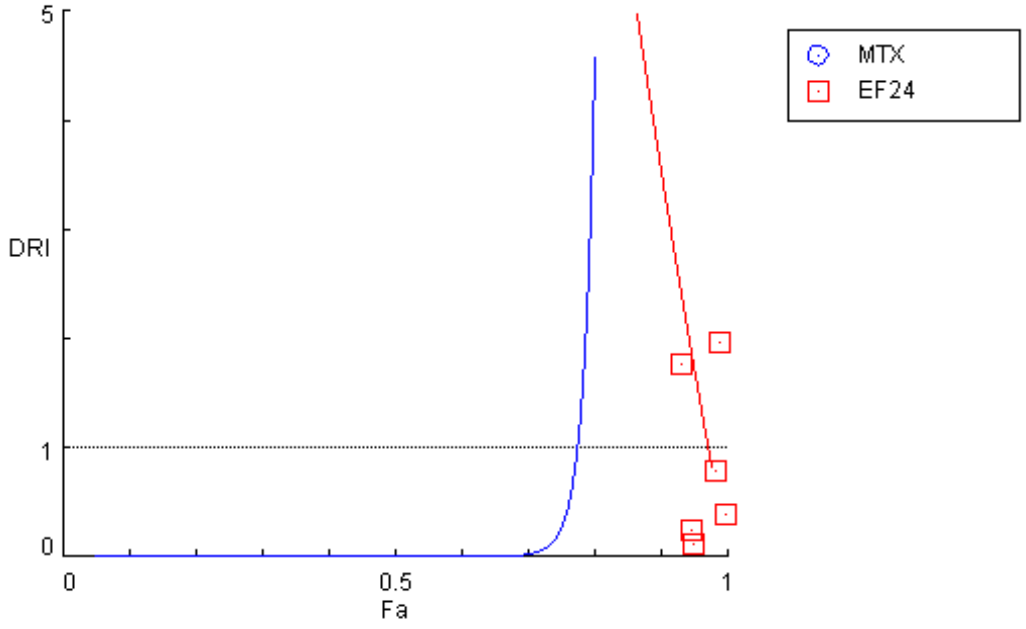


(D)

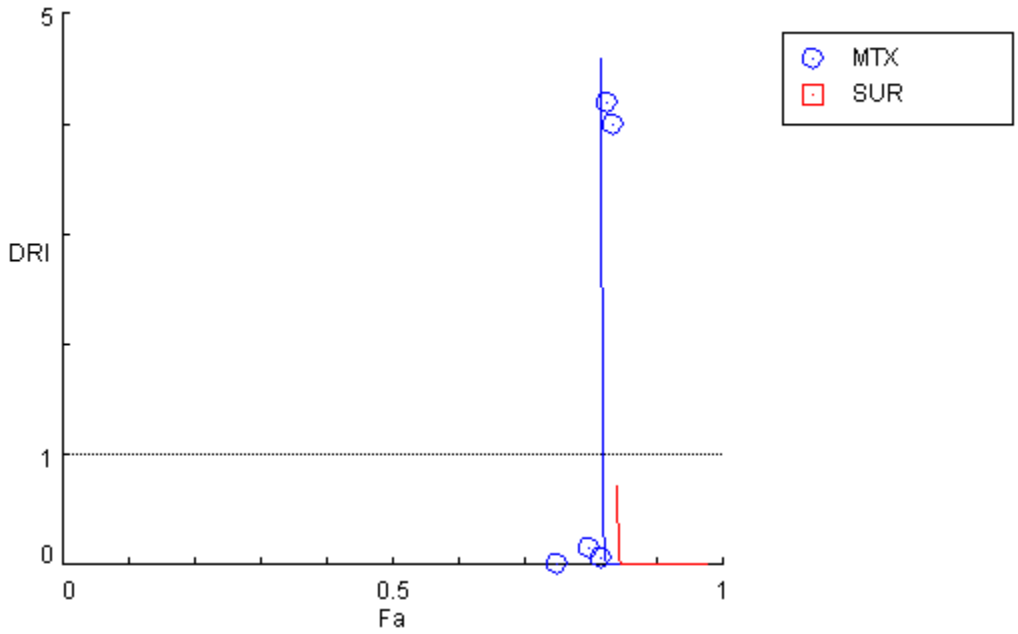


(E)

Figure 5—11. Combination plot and Dose-reduction plots for the coincubation treatments in MIAPACA2 cells. (A) Combination plot for the four MIAPACA2 coincubations. (B) The DRI plot in the combination of gemcitabine and suramin (constant ratio). (C) Combination plot of gemcitabine and EF24 (constant ratio). (D) The DRI plot in the combination of methotrexate and EF4 (constant ratio). (E) The DRI plot in the combination of methotrexate and suramin (constant ratio)

### Methotrexate and Suramin

As previously shown, MTX was initially more cytotoxic than GEM in PANC1 cells (Table 5—1). MIAPAC2 cells also exhibited higher sensitivity towards MTX than GEM (Table 5—1). The conformity of both suramin and methotrexate was higher in PANC1 cells that in MIAPACA2 cells with r values = 0.692 and 0.598, respectively. The MTX:SUR coincubation exhibited synergism across the widest range of concentrations (Table 5—8). The simulated data showed that the CI values for MTX:SUR combination ranged from 10E-225 to 8.1E-21 (Table 5—8). While the lack of conformity may be an issue, the CI plot showed all values to be synergistic (Figure 5—11). Further demonstrating the strong synergistic effects between MTX and SUR. The DRI plot also exhibited that suramin showed a constant favourable DRI while MTX exhibited favourable DRI until high (>0.8) inhibition levels were reached.

| Compound | | Fractional Inhibition | Parameters | | | CI [DRI (MTX); DRI (Suramin)] |
|---|---|---|---|---|---|---|
| MTX (µM) | Suramin (µM) | (Fa) | m | Dm | r | |
| 100 | | 0.843 | 0.09013 +/- 0.04705 | 4.04E-7 | 0.69170 | |
| 50 | | 0.833 | | | | |
| 25 | | 0.866 | | | | |
| 12.5 | | 0.818 | | | | |

| | | | | | | | |
|---|---|---|---|---|---|---|---|
| 6.25 | | 0.813 | | | | | |
| 3.125 | | 0.801 | | | | | |
| | 100 | 0.213 | -0.7701 | +/- | 67817.7 | 0.59827 | |
| | | | 0.14402 | | | | |
| | 50 | 0.283 | | | | | |
| | 25 | 0.286 | | | | | |
| | 12.5 | 0.151 | | | | | |
| | 6.25 | 0.203 | | | | | |
| | 3.125 | 0.161 | | | | | |
| 100 + 100 | | 0.816 | 0.00786 | +/- | 2.5E-82 | 0.03858 | 1298106 [0.06190; 783563] |
| | | | 0.10180 | | | | |
| 50 + 50 | | 0.869 | | | | | 466210 [10.2365; 1.902E8] |
| 25 + 25 | | 0.749 | | | | | 156098 [0.00295; 2561596] |
| 12.5 +12.5 | | 0.799 | | | | | 81774.0 [0.1458; 3.140E7] |
| 6.25 + 6.25 | | 0.834 | | | | | 55249.8 [3.9918; 2.757E8] |
| 3.125 + 3.125 | | 0.826 | | | | | 19414.7 [4.18599; 3.83E8] |
| | | Simulation | | | | | |
| | | 0.05 | | | | | 10E-225 [1.0E224;2.5E24] |
| | | 0.1 | | | | | 5.E-187 [2.1E186;1.4E202] |
| | | 0.15 | | | | | 1.E-163 [9.8E162; 7.0E17] |
| | | 0.2 | | | | | 4.E-146 [2.6E145; 3.5E16] |
| | | 0.25 | | | | | 1.E-131 [8.2E130; 2.7E14] |
| | | 0.5 | | | | | 3.1E-76 [3.18E75; 5.33E8] |
| | | 0.65 | | | | | 5.2E-45 [1.90E44; 1.62E5] |
| | | 0.75 | | | | | 8.1E-21 [1.24E20; 1.04E2] |
| | | 0.95 | | | | | 1.01E73 [9.9E-74; 1.1E-68] |

Table 5—8. Dose and effect data were obtained from the MTT assay (average value of triplicate) and were subjected to CompuSyn analysis in accordance chou et al., [229]. The combination index values can be interpreted as synergistic (CI<1), additive (CI=1) and antagonistic (CI>1) [228]. The combination of methotrexate and suramin was compared.

### Methotrexate and EF24

The combination of MTX and EF24 was suggested to be the most effective combination in PANC1 cells. Suramin (6.25 or 3.125 µM) combined with MTX (1.25 or 6.25 µM) within MIAPACA2 cells, resulted in synergistic CI values of 0.507 and 0.567, respectively. The inhibition fractions (Fa) greater than 0.8 demonstrated that the combination of MTX and EF24 was synergistic at higher levels of inhibition (Table 5—9). The combination of MTX and EF24 also showed favourable dose reduction for both compounds after 0.8 Fa (Table 5—9). This was the only combination to show synergism across values higher than that of the anticancer compound alone. Suggesting that while the strong synergistic effects of the previous combinations were able to enhance the potency of anticancer drugs. The combination of MTX and EF24 showed enhanced cytotoxicity above that of MTX alone. Even at lower inhibition levels, EF24 also showed favourable DRI, while suramin did not (Table 5—9). Surprisingly, this would suggest that MTX is able to make EF24 an already highly potent compound, even more potent. The combination of

MTX:SUR while not the most wide-ranging combination showed enhanced synergism at higher inhibitory levels a pattern not seen in other combinations or in PANC1 cells.

| Compound | | Fractional Inhibition | Parameters | | | CI [DRI (MTX); DRI (EF24)] |
|---|---|---|---|---|---|---|
| MTX (µM) | EF24 (µM) | (Fa) | m | Dm | r | |
| 100 | | 0.843 | 0.09013 +/- 0.04705 | 4.04E-7 | 0.69170 | |
| 50 | | 0.833 | | | | |
| 25 | | 0.866 | | | | |
| 12.5 | | 0.818 | | | | |
| 6.25 | | 0.813 | | | | |
| 3.125 | | 0.801 | | | | |
| | 20 | 1 | 2.42118 +/- 1.72598 | 0.37160 | 0.57423 | |
| | 10 | 0.792 | | | | |
| | 5 | 0.975 | | | | |
| | 2.5 | 0.987 | | | | |
| | 1.25 | 0.996 | | | | |
| | 0.625 | 0.842 | | | | |
| 100 + 20 | | 0.999 | 0.72043 +/- 0.57754 | 0.07420 | 0.52921 | 2.60847 [8.34E26; 0.3834] |
| 50 + 10 | | 0.950 | | | | 7.95189 [1351628; 0.1258] |
| 25 + 5 | | 0.948 | | | | 4.05845 [1556890; 0.2464] |
| 12.5 + 2.5 | | 0.983 | | | | 1.25778 [1.18E12; 0.7951] |
| 6.25 + 1.25 | | 0.990 | | | | 0.50746 [7.54E14; 1.9706] |
| 3.125 + 0.625 | | 0.932 | | | | 0.56883 [575421; 1.75801] |
| | | Simulation | | | | |
| | | 0.2 | | | | 1.07E11 [9.4E-12; 116.099] |
| | | 0.25 | | | | 6.550E9 [1.5E-10; 87.7017] |
| | | 0.3 | | | | 5.711E8 [1.75E-9; 68.6418] |
| | | 0.5 | | | | 152995 [6.54E-6; 30.0469] |
| | | 0.75 | | | | 3.67076 [0.27983; 10.2942] |
| | | 0.8 | | | | 0.34752 [4.56785; 7.77628] |
| | | 0.85 | | | | 0.18805 [134.312;5.53708] |
| | | 0.9 | | | | 0.28363 [11980.1; 3.52681] |
| | | 0.95 | | | | 0.58753 [1.693E7; 1.7021] |
| | | 0.97 | | | | 0.98664 [2.951E9; 1.0135] |

Table 5—9. Dose and effect data were obtained from the MTT assay (average value of triplicate) and were subjected to CompuSyn analysis in accordance chou et al., [229]. The combination index values can be interpreted as synergistic (CI<1), additive (CI=1) and antagonistic (CI>1) [228]. The combination of methotrexate and EF24 was compared.

## Discussion

Suramin, curcumin and EF24 were all able to inhibit MRP3 function demonstrated by their ability to increase the cellular accumulation of CMF. Curcumin and EF24 also showed increased BCECF accumulation, suggesting that they also significantly inhibited MRP5 function. Whether these functional inhibitions were able to illicit positive effects on anticancer drugs was investigated in a combination study. The combination of GEM:EF24, GEM:SUR, MTX:SUR and MTX:EF24 all combined to show synergistic

effects in both MIAPACA2 and PANC1 cells. In PANC1, GEM:EF24 combinations showed that the lower concentrations of EF24 may exhibit an additive relationship towards gemcitabine within the range of gemcitabine's original effectiveness. This was further established by the increases in DRI values seen an the lower Fa regions of the graph. However, the combination of EF24 was unable to increase the Fa of gemcitabine suggesting only increased potency and not cytotoxicity. The GEM:SUR combination also showed synergistic effects at lower inhibition (Fa) ranges. The findings that suramin enhances proliferation at lower doses, accentuate these results further as this initial stimulation was overcome in combination with GEM. However, GEM:SUR unlike GEM:EF24 was unable to achieve inhibition of PANC1 cell viability by more than 50%. The MTX:SUR combination was also able to show synergistic effects at lower fa regions of the graph. While the combination index became more antagonistic at higher fa regions, the data still suggests that the non-cytotoxic compound suramin could improve lower doses of methotrexate. Similar to GEM:SUR, MTX:SUR was also able to overcome the stimulation of cell viability shown in suramin treatments. The most synergistic combination was that of MTX and EF24, which showed synergism for the whole range of sole MTX treatment (up to fa of 0.6). These results suggested that MTX:EF24 showed the most consistent synergistic relationship. It would be beneficial to investigate the combination of GEM/MTX and EF24 at lower concentrations to see whether the synergy observed could be enhanced to cause higher fractional inhibition.

MIAPACA2 exhibited increased sensitivity towards all of the compounds tested. The combination that exhibited the most consistent synergism across the concentrations chosen was the combination of MTX and SUR. While the remaining combinations showed synergism across different ranges of cell viability inhibition. The combination of GEM and SUR in MIAPAC2 cells showed enhanced cytotoxicity approximating around half the maximum inhibition. While, the GEM and EF24 combination also showed synergistic effects across a wide range. However, the combination of MTX and EF24 resulted in synergistic effects that only occurred at higher levels of inhibition. The MTX and EF24 combination did not show synergistic effects across the normal inhibition levels of MTX but only showed synergism at levels higher than that achieved by methotrexate. Suggesting that this combination unlike the other combinations in both MIAPACA2 and PANC1 cells showed that MTX cytotoxicity was enhanced to levels higher than both EF24 and MTX alone.

The mechanisms by which MRP3 inhibition occurs has not been well established. The ability of suramin to inhibit energy production in parasites by inhibiting glycosomal enzymes such as those required for glycolysis, may be the mechanism by which suramin inhibits MRP3 [309, 320]. MRP3, like all ABC transporters require ATP to change conformation and transport substrates [47]. The inhibition of glycolysis a process which

produces ATP shows a clear link between suramin and MRP3 inhibition [321, 322]. Curcumin modulation of ABC transporter function in the case of P-gp appeared to be by direct inhibition of P-gp expression [323]. Furthermore, curcumin competed with verapamil for the binding P-gp binding site, further suggesting direct inhibition of P-gp [323]. Therefore, curcumin may also inhibit MRP3 by direct modulation of MRP3 expression. Little is known about EF24 activity, as EF24, is a derivative of curcumin, EF24 may also directly interact with MRP3 by limiting MRP3 expression and binding sites like its parent molecule, curcumin. However, like suramin, EF24 also showed inhibition of glycolysis, which could suggest a similar mechanism of action for both suramin and EF24 in MRP3 inhibition [169].

This study examined three very different compounds all with the ability to increase MRP3 dependent accumulation of the CMF molecule. Curcumin a natural compound found in turmeric, showed moderate cytotoxicity in PANC1 cells ($IC_{50}$: 24.81 µM) but exhibits inherently low bioavailability [51]. EF24, a natural derivative of curcumin showed strong cytotoxicity in PANC1 cells ($IC_{50}$: 1.76 µM). Suramin, a fully synthetic compound which not only exhibited no cytotoxicity (up to 100 µM) but also enhanced cell proliferation. While previous publications showed the ability of curcumin to inhibit P-gp, MRP1, MRP5 and BCRP transport [55, 162]. This was the first time that curcumin, EF24 and suramin was shown in an *in vitro* model to inhibit MRP3 activity in pancreatic cancer. Furthermore, this was the first time that EF24 has shown MRP5 inhibition and increased BCECF accumulation in pancreatic cancer.

The inhibition of both MRP3 and MRP5 by EF24 suggest that it has retained the ABC transport modulation seen in curcumin. However, EF24 inhibited both MRP3 and MRP5 more potently than curcumin and EF24 showed much higher cytotoxicity as well. This may suggest that EF24 could be used alone or in combination with anticancer drugs to directly treat pancreatic cancer or modulate multidrug resistance caused by ABC transporters.

It was recently shown that accumulation of COG a predominant curcumin metabolite was inhibited by MRP3 [74]. Whether MRP3 transport can also be inhibited by COG alone is not yet known. The preferential transport of glucuronides by MRP3 has been well demonstrated, however the extent to which this exclusivity impacts MRP3 inhibition is of great interest. The combination of suramin and gemcitabine have been studied *in clinic* within non-small cell carcinoma models [178]. Non-small cell carcinoma in particular showed consistent overexpression of ABCC3 within the cancer versus cancer analysis. The clinical trial demonstrated that gemcitabine (1,250 mg/kg) and suramin (<50 µM) was well tolerated, resulting in stable disease in three patients and the highest median time to progression in comparison to combinations with docetaxel and suramin. This data validates the combination of gemcitabine and suramin but the

mechanism of action could be the modulation of MRP3. A phase II clinical trial tested the efficacy of MTX in combination with 5-FU and doxorubicin in advanced pancreatic cancer patents [324]. The combinations were well tolerated in the majority of patients and resulted in modest improvements in response rates of 16% [324]. Further investigation of these combinations within pancreatic cancer as well as the activity of MTX in pancreatic cancer may lead to better treatment outcomes for pancreatic cancer patients.

# Chapter 6 Discussion

## Summary of Results

### Bioinformatic Studies of ABCC3

Dysregulation of ABCC3 in normal and cancerous tissues was well displayed in the oncomine platform. ABCC3 was significantly over and under expressed in cancers affecting the lymphatic and circulatory system or within bladder, brain/CNS, breast, colorectal, oesophageal, head and neck, kidney, lung, skin, pancreatic, and prostate tissues (Table 3—1). Further interrogation of the expression across normal and cancerous tissues showed that ABCC3 expression was significantly differentially over expressed in kidney, lymphoma, bladder and lung cancers which showed the highest fold increase in expression (Table 3—2). While some cancers also showed strong ABCC3 underexpression in lung, prostate, colorectal and melanoma cancers (Table 3—2). The expression of ABCC3 within the oncomine database was also compared across cancer types (Figure 3—1). Kidney, pancreatic and colorectal cancers showed the highest ABCC3 expression across cancer types (Figure 3—2). The heterogeneity of ABCC3 was also tested within the oncomine platform, revealing several cancers that exhibited large and significant differences in expression levels across the respective cancer databases (**Error! Reference source not found.**). Pancreatic cancer showed heterogeneity of ABCC3 expression with the highest COPA score (**Error! Reference source not found.**). Sarcoma, cervical and renal cancer also showed high COPA scores, suggesting high ABCC3 heterogeneity within these cancers (**Error! Reference source not found.**). Oncomine was also used to investigate which targets could be identified that follow a similar expression pattern to ABCC3. Members of various signalling pathways (WNT signalling pathway, sphingosine-1-phosphate pathway and p53-signalling pathway) showed significant correlation with ABCC3 expression. The coexpression of ABCC3 and cytochrome p450s, ENPP1, WNT signalling molecules and other transporters was discovered (Table 3—8). While, ABCC3 expression correlating with cytochrome p540s, WNT signalling expression and SLC transporters expression had already been observed [38, 197, 268]. Links to other targets such as ENPP1, which promotes cell surface localisation to the cell membrane where found. ENPP1 activity with other ABC transporters make it is possible that ENPP1 may also promote MRP3 the cell surface localisation. However, BCRP is highly unique in a number of ways especially in its structure. Therefore further investigation between the coexpression of ENPP1 and MRP3 expression would be needed to better understand the relationship.

The bioinformatic study also utilised the KMplot and STRING databases to evaluate the effects of expression on survival and whether any significant protein-protein interactions could be discovered. The Km plot revealed that the cancers with high ABCC3 expression could either show improved survival or decreased survival. However, for those patients who showed decreased survival they showed a more severe decline in survival than for those who showed moderate improvement in survival (Figure 3—4 and Figure 3—5). The STRING database returned FABP6 and MRPS7, two targets with no clearly documented links with ABCC3 that also require further investigation.

**CRISPR-Cas9 Knockout of ABCC3**

The CRISPR-Cas9 system provided a model that could specifically target and disrupt the expression of ABCC3 [237]. Following knockout of ABCC3 from PANC1 cells, the results showed that both the first and second round of knockouts showed increased accumulation of CMF (Figure 4—4 & Figure 4—5). This decrease in functional activity of MRP3 resulted in decreased drug resistance of PANC1 towards both gemcitabine and methotrexate (Figure 4—8). The reversal of gemcitabine resistance by MRP5 had already been shown [29]. However, this was the first time that gemcitabine resistance had been modulated in an ABCC3 knockout cell line.

**Inhibition of MRP3 by Suramin, Curcumin and EF24**

Suramin, curcumin and EF24 were identified as potential MRP3 inhibitors. Suramin showed low cytotoxicity across both MIAPACA2 and PANC1 cells. Suramin also significantly inhibited MRP3 function in the CMF accumulation assay and exhibited synergistic effects in both the resistant (PANC1) and sensitive (MIAPACA2) cell lines when combined with gemcitabine and methotrexate. EF24, unlike suramin, showed potent cytotoxicity in both PANC1 and MIAPACA2 cells. However, in combination with MTX and GEM, EF24 also exhibited strong synergistic effects especially in the more sensitive MIAPACA2 cells. EF24 also demonstrated functional inhibition of MRP3 and MRP5 by significantly increasing the accumulation of CMF and BCECF, respectively. A recent paper suggested targeting ABC transporters require inhibitors like EF24, which can target multiple ABC transporters [51]. This data demonstrates that modulators of MRP3 function can improve drug resistance in pancreatic cancer cells.

**Limitations**

The cleavage detection across the knockout cell lines only showed successful cleavage of ABCC3 in the gRNA1 cells, while the cells that showed greater modulation of both CMF accumulation and modulation of anticancer drugs did not produce clear cleavage results. The cleavage sites targeted by the CRISPR-Cas9 knockout are sites that exist

in normal human cells, it is unknown whether these target sites have mutated in PANC1 cells. Therefore, while these results suggest some off-target effects causing the phenotypic changes in gRNA2 and gRNA3, cleavage of DNA could have still occurred within the ABCC3 gene. This question would be answered by gene sequencing of gRNA2 and gRNA3 in comparison with WT PANC1 cells.

Furthermore, the cytotoxicity of PANC1 towards gemcitabine was relatively high ($IC_{50}$ >100 µM). However, this cytotoxicity was consistently exhibited across different PANC1 passages and gemcitabine stocks. The variation in $IC_{50}$ values for PANC1 cells across literature is quite surprising with the highest $IC_{50}$ value of 300±33mM and the lowest $IC_{50}$ value of 8.32 nM [319, 325]. Therefore, the gemcitabine found in this study does fall within published results. However, it would be highly beneficial to investigate why there is such variations between gemcitabine $IC_{50}$ values. Furthermore, some papers showed that PANC1 was more resistant towards gemcitabine while others showed that MIAPACA2 was more resistant [319, 325]. This data agreed with the paper by Fryer, R.A., et al that MIAPACA2 cells showed increased sensitivity towards gemcitabine [319]. However, MIAPACA2 also showed enhanced sensitivity towards methotrexate, EF24 and suramin. Potentiating the use of these compounds and combinations in both resistant and sensitive pancreatic cancer cells.

**Future Directions**

This study successfully created MRP3 PANC1 knockout cell lines that reduced both MRP3 functional activity and MRP3-dependent drug resistance. These cells lines could be used to further investigate MRP3 substrates, inhibitors and MRP3 inhibitor mechanisms of action. However, before this can happen single clone populations should be extracted in order to fully observe the effects of ABCC3 knockout on MRP3 function (CMF accumulation), gene sequencing (cleavage detection) and protein expression (surface staining). It may also be useful to try CRISPR-Cas9 knockout of ABCC3 using the sgRNA molecule which would remove the variability imparted by the extra tracrRNA:crRNA annealing step that was required (see methodology).

This research also revealed a number of other cancer targets that highly express MRP3 especially kidney and lung cancer. The CRISPR-cas9 system and the protocols established in the research, could also be used to investigate the MRP3 expression across in these cancers. Finally, the inhibition of MRP3 by curcumin, suramin and EF24 and their combination with MTX or gemcitabine can lead to some valuable results. Further optimization of concentrations for both anticancer drugs and MRP3 inhibitors may improve m, CI and DRI values. The use of EF24 in pancreatic cancer treatments as a sole anticancer agent should also be investigated.

## References


1. Hanahan, D. and R.A. Weinberg, *The hallmarks of cancer.* Cell, 2000. **100**(1): p. 57-70.
2. Murthy, D., K.S. Attri, and P.K. Singh, *Phosphoinositide 3-Kinase Signaling Pathway in Pancreatic Ductal Adenocarcinoma Progression, Pathogenesis, and Therapeutics.* Front Physiol, 2018. **9**: p. 335.
3. Hanahan, D. and R.A. Weinberg, *Hallmarks of cancer: the next generation.* Cell, 2011. **144**(5): p. 646-74.
4. Ulus, G., et al., *The anti-angiogenic potential of (+/-) gossypol in comparison to suramin.* Cytotechnology, 2018. **70**(6): p. 1537-1550.
5. Waltenberger, J., et al., *Suramin is a potent inhibitor of vascular endothelial growth factor. A contribution to the molecular basis of its antiangiogenic action.* Journal of Molecular and Cellular Cardiology, 1996. **28**(7): p. 1523-1529.
6. Hosang, M., *Suramin binds to platelet-derived growth factor and inhibits its biological activity.* J Cell Biochem, 1985. **29**(3): p. 265-73.
7. Pollak, M. and M. Richard, *Suramin Blockade of Insulin-Like Growth-Factor I-Stimulated Proliferation of Human Osteosarcoma Cells.* Journal of the National Cancer Institute, 1990. **82**(16): p. 1349-1352.
8. Myers, C., et al., *Suramin - a Novel Growth-Factor Antagonist with Activity in Hormone-Refractory Metastatic Prostate-Cancer.* Journal of Clinical Oncology, 1992. **10**(6): p. 881-889.
9. Huang, H.W., S.K. Mohan, and C. Yu, *The NMR solution structure of human epidermal growth factor (hEGF) at physiological pH and its interactions with suramin.* Biochem Biophys Res Commun, 2010. **402**(4): p. 705-10.
10. Wu, Z.S., et al., *Suramin blocks interaction between human FGF1 and FGFR2 D2 domain and reduces downstream signaling activity.* Biochem Biophys Res Commun, 2016. **477**(4): p. 861-867.
11. Hsu, Y.L., et al., *Hypoxic lung cancer-secreted exosomal miR-23a increased angiogenesis and vascular permeability by targeting prolyl hydroxylase and tight junction protein ZO-1.* Oncogene, 2017. **36**(34): p. 4929-4942.
12. Nguyen, D.X., P.D. Bos, and J. Massague, *Metastasis: from dissemination to organ-specific colonization.* Nat Rev Cancer, 2009. **9**(4): p. 274-84.
13. Bray, F., et al., *Global cancer statistics 2018: GLOBOCAN estimates of incidence and mortality worldwide for 36 cancers in 185 countries.* CA Cancer J Clin, 2018. **68**(6): p. 394-424.
14. White, M.C., et al., *Cancer prevention for the next generation.* J Adolesc Health, 2013. **52**(5 Suppl): p. S1-7.
15. Yang, Y., *Cancer immunotherapy: harnessing the immune system to battle cancer.* J Clin Invest, 2015. **125**(9): p. 3335-7.
16. Couzin-Frankel, J., *Cancer Immunotherapy.* Science, 2013. **342**(6165): p. 1432-1433.
17. Hay, A.E. and M.C. Cheung, *CAR T-cells: costs, comparisons, and commentary.* J Med Econ, 2019. **22**(7): p. 613-615.
18. Czarnecka, A.M., et al., *Hormone signaling pathways as treatment targets in renal cell cancer (Review).* Int J Oncol, 2016. **48**(6): p. 2221-35.
19. Bodmer, A. and M. Castiglione-Gertsch, *Role of hormonal manipulations in patients with hormone-sensitive metastatic breast cancer.* Eur J Cancer, 2011. **47 Suppl 3**: p. S28-37.
20. Xu, M.J., D.E. Johnson, and J.R. Grandis, *EGFR-targeted therapies in the post-genomic era.* Cancer Metastasis Rev, 2017. **36**(3): p. 463-473.
21. Cohen, S., *Purification of a Nerve-Growth Promoting Protein from the Mouse Salivary Gland and Its Neuro-Cytotoxic Antiserum.* Proc Natl Acad Sci U S A, 1960. **46**(3): p. 302-11.
22. Baskar, R., et al., *Biological response of cancer cells to radiation treatment.* Front Mol Biosci, 2014. **1**: p. 24.
23. Zhang, C.L., et al., *Stem cells in cancer therapy: opportunities and challenges.* Oncotarget, 2017. **8**(43): p. 75756-75766.

24. Frank, T.S., et al., *Genomic profiling guides the choice of molecular targeted therapy of pancreatic cancer.* Cancer Lett, 2015. **363**(1): p. 1-6.
25. Halls, B.S. and P. Ward-Smith, *Identifying early symptoms of pancreatic cancer.* Clin J Oncol Nurs, 2007. **11**(2): p. 245-8.
26. Al-Hawary, M.M., et al., *Staging of pancreatic cancer: role of imaging.* Semin Roentgenol, 2013. **48**(3): p. 245-52.
27. Jeune, F., et al., *Pancreatic cancer surgical management.* Presse Med, 2019. **48**(3 Pt 2): p. e147-e158.
28. Mohammed, S., G. Van Buren, 2nd, and W.E. Fisher, *Pancreatic cancer: advances in treatment.* World J Gastroenterol, 2014. **20**(28): p. 9354-60.
29. Hagmann, W., R. Jesnowski, and J.M. Lohr, *Interdependence of gemcitabine treatment, transporter expression, and resistance in human pancreatic carcinoma cells.* Neoplasia, 2010. **12**(9): p. 740-7.
30. Housman, G., et al., *Drug resistance in cancer: an overview.* Cancers (Basel), 2014. **6**(3): p. 1769-92.
31. Robert Templeton, M.T.a.A.D. *Cancer Projections Incidence 2004–08 to 2014–18*. 2010.
32. Maitra, A. and R.H. Hruban, *Pancreatic cancer.* Annu Rev Pathol, 2008. **3**: p. 157-88.
33. AIHW, *Cancer in Australia: an overview 2014*, A.I.o.H.a. Welfare, Editor. 2014, AIHW: Canberra.
34. Pelosi, E., G. Castelli, and U. Testa, *Pancreatic Cancer: Molecular Characterization, Clonal Evolution and Cancer Stem Cells.* Biomedicines, 2017. **5**(4).
35. Burris, H. and A.M. Storniolo, *Assessing clinical benefit in the treatment of pancreas cancer: gemcitabine compared to 5-fluorouracil.* Eur J Cancer, 1997. **33 Suppl 1**: p. S18-22.
36. Adamska, A., et al., *ABCC3 is a novel target for the treatment of pancreatic cancer.* Adv Biol Regul, 2019.
37. Long, J., et al., *Overcoming drug resistance in pancreatic cancer.* Expert Opin Ther Targets, 2011. **15**(7): p. 817-28.
38. Li, Y., J. Lu, and J.W. Paxton, *The role of ABC and SLC transporters in the pharmacokinetics of dietary and herbal phytochemicals and their interactions with xenobiotics.* Curr Drug Metab, 2012. **13**(5): p. 624-39.
39. Pastan, I. and M. Gottesman, *Multiple-drug resistance in human cancer.* N Engl J Med, 1987. **316**(22): p. 1388-93.
40. Gerlach, J., *[In memoriam Hartwig Kuhlenbeck].* Anat Anz, 1986. **161**(2): p. 89-98.
41. Dean, M., Y. Hamon, and G. Chimini, *The human ATP-binding cassette (ABC) transporter superfamily.* J Lipid Res, 2001. **42**(7): p. 1007-17.
42. Li, Y., et al., *Interactions of dietary phytochemicals with ABC transporters: possible implications for drug disposition and multidrug resistance in cancer.* Drug Metab Rev, 2010. **42**(4): p. 590-611.
43. Keogh, J.P., *Membrane transporters in drug development.* Adv Pharmacol, 2012. **63**: p. 1-42.
44. Prachayasittikul, V. and V. Prachayasittikul, *P-glycoprotein transporter in drug development.* EXCLI J, 2016. **15**: p. 113-8.
45. Dean, M., A. Rzhetsky, and R. Allikmets, *The human ATP-binding cassette (ABC) transporter superfamily.* Genome Res, 2001. **11**(7): p. 1156-66.
46. M, A.L., et al., *Regulatory recruitment of signalling molecules to the cell membrane by pleckstrinhomology domains.* Trends Cell Biol, 1997. **7**(6): p. 237-42.
47. Gottesman, M.M., T. Fojo, and S.E. Bates, *Multidrug resistance in cancer: role of ATP-dependent transporters.* Nat Rev Cancer, 2002. **2**(1): p. 48-58.
48. Goldstein, L.J., *Clinical reversal of drug resistance.* Curr Probl Cancer, 1995. **19**(2): p. 65-124.
49. Zhang, Y.C., et al., *Esters of the Marine-Derived Triterpene Sipholenol A Reverse P-GP-Mediated Drug Resistance.* Marine Drugs, 2015. **13**(4): p. 2267-2286.
50. Fojo, T. and S. Bates, *Strategies for reversing drug resistance.* Oncogene, 2003. **22**(47): p. 7512-23.
51. Dantzic, D., et al., *The Effects of Synthetically Modified Natural Compounds on ABC Transporters.* Pharmaceutics, 2018. **10**(3).
52. Dano, K., *Active outward transport of daunomycin in resistant Ehrlich ascites tumor cells.* Biochim

Biophys Acta, 1973. **323**(3): p. 466-83.
53. Juliano, R.L. and V. Ling, *A surface glycoprotein modulating drug permeability in Chinese hamster ovary cell mutants.* Biochim Biophys Acta, 1976. **455**(1): p. 152-62.
54. Ueda, K., et al., *The mdr1 gene, responsible for multidrug-resistance, codes for P-glycoprotein.* Biochem Biophys Res Commun, 1986. **141**(3): p. 956-62.
55. Li, Y., J. Revalde, and J.W. Paxton, *The effects of dietary and herbal phytochemicals on drug transporters.* Adv Drug Deliv Rev, 2017. **116**: p. 45-62.
56. Thiebaut, F., et al., *Cellular localization of the multidrug-resistance gene product P-glycoprotein in normal human tissues.* Proc Natl Acad Sci U S A, 1987. **84**(21): p. 7735-8.
57. Sugawara, I., et al., *Tissue distribution of P-glycoprotein encoded by a multidrug-resistant gene as revealed by a monoclonal antibody, MRK 16.* Cancer Res, 1988. **48**(7): p. 1926-9.
58. Fromm, M.F., *P-glycoprotein: a defense mechanism limiting oral bioavailability and CNS accumulation of drugs.* Int J Clin Pharmacol Ther, 2000. **38**(2): p. 69-74.
59. Robey, R.W., et al., *Revisiting the role of ABC transporters in multidrug-resistant cancer.* Nat Rev Cancer, 2018.
60. Borst, P., et al., *A family of drug transporters: the multidrug resistance-associated proteins.* J Natl Cancer Inst, 2000. **92**(16): p. 1295-302.
61. Pearce, H.L., et al., *Essential features of the P-glycoprotein pharmacophore as defined by a series of reserpine analogs that modulate multidrug resistance.* Proc Natl Acad Sci U S A, 1989. **86**(13): p. 5128-32.
62. Doyle, L. and D.D. Ross, *Multidrug resistance mediated by the breast cancer resistance protein BCRP (ABCG2).* Oncogene, 2003. **22**(47): p. 7340-58.
63. Li, Y. and J.W. Paxton, *The effects of flavonoids on the ABC transporters: consequences for the pharmacokinetics of substrate drugs.* Expert Opin Drug Metab Toxicol, 2013. **9**(3): p. 267-85.
64. Henrich, C.J., et al., *A high-throughput cell-based assay for inhibitors of ABCG2 activity.* Journal of Biomolecular Screening, 2006. **11**(2): p. 176-183.
65. Huang, X.C., et al., *Lamellarin O, a Pyrrole Alkaloid from an Australian Marine Sponge, Ianthella sp., Reverses BCRP Mediated Drug Resistance in Cancer Cells.* Marine Drugs, 2014. **12**(7): p. 3818-3837.
66. Krapf, M.K., J. Gallus, and M. Wiese, *Synthesis and biological investigation of 2,4-substituted quinazolines as highly potent inhibitors of breast cancer resistance protein (ABCG2).* European Journal of Medicinal Chemistry, 2017. **139**: p. 587-611.
67. Cole, S.P.C., *Multidrug Resistance Protein 1 (MRP1, ABCC1), a "Multitasking" ATP-binding Cassette (ABC) Transporter.* Journal of Biological Chemistry, 2014. **289**(45): p. 30880-30888.
68. Martin-Broto, J., et al., *MRP1 overexpression determines poor prognosis in prospectively treated patients with localized high-risk soft tissue sarcoma of limbs and trunk wall: an ISG/GEIS study.* Mol Cancer Ther, 2014. **13**(1): p. 249-59.
69. Evers, R., et al., *Basolateral localization and export activity of the human multidrug resistance-associated protein in polarized pig kidney cells.* J Clin Invest, 1996. **97**(5): p. 1211-8.
70. Cole, S.P. and R.G. Deeley, *Transport of glutathione and glutathione conjugates by MRP1.* Trends Pharmacol Sci, 2006. **27**(8): p. 438-46.
71. Versantvoort, C.H., et al., *Regulation by glutathione of drug transport in multidrug-resistant human lung tumour cell lines overexpressing multidrug resistance-associated protein.* Br J Cancer, 1995. **72**(1): p. 82-9.
72. van der Schoor, L.W., et al., *New insights in the biology of ABC transporters ABCC2 and ABCC3: impact on drug disposition.* Expert Opin Drug Metab Toxicol, 2015. **11**(2): p. 273-93.
73. Ali, I., et al., *Identification of novel MRP3 inhibitors based on computational models and validation using an in vitro membrane vesicle assay.* Eur J Pharm Sci, 2017. **103**: p. 52-59.

74. Jia, Y.M., et al., *MRP3 Is Responsible for the Efflux Transport of Curcumin Glucuronide from Hepatocytes to the Blood.* Drug Metab Dispos, 2020.
75. Kitamura, Y., H. Kusuhara, and Y. Sugiyama, *Basolateral efflux mediated by multidrug resistance-associated protein 3 (Mrp3/Abcc3) facilitates intestinal absorption of folates in mouse.* Pharm Res, 2010. **27**(4): p. 665-72.
76. Iyer, R. and S.K. Tomar, *Folate: a functional food constituent.* J Food Sci, 2009. **74**(9): p. R114-22.
77. Scialis, R.J., et al., *Multidrug Resistance-Associated Protein 3 Plays an Important Role in Protection against Acute Toxicity of Diclofenac.* Drug Metab Dispos, 2015. **43**(7): p. 944-50.
78. Venkatasubramanian, R., et al., *ABCC3 and OCT1 genotypes influence pharmacokinetics of morphine in children.* Pharmacogenomics, 2014. **15**(10): p. 1297-309.
79. Kool, M., et al., *MRP3, an organic anion transporter able to transport anti-cancer drugs.* Proc Natl Acad Sci U S A, 1999. **96**(12): p. 6914-9.
80. Yang, J., et al., *Effect of variation of ABCB1 and ABCC3 genotypes on the survival of bone tumor cases after chemotherapy.* Asian Pac J Cancer Prev, 2013. **14**(8): p. 4595-8.
81. Zhao, Y., et al., *ABCC3 as a marker for multidrug resistance in non-small cell lung cancer.* Sci Rep, 2013. **3**: p. 3120.
82. Rady, M., et al., *Therapy-relevant aberrant expression of MRP3 and BCRP mRNA in TCC-/SCC-bladder cancer tissue of untreated patients.* Oncol Rep, 2017. **38**(1): p. 551-560.
83. Morse, D.L., et al., *Identification of novel pancreatic adenocarcinoma cell-surface targets by gene expression profiling and tissue microarray.* Biochem Pharmacol, 2010. **80**(5): p. 748-54.
84. Tomonari, T., et al., *MRP3 as a novel resistance factor for sorafenib in hepatocellular carcinoma.* Oncotarget, 2016. **7**(6): p. 7207-15.
85. Nies, A.T., et al., *Expression of the multidrug resistance proteins MRP2 and MRP3 in human hepatocellular carcinoma.* Int J Cancer, 2001. **94**(4): p. 492-9.
86. Fletcher, J.I., et al., *ABC transporters in cancer: more than just drug efflux pumps.* Nat Rev Cancer, 2010. **10**(2): p. 147-56.
87. Balaji, S.A., et al., *Role of the Drug Transporter ABCC3 in Breast Cancer Chemoresistance.* PLoS One, 2016. **11**(5): p. e0155013.
88. O'Brien, C., et al., *Functional genomics identifies ABCC3 as a mediator of taxane resistance in HER2-amplified breast cancer.* Cancer Res, 2008. **68**(13): p. 5380-9.
89. Partanen, L., et al., *Amplification and overexpression of the ABCC3 (MRP3) gene in primary breast cancer.* Genes Chromosomes Cancer, 2012. **51**(9): p. 832-40.
90. Basili, S. and S. Moro, *Novel camptothecin derivatives as topoisomerase I inhibitors.* Expert Opin Ther Pat, 2009. **19**(5): p. 555-74.
91. Brangi, M., et al., *Camptothecin resistance: role of the ATP-binding cassette (ABC), mitoxantrone-resistance half-transporter (MXR), and potential for glucuronidation in MXR-expressing cells.* Cancer Res, 1999. **59**(23): p. 5938-46.
92. Lalloo, A.K., et al., *Membrane transport of camptothecin: facilitation by human P-glycoprotein (ABCB1) and multidrug resistance protein 2 (ABCC2).* BMC Med, 2004. **2**: p. 16.
93. van de Wetering, K., et al., *Intestinal breast cancer resistance protein (BCRP)/Bcrp1 and multidrug resistance protein 3 (MRP3)/Mrp3 are involved in the pharmacokinetics of resveratrol.* Mol Pharmacol, 2009. **75**(4): p. 876-85.
94. Patel, D., S. Shukla, and S. Gupta, *Apigenin and cancer chemoprevention: progress, potential and promise (review).* Int J Oncol, 2007. **30**(1): p. 233-45.
95. Shukla, S. and S. Gupta, *Molecular targets for apigenin-induced cell cycle arrest and apoptosis in prostate cancer cell xenograft.* Mol Cancer Ther, 2006. **5**(4): p. 843-52.
96. Budhraja, A., et al., *Apigenin induces apoptosis in human leukemia cells and exhibits anti-leukemic activity in vivo.* Mol Cancer Ther, 2012. **11**(1): p. 132-42.
97. Lin, C.C., et al., *Apigenin induces apoptosis through mitochondrial dysfunction in U-2 OS human osteosarcoma cells and inhibits osteosarcoma xenograft tumor*

*growth in vivo.* J Agric Food Chem, 2012. **60**(45): p. 11395-402.
98. Saeed, M., et al., *Activity of the dietary flavonoid, apigenin, against multidrug-resistant tumor cells as determined by pharmacogenomics and molecular docking.* J Nutr Biochem, 2015. **26**(1): p. 44-56.
99. Rajesh, E., et al., *Naturally occurring products in cancer therapy.* J Pharm Bioallied Sci, 2015. **7**(Suppl 1): p. S181-3.
100. Rigalli, J.P., et al., *Regulation of multidrug resistance proteins by genistein in a hepatocarcinoma cell line: impact on sorafenib cytotoxicity.* PLoS One, 2015. **10**(3): p. e0119502.
101. Zhu, W., et al., *Breast cancer resistance protein (BCRP) and sulfotransferases contribute significantly to the disposition of genistein in mouse intestine.* AAPS J, 2010. **12**(4): p. 525-36.
102. Falasca, M. and K.J. Linton, *Investigational ABC transporter inhibitors.* Expert Opin Investig Drugs, 2012. **21**(5): p. 657-66.
103. Long, S., et al., *Marine Natural Products as Models to Circumvent Multidrug Resistance.* Molecules, 2016. **21**(7).
104. Boger, D.L., et al., *Total synthesis of ningalin B utilizing a heterocyclic azadiene Diels-Alder reaction and discovery of a new class of potent multidrug resistant (MDR) reversal agents.* J Org Chem, 2000. **65**(8): p. 2479-83.
105. Yang, C., et al., *Extending the structure-activity relationship study of marine natural ningalin B analogues as P-glycoprotein inhibitors.* European Journal of Medicinal Chemistry, 2017. **125**: p. 795-806.
106. Kang, H. and W. Fenical, *Ningalins A-D: Novel Aromatic Alkaloids from a Western Australian Ascidian of the Genus Didemnum.* J Org Chem, 1997. **62**(10): p. 3254-3262.
107. Soenen, D.R., et al., *Multidrug resistance reversal activity of key ningalin analogues.* Bioorganic & Medicinal Chemistry Letters, 2003. **13**(10): p. 1777-1781.
108. Tao, H.C., I.K. Hwang, and D.L. Boger, *Multidrug resistance reversal activity of permethyl ningalin B amide derivatives.* Bioorganic & Medicinal Chemistry Letters, 2004. **14**(24): p. 5979-5981.
109. Chou, T.C., et al., *Potent reversal of multidrug resistance by ningalins and its use in drug combinations against human colon carcinoma xenograft in nude mice.* Cancer Chemother Pharmacol, 2005. **56**(4): p. 379-90.
110. Bin, J.W., et al., *Structure-activity relationship study of permethyl ningalin B analogues as P-glycoprotein chemosensitizers.* J Med Chem, 2013. **56**(22): p. 9057-70.
111. Zhang, P.Y., et al., *Design and syntheses of permethyl ningalin B analogues: potent multidrug resistance (MDR) reversal agents of cancer cells.* J Med Chem, 2010. **53**(14): p. 5108-20.
112. Wang, Z., et al., *Optimization of permethyl ningalin B analogs as P-glycoprotein inhibitors.* Bioorg Med Chem, 2015. **23**(17): p. 5566-73.
113. Chen, L.M., et al., *Reversal of P-gp-mediated multidrug resistance by Bromotetrandrine in vivo is associated with enhanced accumulation of chemotherapeutical drug in tumor tissue.* Anticancer Res, 2009. **29**(11): p. 4597-604.
114. Sun, H., et al., *Reversal of P-glycoprotein-mediated multidrug resistance by the novel tetrandrine derivative W6.* J Asian Nat Prod Res, 2015. **17**(6): p. 638-48.
115. Zhu, J.Y., et al., *Jatrophane Diterpenoids as Modulators of P-Glycoprotein-Dependent Multidrug Resistance (MDR): Advances of Structure-Activity Relationships and Discovery of Promising MDR Reversal Agents.* Journal of Medicinal Chemistry, 2016. **59**(13): p. 6353-6369.
116. Murakami, M., et al., *Synthetic Analogs of Curcumin Modulate the Function of Multidrug Resistance-Linked ATP-Binding Cassette Transporter ABCG2.* Drug Metab Dispos, 2017. **45**(11): p. 1166-1177.
117. Wong, I.L.K., et al., *Potent and Nontoxic Chemosensitizer of P-Glycoprotein-Mediated Multidrug Resistance in Cancer: Synthesis and Evaluation of Methylated Epigallocatechin, Gallocatechin, and Dihydromyricetin Derivatives.* Journal of Medicinal Chemistry, 2015. **58**(11): p. 4529-4549.
118. Yang, Y., et al., *Targeting ABCB1-mediated tumor multidrug resistance by CRISPR/Cas9-based*

*genome editing.* Am J Transl Res, 2016. **8**(9): p. 3986-3994.
119. Fu, L.W., et al., *The multidrug resistance of tumour cells was reversed by tetrandrine in vitro and in xenografts derived from human breast adenocarcinoma MCF-7/adr cells.* Eur J Cancer, 2002. **38**(3): p. 418-26.
120. Wei, N., et al., *H1, a novel derivative of tetrandrine reverse P-glycoprotein-mediated multidrug resistance by inhibiting transport function and expression of P-glycoprotein.* Cancer Chemother Pharmacol, 2011. **67**(5): p. 1017-25.
121. Munoz-Martinez, F., et al., *Celastraceae sesquiterpenes as a new class of modulators that bind specifically to human P-glycoprotein and reverse cellular multidrug resistance.* Cancer Res, 2004. **64**(19): p. 7130-8.
122. Spivey, A.C., M. Weston, and S. Woodhead, *Celastraceae sesquiterpenoids: biological activity and synthesis.* Chem Soc Rev, 2002. **31**(1): p. 43-59.
123. Szakacs, G., et al., *Targeting the Achilles heel of multidrug-resistant cancer by exploiting the fitness cost of resistance.* Chem Rev, 2014. **114**(11): p. 5753-74.
124. Callies, O., et al., *Optimization by Molecular Fine Tuning of Dihydro-beta-agarofuran Sesquiterpenoids as Reversers of P-Glycoprotein-Mediated Multidrug Resistance.* Journal of Medicinal Chemistry, 2016. **59**(5): p. 1880-1890.
125. Barile, E., et al., *Discovery of a new series of jatrophane and lathyrane diterpenes as potent and specific P-glycoprotein modulators.* Organic & Biomolecular Chemistry, 2008. **6**(10): p. 1756-1762.
126. Teodori, E., et al., *Structure-Activity Relationship Studies on 6,7-Dimethoxy-2-phenethyl-1,2,3,4-tetrahydroisoquinoline Derivatives as Multidrug Resistance Reversers.* ChemMedChem, 2017. **12**(16): p. 1369-1379.
127. Bisi, A., et al., *Coumarin derivatives as potential antitumor agents: Growth inhibition, apoptosis induction and multidrug resistance reverting activity.* Eur J Med Chem, 2017. **127**: p. 577-585.
128. Baggetto, L.G., et al., *In vitro and in vivo reversal of cancer cell multidrug resistance by the semi-synthetic antibiotic tiamulin.* Biochemical Pharmacology, 1998. **56**(9): p. 1219-1228.
129. Wong, I.L.K., et al., *Modulation of Multidrug Resistance Protein 1 (MRP1/ABCC1)-Mediated Multidrug Resistance by Bivalent Apigenin Homodimers and Their Derivatives.* Journal of Medicinal Chemistry, 2009. **52**(17): p. 5311-5322.
130. Vaclavikova, R., et al., *Modulation of paclitaxel transport by flavonoid derivatives in human breast cancer cells. Is there a correlation between binding affinity to NBD of P-gp and modulation of transport?* Bioorganic & Medicinal Chemistry, 2006. **14**(13): p. 4519-4525.
131. Lee, S.Y., et al., *Hydrocinchonine, Cinchonine, and Quinidine Potentiate Paclitaxel-Induced Cytotoxicity and Apoptosis via Multidrug Resistance Reversal in MES-SA/DX5 Uterine Sarcoma Cells.* Environmental Toxicology, 2011. **26**(4): p. 424-431.
132. Yuan, J., et al., *Synthesis of methylated quercetin derivatives and their reversal activities on P-gp- and BCRP-mediated multidrug resistance tumour cells.* European Journal of Medicinal Chemistry, 2012. **54**: p. 413-422.
133. Martins, A., et al., *Significant Activity of Ecdysteroids on the Resistance to Doxorubicin in Mammalian Cancer Cells Expressing the Human ABCB1 Transporter.* Journal of Medicinal Chemistry, 2012. **55**(11): p. 5034-5043.
134. Han, H.K. and L.T. Van Anh, *Modulation of P-glycoprotein expression by honokiol, magnolol and 4-O-methylhonokiol, the bioactive components of Magnolia officinalis.* Anticancer Res, 2012. **32**(10): p. 4445-52.
135. Podszun, M.C., et al., *The long chain alpha-tocopherol metabolite alpha-13'-COOH and gamma-tocotrienol induce P-glycoprotein expression and activity by activation of the pregnane X receptor in the intestinal cell line LS 180.* Mol Nutr Food Res, 2017. **61**(3).
136. Zander, S.A., et al., *EZN-2208 (PEG-SN38) overcomes ABCG2-mediated topotecan resistance in BRCA1-deficient mouse mammary tumors.* PLoS One, 2012. **7**(9): p. e45248.
137. Nicolle, E., et al., *Breast cancer resistance protein (BCRP/ABCG2): New inhibitors and QSAR studies by*

*a 3D linear solvation energy approach.* European Journal of Pharmaceutical Sciences, 2009. **38**(1): p. 39-46.
138. Sim, H.M., et al., *In vitro and in vivo modulation of ABCG2 by functionalized aurones and structurally related analogs.* Biochemical Pharmacology, 2011. **82**(11): p. 1562-1571.
139. Kraege, S., et al., *The combination of quinazoline and chalcone moieties leads to novel potent heterodimeric modulators of breast cancer resistance protein (BCRP/ABCG2).* European Journal of Medicinal Chemistry, 2016. **117**: p. 212-229.
140. Danko, B., et al., *Synthesis and SAR Study of Anticancer Protoflavone Derivatives: Investigation of Cytotoxicity and Interaction with ABCB1 and ABCG2 Multidrug Efflux Transporters.* Chemmedchem, 2017. **12**(11): p. 850-859.
141. Talukdar, S., et al., *Evolving Strategies for Therapeutically Targeting Cancer Stem Cells.* Adv Cancer Res, 2016. **131**: p. 159-91.
142. Lania-Pietrzak, B., et al., *Modulation of MRP1 protein transport by plant, and synthetically modified flavonoids.* Life Sci, 2005. **77**(15): p. 1879-91.
143. Paszel-Jaworska, A., et al., *Proapoptotic activity and ABCC1-related multidrug resistance reduction ability of semisynthetic oleanolic acid derivatives DIOXOL and HIMOXOL in human acute promyelocytic leukemia cells.* Chem Biol Interact, 2015. **242**: p. 1-12.
144. Hilgendorf, C., et al., *Expression of thirty-six drug transporter genes in human intestine, liver, kidney, and organotypic cell lines.* Drug Metab Dispos, 2007. **35**(8): p. 1333-40.
145. Durmus, S., et al., *Oral availability and brain penetration of the B-RAFV600E inhibitor vemurafenib can be enhanced by the P-GLYCOprotein (ABCB1) and breast cancer resistance protein (ABCG2) inhibitor elacridar.* Mol Pharm, 2012. **9**(11): p. 3236-45.
146. Mao, Q.C. and J.D. Unadkat, *Role of the Breast Cancer Resistance Protein (BCRP/ABCG2) in Drug Transport-an Update.* Aaps Journal, 2015. **17**(1): p. 65-82.
147. Glavinas, H., et al., *The role of ABC transporters in drug resistance, metabolism and toxicity.* Curr Drug Deliv, 2004. **1**(1): p. 27-42.
148. Qadir, M., et al., *Cyclosporin A is a broad-spectrum multidrug resistance modulator.* Clin Cancer Res, 2005. **11**(6): p. 2320-6.
149. Litman, T., et al., *From MDR to MXR: new understanding of multidrug resistance systems, their properties and clinical significance.* Cell Mol Life Sci, 2001. **58**(7): p. 931-59.
150. Fojo, A.T., et al., *Expression of a multidrug-resistance gene in human tumors and tissues.* Proc Natl Acad Sci U S A, 1987. **84**(1): p. 265-9.
151. Lai, S.L., et al., *MDR1 gene expression in lung cancer.* J Natl Cancer Inst, 1989. **81**(15): p. 1144-50.
152. Kosztyu, P., P. Dolezel, and P. Mlejnek, *Can P-glycoprotein mediate resistance to nilotinib in human leukaemia cells?* Pharmacol Res, 2013. **67**(1): p. 79-83.
153. Ruzickova, E., et al., *Clinically relevant interactions of anti-apoptotic Bcl-2 protein inhibitors with ABC transporters.* Pharmazie, 2017. **72**(12): p. 751-758.
154. Dhillon, N., et al., *Phase II trial of curcumin in patients with advanced pancreatic cancer.* Clin Cancer Res, 2008. **14**(14): p. 4491-9.
155. Kuo, M.L., T.S. Huang, and J.K. Lin, *Curcumin, an antioxidant and anti-tumor promoter, induces apoptosis in human leukemia cells.* Biochim Biophys Acta, 1996. **1317**(2): p. 95-100.
156. Chearwae, W., et al., *Biochemical mechanism of modulation of human P-glycoprotein (ABCB1) by curcumin I, II, and III purified from Turmeric powder.* Biochem Pharmacol, 2004. **68**(10): p. 2043-52.
157. Zeng, Z., et al., *Transport of curcumin derivatives in Caco-2 cell monolayers.* Eur J Pharm Biopharm, 2017. **117**: p. 123-131.
158. Prehm, P., *Curcumin analogue identified as hyaluronan export inhibitor by virtual docking to the ABC transporter MRP5.* Food and Chemical Toxicology, 2013. **62**: p. 76-81.
159. Wahlstrom, B. and G. Blennow, *A study on the fate of curcumin in the rat.* Acta Pharmacol Toxicol (Copenh), 1978. **43**(2): p. 86-92.
160. Ravindranath, V. and N. Chandrasekhara, *Absorption and*

*tissue distribution of curcumin in rats.* Toxicology, 1980. **16**(3): p. 259-65.
161. Sharma, R.A., et al., *Pharmacodynamic and pharmacokinetic study of oral Curcuma extract in patients with colorectal cancer.* Clin Cancer Res, 2001. **7**(7): p. 1894-900.
162. Revalde, J.L., et al., *Heterocyclic cyclohexanone monocarbonyl analogs of curcumin can inhibit the activity of ATP-binding cassette transporters in cancer multidrug resistance.* Biochem Pharmacol, 2015. **93**(3): p. 305-17.
163. Kudo, C., et al., *Synthesis of 86 species of 1,5-diaryl-3-oxo-1,4-pentadienes analogs of curcumin can yield a good lead in vivo.* BMC Pharmacol, 2011. **11**: p. 4.
164. Skoupa, N., et al., *Apoptosis Induced by the Curcumin Analogue EF-24 Is Neither Mediated by Oxidative Stress-Related Mechanisms nor Affected by Expression of Main Drug Transporters ABCB1 and ABCG2 in Human Leukemia Cells.* Int J Mol Sci, 2017. **18**(11).
165. Adams, B.K., et al., *EF24, a novel synthetic curcumin analog, induces apoptosis in cancer cells via a redox-dependent mechanism.* Anticancer Drugs, 2005. **16**(3): p. 263-75.
166. Liu, H., et al., *In vivo and in vitro suppression of hepatocellular carcinoma by EF24, a curcumin analog.* PLoS One, 2012. **7**(10): p. e48075.
167. Yin, D.L., et al., *EF24 inhibits tumor growth and metastasis via suppressing NF-kappaB dependent pathways in human cholangiocarcinoma.* Sci Rep, 2016. **6**: p. 32167.
168. Bertazza, L., et al., *Biological Effects of EF24, a Curcumin Derivative, Alone or Combined with Mitotane in Adrenocortical Tumor Cell Lines.* Molecules, 2019. **24**(12).
169. Zhang, D., et al., *Therapeutic role of EF24 targeting glucose transporter 1-mediated metabolism and metastasis in ovarian cancer cells.* Cancer Sci, 2013. **104**(12): p. 1690-6.
170. Zhang, X., et al., *Effects of curcumin on ion channels and transporters.* Front Physiol, 2014. **5**: p. 94.
171. Gan, Y., et al., *Pharmacodynamics of telomerase inhibition and telomere shortening by noncytotoxic suramin.* AAPS J, 2015. **17**(1): p. 268-76.
172. Cheson, B.D., et al., *Suramin therapy in AIDS and related disorders. Report of the US Suramin Working Group.* JAMA, 1987. **258**(10): p. 1347-51.
173. Eisenberger, M.A. and L.M. Reyno, *Suramin.* Cancer Treatment Reviews, 1994. **20**(3): p. 259-273.
174. Koval, A., K. Ahmed, and V.L. Katanaev, *Inhibition of Wnt signalling and breast tumour growth by the multi-purpose drug suramin through suppression of heterotrimeric G proteins and Wnt endocytosis.* Biochem J, 2016. **473**(4): p. 371-81.
175. Villalona-Calero, M.A., et al., *Noncytotoxic suramin as a chemosensitizer in patients with advanced non-small-cell lung cancer: a phase II study.* Ann Oncol, 2008. **19**(11): p. 1903-9.
176. Marchetti, D., et al., *Inhibition of heparanase activity and heparanase-induced angiogenesis by suramin analogues.* Int J Cancer, 2003. **104**(2): p. 167-74.
177. Margolles-Clark, E., et al., *Suramin inhibits the CD40–CD154 costimulatory interaction: A possible mechanism for immunosuppressive effects.* Biochemical Pharmacology, 2009. **77**(7): p. 1236-1245.
178. Lam, E.T., et al., *Phase I trial of non-cytotoxic suramin as a modulator of docetaxel and gemcitabine therapy in previously treated patients with non-small cell lung cancer.* Cancer Chemother Pharmacol, 2010. **66**(6): p. 1019-29.
179. Pesenti, E., et al., *Suramin prevents neovascularisation and tumour growth through blocking of basic fibroblast growth factor activity.* Br J Cancer, 1992. **66**(2): p. 367-72.
180. Wielinga, P., et al., *The human multidrug resistance protein MRP5 transports folates and can mediate cellular resistance against antifolates.* Cancer Res, 2005. **65**(10): p. 4425-30.
181. Hagner, N. and M. Joerger, *Cancer chemotherapy: targeting folic acid synthesis.* Cancer Manag Res, 2010. **2**: p. 293-301.
182. de Graaf, D., et al., *P-glycoprotein confers methotrexate resistance in 3T6 cells with deficient carrier-mediated methotrexate uptake.*

Proc Natl Acad Sci U S A, 1996. **93**(3): p. 1238-42.
183. Amrutkar, M. and I.P. Gladhaug, *Pancreatic Cancer Chemoresistance to Gemcitabine.* Cancers (Basel), 2017. **9**(11).
184. Ciliberto, D., et al., *Role of gemcitabine-based combination therapy in the management of advanced pancreatic cancer: a meta-analysis of randomised trials.* Eur J Cancer, 2013. **49**(3): p. 593-603.
185. Mohammed, A., et al., *Molecular Targeted Intervention for Pancreatic Cancer.* Cancers (Basel), 2015. **7**(3): p. 1499-542.
186. Nambaru, P.K., et al., *Drug efflux transporter multidrug resistance-associated protein 5 affects sensitivity of pancreatic cancer cell lines to the nucleoside anticancer drug 5-fluorouracil.* Drug Metab Dispos, 2011. **39**(1): p. 132-9.
187. Philip, P.A., *Targeted therapies for pancreatic cancer.* Gastrointest Cancer Res, 2008. **2**(4 Suppl): p. S16-9.
188. Adamska, A. and M. Falasca, *ATP-binding cassette transporters in progression and clinical outcome of pancreatic cancer: What is the way forward?* World J Gastroenterol, 2018. **24**(29): p. 3222-3238.
189. Russo, G., C. Zegar, and A. Giordano, *Advantages and limitations of microarray technology in human cancer.* Oncogene, 2003. **22**(42): p. 6497-507.
190. Rhodes, D.R., et al., *ONCOMINE: a cancer microarray database and integrated data-mining platform.* Neoplasia, 2004. **6**(1): p. 1-6.
191. Li, T., et al., *Identification of hub genes with prognostic values in gastric cancer by bioinformatics analysis.* World J Surg Oncol, 2018. **16**(1): p. 114.
192. Liu, Y., A. Beyer, and R. Aebersold, *On the Dependency of Cellular Protein Levels on mRNA Abundance.* Cell, 2016. **165**(3): p. 535-50.
193. Szklarczyk, D., et al., *The STRING database in 2017: quality-controlled protein-protein association networks, made broadly accessible.* Nucleic Acids Res, 2017. **45**(D1): p. D362-D368.
194. Rhodes, D.R., et al., *Oncomine 3.0: genes, pathways, and networks in a collection of 18,000 cancer gene expression profiles.* Neoplasia, 2007. **9**(2): p. 166-80.
195. Mukaka, M.M., *Statistics corner: A guide to appropriate use of correlation coefficient in medical research.* Malawi Med J, 2012. **24**(3): p. 69-71.
196. Yamada, A., et al., *ABCC1-Exported Sphingosine-1-phosphate, Produced by Sphingosine Kinase 1, Shortens Survival of Mice and Patients with Breast Cancer.* Mol Cancer Res, 2018. **16**(6): p. 1059-1070.
197. Kobayashi, M., et al., *Wnt-beta-catenin signaling regulates ABCC3 (MRP3) transporter expression in colorectal cancer.* Cancer Sci, 2016. **107**(12): p. 1776-1784.
198. McGranahan, N. and C. Swanton, *Clonal Heterogeneity and Tumor Evolution: Past, Present, and the Future.* Cell, 2017. **168**(4): p. 613-628.
199. Hou, G.X., et al., *Mining expression and prognosis of topoisomerase isoforms in non-small-cell lung cancer by using Oncomine and Kaplan-Meier plotter.* PLoS One, 2017. **12**(3): p. e0174515.
200. Soric, B., *Statistical "Discoveries" and Effect-Size Estimation.* Journal of the American Statistical Association, 1989. **84**(406): p. 608-610.
201. Myint, K., et al., *Identification of MRP2 as a targetable factor limiting oxaliplatin accumulation and response in gastrointestinal cancer.* Sci Rep, 2019. **9**(1): p. 2245.
202. Macey, M.G., *Principles of Flow Cytometry*, in *Flow Cytometry: Principles and Applications*, M.G. Macey, Editor. 2007, Humana Press: Totowa, NJ. p. 1-15.
203. Kamentsky, L.A., M.R. Melamed, and H. Derman, *Spectrophotometer - New Instrument for Ultrarapid Cell Analysis.* Science, 1965. **150**(3696): p. 630-+.
204. Fulwyler, M.J., *Electronic Separation of Biological Cells by Volume.* Science, 1965. **150**(3698): p. 910-&.
205. Sweet, R.G., *High Frequency Recording with Electrostatically Deflected Ink Jets.* Review of Scientific Instruments, 1965. **36**(2): p. 131-&.
206. Bigos, M., et al., *Nine color eleven parameter immunophenotyping using three laser flow cytometry.* Cytometry, 1999. **36**(1): p. 36-45.

207. Woo, J., A. Baumann, and V. Arguello, *Recent advancements of flow cytometry: new applications in hematology and oncology.* Expert Rev Mol Diagn, 2014. **14**(1): p. 67-81.
208. Spitzer, M.H. and G.P. Nolan, *Mass Cytometry: Single Cells, Many Features.* Cell, 2016. **165**(4): p. 780-91.
209. Adan, A., et al., *Flow cytometry: basic principles and applications.* Crit Rev Biotechnol, 2017. **37**(2): p. 163-176.
210. Wilkerson, M.J., *Principles and applications of flow cytometry and cell sorting in companion animal medicine.* Vet Clin North Am Small Anim Pract, 2012. **42**(1): p. 53-71.
211. Chen, X. and S. Cherian, *Acute Myeloid Leukemia Immunophenotyping by Flow Cytometric Analysis.* Clin Lab Med, 2017. **37**(4): p. 753-769.
212. Kayser, S. and M.J. Levis, *Advances in targeted therapy for acute myeloid leukaemia.* Br J Haematol, 2018. **180**(4): p. 484-500.
213. Kandeel, E.Z., et al., *Impact of FLT3 Receptor (CD135) Detection by Flow Cytometry on Clinical Outcome of Adult Acute Myeloid Leukemia Patients.* Clin Lymphoma Myeloma Leuk, 2018. **18**(8): p. 541-547.
214. van Dongen, J.J., et al., *Minimal residual disease diagnostics in acute lymphoblastic leukemia: need for sensitive, fast, and standardized technologies.* Blood, 2015. **125**(26): p. 3996-4009.
215. Liu, L., et al., *Epigallocatechin-3-gallate promotes apoptosis and reversal of multidrug resistance in esophageal cancer cells.* Pathol Res Pract, 2017. **213**(10): p. 1242-1250.
216. Hogg, K., et al., *Quantification of proteins by flow cytometry: Quantification of human hepatic transporter P-gp and OATP1B1 using flow cytometry and mass spectrometry.* Methods, 2015. **82**: p. 38-46.
217. Pisco, A.O., D.A. Jackson, and S. Huang, *Reduced Intracellular Drug Accumulation in Drug-Resistant Leukemia Cells is Not Only Solely Due to MDR-Mediated Efflux but also to Decreased Uptake.* Frontiers in oncology, 2014. **4**: p. 306-306.
218. Weiss, J., et al., *Inhibition of MRP1/ABCC1, MRP2/ABCC2, and MRP3/ABCC3 by nucleoside, nucleotide, and non-nucleoside reverse transcriptase inhibitors.* Drug Metab Dispos, 2007. **35**(3): p. 340-4.
219. Gutmann, H., et al., *Evidence for different ABC-transporters in Caco-2 cells modulating drug uptake.* Pharm Res, 1999. **16**(3): p. 402-7.
220. Li, Y., et al., *Modulatory effects of curcumin on multi-drug resistance-associated protein 5 in pancreatic cancer cells.* Cancer Chemother Pharmacol, 2011. **68**(3): p. 603-10.
221. Rau, S., et al., *Expression of the multidrug resistance proteins MRP2 and MRP3 in human cholangiocellular carcinomas.* Eur J Clin Invest, 2008. **38**(2): p. 134-42.
222. Mosmann, T., *Rapid colorimetric assay for cellular growth and survival: application to proliferation and cytotoxicity assays.* J Immunol Methods, 1983. **65**(1-2): p. 55-63.
223. Stone, V., H. Johnston, and R.P. Schins, *Development of in vitro systems for nanotoxicology: methodological considerations.* Crit Rev Toxicol, 2009. **39**(7): p. 613-26.
224. Sieuwerts, A.M., et al., *The MTT tetrazolium salt assay scrutinized: how to use this assay reliably to measure metabolic activity of cell cultures in vitro for the assessment of growth characteristics, IC50-values and cell survival.* Eur J Clin Chem Clin Biochem, 1995. **33**(11): p. 813-23.
225. Wang, P., S.M. Henning, and D. Heber, *Limitations of MTT and MTS-based assays for measurement of antiproliferative activity of green tea polyphenols.* PLoS One, 2010. **5**(4): p. e10202.
226. Stepanenko, A.A. and V.V. Dmitrenko, *Pitfalls of the MTT assay: Direct and off-target effects of inhibitors can result in over/underestimation of cell viability.* Gene, 2015. **574**(2): p. 193-203.
227. N, C.T.a.M., *CompuSyn for Drug Combinations: PC Software and User's Guide: A Computer Program for Quantitation of Synergism and Antagonism in Drug Combinations, and the Determination of IC50 and ED50 and LD50 Values.* 2005.
228. Chou, T.C. and P. Talalay, *Generalized equations for the analysis of inhibitions of Michaelis-Menten and higher-order kinetic systems with two or more mutually exclusive and nonexclusive*

*inhibitors.* Eur J Biochem, 1981. **115**(1): p. 207-16.
229. Chou, T.C., *Theoretical basis, experimental design, and computerized simulation of synergism and antagonism in drug combination studies.* Pharmacol Rev, 2006. **58**(3): p. 621-81.
230. Danna, K. and D. Nathans, *Specific cleavage of simian virus 40 DNA by restriction endonuclease of Hemophilus influenzae.* Proc Natl Acad Sci U S A, 1971. **68**(12): p. 2913-7.
231. Kasarjian, J.K., M. Iida, and J. Ryu, *New restriction enzymes discovered from Escherichia coli clinical strains using a plasmid transformation method.* Nucleic Acids Res, 2003. **31**(5): p. e22.
232. Lai, C.J. and D. Nathans, *Deletion mutants of simian virus 40 generated by enzymatic excision of DNA segments from the viral genome.* J Mol Biol, 1974. **89**(1): p. 179-93.
233. Roberts, R.J., *How restriction enzymes became the workhorses of molecular biology.* Proc Natl Acad Sci U S A, 2005. **102**(17): p. 5905-8.
234. Carroll, D., *Genome engineering with zinc-finger nucleases.* Genetics, 2011. **188**(4): p. 773-82.
235. Scherer, S. and R.W. Davis, *Replacement of chromosome segments with altered DNA sequences constructed in vitro.* Proc Natl Acad Sci U S A, 1979. **76**(10): p. 4951-5.
236. Smithies, O., et al., *Insertion of DNA sequences into the human chromosomal beta-globin locus by homologous recombination.* Nature, 1985. **317**(6034): p. 230-4.
237. Adli, M., *The CRISPR tool kit for genome editing and beyond.* Nat Commun, 2018. **9**(1): p. 1911.
238. Kim, Y.G., J. Cha, and S. Chandrasegaran, *Hybrid restriction enzymes: zinc finger fusions to Fok I cleavage domain.* Proc Natl Acad Sci U S A, 1996. **93**(3): p. 1156-60.
239. Gaj, T., C.A. Gersbach, and C.F. Barbas, 3rd, *ZFN, TALEN, and CRISPR/Cas-based methods for genome engineering.* Trends Biotechnol, 2013. **31**(7): p. 397-405.
240. Schmid-Burgk, J.L., et al., *A ligation-independent cloning technique for high-throughput assembly of transcription activator-like effector genes.* Nat Biotechnol, 2013. **31**(1): p. 76-81.
241. Ishino, Y., et al., *Nucleotide sequence of the iap gene, responsible for alkaline phosphatase isozyme conversion in Escherichia coli, and identification of the gene product.* J Bacteriol, 1987. **169**(12): p. 5429-33.
242. Pickar-Oliver, A. and C.A. Gersbach, *The next generation of CRISPR-Cas technologies and applications.* Nat Rev Mol Cell Biol, 2019. **20**(8): p. 490-507.
243. Barrangou, R., et al., *CRISPR provides acquired resistance against viruses in prokaryotes.* Science, 2007. **315**(5819): p. 1709-12.
244. Jinek, M., et al., *A programmable dual-RNA-guided DNA endonuclease in adaptive bacterial immunity.* Science, 2012. **337**(6096): p. 816-21.
245. Jinek, M., et al., *RNA-programmed genome editing in human cells.* Elife, 2013. **2**: p. e00471.
246. Lee, K., et al., *Synthetically modified guide RNA and donor DNA are a versatile platform for CRISPR-Cas9 engineering.* Elife, 2017. **6**.
247. Guo, Z., et al., *CRISPR/Cas9-mediated knockout of both the PxABCC2 and PxABCC3 genes confers high-level resistance to Bacillus thuringiensis Cry1Ac toxin in the diamondback moth, Plutella xylostella (L.).* Insect Biochem Mol Biol, 2019. **107**: p. 31-38.
248. Schwank, G., et al., *Functional repair of CFTR by CRISPR/Cas9 in intestinal stem cell organoids of cystic fibrosis patients.* Cell Stem Cell, 2013. **13**(6): p. 653-8.
249. Simoff, I., et al., *Complete Knockout of Endogenous Mdr1 (Abcb1) in MDCK Cells by CRISPR-Cas9.* J Pharm Sci, 2016. **105**(2): p. 1017-1021.
250. Muzumdar, M.D., et al., *Survival of pancreatic cancer cells lacking KRAS function.* Nat Commun, 2017. **8**(1): p. 1090.
251. Cutting, G.R., *Cystic fibrosis genetics: from molecular understanding to clinical application.* Nat Rev Genet, 2015. **16**(1): p. 45-56.
252. Fletcher, J.I., et al., *ABC transporters in cancer: more than just drug efflux pumps.* Nature Reviews Cancer, 2010. **10**(2): p. 147-156.
253. Ran, F.A., et al., *Genome engineering using the CRISPR-*

*Cas9 system.* Nature Protocols, 2013. **8**(11): p. 2281-2308.
254. Smits, A.H., et al., *Biological plasticity rescues target activity in CRISPR knock outs.* Nat Methods, 2019. **16**(11): p. 1087-1093.
255. Garibyan, L. and N. Avashia, *Polymerase chain reaction.* The Journal of investigative dermatology, 2013. **133**(3): p. 1-4.
256. Tuma, R.S., et al., *Characterization of SYBR Gold Nucleic Acid Gel Stain: A Dye Optimized for Use with 300-nm Ultraviolet Transilluminators.* Analytical Biochemistry, 1999. **268**(2): p. 278-288.
257. Das, S., S.C. Mohapatra, and J.T. Hsu, *Studies on primer-dimer formation in polymerase chain reaction (PCR).* Biotechnology Techniques, 1999. **13**(10): p. 643-646.
258. Sredni, S.T., et al., *A functional screening of the kinome identifies the Polo-like kinase 4 as a potential therapeutic target for malignant rhabdoid tumors, and possibly, other embryonal tumors of the brain.* Pediatr Blood Cancer, 2017. **64**(11).
259. WHO, *The top 10 causes of death*. 2014.
260. Siegel, R.L., K.D. Miller, and A. Jemal, *Cancer statistics, 2016.* CA Cancer J Clin, 2016. **66**(1): p. 7-30.
261. Society, A.C., *Cancer Facts & Figures 2019.* Atlanta: American Cancer Society, 2019.
262. Arnold, M., et al., *Progress in cancer survival, mortality, and incidence in seven high-income countries 1995-2014 (ICBP SURVMARK-2): a population-based study.* Lancet Oncol, 2019.
263. Higgins, C.F., *ABC transporters: from microorganisms to man.* Annu Rev Cell Biol, 1992. **8**: p. 67-113.
264. Schober, P. and T.R. Vetter, *Survival Analysis and Interpretation of Time-to-Event Data: The Tortoise and the Hare.* Anesth Analg, 2018. **127**(3): p. 792-798.
265. Vogel, C. and E.M. Marcotte, *Insights into the regulation of protein abundance from proteomic and transcriptomic analyses.* Nature Reviews Genetics, 2012. **13**: p. 227.
266. Tomlins, S.A., et al., *Recurrent fusion of TMPRSS2 and ETS transcription factor genes in prostate cancer.* Science, 2005. **310**(5748): p. 644-8.
267. Miksys, S. and R.F. Tyndale, *Cytochrome P450-mediated drug metabolism in the brain.* J Psychiatry Neurosci, 2013. **38**(3): p. 152-63.
268. Toselli, F., et al., *Gene expression profiling of cytochromes P450, ABC transporters and their principal transcription factors in the amygdala and prefrontal cortex of alcoholics, smokers and drug-free controls by qRT-PCR.* Xenobiotica, 2015. **45**(12): p. 1129-37.
269. Afsar, N.A., et al., *Implications of genetic variation of common Drug Metabolizing Enzymes and ABC Transporters among the Pakistani Population.* Sci Rep, 2019. **9**(1): p. 7323.
270. Liptrott, N.J., et al., *The impact of cytokines on the expression of drug transporters, cytochrome P450 enzymes and chemokine receptors in human PBMC.* Br J Pharmacol, 2009. **156**(3): p. 497-508.
271. Yang, Q., et al., *Effects of culture duration on gene expression of P450 isoforms, uptake and efflux transporters in primary hepatocytes cultured in the absence and presence of interleukin-6: implications for experimental design for the evaluation of downregulatory effects of biotherapeutics.* Curr Drug Metab, 2012. **13**(7): p. 938-46.
272. Nitschke, Y. and F. Rutsch, *Generalized arterial calcification of infancy and pseudoxanthoma elasticum: two sides of the same coin.* Front Genet, 2012. **3**: p. 302.
273. Takahashi, R.U., et al., *Loss of microRNA-27b contributes to breast cancer stem cell generation by activating ENPP1.* Nat Commun, 2015. **6**: p. 7318.
274. Wang, J., et al., *Knockdown of cyclin D1 inhibits proliferation, induces apoptosis, and attenuates the invasive capacity of human glioblastoma cells.* J Neurooncol, 2012. **106**(3): p. 473-84.
275. Wang, Y.H., et al., *Knockdown of the Wnt receptor Frizzled-1 (FZD1) reduces MDR1/P-glycoprotein expression in multidrug resistant leukemic cells and inhibits leukemic cell proliferation.* Leuk Res, 2018. **67**: p. 99-108.
276. Yan, H.Q., et al., *Interleukin 6 augments lung cancer chemotherapeutic resistance via ataxia-telangiectasia mutated/NF-*

*kappaB pathway activation.* Cancer Sci, 2014. **105**(9): p. 1220-7.
277. Vlaming, M.L., et al., *Abcc2 (Mrp2), Abcc3 (Mrp3), and Abcg2 (Bcrp1) are the main determinants for rapid elimination of methotrexate and its toxic metabolite 7-hydroxymethotrexate in vivo.* Mol Cancer Ther, 2009. **8**(12): p. 3350-9.
278. Morris, M.E., V. Rodriguez-Cruz, and M.A. Felmlee, *SLC and ABC Transporters: Expression, Localization, and Species Differences at the Blood-Brain and the Blood-Cerebrospinal Fluid Barriers.* AAPS J, 2017. **19**(5): p. 1317-1331.
279. Hendrick, A.G., et al., *Identification and Investigation of Novel Binding Fragments in the Fatty Acid Binding Protein 6 (FABP6).* J Med Chem, 2016. **59**(17): p. 8094-102.
280. Fernandez-Barrena, M.G., et al., *Lack of Abcc3 expression impairs bile-acid induced liver growth and delays hepatic regeneration after partial hepatectomy in mice.* J Hepatol, 2012. **56**(2): p. 367-73.
281. Menezes, M.J., et al., *Mutation in mitochondrial ribosomal protein S7 (MRPS7) causes congenital sensorineural deafness, progressive hepatic and renal failure and lactic acidemia.* Hum Mol Genet, 2015. **24**(8): p. 2297-307.
282. Ferlay, J., et al., *Cancer incidence and mortality worldwide: sources, methods and major patterns in GLOBOCAN 2012.* Int J Cancer, 2015. **136**(5): p. E359-86.
283. Siska, P.J., et al., *Strategies to overcome therapeutic resistance in renal cell carcinoma.* Urol Oncol, 2017. **35**(3): p. 102-110.
284. Buzaid, A.C. and M.B. Todd, *Therapeutic options in renal cell carcinoma.* Semin Oncol, 1989. **16**(1 Suppl 1): p. 12-9.
285. Oguri, T., et al., *Association between expression of the MRP3 gene and exposure to platinum drugs in lung cancer.* Int J Cancer, 2001. **93**(4): p. 584-9.
286. Hodorova, I., et al., *Multidrug resistance proteins in renal cell carcinoma.* Folia Biol (Praha), 2008. **54**(6): p. 187-92.
287. Rosland, G.V. and A.S. Engelsen, *Novel points of attack for targeted cancer therapy.* Basic Clin Pharmacol Toxicol, 2015. **116**(1): p. 9-18.
288. Radon, T.P., et al., *Identification of a Three-Biomarker Panel in Urine for Early Detection of Pancreatic Adenocarcinoma.* Clin Cancer Res, 2015. **21**(15): p. 3512-21.
289. Konig, J., et al., *Expression and localization of human multidrug resistance protein (ABCC) family members in pancreatic carcinoma.* Int J Cancer, 2005. **115**(3): p. 359-67.
290. Hoang, N.T., et al., *A review of soft-tissue sarcomas: translation of biological advances into treatment measures.* Cancer Manag Res, 2018. **10**: p. 1089-1114.
291. Voss, R.K., et al., *Adherence to National Comprehensive Cancer Network Guidelines is Associated with Improved Survival for Patients with Stage 2A and Stages 2B and 3 Extremity and Superficial Trunk Soft Tissue Sarcoma.* Ann Surg Oncol, 2017. **24**(11): p. 3271-3278.
292. Pishas, K.I. and S.L. Lessnick, *Ewing sarcoma resistance to SP-2509 is not mediated through KDM1A/LSD1 mutation.* Oncotarget, 2018. **9**(92): p. 36413-36429.
293. Stahl, M., et al., *Risk of recurrence and survival after relapse in patients with Ewing sarcoma.* Pediatr Blood Cancer, 2011. **57**(4): p. 549-53.
294. Jaluria, P., et al., *A perspective on microarrays: current applications, pitfalls, and potential uses.* Microb Cell Fact, 2007. **6**: p. 4.
295. Ye, S., et al., *NVP-TAE684 reverses multidrug resistance (MDR) in human osteosarcoma by inhibiting P-glycoprotein (PGP1) function.* Br J Pharmacol, 2016. **173**(3): p. 613-26.
296. Rajagopal, A. and S.M. Simon, *Subcellular localization and activity of multidrug resistance proteins.* Mol Biol Cell, 2003. **14**(8): p. 3389-99.
297. Hooijberg, J.H., et al., *Modulation by (iso)flavonoids of the ATPase activity of the multidrug resistance protein.* FEBS Lett, 1997. **413**(2): p. 344-8.
298. Chang, X.B., Y.X. Hou, and J.R. Riordan, *Stimulation of ATPase activity of purified multidrug resistance-associated protein by nucleoside diphosphates.* J Biol Chem, 1998. **273**(37): p. 23844-8.
299. Carrasco-Torres, G., et al., *The transmembrane transporter ABCC3 participates in liver cancer progression and is a potential*

*biomarker.* Tumour Biol, 2016. **37**(2): p. 2007-14.
300. Billington, S., et al., *Transporter Expression in Noncancerous and Cancerous Liver Tissue from Donors with Hepatocellular Carcinoma and Chronic Hepatitis C Infection Quantified by LC-MS/MS Proteomics.* Drug Metab Dispos, 2018. **46**(2): p. 189-196.
301. Wiel, C., et al., *Multidrug resistance protein 3 loss promotes tumor formation by inducing senescence escape.* Oncogene, 2016. **35**(12): p. 1596-601.
302. Lin, S., et al., *MEK inhibition induced downregulation of MRP1 and MRP3 expression in experimental hepatocellular carcinoma.* Cancer Cell Int, 2013. **13**(1): p. 3.
303. Manikandan, S., *Measures of central tendency: The mean.* J Pharmacol Pharmacother, 2011. **2**(2): p. 140-2.
304. Tangri, S., et al., *Validation of cell-based fluorescence assays: practice guidelines from the ICSH and ICCS - part III - analytical issues.* Cytometry B Clin Cytom, 2013. **84**(5): p. 291-308.
305. Vlaming, M.L., et al., *Impact of Abcc2 (Mrp2) and Abcc3 (Mrp3) on the in vivo elimination of methotrexate and its main toxic metabolite 7-hydroxymethotrexate.* Clin Cancer Res, 2008. **14**(24): p. 8152-60.
306. Wu, X., A.J. Kriz, and P.A. Sharp, *Target specificity of the CRISPR-Cas9 system.* Quant Biol, 2014. **2**(2): p. 59-70.
307. Liu, X., et al., *Overexpression of ABCC3 promotes cell proliferation, drug resistance, and aerobic glycolysis and is associated with poor prognosis in urinary bladder cancer patients.* Tumour Biol, 2016. **37**(6): p. 8367-74.
308. Steverding, D., *The development of drugs for treatment of sleeping sickness: a historical review.* Parasit Vectors, 2010. **3**(1): p. 15.
309. Babokhov, P., et al., *A current analysis of chemotherapy strategies for the treatment of human African trypanosomiasis.* Pathog Glob Health, 2013. **107**(5): p. 242-52.
310. Li, H., et al., *Suramin inhibits cell proliferation in ovarian and cervical cancer by downregulating heparanase expression.* Cancer Cell Int, 2015. **15**: p. 52.
311. Gradishar, W.J., et al., *A pilot trial of suramin in metastatic breast cancer to assess antiangiogenic activity in individual patients.* Oncology, 2000. **58**(4): p. 324-33.
312. Cohen, I., et al., *Heparanase promotes growth, angiogenesis and survival of primary breast tumors.* Int J Cancer, 2006. **118**(7): p. 1609-17.
313. Reis, M. and S. Liebner, *Wnt signaling in the vasculature.* Exp Cell Res, 2013. **319**(9): p. 1317-23.
314. Nilsson, L.M., et al., *Nuclear factor of activated T-cells transcription factors in the vasculature: the good guys or the bad guys?* Curr Opin Lipidol, 2008. **19**(5): p. 483-90.
315. Stenman, J.M., et al., *Canonical Wnt signaling regulates organ-specific assembly and differentiation of CNS vasculature.* Science, 2008. **322**(5905): p. 1247-50.
316. Liebner, S., et al., *Wnt/beta-catenin signaling controls development of the blood-brain barrier.* J Cell Biol, 2008. **183**(3): p. 409-17.
317. Avendaño, C. and J.C. Menéndez, *Chapter 9 - Drugs That Inhibit Signalling Pathways for Tumor Cell Growth and Proliferation*, in *Medicinal Chemistry of Anticancer Drugs*, C. Avendaño and J.C. Menéndez, Editors. 2008, Elsevier: Amsterdam. p. 251-305.
318. He, Y., et al., *Bioactivities of EF24, a Novel Curcumin Analog: A Review.* Front Oncol, 2018. **8**: p. 614.
319. Fryer, R.A., et al., *Mechanisms underlying gemcitabine resistance in pancreatic cancer and sensitisation by the iMiD lenalidomide.* Anticancer Res, 2011. **31**(11): p. 3747-56.
320. Fantini, J., et al., *Suramin inhibits cell growth and glycolytic activity and triggers differentiation of human colic adenocarcinoma cell clone HT29-D4.* J Biol Chem, 1989. **264**(17): p. 10282-6.
321. Alfarouk, K.O., et al., *Glycolysis, tumor metabolism, cancer growth and dissemination. A new pH-based etiopathogenic perspective and therapeutic approach to an old cancer question.* Oncoscience, 2014. **1**(12): p. 777-802.
322. Baghdiguian, S., et al., *Short-term suramin treatment followed by the removal of the drug induces terminal differentiation of HT29-D4 cells.* J Cell Physiol, 1992. **150**(1): p. 168-74.

323. Anuchapreeda, S., et al., *Modulation of P-glycoprotein expression and function by curcumin in multidrug-resistant human KB cells.* Biochem Pharmacol, 2002. **64**(4): p. 573-82.
324. Scheithauer, W., et al., *Sequential high-dose methotrexate, 5-fluorouracil, and doxorubicin for treatment of advanced pancreatic cancer.* J Cancer Res Clin Oncol, 1990. **116**(2): p. 132-3.
325. Lou, C., et al., *Ginkgolide B enhances gemcitabine sensitivity in pancreatic cancer cell lines via inhibiting PAFR/NF-small ka, CyrillicB pathway.* Biomed Pharmacother, 2019. **109**: p. 563-572.

# Supplementary Data

A

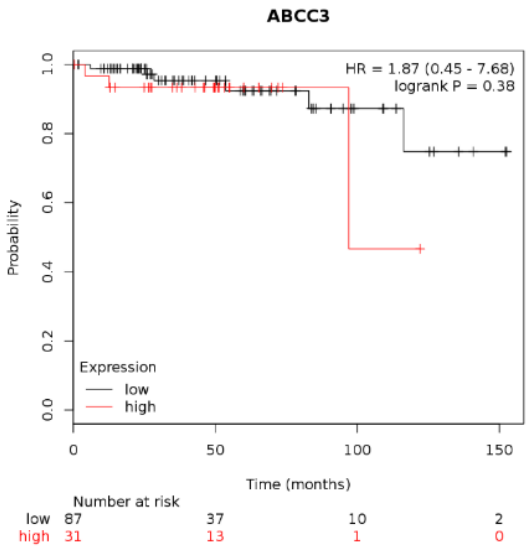


B

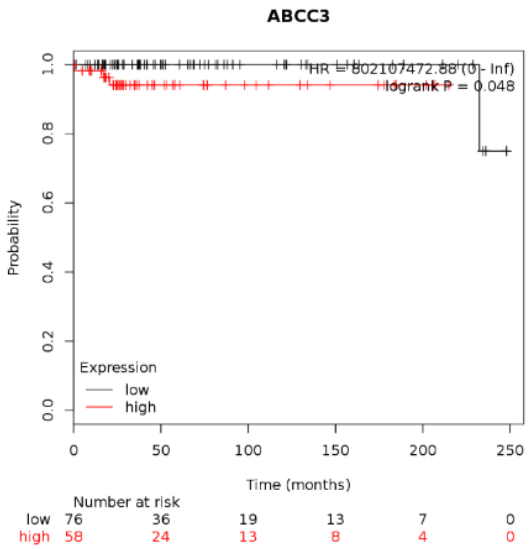


C

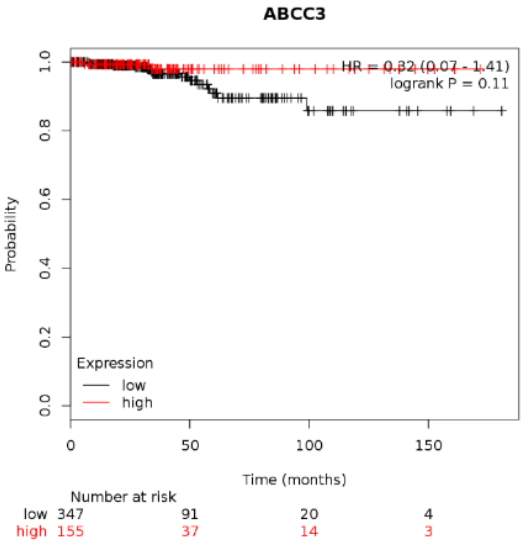


D

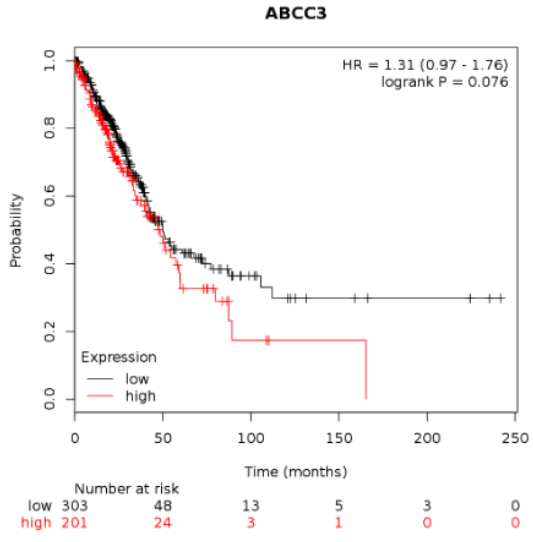


E

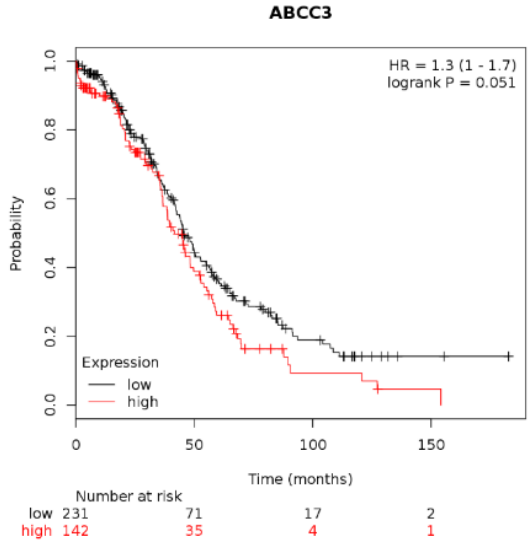


F

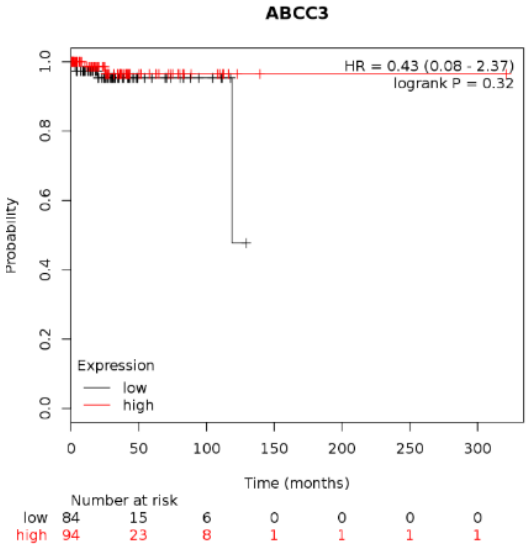

G

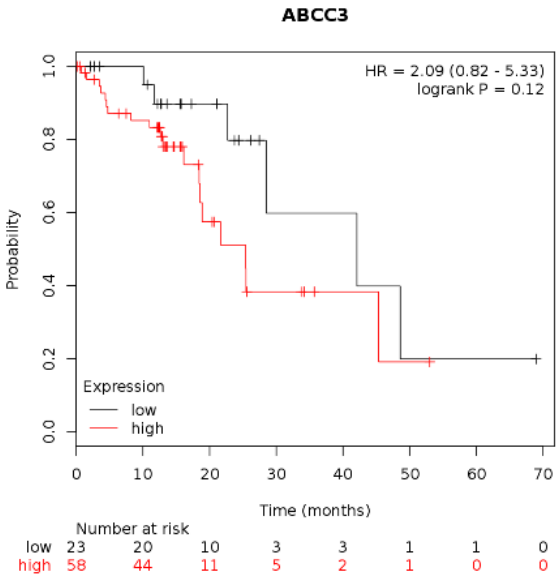


H

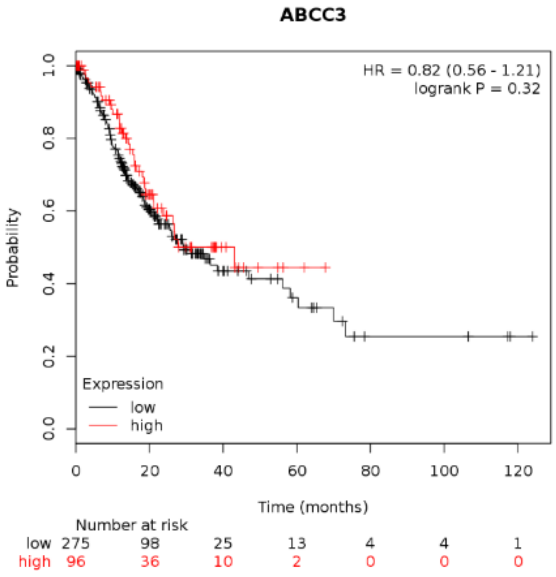


I

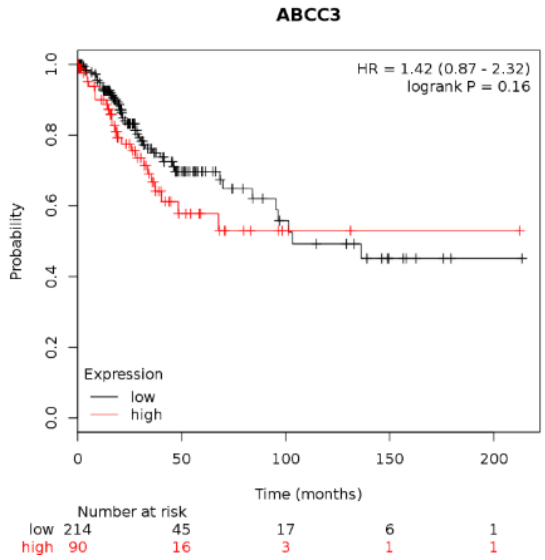


Supplementary Figure 1. Kaplan Meier Survival Plots of ABCC3 expression. Other cancer types that were produced by the KM plotter fof ABCC3 expression. Cancer types in which overall suvival was not significantly affected by ABCC3 includes (A) Thymoma, (B) Testicular Germ Cell Tumour, (C) Thyroid Carcinoma, (D) Lung Adenocarcinoma, (E) Ovarian Carcinoma, (F) Pheochromocytoma and Paraganglioma, (G) Esophageal SCC, (H) Stomach Adenocarcinoma and (I) Cervical Carcinoma.

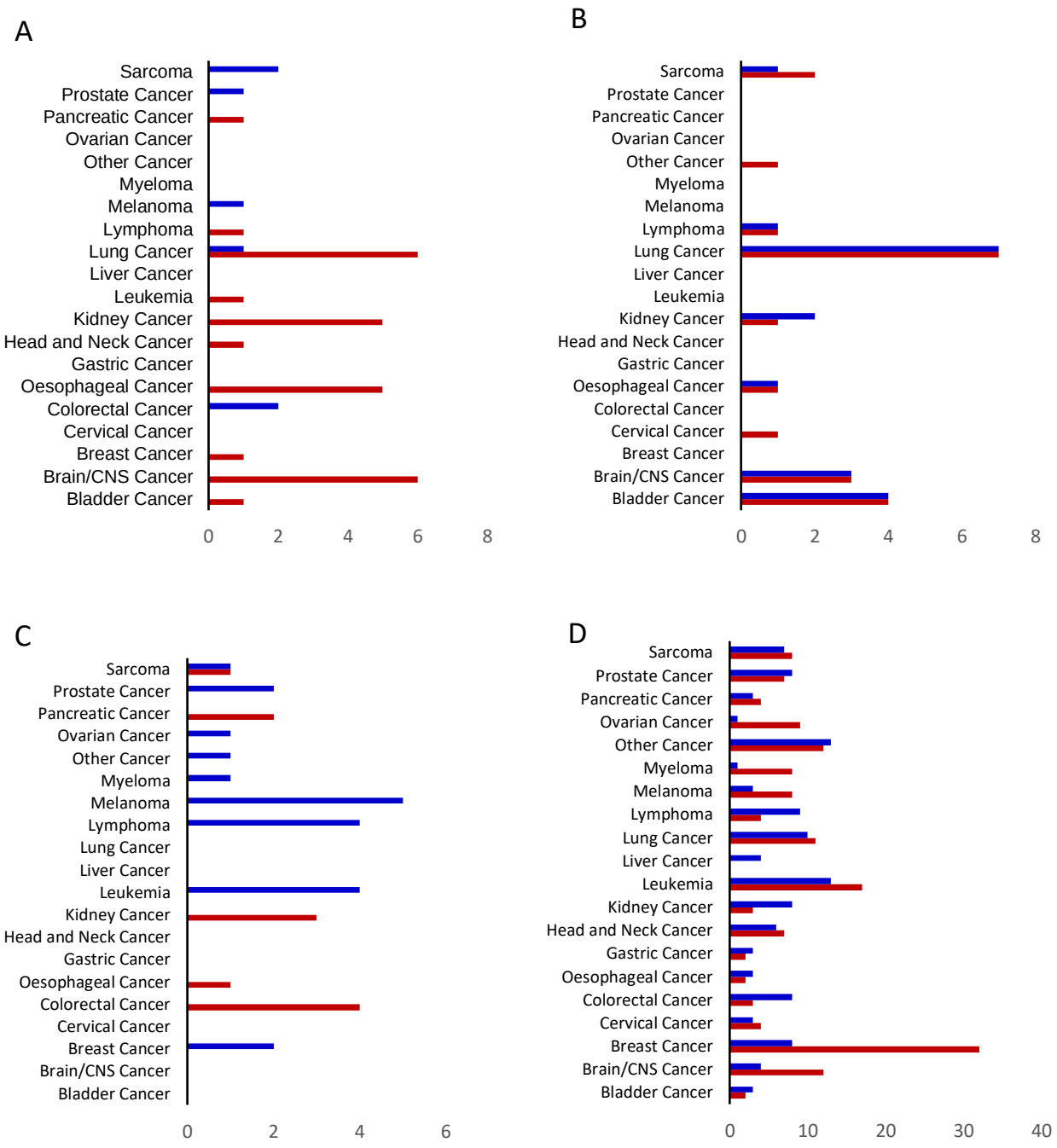


Supplementary Figure 2. Significant analyses shown in response to the ABCC3 search in the oncomine database. Overexpression in red and underexpression in blue. (A) Comparing cancerous samples versus normal samples. (B) Comparing the differential ABCC3 expression between different types of cancerous histology samples. (C) Comparing ABCC3 expression across different cancer types. (D) Comparing the outlying expression of ABCC3 across cancer types. (oncomine.org)

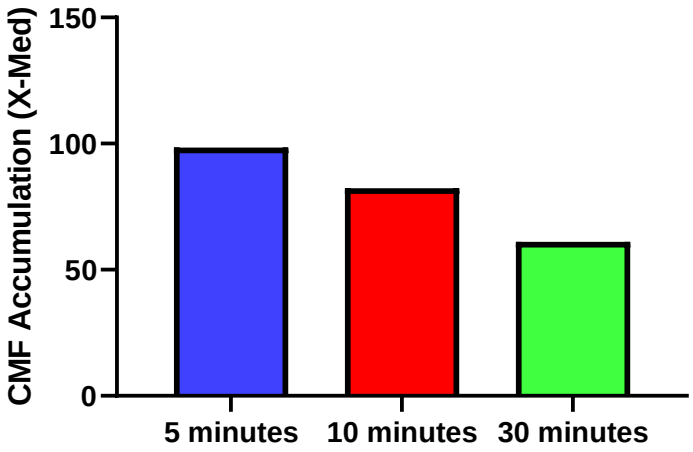


Supplementary Figure 3. MIAPACA2 cells were incubated with CMF and suramin (20 μM) for 5, 10 and 30 minutes to assess which time point should be selected for optimal fluorescent detection.

Supplementary Table 1.Top overexpressing ABCC3 cancer types. The top overexpressing ABCC3 cancer types for each type of oncomine analysis was compared and given a position score, allowing the extropolationg of the top overexpressing ABCC3 cancer types across all analyses performed.

| Cancer vs Normal | Overexpression Rank | Position Score |
|---|---|---|
| Kidney Cancer | 1st | 4 |
| Lymphoma Cancer | 2nd | 3 |
| Bladder Cancer | 3rd | 2 |
| Kidney Cancer | 4th | 1 |
| Cancer vs Cancer (histology) | | |
| Lung Cancer | 1st | 4 |
| Sarcoma | 2nd | 3 |
| Bladder Cancer | 3rd | 2 |
| Lung Cancer | 4th | 1 |
| Cancer vs Cancer (multi-cancer) | | |
| Kidney Cancer | 1st | 4 |
| Pancreatic Cancer | 2nd | 3 |
| Colorectal Cancer | 3rd | 2 |
| Pancreatic Cancer | 4th | 1 |
| Outliers | | |
| Pancreatic Cancer | 1st | 4 |
| Melanoma | 2nd | 3 |
| Sarcoma | 3rd | 2 |
| Brain/CNS Cancer | 4th | 1 |

.

Supplementary Table 2. Coexpression across previously associated pathways. The top seven datasets which showed the highest gene ranks for ABCC3 where compared with pathways that showed ABCC3 modulation in literature

| Concept | Dataset | Cancer/Analysis Type | Rank | P-value | Fold Change | Gene |
|---|---|---|---|---|---|---|
| ABCC3 and Sphingosine-1-phosphate receptor-interpo protein domains and families | | | | | | |
| ABCC3 and Sphingosine-1-phosphate receptor-interpo protein domains and families | Su Multi-cancer | Kidney Cancer | 9 | 1.80E-18 | 24.93 | ABCC3 |
| ABCC3 and Sphingosine-1-phosphate receptor-interpo protein domains and families | Su Multi-cancer | Kidney Cancer | 194 | 1.03E-07 | 6.71 | S1PR1 |
| ABCC3 and Sphingosine-1-phosphate receptor-interpo protein domains and families | Gumz Renal | Clear Cell Renal Cell Carcinoma vs Normal | 66 | 2.38E-09 | 15.08 | ABCC3 |
| ABCC3 and Sphingosine-1-phosphate receptor-interpo protein domains and families | Gumz Renal | Clear Cell Renal Cell Carcinoma vs Normal | 1985 | 3.00E-03 | 2.03 | S1PR1 |
| ABCC3 and Sphingosine-1-phosphate receptor-interpo protein domains and families | Beroukhim Renal | Non-Hereditary Clear Cell Renal Cell Carcinoma vs. Normal | 366 | 1.42E-08 | 4.92 | ABCC3 |
| ABCC3 and Sphingosine-1-phosphate receptor-interpo protein domains and families | Beroukhim Renal | Non-Hereditary Clear Cell Renal Cell Carcinoma vs. Normal | 1692 | 1.14E-04 | 1.67 | S1PR1 |
| ABCC3 and Sphingosine-1-phosphate receptor-interpo protein domains and families | Beroukhim Renal | Hereditary Clear Cell Renal Cell Carcinoma vs. Normal | 522 | 3.35E-09 | 6.56 | ABCC3 |
| ABCC3 and Sphingosine-1-phosphate receptor-interpo protein domains and families | Beroukhim Renal | Hereditary Clear Cell Renal Cell Carcinoma vs. Normal | 1113 | 4.85E-07 | 1.91 | S1PR1 |
| ABCC3 and Sphingosine-1-phosphate receptor-interpo protein domains and families | Bittner Multi-Cancer | Cancer Type: Kidney Cancer | 544 | 2.25E-34 | 2.05 | S1PR1 |

| | | | | | | | |
|---|---|---|---|---|---|---|---|
| ABCC3 and Sphingosine-1-phosphate receptor-interpo protein domains and families | Bittner Multi-Cancer | Cancer Type: Kidney Cancer | 995 | 3.69E-22 | 2.25 | ABCC3 |
| ABCC3 and Sphingosine-1-phosphate receptor-interpo protein domains and families | Su Multi-cancer | Cancer Type: Pancreatic Cancer | 28 | 4.86E-09 | 24.53 | ABCC3 |
| ABCC3 and Sphingosine-1-phosphate receptor-interpo protein domains and families | Su Multi-cancer | Cancer Type: Pancreatic Cancer | 735 | 7.00E-03 | 2.56 | S1PR1 |
| ABCC3 and Sphingosine-1-phosphate receptor-interpo protein domains and families | Bild Lung | Lung cancer type: Non-small Cell Lung Carcinoma | 7 | 2.41E-13 | 3.27 | ABCC3 |
| ABCC3 and Sphingosine-1-phosphate receptor-interpo protein domains and families | Bild Lung | Lung cancer type: Non-small Cell Lung Carcinoma | 1061 | 0.001 | 1.53 | S1PR3 |
| ABCC3 and WNT Signaling Pathway-Biocarta Pathway (Cancer vs Cancer & Cancer vs Normal) | | | | | | |
| ABCC3 and WNT Signaling Pathway-Biocarta Pathway (Cancer vs Cancer & Cancer vs Normal) | Su Multi-cancer | Cancer Type: Kidney Cancer | 9 | 1.80E-18 | 24.93 | ABCC3 |
| ABCC3 and WNT Signaling Pathway-Biocarta Pathway (Cancer vs Cancer & Cancer vs Normal) | Su Multi-cancer | Cancer Type: Kidney Cancer | 57 | 1.98E-11 | 8.14 | CCND1 |
| ABCC3 and WNT Signaling Pathway-Biocarta Pathway (Cancer vs Cancer & Cancer vs Normal) | Su Multi-cancer | Cancer Type: Kidney Cancer | 354 | 5.36E-06 | 5.1 | FZD1 |
| ABCC3 and WNT Signaling Pathway-Biocarta Pathway (Cancer vs Cancer & Cancer vs Normal) | Su Multi-cancer | Cancer Type: Kidney Cancer | 396 | 1.10E-05 | 1.63 | PPP2CA |
| ABCC3 and WNT Signaling Pathway-Biocarta Pathway (Cancer vs Cancer & Cancer vs Normal) | Su Multi-cancer | Cancer Type: Kidney Cancer | 648 | 1.49E-04 | 3.67 | PPARD |

| | | | | | | |
|---|---|---|---|---|---|---|
| ABCC3 and WNT Signaling Pathway-Biocarta Pathway (Cancer vs Cancer & Cancer vs Normal) | Su Multi-cancer | Cancer Type: Kidney Cancer | 885 | 6.56E-04 | 6.8 | HNF1A |
| ABCC3 and WNT Signaling Pathway-Biocarta Pathway (Cancer vs Cancer & Cancer vs Normal) | Su Multi-cancer | Cancer Type: Kidney Cancer | 924 | 7.98E-04 | 1.86 | CNSK2A1 |
| ABCC3 and WNT Signaling Pathway-Biocarta Pathway (Cancer vs Cancer & Cancer vs Normal) | Higgins Renal | Clear Cell Renal Cell Carcinoma vs. Normal | 19 | 8.94E-11 | 5.15 | ABCC3 |
| ABCC3 and WNT Signaling Pathway-Biocarta Pathway (Cancer vs Cancer & Cancer vs Normal) | Higgins Renal | Clear Cell Renal Cell Carcinoma vs. Normal | 192 | 4.83E-05 | 1.68 | CTNNB1 |
| ABCC3 and WNT Signaling Pathway-Biocarta Pathway (Cancer vs Cancer & Cancer vs Normal) | Higgins Renal | Clear Cell Renal Cell Carcinoma vs. Normal | 280 | 3.72E-04 | 4.28 | CCND1 |
| ABCC3 and WNT Signaling Pathway-Biocarta Pathway (Cancer vs Cancer & Cancer vs Normal) | Higgins Renal | Clear Cell Renal Cell Carcinoma vs. Normal | 419 | 2.00E-03 | 1.56 | CSNK1A1 |
| ABCC3 and WNT Signaling Pathway-Biocarta Pathway (Cancer vs Cancer & Cancer vs Normal) | Higgins Renal | Clear Cell Renal Cell Carcinoma vs. Normal | 507 | 4.00E-03 | 3.71 | MYC |
| ABCC3 and WNT Signaling Pathway-Biocarta Pathway (Cancer vs Cancer & Cancer vs Normal) | Higgins Renal | Clear Cell Renal Cell Carcinoma vs. Normal | 733 | 1.60E-02 | 2.16 | FZD1 |
| ABCC3 and WNT Signaling Pathway-Biocarta Pathway (Cancer vs Cancer & Cancer vs Normal) | Gumz Renal | Clear Cell Renal Cell Carcinoma vs. Normal | 66 | 2.38E-09 | 15.08 | ABCC3 |
| ABCC3 and WNT Signaling Pathway-Biocarta Pathway (Cancer vs Cancer & Cancer vs Normal) | Gumz Renal | Clear Cell Renal Cell Carcinoma vs. Normal | 366 | 1.03E-06 | 5.21 | CCND1 |

| | | | | | | |
|---|---|---|---|---|---|---|
| ABCC3 and WNT Signaling Pathway-Biocarta Pathway (Cancer vs Cancer & Cancer vs Normal) | Gumz Renal | Clear Cell Renal Cell Carcinoma vs. Normal | 538 | 7.01E-06 | 1.63 | CSNK1A1 |
| ABCC3 and WNT Signaling Pathway-Biocarta Pathway (Cancer vs Cancer & Cancer vs Normal) | Gumz Renal | Clear Cell Renal Cell Carcinoma vs. Normal | 821 | 4.04E-05 | 2.83 | FZD1 |
| ABCC3 and WNT Signaling Pathway-Biocarta Pathway (Cancer vs Cancer & Cancer vs Normal) | Gumz Renal | Clear Cell Renal Cell Carcinoma vs. Normal | 992 | 9.42E-05 | 6.71 | MYC |
| ABCC3 and WNT Signaling Pathway-Biocarta Pathway (Cancer vs Cancer & Cancer vs Normal) | Gumz Renal | Clear Cell Renal Cell Carcinoma vs. Normal | 1194 | 2.42E-04 | 1.58 | SMAD4 |
| ABCC3 and WNT Signaling Pathway-Biocarta Pathway (Cancer vs Cancer & Cancer vs Normal) | Gumz Renal | Clear Cell Renal Cell Carcinoma vs. Normal | 2604 | 9.00E-03 | 2.37 | PPARD |
| ABCC3 and WNT Signaling Pathway-Biocarta Pathway (Cancer vs Cancer & Cancer vs Normal) | Garnett CellLine | Cancer Type: Kidney Cancer | 253 | 4.45E-06 | 3.83 | ABCC3 |
| ABCC3 and WNT Signaling Pathway-Biocarta Pathway (Cancer vs Cancer & Cancer vs Normal) | Garnett CellLine | Cancer Type: Kidney Cancer | 527 | 1.16E-04 | 1.68 | TLE1 |
| ABCC3 and WNT Signaling Pathway-Biocarta Pathway (Cancer vs Cancer & Cancer vs Normal) | Garnett CellLine | Cancer Type: Kidney Cancer | 878 | 1.00E-03 | 1.94 | CCND1 |
| ABCC3 and WNT Signaling Pathway-Biocarta Pathway (Cancer vs Cancer & Cancer vs Normal) | Jones Renal | Renal Pelvis Urothelial Carcinoma vs. Normal | 70 | 3.07E-16 | 3.7 | SMAD4 |
| ABCC3 and WNT Signaling Pathway-Biocarta Pathway (Cancer vs Cancer & Cancer vs Normal) | Jones Renal | Renal Pelvis Urothelial Carcinoma vs. Normal | 211 | 5.03E-11 | 1.83 | PPARD |

| | | | | | | |
|---|---|---|---|---|---|---|
| ABCC3 and WNT Signaling Pathway-Biocarta Pathway (Cancer vs Cancer & Cancer vs Normal) | Jones Renal | Renal Pelvis Urothelial Carcinoma vs. Normal | 263 | 4.52E-10 | 4.39 | ABCC3 |
| ABCC3 and WNT Signaling Pathway-Biocarta Pathway (Cancer vs Cancer & Cancer vs Normal) | Jones Renal | Renal Pelvis Urothelial Carcinoma vs. Normal | 721 | 9.91E-07 | 1.74 | MAP3K7 |
| ABCC3 and WNT Signaling Pathway-Biocarta Pathway (Cancer vs Cancer & Cancer vs Normal) | Jones Renal | Renal Pelvis Urothelial Carcinoma vs. Normal | 739 | 1.15E-06 | 2.3 | CSNK1A1 |
| ABCC3 and WNT Signaling Pathway-Biocarta Pathway (Cancer vs Cancer & Cancer vs Normal) | Yusenko Renal | Kidney Cancer Type: Renal Carcinoma | 328 | 3.66E-05 | 8.32 | ABCC3 |
| ABCC3 and WNT Signaling Pathway-Biocarta Pathway (Cancer vs Cancer & Cancer vs Normal) | Yusenko Renal | Kidney Cancer Type: Renal Carcinoma | 567 | 1.45E-04 | 1.63 | PPARD |
| ABCC3 and WNT Signaling Pathway-Biocarta Pathway (Cancer vs Cancer & Cancer vs Normal) | Yusenko Renal | Kidney Cancer Type: Renal Carcinoma | 749 | 3.25E-04 | 3.54 | FZD1 |
| ABCC3 and WNT Signaling Pathway-Biocarta Pathway (Cancer vs Cancer & Cancer vs Normal) | Yusenko Renal | Kidney Cancer Type: Renal Carcinoma | 826 | 4.28E-04 | 1.99 | HNF1A |
| ABCC3 and WNT Signaling Pathway-Biocarta Pathway (Cancer vs Cancer & Cancer vs Normal) | Yusenko Renal | Kidney Cancer Type: Renal Carcinoma | 1753 | 4.00E-03 | 1.56 | CSNK1D |
| ABCC3 and WNT Signaling Pathway-Biocarta Pathway (Cancer vs Cancer & Cancer vs Normal) | Yusenko Renal | Kidney Cancer Type: Renal Carcinoma | 2458 | 1.20E-02 | 2.45 | MYC |
| ABCC3 and WNT Signaling Pathway-Biocarta Pathway (Cancer vs Cancer & Cancer vs Normal) | Yusenko Renal | Kidney Cancer Type: Renal Carcinoma | 3730 | 4.40E-02 | 1.93 | CSNK1A1 |

| | | | | | | |
|---|---|---|---|---|---|---|
| ABCC3 and WNT Signaling Pathway-Biocarta Pathway (Cancer vs Cancer & Cancer vs Normal) | Su Multi-cancer | Cancer Type: Pancreatic Cancer | 5 | 2.69E-14 | 6.06 | PPARD |
| ABCC3 and WNT Signaling Pathway-Biocarta Pathway (Cancer vs Cancer & Cancer vs Normal) | Su Multi-cancer | Cancer Type: Pancreatic Cancer | 28 | 4.86E-09 | 24.53 | ABCC3 |
| ABCC3 and WNT Signaling Pathway-Biocarta Pathway (Cancer vs Cancer & Cancer vs Normal) | Su Multi-cancer | Cancer Type: Pancreatic Cancer | 546 | 3.00E-03 | 1.69 | CTNNB1 |
| ABCC3 and WNT Signaling Pathway-Biocarta Pathway (Cancer vs Cancer & Cancer vs Normal) | Su Multi-cancer | Cancer Type: Pancreatic Cancer | 1121 | 2.40E-02 | 1.59 | CSNK1A1 |
| ABCC3 and WNT Signaling Pathway-Biocarta Pathway (Cancer vs Cancer & Cancer vs Normal) | Su Multi-cancer | Cancer Type: Pancreatic Cancer | 1383 | 4.30E-02 | 1.72 | MAP3K7 |
| ABCC3 and WNT Signaling Pathway-Biocarta Pathway (Cancer vs Cancer & Cancer vs Normal) | Barretina CellLine | Cancer Type: Pancreatic Cancer | 69 | 1.31E-17 | 2.6 | CCND1 |
| ABCC3 and WNT Signaling Pathway-Biocarta Pathway (Cancer vs Cancer & Cancer vs Normal) | Barretina CellLine | Cancer Type: Pancreatic Cancer | 229 | 8.71E-12 | 4.21 | ABCC3 |
| ABCC3 and WNT Signaling Pathway-Biocarta Pathway (Cancer vs Cancer & Cancer vs Normal) | Barretina CellLine | Cancer Type: Pancreatic Cancer | 778 | 4.91E-07 | 1.74 | TLE1 |
| ABCC3 and WNT Signaling Pathway-Biocarta Pathway (Cancer vs Cancer & Cancer vs Normal) | Pei Pancreas | Cancer Type: Pancreatic Cancer | 517 | 9.25E-07 | 1.84 | HDAC1 |
| ABCC3 and WNT Signaling Pathway-Biocarta Pathway (Cancer vs Cancer & Cancer vs Normal) | Pei Pancreas | Cancer Type: Pancreatic Cancer | 1541 | 8.17E-05 | 2.13 | ABCC3 |

| | | | | | | |
|---|---|---|---|---|---|---|
| ABCC3 and WNT Signaling Pathway-Biocarta Pathway (Cancer vs Cancer & Cancer vs Normal) | Pei Pancreas | Cancer Type: Pancreatic Cancer | 2228 | 3.75E-04 | 1.7 | CNSK2A1 |
| ABCC3 and WNT Signaling Pathway-Biocarta Pathway (Cancer vs Cancer & Cancer vs Normal) | Pei Pancreas | Cancer Type: Pancreatic Cancer | 2460 | 5.51E-04 | 1.95 | CCND1 |
| ABCC3 and WNT Signaling Pathway-Biocarta Pathway (Cancer vs Cancer & Cancer vs Normal) | Pei Pancreas | Cancer Type: Pancreatic Cancer | 3564 | 3.00E-03 | 1.62 | PPARD |

ABCC3 and p53 Signaling Pathway-Biocarta Pathway (Cancer vs Cancer & Cancer vs Normal)

| | | | | | | |
|---|---|---|---|---|---|---|
| ABCC3 and p53 Signalling Pathway - Biocarta Pathway (Cancer vs Cancer & Cancer vs Normal) | Bild Lung | Lung Cancer Type: Non-small Cell Lung Carcinoma | 7 | 2.41E-13 | 3.27 | ABCC3 |
| ABCC3 and p53 Signalling Pathway - Biocarta Pathway (Cancer vs Cancer & Cancer vs Normal) | Bild Lung | Lung Cancer Type: Non-small Cell Lung Carcinoma | 2268 | 1.20E-02 | 1.22 | ATM |
| ABCC3 and p53 Signalling Pathway - Biocarta Pathway (Cancer vs Cancer & Cancer vs Normal) | Bild Lung | Lung Cancer Type: Non-small Cell Lung Carcinoma | 2382 | 1.40E-02 | 1.45 | CCND1 |
| ABCC3 and p53 Signalling Pathway - Biocarta Pathway (Cancer vs Cancer & Cancer vs Normal) | Su Multi-cancer | Cancer Type: Kidney Cancer | 9 | 1.80E-18 | 24.93 | ABCC3 |
| ABCC3 and p53 Signalling Pathway - Biocarta Pathway (Cancer vs Cancer & Cancer vs Normal) | Su Multi-cancer | Cancer Type: Kidney Cancer | 57 | 1.98E-11 | 8.14 | CCND1 |
| ABCC3 and p53 Signalling Pathway - Biocarta Pathway (Cancer vs Cancer & Cancer vs Normal) | Su Multi-cancer | Cancer Type: Kidney Cancer | 182 | 7.34E+08 | 1.77 | RB1 |
| ABCC3 and p53 Signalling Pathway - Biocarta Pathway | Su Multi-cancer | Cancer Type: Kidney Cancer | 267 | 1.01E-06 | 3.3 | BAX |

| | | | | | | | |
|---|---|---|---|---|---|---|---|
| (Cancer vs Cancer & Cancer vs Normal) | | | | | | | |
| ABCC3 and p53 Signalling Pathway - Biocarta Pathway (Cancer vs Cancer & Cancer vs Normal) | Su cancer | Multi- | Cancer Type: Kidney Cancer | 437 | 1.97E-05 | 3.25 | CDKN1A |
| ABCC3 and p53 Signalling Pathway - Biocarta Pathway (Cancer vs Cancer & Cancer vs Normal) | Su cancer | Multi- | Cancer Type: Kidney Cancer | 625 | 1.21E-04 | 7.06 | ATM |
| ABCC3 and p53 Signalling Pathway - Biocarta Pathway (Cancer vs Cancer & Cancer vs Normal) | Su cancer | Multi- | Cancer Type: Kidney Cancer | 699 | 2.04E-04 | 2.79 | BCL2 |
| ABCC3 and p53 Signalling Pathway - Biocarta Pathway (Cancer vs Cancer & Cancer vs Normal) | Su cancer | Multi- | Cancer Type: Kidney Cancer | 800 | 3.79E-04 | 2.47 | TP53 |
| ABCC3 and p53 Signalling Pathway - Biocarta Pathway (Cancer vs Cancer & Cancer vs Normal) | Su cancer | Multi- | Cancer Type: Kidney Cancer | 1078 | 2.00E-03 | 1.78 | TIMP3 |
| ABCC3 and p53 Signalling Pathway - Biocarta Pathway (Cancer vs Cancer & Cancer vs Normal) | Su cancer | Multi- | Cancer Type: Kidney Cancer | 1248 | 4.00E-03 | 1.79 | GADD45A |
| ABCC3 and p53 Signalling Pathway - Biocarta Pathway (Cancer vs Cancer & Cancer vs Normal) | Su cancer | Multi- | Cancer Type: Pancreatic Cancer | 28 | 4.86E-09 | 24.53 | ABCC3 |
| ABCC3 and p53 Signalling Pathway - Biocarta Pathway (Cancer vs Cancer & Cancer vs Normal) | Su cancer | Multi- | Cancer Type: Pancreatic Cancer | 1039 | 1.80E-02 | 2.97 | BAX |
| ABCC3 and p53 Signalling Pathway - Biocarta Pathway (Cancer vs Cancer & Cancer vs Normal) | Su cancer | Multi- | Cancer Type: Colorectal Cancer | 54 | 1.80E-13 | 16.8 | ABCC3 |
| ABCC3 and p53 Signalling Pathway - Biocarta Pathway | Su cancer | Multi- | Cancer Type: Colorectal Cancer | 338 | 3.16E-07 | 2.29 | PCNA |

| | | | | | | |
|---|---|---|---|---|---|---|
| (Cancer vs Cancer & Cancer vs Normal) | | | | | | |
| ABCC3 and p53 Signalling Pathway - Biocarta Pathway (Cancer vs Cancer & Cancer vs Normal) | Su Multi-cancer | Cancer Type: Colorectal Cancer | 500 | 5.52E-06 | 2.98 | BAX |
| ABCC3 and p53 Signalling Pathway - Biocarta Pathway (Cancer vs Cancer & Cancer vs Normal) | Su Multi-cancer | Cancer Type: Colorectal Cancer | 695 | 6.47E-05 | 1.37 | BCL2 |
| ABCC3 and p53 Signalling Pathway - Biocarta Pathway (Cancer vs Cancer & Cancer vs Normal) | Su Multi-cancer | Cancer Type: Colorectal Cancer | 794 | 1.45E-04 | 1.28 | CDK2 |
| ABCC3 and p53 Signalling Pathway - Biocarta Pathway (Cancer vs Cancer & Cancer vs Normal) | Su Multi-cancer | Cancer Type: Colorectal Cancer | 980 | 5.26E-04 | 1.41 | CDK4 |
| ABCC3 and p53 Signalling Pathway - Biocarta Pathway (Cancer vs Cancer & Cancer vs Normal) | Nakayama Sarcoma | Sarcoma Type: Malignant Peripheral Nerve Sheath Tumour | 15 | 1.32E+14 | 5.92 | ABCC3 |
| ABCC3 and p53 Signalling Pathway - Biocarta Pathway (Cancer vs Cancer & Cancer vs Normal) | Nakayama Sarcoma | Sarcoma Type: Malignant Peripheral Nerve Sheath Tumour | 145 | 4.86E-06 | 1.67 | RB1 |
| ABCC3 and p53 Signalling Pathway - Biocarta Pathway (Cancer vs Cancer & Cancer vs Normal) | Nakayama Sarcoma | Sarcoma Type: Malignant Peripheral Nerve Sheath Tumour | 182 | 1.56E-05 | 2.17 | CCND1 |
| ABCC3 and p53 Signalling Pathway - Biocarta Pathway (Cancer vs Cancer & Cancer vs Normal) | Nakayama Sarcoma | Sarcoma Type: Malignant Peripheral Nerve Sheath Tumour | 492 | 2.00E-03 | 1.77 | TIMP3 |
| ABCC3 and p53 Signalling Pathway - Biocarta Pathway (Cancer vs Cancer & Cancer vs Normal) | Nakayama Sarcoma | Sarcoma Type: Malignant Peripheral Nerve Sheath Tumour | 881 | 1.30E-02 | 1.51 | CDK2 |
| ABCC3 and p53 Signalling Pathway - Biocarta Pathway | Higgins Renal | Clear Cell Renal Cell Carcinoma vs Normal | 19 | 9.84E-11 | 5.15 | ABCC3 |

| | | | | | | |
|---|---|---|---|---|---|---|
| (Cancer vs Cancer & Cancer vs Normal) | | | | | | |
| ABCC3 and p53 Signalling Pathway - Biocarta Pathway (Cancer vs Cancer & Cancer vs Normal) | Higgins Renal | Clear Cell Renal Cell Carcinoma vs Normal | 154 | 1.31E-05 | 1.88 | TP53 |
| ABCC3 and p53 Signalling Pathway - Biocarta Pathway (Cancer vs Cancer & Cancer vs Normal) | Higgins Renal | Clear Cell Renal Cell Carcinoma vs Normal | 280 | 3.72E-04 | 4.28 | CCND1 |
| ABCC3 and p53 Signalling Pathway - Biocarta Pathway (Cancer vs Cancer & Cancer vs Normal) | Higgins Renal | Clear Cell Renal Cell Carcinoma vs Normal | 774 | 1.90E-02 | 2.04 | ATM |
| ABCC3 and p53 Signalling Pathway - Biocarta Pathway (Cancer vs Cancer & Cancer vs Normal) | Bhattacharjee Lung | Lung cancer type: Non-small Cell Lung Carcinoma | 25 | 2.39E-06 | 16.48 | ABCC3 |
| ABCC3 and p53 Signalling Pathway - Biocarta Pathway (Cancer vs Cancer & Cancer vs Normal) | Bhattacharjee Lung | Lung cancer type: Non-small Cell Lung Carcinoma | 643 | 4.00E-02 | 1.49 | MDM2 |